ELECTROCHEMICAL PROMOTION OF AN IrO_2 CATALYST FOR THE GAS PHASE OXIDATION OF ETHYLENE

THÈSE N° 1455 (1995)

PRÉSENTÉE AU DÉPARTEMENT DE CHIMIE

ÉCOLE POLYTECHNIQUE FÉDÉRALE DE LAUSANNE

POUR L'OBTENTION DU GRADE DE DOCTEUR ÈS SCIENCES TECHNIQUES

PAR

Elli VARKARAKI

Ingénieur chimiste diplômée EPF

de nationalité grecque

acceptée sur proposition du jury:

Prof. E. Plattner, directeur de thèse
Dr Ch. Comninellis, corapporteur
Prof. R.M. Lambert, corapporteur
Prof. A. Renken, corapporteur
Prof. C. Vayenas, corapporteur

Lausanne, EPFL
1996

– Παππού αγαπημένε, είπα, δώσ'μου μια προσταγή.

Χαμογέλασε, απίθωσε το χέρι απάνω στο κεφάλι μου· δεν ήταν χέρι, ήταν πολύχρωμη φωτιά· ως τις ρίζες του μυαλού μου περεχύθηκε η φλόγα.

– Φτάσε όπου μπορείς, παιδί μου...

Η φωνή του βαθειά, σκοτεινή, σα να'βγαινε από το βαθύ λαρύγγι της γης.

Εφτασε ως τις ρίζες του μυαλού μου η φωνή του, μα η καρδιά μου δεν τινάχτηκε.

– Παππού, φώναξα τώρα πιο δυνατά, δώσ'μου μιαν πιο δύσκολη, πιο κρητικιά προσταγή.

Κι ολομεμιάς, ως να το πω, μια φλόγα σούριξε ξεσκίζοντας τον αέρα, αφανίστηκε από τα μάτια μου ο αδάμαστος πρόγονος με τις περιπλεμένες θυμαρόριζες στα μαλλιά του κι απόμεινε στην κορφή του Σινά μια φωνή όρθια, γεμάτη προσταγή, κι ο αέρας έτρεμε:

– Φτάσε όπου δε μπορείς!

Νίκος Καζαντζάκης
(Αναφορά στον Γκρέκο)

To my grandfather, my parents

and Christina

ACKNOWLEDGEMENTS

I particularly wish to express my gratitude to Prof. E. Plattner (Institut de Génie Chimique, EPFL), director of this thesis, for his trust and communicative enthusiasm for research.

I gratefully acknowledge Prof. C. Vayenas (Technical University of Patras, Greece), initiator of this project, who invited me to his laboratories at a crucial moment of my Ph.D. work and introduced me, with his team, to the secrets of the NEMCA effect.

I also wish to thank Dr. C. Comninellis and the members of the Institut de Génie Chimique for their friendship and encouragements.

RÉSUMÉ

L'oxydation catalytique de l'éthylène est étudiée sur un catalyseur en IrO_2 supporté sur la zircone stabilisée à l'yttrium. La réaction a lieu entre les réactants à l'état adsorbé, et sa cinétique est de type "Langmuir-Hinshelwood". A faible pression partielle d'éthylène, la réaction est plutôt limitée par l'adsorption d'éthylène et la vitesse de réaction dépend linéairement de la pression partielle de l'éthylène. A faible pression partielle d'oxygène par contre, la vitesse de réaction semble dépendre de la pression partielle de l'oxygène à la puissance 3/2. Cette dépendence indique que la réaction a probablement lieu par le biais d'un intermédiaire.

L'effet NEMCA (Non-faradaic Electrochemical Modification of Catalytic Activity) est démontré pour la première fois sur un catalyseur oxyde. Ce travail contribue donc à la généralisation de l'effet NEMCA, qui, jusqu'à présent, avait été étudié uniquement sur des catalyseurs métalliques. L'activité du catalyseur IrO_2, pour la combustion complète d'éthylène, est accrue de manière remarquable et réversible en polarisant l'interface catalyseur-électrolyte solide. La vitesse de réaction en excès d'oxygène est augmentée d'un ordre de grandeur, quand le catalyseur est polarisé positivement par rapport à une électrode de référence. L'augmentation de la vitesse peut être jusqu'à $1 \cdot 10^4$ fois plus élevée que la vitesse d'apport d'ions O^{2-} vers le catalyseur. La vitesse de réaction peut être augmentée aussi par l'application de potentiels négatifs, sous certaines conditions expérimentales.

La voltamétrie cyclique peut être utilisée pour maintenir la vitesse d'oxydation d'éthylène à un niveau supérieur à sa valeur à circuit ouvert. Cette méthode d'investigation, qui n'a pas souvent été appliquée à l'étude des catalyseurs en régime de fonctionnement, peut donner beaucoup d'informations sur l'état de la surface. La sensibilité de la voltamétrie cyclique est plus grande quand la pression partielle de l'oxygène dans le milieu est faible.

La promotion électrochimique de l'activité catalytique de l'IrO_2 est particulièrement spectaculaire en excès d'oxygène. Elle est expliquée par l'oxydation de l'IrO_2 en $IrO_{2+\delta}$, lors de la polarisation anodique du catalyseur. Il est montré dans ce travail que la vitesse d'oxydation de l'éthylène est en relation linéaire avec la quantité de charge accumulée à l'interface catalyseur-électrolyte. Cette charge est mesurée par voltamétrie cyclique lors de la désactivation du catalyseur après une polarisation anodique. Les voltamogrammes de l'IrO_2 dans l'air ont mis en évidence la présence d'un pic cathodique, lié à la réduction de l'$IrO_{2+\delta}$ formé pendant le balayage anodique.

ABSTRACT

This work contributes to the generalization of the Non-faradaic Electrochemical Modification of Catalytic Activity effect, known under the acronym NEMCA. This effect is observed for the first time over an oxide catalyst, namely IrO_2 supported on yttria-stabilized-zirconia. The activity of the IrO_2 catalyst for the complete ethylene oxidation is remarkably and reversibly increased by polarizing the catalyst-solid electrolyte interface. The reaction rate in excess oxygen is enhanced by at least an order of magnitude, when the catalyst is polarized positively with respect to a reference electrode. The rate enhancement may be up to $1 \cdot 10^4$ times higher than the rate of O^{2-} supply to the catalyst.

The application of low negative potentials generally causes the rate to decrease. However, under a limited range of experimental conditions, namely temperatures above 370°C and high overpotentials, the cathodic polarization induces a rate enhancement.

The ethylene oxidation kinetics over an IrO_2 catalyst exhibits a Langmuir-Hinshelwood behaviour with competitive adsorption of reactants. The rate dependence on the oxygen partial pressure indicates that the reaction may proceed via an intermediate. The electrochemical promotion of the catalyst is most effective in oxygen-rich gas phase compositions, where the rate is essentially limited by the ethylene adsorption.

In-situ cyclic voltammetry is used to maintain the reaction rate at a higher value than under open-circuit conditions. This simple method of investigation has just entered in the world of catalysis and provides valuable information on the state of the catalyst surface. The redox processes involving very small amounts of electroactive species can only be studied in low oxygen pressures.

The main finding of this work is the experimental evidence that the electrochemical promotion of the ethylene oxidation rate is linearly related to the electrical charge stored at the electrode-electrolyte interface, measured by cyclic voltammetry. The voltammetric analysis of the IrO_2 catalyst in air shows that, upon positive polarization, the catalyst surface is oxidized to a higher oxide $IrO_{2+\delta}$ which is responsible for the rate enhancement observed.

CHAPTER 1

INTRODUCTION - AIM OF THE WORK

The writings of Jabir ibn Haiyan, an Arabic alchemist, attest that sulfuric acid was used in the eighth century as a catalyst for the dehydration of alcohol to ether. The word catalysis in its modern connotation, however, is due to Berzelius (1835). The discovery in 1823 of Döbereiner's lighter, based on the platinum catalyzed water synthesis, became the first commercial application of a catalytic process [Thomas, 1994]. In the 1840s, Grove invented the "gas battery" or fuel cell using platinum as an electrocatalyst. In the same period, Phillips patented a platinum catalyst for the conversion of SO_2 to SO_3, preparing the way for the manufacture of sulfuric acid. The Haber process for the ammonia synthesis initiated in 1909, the Fischer-Tropsch conversion of syngas in 1922 and the production of ethylene oxide over silver by Union Carbide in 1937 are also landmarks in the history of catalysis, which still certify the importance of heterogeneous catalysis in the chemical industry.

The promotion and control of catalyst activity and selectivity is a long-sought goal in catalysis. The geometric and electronic factor, the spillover phenomenon, the metal-support interaction and the bifunctional character of catalysts are concepts developed to explain promotion effects. Despite the theoretical advance and the formulation of new ideas in the catalysis field, research remains quite empirical as is evidenced by the still widespread use of catalyst screening for technical applications. New tools and techniques rather than new concepts are responsible for the progress in the identification of elementary steps and in the understanding of catalytic mechanisms.

The aim of this work is to study the recently discovered Non-faradaic Electrochemical Modification of Catalytic Activity (NEMCA) effect [Vayenas, 1992a]. The electrochemical polarization of a catalyst film supported on an ionic conductor acts as a promoter for the catalyzed reaction. This effect, which has already been tested with several reactions on different metal catalysts, seems to be of a general validity. In order to prove the wide applicability of the NEMCA effect, this work will deal with the ethylene oxidation over an iridium oxide catalyst, the first metallic oxide to be tested. The IrO_2 catalyst is supported on ZrO_2 stabilized in the cubic phase with 6-8% mol of Y_2O_3.

An important characteristic of the NEMCA effect studies is the coupling of heterogeneous catalysis and electrocatalysis, which have been growing apart for years, probably due to the high complexity of the respective systems. Actually, they have many points in common and their simultaneous study is a practical and theoretical challenge.

CHAPTER 2

THEORY AND LITERATURE REVIEW

The study of a catalytic reaction under an electrochemical polarization regime necessitates the use of concepts and techniques from two distinct areas of chemistry: electrochemistry and heterogeneous catalysis. Generally, electrochemists are not acquainted with the terms and experimental methods applied in catalysis, and vice-versa. The literature review is divided in four sections. The first section is dedicated to the electrochemistry, and especially to its high temperature applications. The accent is put on the properties of solid electrolytes and particularly of the cubic zirconia which is used as a catalyst support in this study. The second section deals with the electrocatalytic and catalytic properties of the catalyst, namely iridium oxide. The third section is dedicated to the heterogeneous catalysis and the ethylene oxidation in the gas phase, which is the reaction under study. The state of the art on the NEMCA effect is overviewed in the last section, since it is based on a synthesis of electrochemical and catalytical theories.

2.1 SOLID ELECTROLYTES AND HIGH TEMPERATURE ELECTROCHEMISTRY

2.1.1 Solid electrolytes: properties and applications

In 1834, Michael Faraday observed for the first time that solid PbF_2 becomes an electrical conductor when heated to 500°C. It took almost a century to explain this experimental observation by F^- ion conduction [Vayenas, 1995].

A solid electrolyte is an ionically conducting solid medium. In the non-conducting state ions vibrate around a given lattice position, whereas in the conducting state they undergo long range translation. Most of the solid electrolytes used in high temperature electrochemistry are oxides and salts. The ionic conductivity of such materials can be described in terms of a mobile sublattice of one set of ions in a rigid framework. It is generally due to the presence of intrinsic or extrinsic point defects in their structure, namely vacancies, interstitials, misplaced atoms, impurities, Schottky and Frenkel defects [Choudhary, 1980].

Schottky defects correspond to anion-cation vacancy pairs and the charge transfer is due to motion of vacancies through the lattice by successive ion hops. Frenkel defects correspond to ions promoted to interstitial sites and the conductivity, which is much higher, is due to ion displacement through a series of interstitial sites.

The concentration of mobile species can be increased by means of doping with heterovalent ions. The charge balance can then be achieved by four ionic mechanisms. Doping with a higher valent cation leads to the creation of cation vacancies or anion interstitials, whereas doping with lower valent cations necessitates the creation of anion vacancies or cation interstitials [West, 1995]. The dopant size is of primary importance for the conductivity enhancement. For any oxide structure, a significant increase in the

oxygen vacancy concentration due to doping can result in phase transitions at temperatures considerably lower than those of the pure oxides [Johannesen, 1989].

Classification of solid electrolytes

A useful classification of crystalline electrolytes is based on the ion responsible for their conductivity. Silver ion conductors generally present the highest conductivities. Sodium ion conduction has been extensively studied in the β-alumina, where Na^+ ions can only migrate in two dimensions. β-alumina are layered structures in which dense blocks with spinel-like structure alternate with open "conduction planes" containing the mobile Na^+ ions [West, 1995]. Lithium ion conductors are interesting, because high voltages and power densities can be obtained with lithium batteries.

Oxide ion conductors are among the most useful electrolytes, especially the ones with fluorite structures based on ZrO_2, CeO_2, ThO_2 and Bi_2O_3. The Bi_2O_3-based materials are the best conductors, but they are easily reduced at low oxygen partial pressures. Usually, the activation energy for oxide ion conduction is at least 0.8eV (77 kJ/mol) [West, 1995]. Materials with the perovskite structure are capable of high oxide ion conductivity but they often are electronic conductors as well. In certain perovskites, proton conduction at high temperatures has been discovered too. Fluoride ion conduction is also common in materials with the fluorite structure [West, 1995].

Electrical conductivity of solid electrolytes

Ionic conductivity by ion hopping from site to site, through a crystal structure, can occur if not all of the energetically equivalent or near-equivalent sites are occupied. Each hop generates local departures from electroneutrality, which must be restored by a redistribution of the surrounding ions before the next hop can take place. The *random walk* theory provides a semi-quantitative description of ionic conductivity, assuming that the ions move independently of one another [Goodenough, 1995]. This theory is particularly suitable for dilute defect systems, where the electrostatic interaction between mobile ions can be neglected. This is not the case in systems with high carrier concentrations, where each ion must drag along its associated ion atmosphere, for long range conduction to occur.

In ionic solids with dense crystal structures, there are no well-defined conduction pathways and the activation energy for ion hopping is large, usually 1eV (96 kJ/mol). In solid electrolytes, by contrast, there are open conduction pathways and the activation energy can be as low as 0.03eV in AgI, 0.15eV in β-alumina and 0.9eV in yttria-stabilized-zirconia (YSZ) [West, 1995].

The conductivity is a tensor quantity relating the current density i to the applied electric field E. The scalar expression for the mobile ion current density in one direction is

$$i = \sigma_i E = c_i\, q\, v$$

where v is the mean velocity of the mobile ions of charge q at a concentration c_i [Goodenough, 1995]. From the definition of the charge carrier mobility $u \equiv v/E$, the conductivity is obtained:

$$\sigma_i = c_i q u_i \tag{2.1}$$

and upon substitution of the Nernst-Einstein relationship:

$$u_i = q D / k_b T$$

$$\sigma_i = c_i q^2 D / k_b T \tag{2.2}$$

The diffusion coefficient

$$D = D_o \exp(-\Delta G_m / k_b T)$$

contains the motional free energy

$$\Delta G_m = \Delta H_m - T \Delta S_m$$

In addition, for a temperature-independent mobile-ion site occupancy on energetically equivalent sites we have [Goodenough, 1995]:

$$E_a = \Delta H_m$$

The temperature dependence of the ionic conductivity can therefore be described by the equation:

$$\sigma = (\sigma_o / T) \exp(-E_a / k_b T) \tag{2.3}$$

where σ_o is a function of the ionic charge, the concentration and the attempt frequency of the mobile ions, E_a is the activation energy for defect motion (on the order of 0.5 to 2 eV) and k_b is the Boltzmann constant [Vayenas, 1995]. It is clear from equation 2.1 that it is not possible to obtain independent estimations for c_i and u_i by conductivity measurements alone. Hall effect measurements, which provide a means of separating c_i and u_i in electronic conductors, give voltages at the nanovolt level in ionic conductors [West, 1995].

The temperature dependence of the ionic conductivity of some solid electrolytes is presented in figure 2.1 where it is compared to the conductivity of concentrated sulfuric acid [Rickert, 1982]. Note that the transition to a conducting state may be abrupt, as in the case of α-AgI, or continuous, as in the case of $ZrO_2(Y_2O_3)$ [Khandkar, 1993].

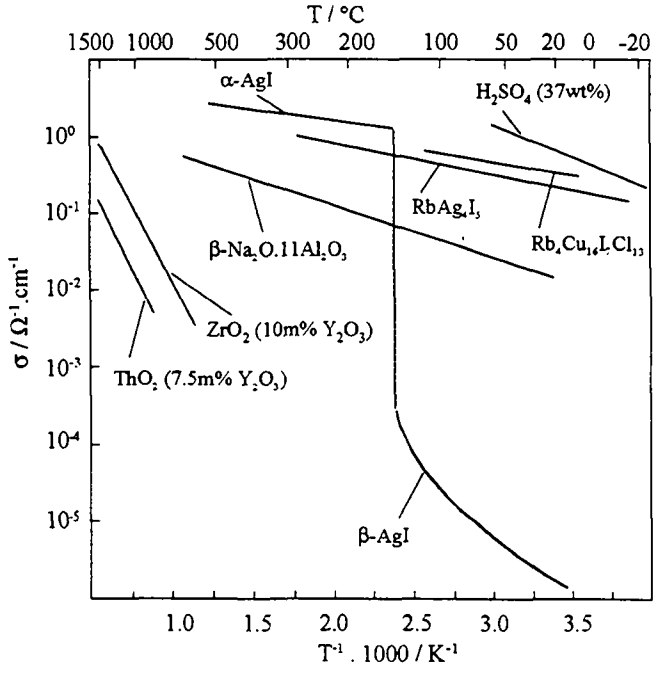

Fig. 2.1 Temperature dependence of the ionic conductivity of some solid electrolytes [Rickert, 1982]

Interfaces and boundaries strongly influence the mass transport, which is due to the chemical potential difference of the mobile species across the electrolyte. Dislocations, grain boundaries and free surfaces are potential pathways for fast diffusion, which can short-circuit diffusion through the lattice [Atkinson, 1989]. Ion blocking effects at grain boundaries are particularly important in the case of electrolytes with anisotropic conductivity [Weber, 1993]. They are mainly due to the introduction of impurities during the fabrication process, which tend to segregate at grain boundaries and at the external surface during processing. In stabilized zirconia, which has an isotropic conductivity, the influence of grain boundaries can be considerable below 700°C [Minh, 1993].

Basic research aims at establishing relationships between ionic transport and local atomic structure of the electrolyte. The structural and diffusional properties of simple systems can be quantitatively calculated with molecular-dynamics simulations. In the case of more complex systems however, the ionic hopping approach is more convenient [Dieterich, 1990].

Ionic conductors may also contain some electronic defects such as free electrons and electron holes. Therefore, they can exhibit some electronic conduction, especially at high temperatures, which is generally undesirable because it causes a reduction of the ion flux. Such a mixed conduction is always present at the interface electrode/electrolyte [Lohrengel, 1993; Wiemhofer, 1993]. The theoretical study of many processes is easier when the conduction is assumed to be purely ionic. Lin et al. [Lin, 1994] recently presented an interesting approach for the modelization of oxygen permeation mechanisms through solid electrolytes assuming mixed conduction.

Preparation methods

Various methods have been investigated for the preparation of solid electrolytes, because the morphology, density and the presence of impurities or defects greatly influence their electric and thermodynamic properties.

Strong, dense and impermeable sheets of stabilized zirconia, less than 0.03 cm thick, have been fabricated by tape-casting, extrusion, hot-rolling, etc. Such fine sheets are particularly important for the solid oxide fuel cell (SOFC) development in planar configuration. The electrochemical vapour deposition technique is more appropriate for the deposition of gas-tight electrolyte thin layers in the tubular SOFC geometry [Yamamoto, 1995].

Slightly porous calcia-stabilized zirconia can be formed by spray pyrolysis [Setoguchi, 1990]. Hot isostatic pressing densifies the sample without grain growth and improves the fracture strength and thermal shock resistance of the electrolyte [Sato, 1988].

An rf-sputtered YSZ film can be used at lower temperature compared with sintered bulk materials and seems promising for the realization of new devices in combination with integrated circuit technology [Miyahara, 1992].

Solid electrolyte applications

Solid electrolytes have found many applications during the last decades in batteries [Yamamoto, 1995], gas sensors [Wright, 1995; Baker, 1994; Miura, 1994; Sadaoka, 1992; Liaw, 1990; Burkhard, 1991; Kleitz, 1983; Mizusaki, 1983], fuel cells [Murphy, 1994; Sawata, 1990; Minh, 1993; Forbes, 1993; VanHerle, 1992; VanHerle, 1994; VanHerle, 1993], electrochromic devices [Monk, 1995], ceramic membranes for gas separation [Scholl, 1993], electrochemical and catalytic reactors [Michaels, 1986; Eng, 1991a; Eng, 1991b; Sammes, 1994; Chiang, 1992], electrochemical potential memory devices [Yamamoto, 1995]. Electrochromic devices, such as SMART windows, are electrochemical cells which can change their opacity by a small charge passage [Bruce, 1995]. Recently, a solar water-splitter was conceived as a reactor with two membranes, a solid electrolyte membrane for the oxygen-side and a membrane semipermeable to hydrogen for the other side [Scholl, 1993]. Gozzi et al. [Gozzi, 1988] studied metal corrosion at high temperature, based on the coupling of two electrochemical cells (an oxygen generator and an oxygen sensor), with YSZ as electrolyte. Belzner et al. [Belzner, 1990] measured the oxygen chemical diffusion coefficient in mixed conductors in a solid state electrochemical cell with an YSZ electrolyte acting simultaneously as a pump and a sensor for oxygen.

Solid electrolyte sensors have been developed for the detection of various gases, such as O_2, H_2, SO_2, CO_2, etc. The potentiometric sensor is based on the measurement of the chemical potential difference across the solid electrolyte. Such oxygen sensors using an YSZ electrolyte are among the most successful commercial sensors to date. In the analysis of exhaust gases from combustion engines, they are used to control the air/fuel ratio near the stoechiometric value. The amperometric sensor consists of a pumping and a sensing cell, and is based on the measurement of the charge passed through the pumping cell electrolyte. It can be used with both high and low air/fuel ratios [Yamamoto, 1995].

SOFCs are power generation devices which convert chemical to electrical energy without the intermediate of thermal energy, so their conversion efficiency is not subject to the Carnot limitation. Their operating principle is the following: oxygen is reduced at the porous cathode to oxide ions which migrate through the solid electrolyte to the anode where they react with the fuel (H_2, CO, hydrocarbons, etc.) to produce H_2O and/or CO_2. A good SOFC electrolyte has to meet the following requirements: high ionic and low electronic conductivity, chemical and physical stability under reducing and oxidizing atmospheres and a resistance contribution of less than 0.2 $\Omega \cdot cm^2$ at the operating temperature (>700°C) [Yamamoto, 1995].

In 1937, Bauer and Preis constructed the first SOFC using an YSZ electrolyte [Yamamoto, 1995], but several other ionic conductors have been tested since. The CeO_2 and Bi_2O_3 systems present a high ionic conductivity but they are not stable at low oxygen pressures because Ce^{4+} and Bi^{3+} ions are easily reduced. Presently, SOFCs of planar, monolithic and tubular geometries are under investigation. Most progress has been achieved with the Westinghouse tubular cell, with 25kW scale systems being tested [Yamamoto, 1995]. There is actually a great interest in SOFCs as a clean means of producing electricity and many studies are dedicated to the optimization of electrocatalysts to obtain the maximum power output [VanHerle, 1992; Suzuki, 1991].

A relatively new research field, related to the SOFCs, is the development of "chemical cogeneration" units, where electricity generation is coupled to the production of useful chemicals [Vayenas, 1992a].

Watanabe et al. [Watanabe, 1994] employed highly dispersed noble metal catalysts (Ru, Rh, Pt and Ir) on mixed conducting oxide particles (samaria-doped ceria) as the anode material and found that, in hydrogen, the anodic polarization resistance and its activation energy were greatly decreased. The use of mixed conducting oxide anodes results in an enlarged electrochemical reaction zone beyond the three-phase-boundary.

In this work, interest is particularly directed towards applications where electrochemical methods have been applied to study catalytic reactions. An important contribution is due to Wagner [Wagner, 1970], who proposed the use of a solid electrolyte electrochemical cell for the measurement of the activity of oxygen adsorbed on metal or metallic oxide catalysts. This technique, which was subsequently termed Solid Electrolyte Potentiometry (SEP), has been used in conjunction with kinetic measurements to study the mechanism of catalytic reactions [Vayenas, 1992a; Hildenbrand, 1990; Hildenbrand, 1989; Gellings, 1988].

The measurement of oxygen activity is based on the assumptions that the solid electrolyte is a pure oxygen ion conductor, no reactions other than oxygen transfer occur at the electrodes and that concentration gradients in the catalyst are absent [Vayenas, 1992a]. When equilibrium is established for the oxygen reaction in a divided cell:

$$O_2(a) + 4e^- = 2O^{2-} \qquad \text{or} \qquad 2O(a) + 4e^- = 2O^{2-}$$

then the open-circuit emf of the cell is given by:

$$V^\circ_{WR} = (1/4F)\,[\,\mu_{O2,W} - \mu_{O2,R}\,] \tag{2.4}$$

where $\mu_{O2,W}$ and $\mu_{O2,R}$ are the oxygen chemical potentials at the catalyst and reference electrodes, respectively. The oxygen activity a_o on the catalyst can be defined by the equation:

$$\mu_{O2,W} = \mu^\circ_{O2,(g)} + RT \ln a_o^2 \tag{2.5}$$

and the chemical potential of oxygen adsorbed on the reference electrode in air by:

$$\mu_{O2,R} = \mu^\circ_{O2,(g)} + RT \ln P_{O2(ref)} \tag{2.6}$$

where $\mu^\circ_{O2,(g)}$ is the standard chemical potential of gaseous oxygen at the temperature T. Finally, we obtain a form of the Nernst equation:

$$V^\circ_{WR} = (RT/4F) \ln [a_o^2 / P_{O2(ref)}] \tag{2.7}$$

Therefore, a_o^2 expresses the partial pressure of gaseous oxygen that would be in thermodynamic equilibrium with oxygen adsorbed on the catalyst surface, if such an equilibrium were established. If $a_o^2 = pO_2$, then the oxygen adsorption is not rate limiting, whereas if $a_o^2 < pO_2$, then oxygen adsorption is rate limiting [Vayenas, 1992a].

2.1.2 Yttria-Stabilized-Zirconia (YSZ)

Zirconium dioxide has a melting point of approximately 2700°C, depending on its preparation or origin, a good resistance to corrosion and is promising as a catalyst support since it presents a high thermal stability and both acidic and basic properties [Yamaguchi, 1994]. The relatively high thermal expansion of zirconia among refractory oxide ceramics makes it a prime candidate for high temperature applications where metal contact is required [Ownby, 1991]. Zirconia displays three polymorphic phases: a non-conducting monoclinic one at low temperatures, a tetragonal one that is stable between 1100 and 2400°C and a cubic one (Fm3m) at higher temperatures [Jacob, 1993; Strekalovskii, 1972].

Metastable tetragonal zirconia inclusions dispersed in a ceramic matrix improve its mechanical properties [Zschech, 1991]. The monoclinic and tetragonal phases are used as catalysts for various reactions such as CO and olefin hydrogenations, selective dehydration, etc. Recently, zirconia was also found to exhibit a pronounced activity for the photocatalytic total decomposition of water [Yamaguchi, 1994].

Takeuchi et al. [Takeuchi, 1995] created oxygen vacancies on an ordered ZrO_2 surface, through argon ion bombardment. While water adsorbs readily at low temperatures on the unsputtered surface and desorbs upon heating, on the sputtered surface it partially dissociates producing hydrogen and supplying oxygen atoms to the lattice of the defective oxide film.

In the face-centered cubic structure (Fig. 2.2), the anions occupy the tetraedral sites of the zirconia lattice (fluorite type). Each metal cation is surrounded by eight oxygen anions and each oxygen anion is tetraedrally coordinated with four metal cations. This is a rather open arrangement, with a large number of octaedral interstitial voids and it is suitable for fast oxygen ion diffusion at high temperature [Ferloni, 1994]. Doping of the zirconia with divalent or trivalent ions stabilizes the cubic structure down to ambient temperature and creates oxygen vacancies by charge compensation according to the following equation (written in Kröger-Vink notation for yttria doping):

$$Y_2O_3 \xrightarrow{ZrO_2} 2Y'_{Zr} + V_{\ddot{o}} + 3O_{O^x}$$

The incorporation of oxygen from the gas phase into the vacancies is described by two equations:

$$\frac{1}{2}O_2\,(g) + V_{\ddot{o}} = O_{O^x} + 2h^{\cdot} \qquad \text{and}$$

$$\frac{1}{2}O_2\,(g) + V_{\ddot{o}} + 2e' = O_{O^x}$$

The corresponding laws of mass action are given by

$$P_{O_2}^{1/2}\,[V_{\ddot{o}}]\,c_{h^{\cdot}}^{-2} = K_1 \qquad \text{and}$$

$$P_{O_2}^{1/2}\,[V_{\ddot{o}}]\,c_{e'}^{2} = K_2$$

The concentration of the oxygen vacancies is essentially fixed by the dopant concentration, while the concentrations of electrons and holes obey the following relations [Rickert, 1982; VanHassel, 1992b]:

$$c_{h^{\cdot}} = 1.72 \cdot 10^{21} \exp\left(-\frac{60\,\text{kJ/mol}}{RT}\right) P_{O_2}^{1/4} \qquad \text{and}$$

$$c_{e'} = 1.04 \cdot 10^{32} \exp\left(-\frac{192\ \text{kJ/mol}}{RT}\right) P_{O_2}{}^{-1/4}$$

In the lattice, the oxygen vacancies may be surrounded by two Y^{3+} and two Zr^{4+} ions (neutral vacancy), or by three Zr^{4+} and one Y^{3+} (single-charged vacancy), or by four Zr^{4+} ions (double-charged vacancy) [Azzoni, 1991].

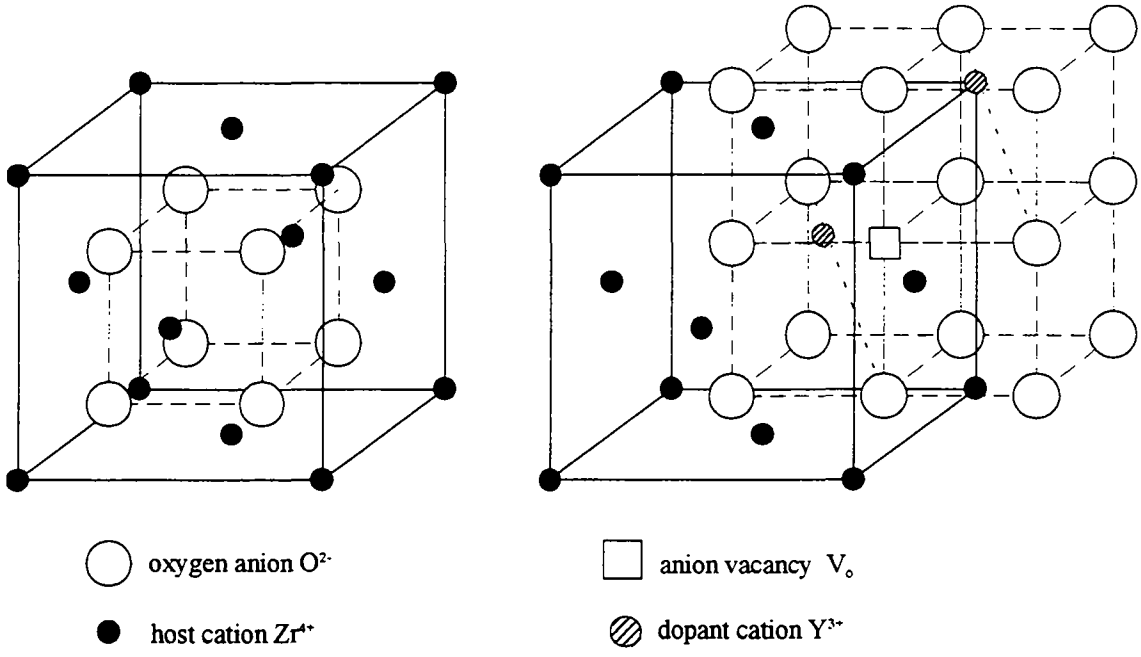

Fig. 2.2 The face-centered cubic structure of the zirconia lattice

In the temperature range from 200 to 500°C, the thermal diffusivity of YSZ (5-7% mol) single crystals is approximately $8 \cdot 10^{-7}$ m^2/s [Youngblood, 1988].

Nernst observed oxide ion conductivity in ZrO_2 - 9% mol Y_2O_3 as early as 1899 [Yamamoto, 1995]. He described how yttria-doped-zirconia would emit a bright white light on the passage of a current at high temperature [Bruce, 1995]. If cubic YSZ (8% mol) alloys are rapidly cooled (in less than 10 s) from high temperature (1200°C) to room temperature, the cubic phase is not affected. The same treatment, applied on YSZ (3-7% mol) alloys, is accompanied by a cubic-to-tetragonal transition [Sakuma, 1988].

The variation of the ionic conductivity of stabilized zirconia with dopant concentration is shown in figure 2.3 [Minh, 1993]. The conductivity is maximal for a 9% mol Y_2O_3 concentration at 1000°C and decreases at higher dopant concentration possibly because of defect association or electrostatic interaction [Choudhary, 1980]. This conductivity maximum is close to the stability limit of the cubic phase and shifts to 8% mol Y_2O_3 at 800°C, and 7.5% mol at 600°C ($3.3 \cdot 10^{-3}$ $Ohm^{-1}cm^{-1}$) [Takahashi, 1967]. Orliukas et al. [Orliukas, 1991] attribute the decrease in conductivity by increasing Y_2O_3 doping to reduced vacancy mobilities and not to the formation of immobile vacancy associates. They proved that the higher activation energy of the total conductivity at low temperature is due to grain boundary effects.

Takahashi et Suzuki [Takahashi, 1967] studied the time dependence of the stabilized zirconia electrical conductivity. They attributed the resistivity increase on prolonged heating to the ordering of oxygen ion vacancies or to the separation of a tetragonal phase from the cubic structure.

The ionic conductivity of YSZ (9% mol) at 400°C ($1.8 \cdot 10^{-4}$ Ohm^{-1} cm^{-1}) is too low for fuel cell constructions, but is sufficient for "Non-faradaic Electrochemical Modification of Catalytic Activity" (NEMCA) applications [Vayenas, 1992a].

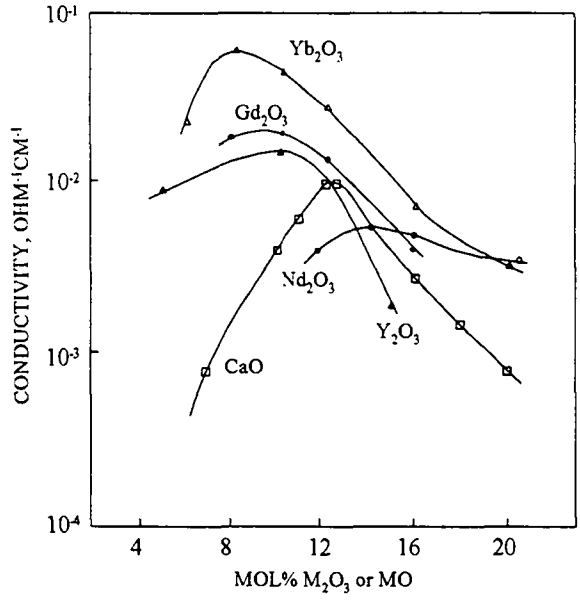

Fig. 2.3 The ionic conductivity of stabilized zirconia as a function of dopant concentration at 807°C [Minh, 1993]

Over a wide range of temperature, the conductivity of stabilized zirconia is independent of oxygen partial pressure and can be considered purely ionic as the ionic transport number is close to unity. Electronic conductivity becomes significant only at extremely low (n-type) or high (p-type) oxygen partial pressures [Ramanarayanan, 1991]. The transition from p- to n-type conductivity occurs at an oxygen partial pressure of 10^{-10} atm at 900°C and shifts to lower partial pressures as temperature decreases. This is due to the lower activation energy of the conductivity of the holes compared to the electrons. At 700°C, in YSZ (10% mol), the electronic conductivity is about 10^{-7} Ohm^{-1} cm^{-1} at an oxygen partial pressure of 0.2 atm. In comparison, at the same temperature, the ionic conductivity is about 10^{-3} Ohm^{-1} cm^{-1} [Weppner, 1977a]. The surface conductance has a different oxygen partial pressure dependence from the bulk conductance [Bae, 1992].

At very low partial pressures, localized states near the conduction band are partially occupied. These states are responsible for the observable electronic conductivity under reducing conditions. Some authors assume excess electrons to be localized on oxygen vacancies whereas others suggest Zr^{3+} -states in the lattice [Wiemhoefer, 1992]. At intermediate oxygen pressures, electronic conductivity can be enhanced by doping the stabilized zirconia with a multivalent cation. The addition of metallic oxides into YSZ (10%

mol) promotes the cubic structure stabilization but results in a conductivity decrease. The conductivity remains ionic with a content of CoO and NiO up to 30%, Fe_2O_3 up to 10% and Mn_3O_4 up to 5%, while mixed conduction sets in with higher amounts of oxides [Neuimin, 1972].

Large current passage often provokes a partial decomposition of the electrolyte ("current blackening") which leads to a decrease in the cell potential at steady current. The large current effect is more pronounced at lower temperatures and for thicker electrolytes, the electrolyte resistance being higher [Badwal, 1990]. Weppner [Weppner, 1977a] measured a decomposition voltage of 2.23 V relative to air at 900°C.

When stabilized zirconia is exposed to reducing atmospheres or to high electrical currents it becomes coloured and its electronic conduction is enhanced [Orera, 1991; Ben-Michael, 1991]. Orera et al. investigated the local structure of the defects in undoped [Orera, 1990] and ceria-doped [Orera, 1994] stabilized zirconia, in order to explain this coloration. Although the overall crystal is neutral, oxygen vacancies and yttrium ions produce locally charged regions which can be good traps for electrons or holes. Upon reduction of the sample, the characteristics of Electron Paramagnetic Resonance (EPR) signals indicate that the unpaired electrons occupy a cation d^1 orbital rather than a 1s vacancy level. The authors ruled out causes such as the presence of impurities, F centers (electrons trapped in oxygen vacancies), or defect aggregates and believe that coloration is due to electrons trapped at sixfold- and sevenfold-coordinated Zr^{3+} ions. The concentration of such Zr^{3+} defects is estimated at 0.1% approximately. During the reoxidation step, the colour front is visible and proceeds from the sample edges towards its center. On the contrary, reduction occurs uniformly and the front is not clear [Orera, 1990].

Nguyen et al. [Nguyen, 1986a] blackened electrically a scandia-stabilized-zirconia disk by applying 1A current (about 3V voltage) under Ar flow at 850°C for half an hour. The XPS analysis of the blackened specimen give quantitative evidence of the presence of the suboxide (ZrO_{2-x}), with $x<0.1$. This electrolyte reduction leads to a three orders of magnitude increase in the cathodic and anodic current density at a given overpotential, whether Pt or Au were used to form the porous electrodes. The current-overpotential behaviour during the electro-oxidation of several different fuels was also similar with Au and Pt electrodes. The authors believe that the major electrochemical steps occur at active sites on the electrolyte surface rather than on the metal electrodes.

The electrolyte reduction phenomenon at high cathodic overpotentials has also been observed on doped ceria whether Pt or Au cathodes were used [Wang, 1980]. The limiting current behaviour at lower overpotentials is the same as in the case of a zirconia electrolyte and is also believed to be due to the slow oxygen adatoms supply at the cathode. Ionic current flows predominantly near the three phase boundary (TPB) and the central area under the gold electrode becomes blocking with the possibility for electron injection directly into the electrolyte. The difficulty in diffusing along the interface should be minimized for electrodes with a poor adherence, where there is no strong chemical bonding between the electrode and the electrolyte [Wang, 1981].

2.1.3 Electrocatalysis with solid electrolytes at high temperature

Solid state electrochemistry is an interdisciplinary area related to chemistry, crystallography, solid state physics and materials science. Although the ionic conduction in solid phases was experimentally evidenced at the end of the last century, the fundamental and applied research in this field remained scarce for many decades. After Faraday's pioneering work, solid and liquid electrochemistry grew apart and developed separately for a long period of time. The theoretical treatment of electrochemical processes has been mainly based on the solid-liquid interface and especially in aqueous solutions. The first books dedicated exclusively to solid state electrochemistry have only been published recently [Deportes, 1994; Bruce, 1995].

The term electrocatalysis was not introduced into the language of the electrochemical community earlier than 1963 and is principally related to the fuel cell development and the revolution in the chloralkali industry by the dimensionally stable anodes (DSA) introduction. Electrocatalysis means the catalytic enhancement of electrochemical reaction rates which is manifested in reduced overpotentials [Wendt, 1994]. It is due to the catalytic acceleration of the slow chemical rather than the relatively fast charge-transfer steps, which together constitute an electrochemical reaction. The broad meaning of the term electrocatalysis is defined by Trasatti [Trasatti, 1991] as "the dependence of the electrode reaction rate on the nature of the electrode material".

At high temperature, the reaction rates are faster, and this is particularly important for the oxygen electrochemistry which has relatively high activation energies. Therefore, the choice of electrode materials is predominantly based on their thermal stability rather than on their activity.

2.1.3.1 Electrode thermodynamics and kinetics

The fundamental concepts of electrochemistry will briefly be overviewed as applied in the context of solid electrolytes, namely the electrochemical interface and the overpotential. The definition of the various potentials will also be recalled.

The Volta or outer potential ψ is defined so that $e\psi$ is the work done in bringing an electron from "infinity" (vacuum) to a point just outside the electrode, where the image forces are negligible (typically less than 1μm from the surface). The subsequent work done in taking the electron through the charged surface inside the material phase defines the surface potential χ. The surface potential is structure sensitive and varies from face to face of a single crystal [Gundry, 1968]. The Galvani or inner potential ϕ is the sum of the outer ψ and surface χ potentials:

$$\phi = \psi + \chi \qquad (2.8)$$

It is defined so that $e\phi$ is the energy required to bring an electron from "infinity" to a point inside the electrode, without taking into account the interactions with other particles of the material phase. These interactions define the chemical potential μ of the electron. The electrochemical potential $\bar{\mu}$ is the sum of the inner and the chemical potentials:

$$\bar{\mu} = \mu + (-e)\,\phi \qquad (2.9)$$

It is identical to the Fermi level E_F which represents the mean energy of the electrons participating to the conduction. In a metallic conductor, E_F lies at the highest occupied energy level of the uncompletely filled band. It should not be confused with the Fermi energy [μ] which is the energy difference between the bottom of the conduction band and the Fermi level, and provides a measure of the average kinetic energy of the electrons at the Fermi level [Vayenas, 1992a].

The work function $e\Phi$ of a metal (where Φ is the electron extraction potential) is the energy required to take an electron from the Fermi level of the electrode to a point just out of reach of the image forces from the electrode. It is the equivalent for ionization potential of an atom, but a smaller quantity, because the resulting positive charge is better screened in a metal. It increases when moving from left to right in the periodic table [Nieuwenhuys, 1993]. Although the Fermi level E_F is spatially uniform, this is not the case for $e\Phi$ which depends on the surface structure and crystallographic planes. The various potentials are schematically presented in figure 2.4.

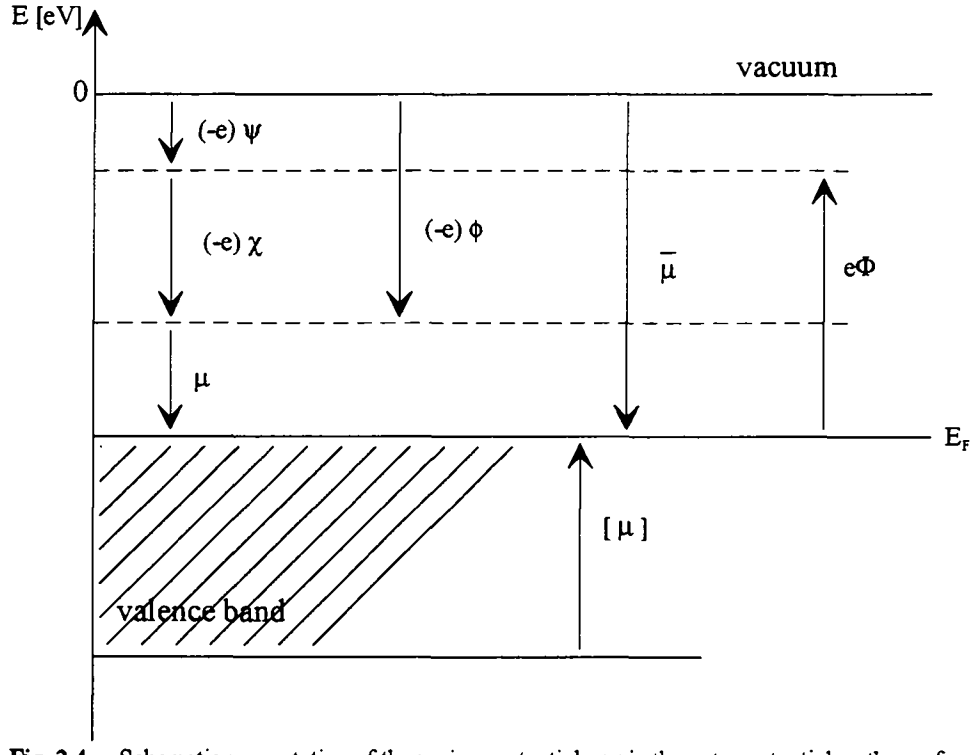

Fig. 2.4 Schematic presentation of the various potentials: ψ is the outer potential, χ the surface potential, ϕ the inner potential, μ the chemical potential, $\bar{\mu}$ the electrochemical potential, Φ the electron extraction potential, and E_F the Fermi level (for an electronic conductor)

In the bulk of a material, at equilibrium, the forces operating on charged particles are isotropic and electroneutrality prevails. Near the phase surface however, these forces become anisotropic and, as a consequence, the surface always carries an excess charge. In reality, every phase surface is a phase boundary or interface, since it is in intimate contact with another phase. So, in the absence of an external electric field, both sides of an interface are charged, although the interphase region as a whole is electrically neutral.

An interface formed by two phases is the apparent two-dimensional surface of contact of these phases. It is an apparent surface because, in reality, there is a region where occurs the continuous transition from the properties of one phase to the properties of the other. The term interphase is more appropriate for this three-dimensional transition region [Bockris, 1970].

The term electrochemical double layer is a near-synonym for electrified interface and describes the arrangement of charges constituting the interphase region at the boundary of an electrolyte. The electrical and structural aspects of the double layer are intimately related. Several models have been proposed for the double layer structure at a metal-solution interface. The theories of Gouy-Chapman and Stern involve the existence of a diffuse layer of charge in the fluid phase. The Helmholtz model is simple and implies that any excess charge, whether on the metal or in the solution, resides at the surface. This structure is equivalent to a parallel-plate capacitor with a differential capacitance given by

$$C_d = \varepsilon \varepsilon_o / d$$

where ε is the dielectric constant of the medium, ε_o is the permittivity of free space, and d is the interplate spacing [Bard, 1980; BarlowJr., 1970].

The double layer at the interface with a solid ionic conductor can be simply described based on the assumption that the partial free enthalpy of formation of the anionic and the cationic defects is different [Deportes, 1994]. This model implies that the double layer is a specific property of the material. The mean thickness of the layer is called Debye length L_D and is given by the relation:

$$L_D = \sqrt{\frac{\varepsilon k T}{4\pi e^2 \sum_i z_i^2 c_i}}$$

where c_i is the concentration of the mobile charge carriers in the bulk and z_i is the charge of the carriers [Deportes, 1994].

Another description of the solid-solid interface is due to Blakely [Deportes, 1994] and consists in distributing the mobile ions over all the accessible sites, excluding the simultaneous presence of two ions on the same site.

A simple equivalent electrical circuit for an electrified interface is a capacitor and resistor connected in parallel (Fig. 2.5). Upon applying a potential difference, if the resistance to charge-transfer is very high, the capacitor charges up; this is the behaviour of a polarizable interface (Fig. 2.5a). If the resistance is very low, the capacitor cannot be charged due to the charge leakage through the low resistance path; this is the behaviour of a nonpolarizable interface (Fig. 2.5b). Note that the resistance to transfer is not really an ohmic one, because its value generally depends on the applied potential.

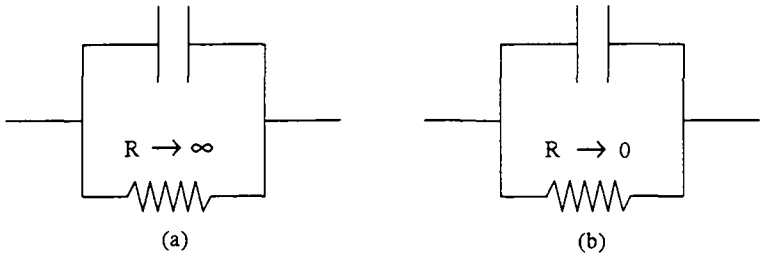

Fig. 2.5 Equivalent circuit for an electrified interface (a) ideally polarizable and (b) nonpolarizable.

An electrochemical cell is composed of at least two interfaces. Consider a triple contact between two solid phases and a gas, as in the case of an oxygen electrode: O_2 (g) / IrO_2 / YSZ

Since the oxygen reaction needs the contribution of species in the three distinct phases gas, electronic conductor and solid electrolyte, in theory it can only take place at the TPB. In practice, however, it occurs in a certain volume at the proximity of the TPB. Note that, unlike in aqueous solutions, the gas is generally insoluble in the gas tight solid electrolyte membrane. The triple contact can be treated as the sum of double contacts (junctions) in series or in parallel. For an ideally dense electrode, the TPB is limited to the periphery of the electrode (Fig. 2.6a). For a porous electrode, the TPB length is much higher (Fig. 2.6b).

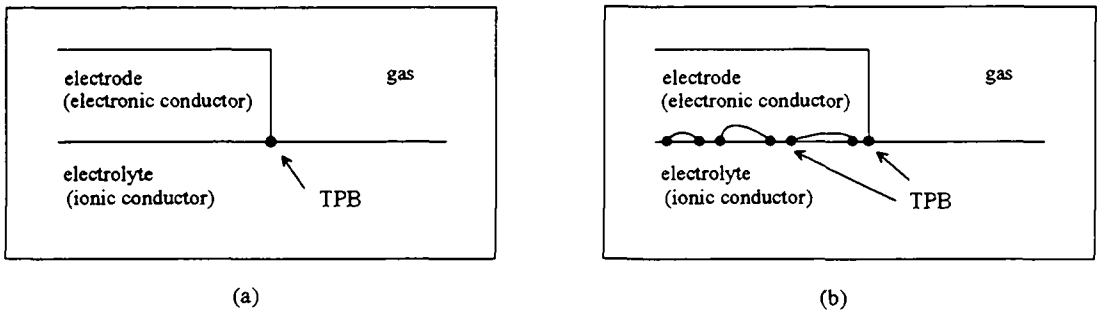

Fig. 2.6 Schematic representation of the TPB in a gas / electrode / electrolyte half cell (a) for dense electrodes and (b) for porous electrodes

A specific feature of solid state electrochemistry is the fact that it is very difficult to obtain a well-defined and reproducible contact area between the electrode and the solid electrolyte. In addition, the current passage may provoke a variation of the contact area due to the electrode dissolution or growth and even lead to the contact rupture. The double-layer capacity can be used as a measure of the electrode-electrolyte contact area [Kenjo, 1990].

Electrode impedance measurements are currently used for the elucidation of electrochemical reaction mechanisms [Pilla, 1967; Velle, 1991; Nakagawa, 1992; Moghadam, 1986; Wang, 1979b]. However, D.C. polarization curves can also be of great interest [Isaacs, 1982; Mizusaki, 1994; Wang, 1979a]. The presence of inflections or hysteresis in the curves demonstrate that there is more than one distinct process controlling the electrochemical reaction rates. The current response to a potential step is the sum of the capacitive current produced by the charging of the double layer at the electrode-electrolyte interface and the faradaic current due to one or more charge-transfer reactions.

The electrode overpotential η can be regarded as the potential difference which is needed to compensate the sum of the voltage drops through the electrochemical interface. When a reaction takes place at the interface between the electronically and ionically conducting medium, the rate may be limited by the charge-transfer process (activation overpotential) or the mass-transfer process (concentration overpotential). Although the overpotential is usually associated with electrode-electrolyte interfaces, it refers to the deviation of the electrode potential only [Vayenas, 1992a].

The overpotential is generally composed of three terms:

$$\eta = \eta_{activation} + \eta_{concentration} + \eta_{ohmic}$$

When mass transfer limitations are excluded, the rate of charge transfer for a given electrochemical reaction varies exponentially with the overpotential η, according to the generalized Butler-Volmer equation:

$$I = I_o \left[\exp\left(\frac{\alpha_a \, nF \, \eta}{RT} \right) - \exp\left(\frac{-\alpha_c \, nF \, \eta}{RT} \right) \right] \qquad (2.10)$$

where α_a and α_c represent the anodic and cathodic charge-transfer coefficients respectively, and n is the number of electrons implied in the charge-transfer reaction.

The exchange current I_o expresses the rates of the forward and reverse electrocatalytic reaction when no net current flows in the cell [Vayenas, 1992a].

For $|\eta| > 100$mV, the Butler-Volmer equation reduces to the "high field approximation", or Tafel relation, for anodic and cathodic operation, respectively:

$$\ln (I / I_o) = \alpha_a n F \eta / RT$$

$$\ln (-I / I_o) = -\alpha_c n F \eta / RT \qquad (2.11)$$

For $|\eta| < 30$mV, the "low-field approximation" is valid:

$$I / I_o = (\alpha_a + \alpha_c) F \eta / RT \qquad (2.12)$$

The concentration overpotential is due to the slow supply of reactants at the reaction sites and can be estimated in terms of the limiting current I_L which is the highest current obtained when the reaction is completely mass-transfer controlled.

2.1.3.2 The oxygen reaction

There are relatively few electrode reactions investigated in the field of solid electrolytes at high temperature. The major part of the studies aim to elucidate the kinetics and mechanism of reactions related to the development of zirconia sensors and SOFCs. These reactions include CO oxidation or CO_2 reduction [Mizusaki, 1992; Copcutt, 1992; Etsell, 1971; Kleitz, 1967a] and H_2 oxidation or H_2O reduction [Schouler, 1987; Mizusaki, 1994; Kleitz, 1967a].

The oxygen reaction on stabilized zirconia supported electrodes is certainly the most studied reaction in the solid electrolyte field at high temperature, because a good comprehension of its mechanism is fundamental for the SOFC and oxygen sensors development. Most studies have been conducted on platinum electrodes supported on YSZ, but there still is considerable disagreement on the reaction

mechanism. Among the reaction pathways and the rate-determining-steps (RDS) proposed, some will be discussed in greater detail because they seem valid in the case of an IrO_2 electrode too.

The overall reaction of oxygen exchange between the gas phase and the solid electrolyte can be expressed in Kröger-Vink notation as:

$$O_2\,(g) + 2\,V_{\ddot{o}} + 4e' = 2\,O_o^x$$

where V_o is a vacancy at a normal oxygen site in the lattice and O_o^x is a mobile oxygen anion.
It is generally considered to consist of an adsorption step followed by the charge transfer process:

$$O_2\,(g) + 2\,V_{ad} = 2\,O_{ad}$$

$$2\,(O_{ad} + 2\,e' + V_{\ddot{o}}) = 2\,(O_o^x + V_{ad})$$

Depending on the electrode and electrolyte material, oxygen partial pressure, temperature, overpotential etc., this reaction can take place via various pathways, some of which are schematically depicted in figure 2.7.

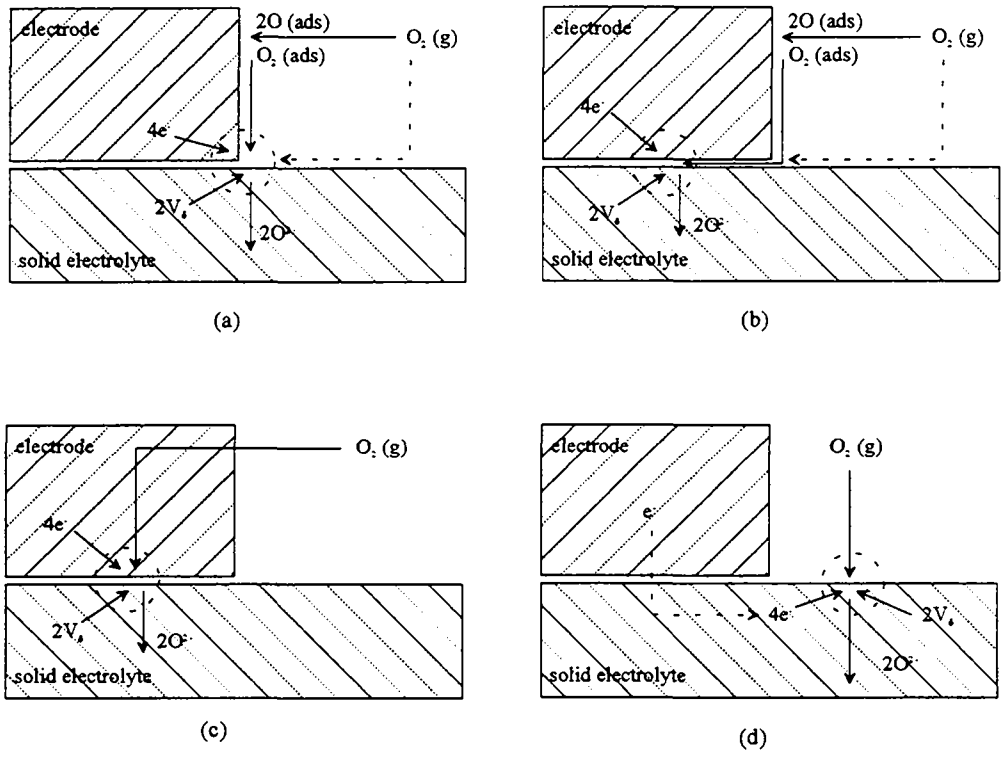

Fig. 2.7 *Possible pathways for the oxygen exchange reaction:* (a) adsorption (dissociative or not) on the electrode, eventually on the electrolyte and surface diffusion to the reaction sites on the TPB, (b) adsorption and diffusion to the reaction sites on the electrode-electrolyte interface, (c) dissolution in the electrode and bulk diffusion to the interface, and (d) adsorption and reaction on the electrolyte

Proposed RDS include internal diffusion of oxygen in the electrode pores, adsorption and/or dissociation of oxygen on the electrode and/or the electrolyte, surface diffusion of oxygen to the electrochemical reaction sites, bulk diffusion of oxygen through the electrode or the electrolyte and charge transfer reaction. Some of the differences in the proposed mechanisms can be attributed to variations in the

electrode morphology or the temperature range covered in the study. As far as electrochemical measurements are concerned, many results cannot be compared because of important variations in the disposition of the electrodes (working, counter and reference electrodes). The influence of many factors on the electrode impedance and polarization phenomena is still unclear. These factors include the thickness, preparation procedure, thermal or electrochemical treatment of the electrodes, as well as the composition, thickness and surface treatment of the electrolyte.

The different kinetic models can be separated in two groups depending on the location of the electrochemical reaction sites. In the first group, the electrochemical reaction is assumed to proceed at the TPB [Okamoto, 1983; Moghadam, 1986], i.e. the region where the electrode, electrolyte and gas phase meet. In the second group, the reaction sites are located at the electrode-electrolyte interface [Wang, 1981; Kenjo, 1990]. In all these models, the electrode acts as the electron donor or acceptor.

A special case is often reported at high voltages (> 2V relative to air), where the oxygen reaction is supposed to take place over the free solid electrolyte surface, with the electrolyte assuming the role of electron donor or acceptor [Yanagida, 1970; Brook, 1971; Nguyen, 1986a].

Most models include oxygen dissociative adsorption and diffusion to the electrochemical reaction sites. Over a wide range of oxygen partial pressure P_{O2} and temperature, the oxygen reaction rate over a Pt electrode is limited by diffusion of atomic oxygen over the electrode surface to the TPB, at high overvoltages, where anodic and cathodic limiting currents are observed [Robertson, 1990; Moghadam, 1986]. This atomic oxygen diffusion limitation has also been reported for low overvoltages, near the equilibrium potential [Kuzin, 1990]. Mizusaki et al. [Mizusaki, 1987] agree that diffusion is the RDS above 600°C, but argue that dissociative oxygen adsorption is limiting at temperatures below 500°C. On the other hand, Gür et al. [Gür, 1980] propose the diffusion of molecular oxygen in the gas phase through a boundary layer near the interface as the RDS at high overvoltages.

Pizzini et al. [Pizzini, 1973] suggest that on porous Pt electrodes and at temperatures greater than 650-700°C, the RDS is the desorption of strongly chemisorbed oxygen, with water vapour acting as a poison. At lower temperatures, they agree with a limitation by oxygen surface diffusion. The same RDS is reported by Yanagida et al. [Yanagida, 1970] for voltages up to 2V, on calcia-stabilized-zirconia (CSZ) supported Pt electrodes, at 560°C. At higher voltages, however, these authors believe that the reaction takes place over the solid electrolyte surface.

A square root dependence of the cathodic limiting current is accounted for by assuming atomic oxygen as the partner in the RDS [Pizzini, 1973]. On the other hand, Etsell and Flengas [Etsell, 1971] propose the diffusion of molecular oxygen in the pores of a Pt electrode to explain the linear dependence of the cathodic limiting currents on the oxygen partial pressure.

The reaction control by bulk diffusion of atomic oxygen through the electrode has been reported for Pt [Brook, 1971], but mainly for Ag electrodes [Moghadam, 1986].

At low overvoltages and current densities, charge transfer may also be the RDS [Winnubst, 1984]. The charge transfer resistance is known to decrease with increasing temperature [Velle, 1991]. Note that the

relative contribution of the charge transfer and diffusion processes to the overall interface resistance strongly depend on the microstructure of the electrode [Inoue, 1993].

Wang [Wang, 1990] proposes a general model for the electrode reaction at the surface of oxide conductors, which combines charge transfer mechanism and current-limiting steps. According to this model, the electrode polarization can be negligible, ohmic, Tafel sloped, or current limiting, depending on the individual situation.

The comparison of various electrode materials as oxygen catalytic electrodes at 1000°C in air showed a correlation between the heat of adsorption and the electrocatalytic activity [Isaacs, 1982]. Rhodium has the highest initial heat of adsorption and highest electrode kinetics among the noble metals, followed by Pd and Pt and finally Au. The use of mixed electronic-ionic conductors as electrodes, typically lanthanide perovskites, improves the electrode kinetics by "delocalizing" the triple contact [Schouler, 1987].

The electrode conductance σ_e is defined by

$$\sigma_e = \lim_{i \to 0} di/d\eta$$

It reflects the electrode activity and depends on the TPB length [Copcutt, 1992]. It is related to the exchange current density i_o by the equation

$$\sigma_e = i_o \, n \, F / RT$$

where n is the number of electrons involved in the rate-determining reaction [Mizusaki, 1994]. In a wide range of oxygen/inert gas mixtures, Kuzin and Komarov [Kuzin, 1990] found that the conductance is proportional to the square root of the oxygen partial pressure, while Mizusaki et al. [Mizusaki, 1987] observed a conductance maximum for a 50% surface coverage by atomic oxygen. Yanagida et al. [Yanagida, 1970] agree that the conductance varies as $P_{O2}^{1/2}$ as long as $P_{O2} >> P_{H2O}$, but they found a weaker P_{O2} dependence when H_2O is the main oxygen-containing species.

The exchange current density can give valuable information on adsorption states on the electrodes. In an oxygen concentration cell with Pt electrodes, i_o has a maximum at a specific oxygen partial pressure, which increases with temperature [Okamoto, 1983].

2.1.3.3 The gold electrode

The choice of the gold metal as a counter electrode in our electrochemical cell is based on the fact that gold is an excellent electronic conductor and has a very low catalytic activity [Goffe, 1981; Hayakawa, 1994]. The inert character of gold and its limited affinity for gas adsorption is due to the completely filled 5d electron shell [Schwank, 1983]. In addition, it is frequently cited in the literature as a poor electrocatalyst in comparison with platinum or iridium oxide [Srinivasan, 1967; Wendt, 1994].

Hayakawa et al. [Hayakawa, 1994] studied the ethane and ethylene oxidation over an Au // YSZ anode, at 475°C. Under open-circuit conditions, no oxidation occurs in presence of gaseous oxygen. The reaction proceeds only by the "active oxygen species" generated electrochemically. The ethylene oxidation produces CO together with acetaldehyde and CO_2. In another study, the electrocatalytic oxidation of hydrocarbons at 700°C, over a gold electrode supported on scandia-stabilized-zirconia is supposed to occur

primarily on the solid electrolyte [Goffe, 1981].

Norby et al. [Norby, 1993] found the Au // YSZ electrode to be a slower anode for oxygen pumping than the Au + $SrFeO_{3-\delta}$ // YSZ anode, but a better catalyst for the methane oxidation. Using co-fed oxygen gas $^{18}O_2$ as well as electrochemically supplied oxygen, they proved that the methane oxidation occurs on the Au // YSZ catalyst via adsorbed oxygen, not lattice oxygen [Norby, 1995].

Mar'ina et al. [Mar'ina, 1992] also found that the Au // YSZ catalyst is quite active for the methane oxidation at 700°C under open-circuit conditions. The catalyst anodic polarization has almost no effect on the rate while the cathodic polarization induces some enhancement. This rate enhancement is explained by the direct electrochemical oxidation of methane [Mar'ina, 1993] and might be connected to the presence of oxygen species such as O_2^-(ads) and O^-(ads).

Gold is considerably active for the oxidative dehydrogenation of alcohols and quite selective because the weak oxygen adsorption inhibits the complete oxidation [Wachs, 1983]. The gold catalytic activity can be enhanced by a synergistic effect, when highly dispersed gold nanoparticles are deposited on reducible metal oxides. So, the high activity for low temperature CO oxidation would be due to the gold-metal oxide interfacial perimeter, which provides the oxygen adsorption sites [Haruta, 1993].

The studies in aqueous electrochemistry present many similarities with the ones at high temperature solid state electrochemistry. The anodic oxidation of ethylene in 1.5M sulfuric acid at a gold-coated platinum electrode is reported to produce CO_2, acetone, acetaldehyde and propionaldehyde [Hartley, 1970]. At 80°C, the faradaic efficiency is only 20% for the conversion to CO_2 at 0.79V (vs NHE). The rate-determining step involves the adsorbed C_2H_4 species and the reaction becomes diffusion-controlled at a limiting current density of approximately 1mA/cm^2 [Hartley, 1970].

Oxygen adsorption

Although it is well known that gold does not form a thermodynamically stable bulk oxide [Schrader, 1977] nor does it chemisorb oxygen at room temperature [Wang, 1981], literature is still controversial as to the adsorption behaviour at high temperature.

Schrader [Schrader, 1977] observed oxygen chemisorption on the Au (111) surface in the temperature range 100°C to 600°C and proposes an adsorption mechanism which involves an initial dissociative chemisorption on some surface active sites, followed by migration of oxygen atoms to less active sites. Légaré et al. [Légaré, 1980] did not notice any significant adsorption on decontaminated gold surfaces below 300°C. They found that the presence of impurities such as calcium promotes the oxygen adsorption. Chesters and Somorjai [Chesters, 1975] report that the oxygen dissociative adsorption occurs only above 500°C, with formation of a surface oxide, which can also be produced by treatment in water vapour. The stability to high temperature of this oxide is explained by the changing valency of the gold surface atoms, which provides a higher heat of formation than in the case of the bulk oxide. As far as ethylene is concerned, no adsorption takes place below 550°C at low pressures (approximately 10^{-9} atm) [Chesters, 1975].

On the other hand, Canning et al. [Canning, 1984] attribute this oxide on gold to the undetected presence of silicon, which diffuses out of the bulk and reacts with oxygen on heating. They did not detect any oxygen adsorption up to 600K. Chemisorption of oxygen atoms could however be induced, by placing a platinum filament near the gold surface for oxygen dissociation to occur.

Oxygen reaction

Generally, the current-overpotential curves of the Au // YSZ system are not symmetrical [Nguyen, 1986b; VanHassel, 1992a; Boukamp, 1993]. During anodic polarization, when oxide anions are oxidized to oxygen atoms, the current is higher than during cathodic polarization. This indicates that gold is a much better anode than cathode for this reaction. Since oxidation seems to occur readily enough on gold and since we principally used the counter electrode as a cathode in our study (oxygen pumping to the working electrode), we will focus on the oxygen reduction at the Au // YSZ cathode:

$$O_2\,(g) + 4e^-\,(electrode) + 2\,V_{\ddot{o}}\,(YSZ) \longrightarrow 2\,O_o^x\,(YSZ)$$

Nguyen et al. [Nguyen, 1986b] propose that the electrochemical reaction sites for the oxygen reduction on a porous Au // YSZ (10mol%) electrode are located in the two-phase region between the metal electrode and the solid electrolyte and that molecular oxygen adsorbs on the electrolyte rather than on gold. At low to moderate overpotentials, the current-overpotential curves indicate a rate limitation by one or more slow electrochemical steps. At high overpotentials however, they believe that surface diffusion of oxygen through the two-dimensional Au - YSZ interface is the RDS. A concentration gradient of the electrochemically active species may then be created along the two-phase region [Nguyen, 1986b]. The exchange current density for the charge transfer process is proportional to the oxygen partial pressure as $I_o \propto P_{O2}^{1/4}$ which changes into $I_o \propto P_{O2}^{5/8}$ when there is competition with mass transport along the Au - YSZ interface [VanHassel, 1991].

Boukamp et al. [Boukamp, 1993] believe that the oxygen adsorption is dissociative and gives rise to two different adsorbed oxygen species O_{ad} and O^-_{ad}. The surface modification of the solid electrolyte by Fe-implantation does not change the type of electrode reaction, but provides some mixed conductivity in a thin surface layer and increases the exchange current density by a factor of 50 [Boukamp, 1993]. An increased surface oxygen exchange rate is also observed for the Fe-YSZ sample in ^{18}O isotope exchange experiments. It can be interpreted as an increase in concentration of reaction sites, which would lead to an enhancement of the electrode reaction rate [VanHassel, 1992a].

On the Au // YSZ system, van Herle et al. [VanHerle, 1994] observed that, upon current interruption from a high voltage value, V_{WR} decays slowly with time through a polarographic half-wave like feature. This is explained by the slow reoxidation of the electrolyte subsurface which had been reduced by electron injection during the preceding polarization. The energy barrier height between the gold and the electrolyte determines if the contact is blocking or rectifying. It depends on the cleanliness of the interface and is related to the difference between the metal work-function and the electrolyte electron affinity [Mayer, 1984].

For the oxygen reduction on a dense gold cathode at T > 800°C, Van Herle proposes the adsorption of oxygen on gold or the diffusion of adsorbed oxygen to the TPB region as the rate-limiting-step [VanHerle, 1992]. The current values were found to be TPB length-dependent rather than area-dependent. Limiting current behaviour was observed in a wide P_{O2} range (from 0.01 to 0.2 atm), indicating a concentration overpotential control [VanHerle, 1994].

At high overpotentials and beyond the limiting region, the current increases rapidly. This is attributed to the onset of an additional charge-transfer reaction, possibly electron injection into the electrolyte, gold functioning as an ion blocking electrode [VanHerle, 1994]. A similar observation was made for a platinum electrode by Robertson and Michaels [Robertson, 1990], who believe that this reaction may be responsible for the hysteresis in the current-voltage curves of their system: the current is higher when the absolute value of the potential is reduced from high to low potentials rather than vice-versa.

2.1.3.4 Cyclic linear sweep voltammetry

Linear sweep voltammetry is a very powerful tool for the in situ investigation of electrochemical systems. The theory of cyclic voltammetry has been developed for aqueous electrochemistry and has been reviewed in a comprehensive way by Bard and Faulkner [Bard, 1980] and the Southampton electrochemistry group [Greef, 1990]. It can be transposed to solid state electrochemistry, although the absence of a well-defined reference state in solid electrolytes is a serious handicap. The theory of cyclic linear sweep voltammetry for aqueous solutions will be briefly surveyed here.

From the current-voltage curves, it is possible to check the system's reversibility, to establish whether multiple steps are involved, to recognize adsorption-desorption processes and to detect electroactive intermediates [Yeager, 1970]. Brainina and Neyman [Brainina, 1993] have presented a systematic study of various voltammogram types. The electrochemical charge-storage capacity of a cell can be studied by integration of the current-voltage curves. The charging process involves not only the surface but an adjacent part of the bulk volume as well. It can be considered to be due to two separate contributions: the double-layer charging of the electrode/electrolyte interface capacity and the eventual oxidation-state changes of the metal ions involved [DeBattisti, 1991].

In the following, the model reaction will be a reduction process at a plane electrode, assuming semi-infinite linear diffusion:

$$Ox + ne^- \Leftrightarrow Red$$

In cyclic voltammetry, the voltage is scanned at a constant rate between two voltage limits and the corresponding current is measured. The potential as a function of time is given by the relations:

$$E = E_i - v\,t \qquad 0 < t \leq \lambda$$

$$E = E_i - 2\,v\,\lambda + v\,t \qquad \lambda \leq t$$

where E_i is the initial potential, v is the voltage scan rate and λ is the time at which the sweep is reversed.

The observed current is the sum of a capacitive component I_{dl} and a faradaic component I_f:

$$I = I_{dl} + I_f = A\,C_d\,v + I_f$$

where A is the electrode surface and C_d is the double-layer capacitance. The non-faradaic component is not constant, since the double-layer capacitance depends on the potential. At slow voltage scan rates v, the capacitive current is usually small compared to the faradaic one. At faster scan rates however, the nonfaradaic component may become quite large and influence the shape of the voltammetric curve [Yeager, 1970].

The exact form of the cyclic voltammogram can be determined mathematically by solving Fick's second law for Ox and Red, with the appropriate initial and boundary conditions:

$$\frac{\partial C_{Ox}}{\partial t} = D_{Ox} \frac{\partial^2 C_{Ox}}{\partial x^2}$$

$$\frac{\partial C_{Red}}{\partial t} = D_{Red} \frac{\partial^2 C_{Red}}{\partial x^2}$$

where D_{Ox} and D_{Red} are the diffusion coefficients for Ox and Red and C_{Ox} and C_{Red} are the concentrations of the respective species.

Reversible (Nernstian) systems

Consider a reversible reaction: $Ox + ne^- \Leftrightarrow Red$

As soon as the reduction potential of Ox is reached, the surface concentration of Ox decreases from its bulk value in order to satisfy the Nernst equation and a concentration gradient is set up [Greef, 1990]. As a result a faradaic current proportional to this gradient flows in the circuit. The gradient can increase until the surface concentration of Ox reaches zero and then starts to decrease, due to the diffusion induced relaxation. This behaviour gives rise to a peak-shaped current-potential curve.

The faradaic current is proportional to the square root of the scan rate and the peak current is given by the equation [Nicholson, 1964]:

$$I_p = 0.4463\, nFA \sqrt{\frac{nF}{RT}}\, C_{Ox,b} \sqrt{D_{Ox}} \sqrt{v} \qquad (2.13)$$

where the electrode surface A is expressed in cm^2, D_{Ox} is the diffusivity in cm^2/s, v is the voltage scan rate in V/s, and $C_{Ox,b}$ is the bulk concentration of the active species expressed in mol/cm^3.

The peak potential E_p is independent of the scan rate v. It is related to the half-peak potential $E_{p/2}$ (potential at which the current is equal to $I_{p/2}$) by the equation [Bard, 1980]:

$$| E_p - E_{p/2} | = 2.2\ (RT / nF)$$

The current on the reverse sweep should also exhibit a peaked response. However, a reversible cyclic voltammogram can only be observed if both Ox and Red are stable and the electron transfer rates are always greater than the rate of mass transport, so that surface concentrations follow the Nernst equation [Greef, 1990]. The reverse peak will then obey the relations:

$$| I_{pa} / I_{pc} | = 1 \text{ and}$$

$$E_{pa} - E_{pc} = 2.3\ (RT / nF)$$

where I_{pa}, I_{pc} are the anodic and cathodic peak currents and E_{pa}, E_{pc} the anodic and cathodic peak potentials respectively. As the sweep rate is augmented, the diffusion layer thickness decreases and the rate of mass

transport increases. If the latter becomes comparable to the rate of electron transfer, then an enhancement of the peak separation may occur.

Irreversible systems

Consider a totally irreversible reduction: $Ox + ne^- \xrightarrow{k} Red$

where $k = k_o \exp[(-\alpha n_a F / RT)(E - E_o)]$, α is the charge transfer coefficient and n_a is the number of electrons implied in the RDS.

The faradaic current is still proportional to the square root of the scan rate, but there is no reverse peak. The current peak is now given by the equation [Nicholson, 1964]:

$$I_p = 0.4958\, nFA \sqrt{\frac{\alpha n_a F}{RT}}\, C_{Ox,b} \sqrt{D_{Ox}} \sqrt{v} \qquad (2.14)$$

In addition, the peak potential E_p is a function of the scan rate and shifts by an amount of $-1.15RT/\alpha n_a F$ for each tenfold increase in v [Bard, 1980]:

$$E_p = E_o - \frac{RT}{\alpha n_a F}\left[0.78 + \ln\left(\frac{\sqrt{D_{Ox}}}{k_o}\right) + \ln\sqrt{\frac{\alpha n_a F v}{RT}}\right] \qquad (2.15)$$

It is related to the half-peak potential by the equation:

$$| E_p - E_{p/2} | = 1.857\, (RT/\alpha n_a F)$$

Note that the total absence of a reverse peak can also be due to a fast following chemical reaction. So, this feature does not necessarily imply an irreversible electron transfer process.

A process that is reversible at low sweep rates may become irreversible at higher sweep rates after having passed through a *quasi-reversible* region [Greef, 1990]. This transition can be seen from a plot of I_p as a function of $v^{1/2}$ (Fig. 2.8) and occurs when the relative rate of the electron transfer with respect to that of mass transport is insufficient to maintain Nernstian equilibrium at the surface. In the quasi-reversible region, the cathodic peak potential E_{pc} shifts negatively with increasing v. The peak separation $| E_{pa} - E_{pc} |$ increases with v and this feature allows the determination of the charge transfer kinetic parameters.

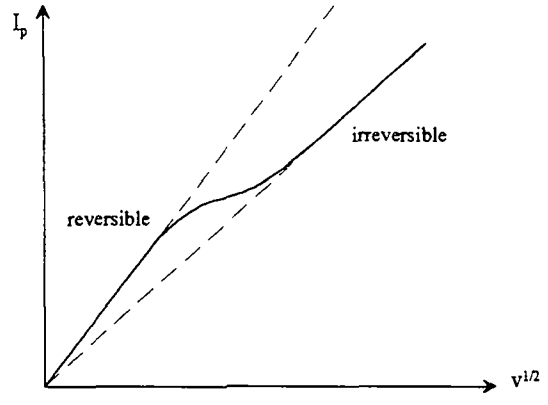

Fig. 2.8 The dependence of the peak current I_p on the square root of the voltage scan rate v, showing the transition from reversible to irreversible behaviour [Greef, 1990].

Chemical reaction preceding the charge-transfer reaction

Consider the reaction

$$Z \Leftrightarrow Ox$$

$$Ox + ne^- \Leftrightarrow Red$$

If the chemical step is very slow, there will be no peaks on the cyclic voltammogram. The current is kinetically controlled and the chemical rate constants can be calculated from the limiting current. A very fast chemical reaction will not affect the voltammogram at all. Under intermediate conditions, the concentration of the reducible species is partially controlled by the chemical reaction and the cathodic peak current will be lower than in the absence of kinetic effects. So, the ratio $I_{pc} / v^{1/2}$ decreases as the scan rate increases [Greef, 1990].

In systems with two electroactive species in equilibrium, where one species is reduced at a less negative potential than the other, the ratio of their peak heights is a function of scan rate; as v is decreased, the first peak becomes more and more important.

Charge-transfer reaction preceding the chemical reaction

$$Ox + ne^- \Leftrightarrow Red$$

$$Red \Leftrightarrow Z$$

If the charge transfer is irreversible, the voltammogram will not be influenced by the presence of the chemical reaction. In the case of a reversible charge transfer, the effect of the chemical reaction is more pronounced when the latter is rapid and irreversible. Since Red is continuously removed, there will be no reverse peak at low scan rates, although the peak may appear at higher scan rates. As long as the cathodic peak is concerned, increasing the scan rate will cause the ratio $I_{pc} / v^{1/2}$ to decrease and the potential E_{pc} to shift negatively [Greef, 1990].

Charge-transfer reaction with adsorbed species

If only the adsorbed forms of Ox and Red are electroactive, then I_p and E_p depend on the type of adsorption isotherm involved and the relative adsorption strength of Ox and Red. For an adsorption described by a Langmuir isotherm, we have:

$$E_{pa} = E_{pc} \qquad \text{and}$$

$$I_{pc} = \frac{nFQ_c}{4RT} v \tag{2.16}$$

where Q_c is the charge consumed for the adsorbed layer reduction and is given by the area under the cathodic peak.

If the species involved in the charge-transfer reaction are electroactive, whether they are adsorbed or diffuse from the bulk, the voltammogram is more complex. The reactant from the bulk is responsible for a peak which increases linearly with concentration and the adsorbed form gives rise to a post-peak which increases with concentration until a limiting value is reached. The separation between the main peak and

the post-peak increases with increasing adsorption strength. If the adsorption is very weak, the post-peak may not be discernible. The product adsorption favours the reaction, so it gives rise to a pre-peak.

The reduction of protons at a Pt electrode is known to exhibit strong product adsorption: there are two pairs of pre-peaks due to the adsorption and desorption of hydrogen at two different types of site. In the cathodic scan, the pre-peak of the strongly adsorbed hydrogen H_s precedes the one due to the weakly adsorbed hydrogen H_w.

From the experimental point of view, the dynamic study of a system by cyclic voltammetry is mainly based on the variation of four parameters: the voltage scan rate, the potential limits of the scan, the concentration of the electroactive species involved and the temperature. The diagnostic criteria presented above are very useful for the qualitative and quantitative (when possible) characterization of an unknown system. However, there are two important complications which should be taken into account while interpreting a voltammogram: the double layer charging effect and the ohmic potential drop IR_u due to the uncompensated resistance R_u.

Although we did not remind it systematically, all the relations concerning the peak current refer to the faradaic current. The cyclic voltammogram can be distorted by the double layer charging current, especially at high scan rates and if the capacitance C_d strongly varies over the range of conditions used.

As far as the IR_u drop is concerned, its effect is not easily established. If the uncompensated resistance or the voltage scan rate are too high, the assumption made for the mathematical description of the voltammograms $E \approx E - IR_u$ is not valid. Since now the term IR_u is no longer constant, like in the steady-state current-potential curves, the voltage sweep becomes non-linear. As a consequence, the peak heights decrease and the peak separations increase [Greef, 1990].

2.2 IRIDIUM OXIDE IN CATALYSIS AND ELECTROCATALYSIS

IrO_2 is the most common stable oxide of iridium at ambient conditions and has a blue-black colour. It is a metallic conductor with five d electrons and a Fermi level in the conduction band [Vallet, 1993]. It crystallizes in the undistorted rutile structure (Fig. 2.9 [Honig, 1980]) with a = 4.498 Å, c = 3.154 Å (Ir-Ir separation) and an Ir-O bond length of 1.99 Å [McDaniel, 1967]. Iridium can exist in a variety of oxidation states and therefore possesses high values of charge injection density upon polarization [Williams, 1992]. In solution, it can be electrochemically oxidized to Ir(V) and (VI). IrO_2 has a low overpotential for oxygen and chlorine evolution but it is not very stable in acid solutions [Hoare, 1964; Hoare, 1967].

Oxides such as IrO_2 possess high energy surfaces with a strong hydrophilic character. Water molecules become bonded to the metal cations (behaving as Lewis acids), usually with transfer of a proton to a neighbouring oxygen site (although undissociated water molecules may also be present). Thus, the surface is finally covered with OH groups [Trasatti, 1991].

Considerable oxidation of iridium to IrO_2 is detected in air above 600°C [Vol, 1986]. Upon heating at 1100°C in oxygen, gaseous IrO_3 is formed [Gulliver, 1982]. Ca_3IrO_6 was the first Ir(VI) oxide to be reported, but the publication is inaccessible [Roof, 1976]. Recently, Ir(VI) has been stabilized in Sr_2MIrO_6 (M = Ca, Mg) oxides with an Ir(VI)-O bond length of 1.90 by use of high oxygen pressure [Jung, 1995]. The samples present a perovskite structure and show semiconducting behavior. Due to the position of Ir (5d) in the periodic table and the high oxidation state, the Ir(VI)-O bond could be one of the strongest chemical bonds in an oxygen lattice.

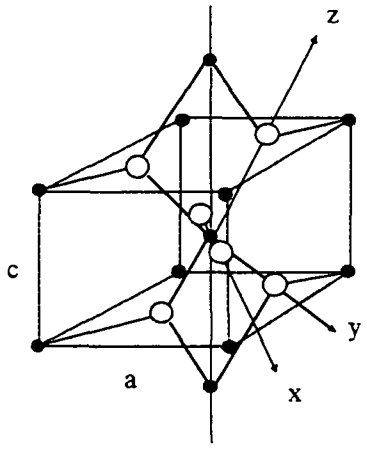

Fig. 2.9 The rutile lattice and its band structure scheme [Honig, 1980]

2.2.1 Preparation methods

Since catalytic activity depends on the surface area and the microstructural defects of a material, the preparation method used is important because it has a strong influence on the morphology and the properties of the final product. For supported catalysts, the nature and the surface state of the support are also of primary interest [Trasatti, 1980].

Thereafter, three of the most interesting preparation methods, namely reactive sputtering, thermal decomposition and electrochemical growth, will be briefly presented.

a) reactive sputtering

"Dry" iridium oxide films prepared by reactive sputtering decompose in air at around 400°C, whereas partially hydrated films decompose at 350°C. After the thermal treatment, both kinds of films exhibit rutile structures. In vacuum, the decomposition takes place at lower temperatures to give only Ir metal phase. The decomposition temperatures change after polarization of the films in an electrolytic cell. The thermal stability of the different species increases in the order: $Ir(OH)_3$ < $IrO(OH)_2$ < IrO_2. Some hydroxyl and water groups can remain adsorbed on the surface at temperatures as high as 600°C in ultra-high vacuum [Sanjinés, 1989]. The desorption of chemically bound water on group VIII metal-oxide surfaces is known to be slow and incomplete indeed [De Battisti, 1991].

Iridium coatings made by sputter deposition on polished supports are more porous than on supports which have been submitted to acid treatment [Williams, 1992].

b) thermal decomposition in air

IrO_2 electrodes as obtained by thermal decomposition of a chloride in solution are generally "dry" and crystalline. The conductivity takes probably place with an "electron-hopping" mechanism from grain to grain [Trasatti, 1991]. The solvent seems to play an important role in determining the crystallinity and even the non-stoechiometry of the oxide layer [Ardizzone, 1981]. In-depth chemical analysis proved that some Cl remains in the film after the decomposition of the chlorides. The Cl content decreases and the O content increases towards the surface [Trasatti, 1980].

The thermal decomposition of $IrCl_3.xH_2O$ in an isopropanolic solution gives rise to IrO_2 rutile with a relatively high chlorine content. Upon annealing of the sample, the crystallite size increases but the conductivity of the film is not necessarily improved [Lodi, 1990]. When the solvent is a mixture of isopropanol and water and the coating is prepared at 400°C, iridium metal is always present together with IrO_2, regardless of further thermal treatment. However, for samples prepared above 500°C no metal is detected in the final product. Iridium metal is also absent when the solvent is almost anhydrous [Lodi, 1988]. The IrO_2 crystallites show no strain, which means that ion-exchange processes across them are minimized and the ions' mobility is limited. On the other hand, the intergranular region seems quite large, so diffusion of small ions such as protons should be facilitated [Benedetti, 1991].

The use of the same precursor ($IrCl_3.xH_2O$) in anhydrous ethanol for the sol-gel preparation of IrO_2 particles gave contradictory results, since the particles contain both iridium oxide and metal at all preparation temperatures [Murakami, 1994].

The dissociation of H_2IrCl_6 in the aqueous phase is complex: depending on the pH of the solution, Ir^{4+} may exist as $IrO_2.2H_2O$, $[Ir(OH)_4Cl_2]^{-2}$, $[Ir(OH)_2Cl4]^{-2}$, or $[IrCl_6]^{-2}$. There still is considerable disagreement on the exact nature of the products of the decomposition of the chloroiridic acid upon drying. The following species have been reported: $IrCl_2$, IrO_2Cl, $IrCl_3$, $IrCl_4$, $Ir(OH)_3Cl$ and IrO_2 [Subramanian, 1991].

Generally, the electrochemical reversibility of the thermally prepared oxide (studied by cyclic voltammetry) is less than that of the electrochemically formed multilayers [Augustynski, 1984].

c) electrochemically grown films

The iridium oxide films formed electrochemically [Butler, 1936; Buckley, 1975; Burke, 1980; Pickup, 1988a; Podlovchenko, 1990; Ferrer, 1994; Woods, 1976] are poorly crystalline, open-structured and highly hydrated. They exhibit an electrochromic effect due to a reversible redox reaction of the iridium in the bulk of the electrode. The oxide growth cannot occur on Ir at a fixed potential and is difficult in basic solutions. Iridium oxides are generally grown to different thicknesses by potential cycling in acidic medium: the oxide formed in the anodic sweep is incompletely reduced in the cathodic sweep and accumulates in a hydrated form [Mozota, 1983; Conway, 1983]. The accumulation is slower when the potential is scanned between critical upper and lower limits than when it is stepped [Pickup, 1987]. The builiding up of a thick film seems to be accompanied by the transformation of $Ir(OH)_4$, which is the main constituent of the thinner film, into hydrated IrO_2 [Augustynski, 1984]. Upon anodization above 1.6V approximately, the active outer layer is oxidized to a soluble Ir(VI) species [Buckley, 1975].

The ions from the electrolyte solution seem to play an important role in the charging and discharging of iridium oxide films in aqueous media. Voltammetry and ion analysis revealed a transient insertion of such ions during oxide reduction, due to pH changes within the oxide [Pickup, 1988b].

The potential of the main peak in the voltammogram of electrochemically grown iridium oxide films decreases on increasing the pH by a rather unusual factor (ca. 90 mV per pH unit) as compared to films prepared by reactive sputtering (ca. 60mV per pH unit) [Burke, 1980; Hüppauff, 1993]. This unusual pH dependence of the hydrous oxide may be related to the more acidic character of the Ir(IV) species, i.e. its greater tendency to hydrolyze due to the increased charge density around the metal ion. As the pH of the solution is increased, hydroxy complexes become more stable or the metal ion activity is reduced [Burke, 1984b].

2.2.2 Iridium compounds in heterogeneous catalysis

In the heterogeneous catalysis field, often no distinction is made between the iridium metal and its oxide. This fact makes the literature research on the subject very difficult. Much work has been published on metallic iridium catalysts and the presence of iridium oxide subsequent to an oxidative treatment is sometimes mentioned but is considered as a detail. The ambiguity may be due to the fact that many authors do not make any difference between chemisorbed oxygen on a metal and a metallic oxide. The X-ray diffraction analysis can reveal the existence of a separate phase but is not systematically done.

The catalysts are generally prepared by impregnation of the support with a solution of an iridium salt followed by drying, calcination in air or oxygen and a final reduction step in hydrogen. This reduction step is not always present and iridium oxide may be formed. In the two following sections, a distinction will be attempted between the applications in catalysis attributed to metallic iridium and those where iridium oxide is eventually present.

2.2.2.1 Iridium metal

The use of metallic iridium in heterogeneous catalysis seems to be restricted to reduction reactions like hydrogenation of unsaturated hydrocarbons [Parravano, 1970; Mann, 1970; DaSilva, 1989; Moulijn, 1993] and hydrazine decomposition [Smith, 1982].

Some interesting studies deal with the adsorption of simple molecules on reconstructed iridium surfaces. Kanski et Rhodin [Kanski, 1977] observed a partially dissociative adsorption of nitric oxide on single crystal Ir(111) and Ir(100)-(5x1) surfaces at 300K and a complete dissociation at 500K. The binding energy of the 2π level should be much lower for the NO/Ir system than for the NO/Pt system, where only molecular NO adsorption occurs.

Verhoef et al. [Verhoef, 1994] measured the initial probability of dissociative chemisorption of molecular oxygen on a reconstructed Ir(110) surface as a function of incident energy. When the incident energy is less than 17 kJ/mol, the probability of chemisorption decreases with increasing incident energy, indicative of a trapping-mediated mechanism. The adsorption energy of oxygen on a well ordered Ir(111) surface was evaluated from flash desorption spectra to be E_{ad} = 293 kJ/mol [Küppers, 1976]. The maxima of the flash curves shift towards lower temperatures with increasing coverage, indicating second-order desorption and thus atomic oxygen in the adsorbed state. These authors also found that a CO-precovered surface adsorbs oxygen negligibly, while additional CO uptake takes place with preadsorbed oxygen.

synthesis gas reactions

Iridium presents some activity for the Fischer-Tropsch synthesis, especially when its structure has many defects [Moulijn, 1993; Snel, 1987]. It is clear from hydrogen and CO chemisorption studies on iridium catalysts [Tournayan, 1991; Kip, 1986; Krishnamurthy, 1982] that the support also plays an important role.

In syngas conversion over iridium catalysts, the activity and the selectivity towards alcohol formation can be greatly promoted by additives such as Mo and Cr. Formation of methyl chloride is also possible if chloride ions from the precursor remain on the surface after the fabrication process [Inoue, 1991]. The high activity and selectivity in methanol synthesis of FeIr/MgO catalysts is attributed to the presence of highly dispersed iridium particles [Psaro, 1995].

catalytic reforming

The purpose of catalytic reforming is to boost the octane number of the naphta fraction. This production of gasoline components of high antiknock quality is achieved by the conversion of n-hydrocarbons to branched or cyclic ones. A hydrotreatment step precedes the reforming reactor in order to remove the nitrogen-containing bases and sulphur-containing compounds which poison the reforming catalysts. Hydrocarbon conversions are generally accompanied by coke formation which also affects the catalyst life and a regeneration cycle is often needed.

The Pt-Ir bimetallic catalysts have retained much attention in the petrochemical industry for the production of high octane number gasoline [Rasser, 1977; Yang, 1994; Marecot, 1990a; Marecot, 1990b; Huang, 1989; Fung, 1994; Sinfelt, 1979; Foger, 1981; Biswas, 1988]. The addition of iridium to the platinum catalyst improves its activity, its selectivity towards isomerization and its stability against coke formation and sintering [Rasser, 1977]. The incorporation of Pt into Ir clusters decreases the cracking activity of the iridium component and retards its oxidative agglomeration [Huang, 1989], thanks to an electron donation from the platinum to iridium [Biswas, 1988].

The hydrogen chemisorption capacity and the n-hexane reforming activity of supported iridium catalysts prepared by impregnation was found to decrease for higher calcination temperatures prior to hydrogen treatment. This was attributed to the formation of large IrO_2 crystallites during calcination in oxygen at 773K, which are converted to large iridium crystallites upon treatment with hydrogen [Yang, 1994]. If the calcination is preceded by a reduction treatment, the oxidative agglomeration is even higher [Huang, 1989].

Supported iridium catalyst is known to be very active for hydrogenolysis reactions and the coke deposited on its surface during hydrocarbon conversions is completely destroyed by hydrogen treatment [Marecot, 1990a]. During regeneration of a Pt-Ir catalyst by oxygen treatment, an unexpectedly high quantity of carbon is removed at low coke burn temperature. This may be due either to the oxygen activated by iridium or to the high mobility of the iridium oxide species and improved contact with coke deposits throughout the support [Fung, 1994].

2.2.2.2 Iridium oxide

During oxidation reactions, the catalyst is most likely in an oxidized form whether iridium metal or its oxide were initially prepared. However, the use of iridium oxide as a catalyst is not limited to oxidation reactions. An iridium containing sulfate-supported zirconia superacid was found to present the highest

activity for the skeletal isomerization of butane to isobutane among the platinum-group metals [Hino, 1995]. The presence of iridium oxide was confirmed with XPS measurements.

CO oxidation

The structure insensitivity of the CO oxidation has been proved by the match of the rates observed on supported, nonoriented iridium catalysts and on single crystals. Berlowitz et al. [Berlowitz, 1988] observed a mean activation energy of 92 kJ/mol for the CO oxidation, close to the desorption energy of CO from the iridium catalyst surface. The rate dependence upon the CO partial pressure at constant oxygen pressure and temperature presents a maximum for an O_2:CO ratio of 12:1. The reaction order in CO is 1 below the maximum and -1 above the maximum. The rate dependence upon the oxygen partial pressure is similar. The negative-order dependence on O_2 partial pressure, under highly oxidizing conditions, indicates the presence of a strongly bound oxygen species. The oxygen species is similar to iridium oxide formed by deliberate oxidation and could be detected as CO_2 desorbing at high temperatures. The oxidation of the iridium catalyst results in a rate decrease without affecting the activation energy, indicating that the oxide serves only as a site blocker.

Berlowitz et al. [Berlowitz, 1988] propose a Langmuir-Hinshelwood rate expression for the CO-rich region. Neglecting the recombinative desorption of oxygen and the dissociative chemisorption of CO_2, the reaction steps may be written as:

$$CO\ (g) \leftrightarrow CO\ (ads) \qquad (1)$$

$$O_2\ (g) \rightarrow 2O\ (ads) \qquad (2)$$

$$CO\ (ads) + O\ (ads) \rightarrow CO_2\ (g) \qquad (3)$$

Assuming that the primary surface species is CO, the rate is governed by the desorption of CO, and the pressure dependence reflects the competition for adsorption sites between oxygen and CO. The rate expression can be formulated as:

$$d[CO_2]/dt = k \exp(-E_{des,CO}/RT)\ P_{O2}/P_{CO}$$

Cant et al. [Cant, 1978] found similar results for the CO oxidation over a 5% Ir/SiO_2 catalyst. They observe an activation energy of 100kJ/mol, a first-order dependence in oxygen pressure and a negative-first-order dependence in CO partial pressure. However, upon calcination of the catalyst at 1000K, a three-fold decrease of the dispersion took place and resulted in a three-fold apparent increase in the catalyst activity, as expressed by the turnover number, based on the surface atoms. The calcination treatment did not affect the activation energy.

Carbon monoxide oxidation may present oscillatory behavior on Ir catalysts for a certain temperature range and reactants partial pressure interval [Turner, 1981]. It is believed that the oscillations occur between two branches of a Langmuir-Hinshelwood reaction mechanism. Chemisorbed oxygen may penetrate one or two monolayers below the iridium catalyst surface. This subsurface oxygen is less reactive than oxygen chemisorbed on the surface and may be regarded as oxygen dissolved into the metal, a necessary precursor to the formation of a metal oxide. The authors believe that the slow formation and

removal of this subsurface or dissolved oxygen drives the reaction between the two branches [Turner, 1981]. They propose the following qualitative description of an oscillation: when the surface of the catalyst is mainly covered with dissociated chemisorbed oxygen, the CO_2 production rate is high and some oxygen, instead of reacting, converts to the "unreactive" subsurface oxygen species. Surface sites are thus being blocked and a rapid transition occurs to the lower reaction branch. At this stage, the catalyst surface is mainly covered with adsorbed CO, the rate is quite low and some CO, instead of reacting with the available chemisorbed oxygen, reduces the "unreactive" dissolved oxygen.

CO - NO -O_2 reaction

The favorable partitioning of CO between NO and O_2 under oxidizing conditions in automobile exhaust is another interesting application of supported iridium catalysts [Taylor, 1989]. Three-way catalysts are used in automobile catalytic converters for the simultaneous treatment of the two reducing pollutants, carbon monoxide and uncombusted hydrocarbons, and the oxidizing pollutant, nitrogen oxides. Although iridium is not used in current commercial three-way catalysts because of scarcity, prohibitive cost and volatilization losses, it has a much superior selectivity than any other noble metal, even at very low metal loadings [Shelef, 1994].

Tauster and Murrell [Tauster, 1976] found that Ir/η-Al_2O_3 promotes the reaction CO + NO $\rightarrow$ N_2 + CO_2 in excess oxygen. The catalysts were prepared by impregnation of the support with H_2IrCl_6 solution, followed by drying at 120°C and reduction by hydrogen at 500°C. The reaction however was studied in oxidizing conditions and some preliminary experiments revealed that oxygen is readily adsorbed on the catalyst and does not desorb at T < 700°C. The formation of IrO_2 cannot thus be excluded.

Another study of the simultaneous conversion of nitrogen oxide and carbon monoxide over Ir, Rh, Pt and Pd catalysts gave similar results [Taylor, 1980]. Only the Ir/γ-Al_2O_3 catalyst favored the NO reduction under net fuel lean conditions. Although the authors consider that the catalyst is metallic iridium, the preparation procedure gives strong evidence that they were working with iridium dioxide instead: after impregnation with an aqueous solution of $IrCl_4$, the catalyst was heated in air at 500°C for 4 hours without any further reducing treatment. In addition, prior to activity measurements, the catalysts were heated to the reaction temperature (550°C) in the absence of a reducing agent. At prolonged experiments at this temperature some catalyst was lost, probably due to the formation of a volatile oxide (IrO_3). It was found that an increase in CO concentration inhibits the NO and O_2 conversions at low temperature (350°C) and enhances them at higher temperature (450°C). A slight inhibiting effect of NO on oxygen conversion suggested that NO and O_2 compete for surface sites. An explanation for the higher activity of Ir towards NO conversion as compared to Pt was based on the consideration of molecular NO adsorption on Pt and partially dissociative adsorption on Ir [Kanski, 1977].

A systematic study of sintering was done on Ir/Al_2O_3 catalysts prepared by the same procedure as in the previous cases [McVicker, 1978]. Ir oxidatively sintered into IrO_2 crystallites, in contrast to Pt, which grows as the metal. It was also established that the gaseous IrO_3 intermediate responsible of the vapor transport of Ir can be generated more easily from Ir metal than from IrO_2. The addition of CaO, SrO or BaO

was proposed for preventing sintering and maintaining high metal dispersions of Ir/Al_2O_3 catalysts under oxygen atmospheres.

C_2H_4 oxidation

The only references found in the literature on the ethylene oxidation over supported iridium catalysts are due to the work of Cant and Hall [Cant, 1970; Cant, 1972]. The ethylene conversion to acetic acid, with approximately 12% selectivity, in the presence of iridium metal, is reported in a patent [Cant, 1972], without any information on the kinetics of the reaction. The catalytic ethylene oxidation over silica-supported iridium is presented in more detail in an article [Cant, 1970]. The silica was impregnated with an aqueous solution of H_2IrCl_6 and dried under flowing hydrogen, while the temperature was raised to 300°C. The reduction continued for approximately 6 hours at 300°C following which the system was purged with helium. The authors believe that "reduction was almost certainly complete" under these conditions, based on experiments reported in the literature. However, they did not make any analysis, so their catalyst may contain some IrO_2 .

The reaction was studied in a temperature range from 80° to 150°C and an apparent activation energy of 71 kJ/mol is reported for the total oxidation of ethylene [Cant, 1970]. CO_2 and H_2O were the chief products, but acetic acid and traces of acetaldehyde were also present. The rate increased with olefin pressure and was weakly inhibited by increasing oxygen pressure.

2.2.3 Iridium oxide in electrocatalysis

In the field of electrochemistry, iridium oxide has retained much attention during the last two decades because of two possible applications. The first is in electrochemical energy conversion, especially as an active component in DSA® electrodes (Dynamically Stable Anodes), because of its low oxygen and chlorine overvoltage in acidic solutions. The second is in electro-optic display devices, where one takes advantage of its electrochromic properties: a change of color accompanies the passage of an oxidative to a reductive state.

A DSA® electrode is composed of an electrochemically active coating, generally a binary mixture of a conducting and an inert oxide, deposited on a base metal. The most popular DSA® electrode is the Ti/RuO_2-TiO_2 anode, especially in the chlor-alkali industry [Comninellis, 1991b]. Much work has been done on pure IrO_2 as electrocatalyst [Böld, 1961; Dufour, 1988] and on binary [Rolewicz, 1987; Rolewicz, 1988; Vercesi, 1990; Comninellis, 1991a; Aramata, 1992; Takasu, 1992; Balko, 1991] or ternary [Lin, 1993; Kameyama, 1994; Hutchings, 1984] oxide mixtures with IrO_2 as the conductive component. Most studies focused on the electrocatalysis of the oxygen evolution reaction (OER) for which iridium oxide is very active in acidic medium but has a low resistance to corrosion, especially for electrochemically grown films [Vukovic, 1987]. Porosity, adhesion and stress are the three main factors affecting corrosion processes.

Thermally prepared IrO_2 favors electrochemical conversion of organic "non-biocompatible" pollutants to "biocompatible" carboxylic acids prior to biological treatment [Comninellis, 1994].

The electrochromism and the charge storage capacity of iridium oxide can be explained by a cation-insertion mechanism: in aqueous medium, the electron transfer during oxidation or reduction of the film is compensated by a proton transfer between the electrolyte and the bulk of the film. According to an investigation with in situ infrared spectroscopy, the colored form (Ir^{4+}) contains no hydroxyl species and could be described as $IrO_2.xH_2O$ whereas the bleached form (Ir^{3+}) could be formulated as $IrOOH.yH_2O$ [Lezna, 1987].

Upon anodic polarization of electrochemically grown iridium oxide films in acid solution, the total amount of oxygen remains constant while the contribution of oxide species grows at the expense of hydroxide ones. This has been evidenced by deconvoluted XPS spectra assuming the presence of only three oxygen species with O1s binding energies of 533.1 eV (water), 531.0 eV (hydroxide) and 529.6 eV (oxide). A model for charge storage and oxygen evolution on iridium oxide electrodes was thus proposed, including deprotonation steps and adsorption/desorption of water molecules: starting from $Ir(OH)_3$, successive deprotonation steps lead to $IrO(OH)_2$, then $IrO_2(OH)$, and finally IrO_3. By oxygen liberation and simultaneous water uptake, IrO_3 is transformed back to $IrO(OH)_2$. As an alternative, IrO_3 can corrode with water uptake to give $2H^+$ and IrO_4^{2-} [Kötz, 1984]. This model is supported by X-ray absorption spectroscopy measurements of the valence of iridium during a voltage scan. The valence was found to vary between 3.0 and 4.8. An increase in the valence was accompanied by a shrinkage of the first coordination shell around the iridium ion [Hüppauff, 1993].

The activity of an electrode for the oxygen evolution reaction may be quantified in terms of the exchange current density (i_0) and the Tafel slope (dE/dlogi). A good electrocatalyst is associated with a high value of i_0 and a low Tafel slope. Tafel plots are very sensitive to the existence of different surface layers and a change in their slope may indicate a change in the rate-determining step of the OER. When the oxidation state of the oxide is increased prior to, or simultaneously with, the beginning of oxygen evolution, the electrocatalyst is probably activated for two reasons: first, the formation of a mixed-valence defect structure in the bulk of the oxide should allow a better electronic conductivity and second, the production of active sites in the form of metal ions with a higher positive charge should enhance the chemisorption of OH or O intermediates [Gottesfeld, 1978].

Ferrer et al. studied the oxygen evolution reaction by electrochemical impedance spectroscopy [Ferrer, 1994]. They proposed the following mechanism at low overpotential in acid medium:

$$IrO_2 + H_2O \rightarrow IrO_2(OH) + H^+ + e^- \qquad \text{(step1)}$$

$$IrO_2(OH) \rightarrow IrO_3 + H^+ + e^- \qquad \text{(step2)}$$

$$IrO_3 \rightarrow IrO_2 + 1/2\ O_2 \qquad \text{(step3)}$$

This mechanism would lead to a saturation of the oxygen evolution reaction with increasing potential, by accumulation of Ir(VI) oxide. This saturation was not observed. It was thus assumed that, at high potentials,

when the amount of IrO_3 starts to be considerable, a new charge transfer process occurs in parallel to the third step. This change in the OER mechanism is supported by a break in the Tafel characteristic, which has often been reported at around 1.34V [Vukovic, 1987; Gottesfeld, 1978]. The alternative path consists in the formation of an oxide-peroxide which decomposes in a very fast chemical step:

$$IrO_3 + H_2O = IrO_2(OO) + 2H^+ 2e^- \qquad \text{(step3')}$$

$$IrO_2(OO) = IrO_2 + O_2 \qquad \text{(step4)}$$

The cyclic voltammetric response of electrochemically grown films depends on the time spent in the reduced state. In acidic solutions, a positive shift of the principal anodic peak and a decrease in the cathodic charge take place when the potential is held for some time in the cathodic region. This reversible "ageing", characterized by slower reaction kinetics, is more pronounced for thicker films. It seems to be due to the partial dehydration of the oxide film and subsequent inhibition of ion/solvent transport processes in the film. The absence of such an "ageing" effect in alkaline solutions supports the idea that it does not simply result from the complete reduction of Ir(IV) to non-conducting Ir(III) sites [Elzanowska, 1993].

Many of the reactions reported for the electrochemically produced layers are not observed with the thermal oxide. The loss of water molecules, the lowering of bulk defect density and the surface rearrangement, involved in sintering, leave the cations in the heated oxide in a less reactive state. However, cations at the surface of these oxides may still undergo redox reactions such as the proton incorporation, represented as:

$$IrO_2 + H^+ + e^- = IrOOH$$

Although rarely observed with the platinum metals, this reaction is quite common in oxides of the non-noble metals, e.g. Mn and Ni [Burke, 1980].

T. Goto et al. deposited Ir films on yttria stabilized zirconia by metallorganic chemical vapour deposition (MOCVD) using a metal-acetylacetonate precursor. To our knowledge, this is the first study of the oxygen evolution reaction on Ir containing electrodes in high temperature electrochemistry by A.C. impedance spectroscopy and D.C. polarization. The Ir electrodes prepared without any oxygen addition contain impurity carbon and show superior electrical properties in comparison to Pt electrodes prepared in the same way. They pass the highest ionic current under a small overvoltage at 550°C in air; the ionic current is higher for Ir than for Pt electrodes. The Arrhenius plot for the conductivity of the process associated to the oxygen electrode presents a breaking point at around 500°C. This breaking point may be associated with the oxidation of impurity carbon or the morphology change of the fine metal particles due to sintering. When a small amount of oxygen is added to the argon carrier gas during deposition, impurity carbon is easily removed by subsequent argon sputtering. The interfacial reaction seems more difficult on these "clean" Ir electrodes [Goto, 1993].

2.3 CATALYTIC ETHYLENE OXIDATION

The catalytic oxidation of hydrocarbons is an important step in many industrial processes, including petroleum processing and automotive exhaust pollutant control. A silica or alumina supported noble metal such as Pt, Pd or Rh is generally employed. The complete ethylene oxidation to carbon dioxide and water is a model reaction for the study of such processes.

Ethylene figures among the top 5 chemicals produced worldwide and is mainly used for the fabrication of polyethylene. In the United States, ethylene oxide and ethylene glycol are ranked by production volume in the top 30 chemicals for 1994 [Kirschner, 1995]. Ethylene oxide, produced by the selective ethylene oxidation, is a most valuable intermediate for many organic syntheses (i.e. ethylene-glycols, tensioactive agents, etc.). Industrial catalysts for ethylene oxide production are based on silver which is known to be particularly selective for the ethylene oxidation.

Consider a gas phase reaction which may either occur homogeneously or be catalyzed heterogeneously. In order for the reaction to be noticeably catalyzed, the catalyst must provide a pathway whereby the activation energy for the formation of an intermediate surface complex is considerably less than for the homogeneous reaction. A simple catalytic reaction with no intermediates can be divided in a series of successive steps, one or more of which may be rate-determining:

a) external diffusion of the reactants through the gas film
b) internal diffusion of the reactants through the catalyst pores
c) adsorption of the reactants on the active sites
d) reaction on the surface
e) desorption of the products
f) internal diffusion of the products through the catalyst pores
g) external diffusion of the products

The changes in energy associated with the different steps in a simple exothermic reaction are shown in figure 2.10. E_{hom} is the activation energy for the homogeneous reaction, E_{ads} for adsorption of reactants, E_a for the formation of the activated complex, and E_{des} for the desorption of products. ΔH_{ads} is the heat of adsorption of reactants, taken to be exothermic, and ΔH_{des} the heat of desorption of products, taken to be endothermic.

It is convenient to divide oxidation reactions in electrophilic oxidations with molecular or atomic oxygen, and nucleophilic oxidations with lattice oxygen. The latter proceed by the Mars and van Krevelen mechanism, according to which lattice oxygen from the catalyst appears in the products and the vacancies are replenished by dissociative oxygen adsorption [Nieuwenhuys, 1993]. The oxygen in metal oxide lattices is of a low mobility and reacts slowly at low temperatures [Margolis, 1963]. The proposed scheme for olefin oxidation on metals and semiconductors is [Margolis, 1963]:

olefin $\rightarrow$ acetaldehyde $\rightarrow$ acid $\rightarrow$ CO $\rightarrow$ CO_2

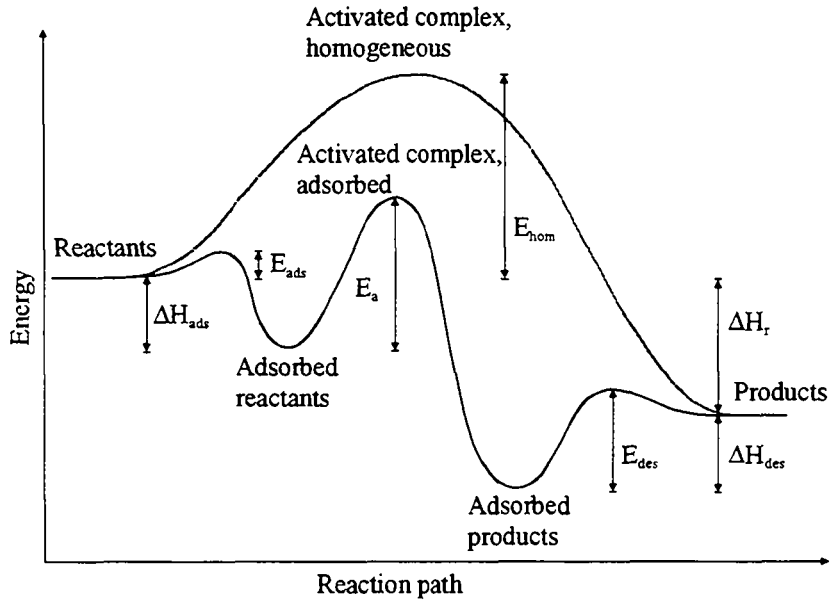

Fig. 2.10 Energy changes associated with the individual steps of an exothermic reaction [Satterfield, 1980].

Heterogeneous catalysis and electrocatalysis have many important points in common. The long-term stability of the catalytic activity and the catalyst adhesion to the support are threatened by poisoning, erosion, corrosion and loss of active surface by sintering. The corrosion may render the catalyst/electrocatalyst material more soluble in a liquid electrolyte or may form a volatile species which evaporates in the gas phase. In electrocatalysis, as in chemical catalysis, catalysts are usually highly porous in order to increase the effective catalyst surface, and mass-transfer limitations are possible, due to an insufficient supply of the catalyst inner surface with reactants. Diffusional control is generally undesirable because it masks the surface effects. Mass-transfer resistances can be minimized by the choice of adequate experimental conditions.

Generally, electrochemical and chemical processes follow very similar if not the same pathways. In the electrochemical reaction of oxygen evolution, metal-oxygen bonds are formed and broken exactly as in the case of O_2 adsorption-desorption in the gas phase. So, oxygen adsorption on oxide surfaces is the gas phase analogue of "oxide anodization": adsorption of oxygen entails "oxidation" of the given oxide to a higher one, with the Gibbs energy of the lower-to-higher oxide transition as the chemical driving force.

2.3.1 Adsorption, Desorption

Adsorption represents the primary step of catalysis and many studies have focused on its mechanisms or the state and interactions of the adsorbed molecules. Since adsorption controls the transition of the reactant molecules to the active state, it may provide information on the different possible routes of a process.

Chemisorption is generally accompanied by electron transfer between the adsorbate and the catalyst, which leads to charging of the surface. The electron transfer direction depends on the Fermi level position in the crystal and on the energy level of the adsorbate. Margolis [Margolis, 1963] found that for

most metal and metallic oxide catalysts, the adsorption of oxygen molecules (electron acceptors) results in a negative surface charge, while a positive charge is observed for ethylene (electron donor) and other hydrocarbons, irrespective of their structure. Water slightly charges the surface positively, causing the work function to decrease [Heras, 1988].

Molecular adsorption often prevails at low temperatures and dissociative adsorption occurs at higher temperatures. Dissociative adsorption requires a cluster of contiguous free metal atoms in an ensemble on the surface. Therefore, dissociation is favoured when the coverage is low. A diatomic molecule has to be adsorbed parallel to the surface in order to dissociate. In general, close-packed and smooth surfaces are less active in dissociation than surfaces with steps or kinks. Adsorption of atoms is favoured by metals with a partially filled d valence electron band or metals of low work function. The dissociation energy of molecules decreases when they are adsorbed with considerable electron transfer from the metal surface to the adsorbate (back donation) [Nieuwenhuys, 1993].

The Sabatier principle states that optimum activity is obtained when catalysts neither bind intermediates too strongly, which would inhibit adsorption to the surface, nor interact too weakly, which would prevent the initiation of the reaction [Nieuwenhuys, 1993]. The Sabatier principle is illustrated in "volcano plots", such as the one in figure 2.11, where the activity for CO oxidation for different metals is plotted as a function of the heat of oxygen adsorption.

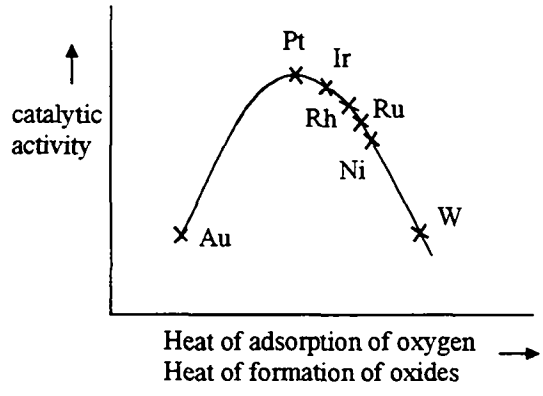

Fig. 2.11 Volcano plot for the CO oxidation over several metal catalysts [Nieuwenhuys, 1993].

An adsorption isotherm shows how an amount adsorbed depends upon the equilibrium pressure of the gas at constant temperature. The Langmuir isotherm is the most used for formulating kinetic expressions and is based on the following assumptions:

i) adsorption occurs on localized sites with each site accomodating only one adsorbed entity, so that the maximum adsorption possible corresponds to a monolayer;

ii) all sites are equivalent (uniform surface) and the energy of adsorption is independent of surface coverage.

Consider the adsorption of a substance A and let the occupied fraction of sites be θ_A. The rate of adsorption r_{ads} is proportional to the rate of collisions with unoccupied sites:

$$r_{ads} = k_{ads} (1-\theta_A) P_A$$

The rate of desorption is proportional to the number of molecules adsorbed:

$$r_{des} = k_{des}\,\theta_A$$

At equilibrium, the rate of adsorption equals the rate of desorption, so that

$$\theta_A = \frac{K_A P_A}{1 + K_A P_A}$$

where the adsorption equilibrium constant $K_A = k_{ads}/k_{des}$

If the adsorption is dissociative, the relation becomes:

$$\theta_A = \frac{\sqrt{K_A P_A}}{1 + \sqrt{K_A P_A}}$$

and if another substance B adsorbs reversibly on the same sites:

$$\theta_A = \frac{K_A P_A}{1 + K_A P_A + K_B P_B}$$

Very few chemisorptions are known to conform to the Langmuir equation over the entire range of surface coverage, because the heat of chemisorption generally decreases with increasing coverage. This observation is due to surface heterogeneity and some degree of repulsive interaction.

In the Freundlich isotherm, the heat of adsorption is assumed to decrease logarithmically with increasing coverage: $\theta_A = \text{const.} \cdot P_A^{1/n}$; $n>1$

In the Temkin (Slygin-Frumkin) isotherm, the fall in heat of adsorption with increasing coverage is supposed to be linear: $\theta_A \propto \ln(\text{const.} \cdot P_A)$

There are three types of surface centers for adsorption on oxides: the hydroxyl-hydrate cover, the electron-acceptor metal cations and the electron-donating oxygen anions. The composition and structure of the solid and the surface treatment determine the chemical properties of these adsorption centres. Any real solid surface hosts a set of surface compounds, produced by the interaction of coordinatively or valently unsaturated surface atoms with molecules of the medium, such as H_2O and CO_2 [Davydov, 1990].

Upon dissociation of water molecules, hydrogen is attached to each O atom, whereas hydroxyl groups are bonded to metal atoms. The oxygen of the OH group can be bound to several metal atoms, depending on their mutual arrangement. The hydroxylated face (110) of the rutile lattice is schematically depicted in figure 2.12.

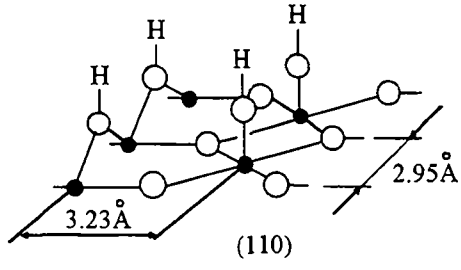

Fig. 2.12 The hydroxyl cover of the (110) face of an oxide which crystallizes in the rutile structure [Davydov, 1990].

2.3.1.1 Oxygen adsorption on oxidation catalysts

Oxygen is readily chemisorbed on metal oxides and in some cases it is partly dissolved in the lattice [Margolis, 1963]. The formation of metal-oxygen groups of an ionic nature on oxide surfaces can proceed by the transfer of oxide electrons to adsorbed oxygen:

$$O_2 (gas) + e^- \Leftrightarrow O_2^- (ads)$$

$$O_2^- (ads) + e^- \Leftrightarrow 2O^- (ads)$$

$$2O^- (ads) + 2e^- \Leftrightarrow 2O^{2-} (ads)$$

By far the most commonly reported species on oxides is the O_2^- (superoxide) ion, which plays a predominant role in nonselective oxidations [Che, 1983]. The presence of coordinatively unsaturated cations on the surface of oxide catalysts should promote the adsorption of uncharged molecular oxygen (not accompanied by electron transfer into the oxygen molecule).

The isotope exchange method, which consists in monitoring the isotopic composition of the gas phase, was used to determine the O_2 and CO_2 exchange rates and their adsorption-desorption characteristics on zirconia surfaces. The interphase exchange rate in CO_2 is much higher than in O_2, due to their different exchange mechanisms: an associative one for CO_2, via CO_3^{2-} formation, and a dissociative one for O_2. The application of a silver or platinum film on zirconia enhanced the oxygen interphase exchange in an atmosphere of oxygen but had no effect in an atmosphere of carbon dioxide [Kurumchin, 1990]. The oxygen adsorption-desorption rates for oxygen ion conductors are much lower than the rate of O^{2-} supply to the surface, which favours the formation of nonselective oxygen species [Voskresenskaya, 1995].

Preadsorbed oxygen promotes the H_2O decomposition at low temperatures, to form an OH overlayer. This effect has been reported for Ir (110) among others metals [Heras, 1988]. In addition, during temperature-programmed-desorption, even a low oxygen coverage gives rise to high-temperature H_2O desorption peaks, because of the stabilization of the undissociated, adsorbed water molecules [Heras, 1988].

2.3.1.2 Ethylene adsorption on oxidation catalysts

The investigation of hydrocarbon adsorption on metal oxides is difficult, due to side processes such as pyrolysis and oxidation at high temperatures. The rates of hydrocarbon adsorption are very high and the surface often needs an oxygen treatment to be freed from the strongly sorbed hydrocarbon.

Margolis [Margolis, 1963] studied ethylene adsorption on silver. Ethylene sorbs reversibly and the coverage degree is low on an oxygen-free silver surface. On an oxygen-precovered surface, only a certain amount of the adsorbed ethylene can be removed by outgassing, while a considerable part becomes strongly bound with surface oxygen. The overall process has an activation energy of 8-13 kJ/mol. Oxygen, presorbed on a cobaltous oxide surface, also enhances the adsorption of ethylene [Thomas, 1967].

The adsorption of hydrocarbons on oxide surfaces is known to involve the formation of several species [Davydov, 1990]. The interaction of alkenes with oxide surfaces depends on the acid-base properties of surface hydroxyls because alkenes are weak bases. The electron-donor properties of ethylene and the presence of coordinatively unsaturated electron-accepting cations on the oxide surfaces result in the formation of ethylene π-complexes, which weaken the C=C bond.

The adsorption isotherms for ethylene on a series of oxide catalysts indicate a uniform cation distribution on the surface and that only 10% of the surface cations are capable of coordinating alkenes. Among the various species detected, the singly bound and π-complexed species are the most reactive forms, while the multiply-bound species are rather unreactive [Nieuwenhuys, 1993]. The adsorption of ethylene involving two surface sites per molecule favours the fragmentation of ethylene, in contrast to single-site adsorption which provides the necessary intermediate for epoxide formation [Margolis, 1963].

2.3.2 Ethylene oxidation

The following global reactions represent the complete and partial ethylene oxidation respectively:

$$C_2H_4 + 3\ O_2 \rightarrow 2\ CO_2 + 2\ H_2O \qquad \Delta H_{r,\,600K} = -\ 1322\ kJ/mol$$

$$C_2H_4 + 1/2\ O_2 \rightarrow C_2H_4O \qquad \Delta H_{r,\,600K} = -107\ kJ/mol$$

Kinetic models are frequently formulated assuming that one step in the reaction is rate-determining. The Langmuir-Hinshelwood model is based on the assumption that the reaction between chemisorbed species is the RDS, while adsorption equilibrium is established at all times. The Eley-Rideal model is applied when the reaction between a chemisorbed species and a molecule from the gas phase is the RDS.

The formulation of Langmuir-Hinshelwood kinetic models is generalized in the expression:

$$-r = \frac{(\text{kinetic term})(\text{potential term})}{(\text{adsorption term})^n}$$

where the different terms are tabulated in many books on heterogeneous catalysis. For example, in the case of a bimolecular reaction between a dissociatively adsorbed atom A and a molecularly adsorbed B atom

$$A_2 \Leftrightarrow 2A$$

$$A + B \rightarrow C$$

the rate expression becomes:

$$-r = k\theta_A\theta_B$$

$$-r = \frac{kK_AK_BP_AP_B}{\left(1+\sqrt{K_AP_A}+K_BP_B+K_CP_c\right)^2}$$

An Eley-Rideal kinetic scheme is proposed by Vayenas et al. [Vayenas, 1992a; Vayenas, 1980; Vayenas, 1981] for the complete ethylene oxidation on Pt:

$$\frac{1}{2}\left[\begin{array}{c} O_2(g) \xrightarrow{k_{ads}} O_2(a) \\ O_2(a) \rightarrow 2O(a) \end{array}\right]$$

$$C_2H_4(g) + O(a) \xrightarrow{k} P \xrightarrow{5/2O_2} 2CO_2 + 2H_2O$$

They found that, at temperatures above 280°C, the open-circuit kinetics can be quantitatively described by the rate expression

$$r_o = k\, k_{ads}\, P_{C_2H_4}\, P_{O_2} / \left(k\, P_{C_2H_4} + k_{ads} P_{O_2}\right)$$

On the fuel-lean region, where the oxygen coverage is near unity, the reaction is the rate determining step and the rate expression can be simplified to:

$$r_o = k\, P_{C_2H_4}$$

On the fuel-rich side, oxygen adsorption is the limiting step and the rate expression reduces to:

$$r_o = k_{ads}\, P_{O_2}$$

The selective oxidation of ethylene to ethylene oxide has been extensively studied over Ag powders and supported Ag catalysts [Grant, 1985; Schmid, 1988; Borman, 1995]. It has also been the subject of many reviews [Margolis, 1963; Moulijn, 1993; vanSanten, 1987; Sachtler, 1981; Thomas, 1967]. Generally, the reaction proceeds between both reactants in an adsorbed state, and a Langmuir-Hinshelwood model can describe the reaction kinetics. Generation of ethylene oxide and CO_2 show a bell-shaped dependence on the concentration of preadsorbed oxygen, but the maximum for ethylene oxide falls at higher oxygen surface concentration than does the maximum for CO_2 formation [vanSanten, 1987].

Paspek [Paspek, 1980] also found that the complete ethylene oxidation over highly dispersed Pt on alumina can be modelized by a Langmuir-Hinshelwood type model. The complete ethylene oxidation over a CeO_2 catalyst proceeds via a formate species intermediate, with the participation of surface lattice oxygen in the absence of gaseous oxygen [Li, 1993b].

Acetaldehyde, acetic acid and oxalic acid have been identified as reaction intermediates for CO_2 formation over silver [Grant, 1985]. However, the rate of formation of ethylene oxide over Ag was found to increase, and the rate of formation of CO_2 to decrease, in the presence of formaldehyde and acetaldehyde. Therefore, the principal precursor to the formation of CO_2 from either ethylene or ethylene oxide would not be the acetaldehyde, but rather an adsorbed ionic intermediate such as ($C_2H_4O_2$) [Thomas, 1967].

Oscillatory behaviour is common in bimolecular oxidation reactions catalyzed by transition metals. The oxidation of ethylene over a Pt/YSZ catalyst exhibits self-sustained oscillations in a certain temperature range and in an excess of ethylene [Slin'ko, 1994; Vayenas, 1981]. The dependence of the adsorption heat on surface coverage, the surface temperature oscillations, and a surface oxidation-reduction mechanism have been proposed to explain this behaviour. The latter mechanism of oxygen storage, involving the periodic formation and destruction of surface platinum oxide, is supported by measurements of the oxygen activity at the surface [Vayenas, 1981].

The detailed mechanism of the complete and selective ethylene oxidation is still a matter for debate. The reported values of the activation energy vary from 50 to 109 kJ/mol for the epoxidation and from 63 to 142 kJ/mol for the complete ethylene combustion. Large discrepancies also exist in the reported values for the reaction order. Apparent orders from -0.3 to 2 are found with respect to oxygen and from 0 to 1 with respect to ethylene.

2.4 NON-FARADAIC ELECTROCHEMICAL MODIFICATION OF CATALYTIC ACTIVITY

The term promotion does not occur frequently in the titles of papers on catalysis, yet the majority involve modification or enhancement of the catalytic activity. The phenomenon called promotion is defined by Margolis [Margolis, 1963] as the "increase in catalytic activities of various semiconductors and metals by addition of certain impurities". It is a relative phenomenon since it suggests an improvement compared to some baseline condition. The action of promoters can be explained by support effects, site creation, electronic and geometric effects, synergism, increased catalyst lifetime and redox effects.

2.4.1 Promotion in heterogeneous catalysis

In his review on promotion [Thomson, 1987], Thomson remarks that the application of electric fields to catalysis has been neglected, yet important changes had been observed not only in rates of reaction and yields, but also in extents of adsorption. Lincoln and Olinger [Lincoln, 1975] proved that surface interactions of a fluid and solid could be affected through application of an appropriate electric field. The adsorption of some gases on metal surfaces was enhanced by the application of a 4 kV AC voltage. In the catalytic ethylene hydrogenation on Ni, a mechanism shift and higher reaction rates were apparent in the kinetically controlled process, but no effect of the imposed voltage was apparent in the diffusion-controlled process.

The idea that the electronic properties of metals, alloys or semi-conductors are intimately related to the chemisorptive and catalytic activities of these solids forms the basis of the "electronic factor" in catalysis. The electronic approach aims at establishing a relationship between the catalytic activity of solids ant the electronic structure of the bulk solid. Adsorption influences the catalyst work function due to the formation of a double electrical layer accounted for by dipoles of adsorbed particles [Margolis, 1963]. Adsorbates displaying a higher electronegativity than the catalyst increase the work function and form dipoles with the negative charge outwards. This is the case for adsorbed oxygen, while the contrary is observed for ethylene. The same explanation was proposed for the effect of impurities on the reaction rate [Margolis, 1963]. The addition of electron acceptors provokes an increase in the work function $e\Phi$ and the addition of donors a decrease.

Metal-support interactions influence both the electronic state of the metal and its precise morphology. Electronic interactions are often believed to modify activation energies, whereas structural alterations would affect pre-exponential factors. However, structural changes may occur due to electronic factors like in the case of alkali-metal modifiers on Ag. The modifiers induce the reconstruction of the open (110) surface to the close-packed (111) one which favours epoxidation [Thomson, 1987].

The interfacing of catalysis and electrochemistry is at the origin of the electrochemical oxygen pumping technique, which consists in applying an external electrical field to a solid electrolyte cell and modifying the catalytical properties of the electrode-catalyst. This technique was applied in the study of methane conversion over Ag-Ni and Cu catalysts supported on YSZ [Belyaev, 1993]. This reaction occurs to

a negligible extent under open-circuit conditions and is enhanced by electrochemical oxygen pumping (EOP) to the catalyst. However, under continuous electrochemical supply of oxygen, an important decrease in rate and selectivity towards C_2 hydrocarbons was observed with time. The conversion of oxygen pumped to the reaction zone was complete. The results were explained by the formation of Ni and Cu oxides, promoters of complete oxidation, upon electrochemical pumping. The rate and selectivity could be enhanced by a factor 2, if the current was switched off for 1 min every 8-10 min. The oxides were then reduced by methane [Belyaev, 1993].

This unsteady-state mode of operation is similar to the periodic operation of catalytic reactors, where flow-cycling, reactor-temperature cycling and periodic composition forcing are used to enhance reaction rates or selectivities. As input variables are cycled between two or more conditions, reaction rates vary because of adsorbate changes as well as changes in the activation energy and the frequency factor. If surface or bulk phase transitions are slow relative to the forcing period, the catalyst will operate in a transient state, which can lead to improved rates, selectivity, or yields [Silveston, 1995]. They regretted that models predicting improved performance under cycling are not supported by experimental data, whereas experimental systems with confirmed improvement do not have adequate models [Silveston, 1995].

Actually, the work of Vayenas and co-workers on the NEMCA effect is an attempt to change the above mentioned situation. In many respects, this electrochemical promotion can be considered a periodic operation with the applied voltage as input variable. It is a tool for the control of conversion or selectivity in a chemical reactor. Although it is more complicated and more expensive than steady operation, industrial applications may appear reasonable in particular cases such as in-situ regeneration of an expensive catalyst, increased selectivity towards particular fine chemicals or reactions with limited conversion per pass.

2.4.2 General features of NEMCA

Vayenas et al. used the EOP technique to study the influence of oxygen pumping on the catalyst activity and selectivity. In 1988, they proposed the term "Non-faradaic Electrochemical Modification of Catalytic Activity" (NEMCA) to describe the remarkable effects of non-faradaic origin they observed [Bebelis, 1989]. The more general term "electrochemical promotion" was later proposed by Pritchard [Pritchard, 1990].

External voltages provoke a remarkable, reversible enhancement of the catalyst activity and selectivity when applied to cells of the type:

gaseous reactants, metal catalyst / solid electrolyte / metal, O_2

The rate of ions supply to or removal from the catalyst is given by $G = I / nF$, assuming that all the current is ionic. In the case of oxygen ion conductors, the electrochemical supply rate is defined as

$$G_o = I / 2F \text{ [molO/s]} \qquad (2.17)$$

and the current is taken as positive when O^{2-} are supplied to the catalyst [Yentekakis, 1988].

Under open-circuit conditions, the regular catalytic rate is r_o and the catalyst potential $V°_{WR}$. Upon changing the catalyst potential V_{WR} with respect to the reference electrode, the catalytic reaction rate becomes r'. The following terms are useful for the description of NEMCA:

$$\Delta r = r' - r_o \text{ [molO/s]} \quad (2.18)$$

is the induced change in the catalytic reaction rate,

$$\rho = r' / r_o \text{ [-]} \quad (2.19)$$

is the reaction enhancement ratio, and

$$\Lambda = \Delta r / G_o \text{ [-]} \quad (2.20)$$

is the enhancement factor which allows the comparison between the induced catalytic rate change and the electrochemical rate of ion supply.

The term "non-faradaic" implies that the change in the catalytic reaction rate exceeds the electrocatalytic rate of the oxygen transport reaction [Bebelis, 1989]. So, a system is considered to exhibit the NEMCA effect when $|\Lambda| > 1$. The effect is called electrophobic when $\Lambda > 1$ and the rate enhancement is due to the positive polarization of the catalyst. It is called electrophilic when $\Lambda < 1$ and the rate enhancement is provoked by the application of negative potentials to the catalyst.

The exchange current I_o is a measure of the electrocatalytic activity of the catalyst-zirconia interface for the reaction:

$$O^{2-} \Leftrightarrow O(a) + 2e^-$$

The value of I_o is proportional to the TPB length and depends on the chemisorbed oxygen coverage of the catalyst surface. Low I_o values indicate a highly polarizable interface across which small currents create high overpotentials and consequently large NEMCA effects [Vayenas, 1994a]. The magnitude of the enhancement factor can be predicted for a given system from the relation:

$$\Lambda \approx 2Fr_o / I_o$$

The relaxation time τ_N is defined as the time required for the rate increase to reach 63% of its final steady-state value. This definition is based on the assumption that the observed transients behave like first-order systems, which is usually the case and

$$\Delta r = \Delta r_{max} (1-\exp(-t/\tau_N)).$$

The order of the relaxation time is

$$\tau_N \approx 2FN_t / I$$

where N_t [molO] is the total number of catalyst surface sites, measured as the atomic oxygen uptake on the catalyst. So, τ_N corresponds to the time required to form a monolayer of an oxygen specie on a surface with N_t sites, when it is supplied at a rate G_o. This relation shows that the NEMCA is a catalytic effect taking place over the entire catalyst surface [Vayenas, 1992a]. It does not create any new catalytic reaction pathways, but simply accelerates the existing ones. In addition, the fact that τ_N is so long, typically many minutes, rules out the possibility of any purely electrochemical interpretation [Vayenas, 1993a].

The central parameter for understanding the NEMCA effect is not the enhancement factor Λ, but the catalyst-electrolyte activation overpotential $\eta = V_{WR} - V^{\circ}_{WR}$, where V_{WR} is the ohmic-drop-free catalyst potential [Bebelis, 1989].

It was shown both theoretically [Bebelis, 1989; Vayenas, 1992a] and experimentally [Ladas, 1991] by means of a Kelvin probe, that solid electrolyte cells are work function probes for their gas-exposed electrode surfaces:

$$e\cdot\Delta V_{WR} = \Delta e\Phi \tag{2.21}$$

This equation plays a key role in understanding and interpreting the NEMCA effect, so the theoretical explanation will be provided here [Vayenas, 1992b].

Consider a porous metal film deposited on YSZ, schematically depicted in figure 2.13. The electronic properties of the metal-solid electrolyte interface E are altered by electrochemical polarization. This perturbation is then propagated via the spatial constancy of the Fermi level throughout the metal film to the metal-gas interface C, altering its electronic properties.

The measured potential difference (ohmic-drop-free) between the working and reference electrodes is the difference in the Galvani potentials of the two electrodes:

$$V_{WR} = \phi_W - \phi_R \tag{2.22}$$

Taking into account the electrochemical potential $\bar{\mu} = \mu - e\phi$, equation (2.9) becomes:

$$eV_{WR} = \bar{\mu}_R - \bar{\mu}_W + (\mu_W - \mu_R) \tag{2.23}$$

The electrochemical potential is also equal to the sum of the work function $e\Phi$ and the Volta potential $e\psi$ (§2.1.3):

$$\bar{\mu} = -e\Phi - e\psi \tag{2.24}$$

Although $e\Phi$ and $e\psi$ are not necessarily uniform over the metal surface, their sum has to be spatially uniform. This is true even when an electrical current is passing through the metal film , provided that the ohmic drop in the film is negligible. Note that, by definition, ψ vanishes if there is no net charge on the metal surface. Combining equations (2.23) and (2.24):

$$eV_{WR} = e\Phi_W - e\Phi_R + e(\psi_W - \psi_R) + (\mu_W - \mu_R) \tag{2.25}$$

This equation is valid under open-circuit and closed-circuit conditions for the surface E in contact with the electrolyte and the gas-exposed surface C:

$$eV_{WR} = e\Phi_{W,E} - e\Phi_{R,E} + e(\psi_{W,E} - \psi_{R,E}) + (\mu_W - \mu_R) \tag{2.26}$$

$$eV_{WR} = e\Phi_{W,C} - e\Phi_{R,C} + e(\psi_{W,C} - \psi_{R,C}) + (\mu_W - \mu_R) \tag{2.27}$$

Assuming that, when V_{WR} is changed by ΔV_{WR}, the properties of the reference electrode remain unaffected and μ which is a pure bulk property also remains constant, equation (2.27) is written as:

$$e\Delta V_{WR} = \Delta e\Phi_{W,C} + e\Delta\psi_{W,C}$$

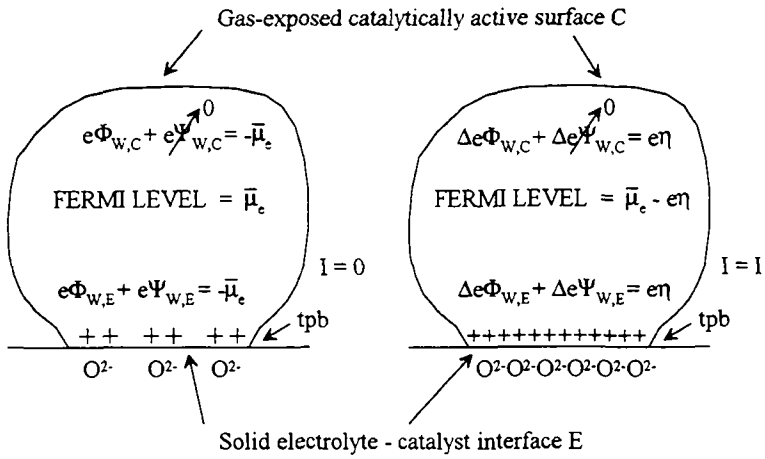

Fig. 2.13 Schematic representation of a metal crystallite deposited on YSZ and of the changes induced in its electronic properties upon polarizing the catalyst-solid electrolyte interface [Vayenas, 1992a].

All the net charge in the metal will be localized in region E facing an equal and opposite charge in the solid electrolyte. No net charge can be sustained in region C, therefore $\psi_{W,C} = 0$ under both open-circuit and closed-circuit conditions:

$$e\Delta V_{WR} = \Delta e\Phi_{W,C} \tag{2.28}$$

This equation is valid even if the reference electrode is not of the same bulk material as the working electrode. If, however, the reference electrode and the catalyst are of the same metal and are both at the same temperature, then $\mu_W = \mu_R$ and the equation (2.27) under open-circuit conditions becomes:

$$eV^{\circ}_{WR} = e\Phi_{W,C} - e\Phi_{R,C} \tag{2.29}$$

For the work function to change something must have changed on the surface. There is strong experimental evidence that the work function modification is due to spillover ions originating from the solid electrolyte and spreading over the catalytically active surface of the catalyst [Vayenas, 1992b]. The spillover mechanism will be presented in more detail later in the chapter section on the origin of NEMCA.

An important finding in all previous NEMCA studies is that, over wide potential ranges (0.2 - 0.8V), the catalytic rates r' depend exponentially on the ohmic-drop-free catalyst potential or, equivalently, on the work function of the catalyst surface [Ladas, 1991]:

$$\ln (r'/r_o) = \alpha \cdot e \cdot (V_{WR} - V^*_{WR}) / k_bT \tag{2.30}$$

$$\ln (r'/r_o) = \alpha \cdot e \cdot (\Phi - \Phi^*) / k_bT \tag{2.31}$$

where α, V^*_{WR}, and Φ^* are reaction- and catalyst-specific constants, and k_b is the Boltzmann's constant. Over the same potential ranges, the activation energy of catalytic reactions changes significantly and usually linearly with V_{WR} and $e\Phi$.

Similar variations of the reaction rate and activation energy with work function have already been reported for catalysts modified by the addition of impurities [Margolis, 1963]. A linear dependence of the

activation energy on eΦ has been observed for oxygen chemisorption and formation of acrolein and CO_2 from propene over CuO catalysts. The selectivity of the propene oxidation towards acrolein synthesis increased linearly with eΦ [Margolis, 1963]. The catalytic rate dependence on eΦ was exponential to a first approximation, but more complicated than equation (2.31). The rate of CO_2 formation from acrolein was represented as:

$$r = K_o \cdot C_{acr} \cdot \exp\left(\frac{-E_{O_2} + Q_r + \Delta e\Phi}{RT}\right)$$

where the activation energy E_{O_2} depended linearly on eΦ, while the preexponential factor K_o varied exponentially with eΦ in a limited work function range [Margolis, 1963]. The isotopic oxygen exchange rate increased with eΦ, indicating that the surface concentration of oxygen is controlled by the electron work function.

The nature of ethylene oxidation kinetics over Ag was also explained by the variation of surface concentrations with eΦ. The addition of acceptor impurities to Ag was found to raise the reaction order for oxygen and decrease it for ethylene. The decrease in reaction rate with increasing eΦ was greater for a higher reaction order with respect to oxygen. The changes in reaction rates with work function were different for low and high conversions [Margolis, 1963].

The above results support the idea that the β"-Al_2O_3 electrolyte acts as a reversible Na^+ donor which controls precisely in situ the Na coverage and eΦ of the Pt surface [Yentekakis, 1994].

2.4.3 Reactions exhibiting NEMCA

Until today, more than 30 catalytic reactions on Pt, Pd, Rh, Ag, Au and Ni, supported on O^{2-}, F^-, Na^+ and H^+ conducting solid electrolytes, have been found to exhibit the NEMCA effect. Work prior to 1992 has been reviewed in a monograph [Vayenas, 1992a]. In addition to the group of Vayenas which first reported the effect [Yentekakis, 1988; Bebelis, 1989; Vayenas, 1991a; Vayenas, 1992b; Vayenas, 1993c; Vayenas, 1994b; Vayenas, 1993b; Vayenas, 1994a; Ladas, 1993], many other research groups have also made significant contributions in this area [Harkness, 1995; Andersen, 1994; Eng, 1991a; Stoukides, 1991; Stoukides, 1993; Saracco, 1994; Mar'ina, 1992; Mahmood, 1992; Mar'ina, 1993; Sobyanin, 1993; Yentekakis, 1994; Bockris, 1994]. Recently, a similar effect of electrochemical enhancement was observed in aqueous solution at ambient temperatures [Neophytides, 1994].

Some of the catalytic reactions exhibiting the effect are listed in table 2.1, where they are classified in electrophobic and electrophilic ones [Vayenas, 1992a]. A change in product selectivity ΔS upon polarization is also indicated. Note that the last reactions in each section exhibit both electrophobic and electrophilic NEMCA, depending on the partial pressure of the reactants and the value of the applied potential.

More care is needed when β"-Al_2O_3 is used as solid electrolyte than when the support is YSZ. It must be always stocked in dry air to prevent extensive substitution of Na^+ by protons from water.

Table 2.1 Catalytic reactions exhibiting the NEMCA effect [Vayenas, 1992a]; the reactions noted (*) are from reference [Vayenas, 1995].

Reactants	Products	Catalyst	Electrolyte	T [°C]	Λ_{max}	ρ_{max}	ΔS
Electrophobic effect ($\Delta r > 0$ with $I > 0$)							
C_3H_6, O_2	C_3H_6O, CO_2	Ag	ZrO_2-Y_2O_3	320-420	300	2	yes
C_2H_4, O_2	C_2H_4O, CO_2	Ag	ZrO_2-Y_2O_3	320-470	300	3	yes
C_2H_4, O_2	C_2H_4O, CO_2	Ag	β"- Al_2O_3	350-410	$3 \cdot 10^3$	3	yes
C_2H_4, O_2	CO_2	Pt	ZrO_2-Y_2O_3	260-450	$3 \cdot 10^5$	55	
C_2H_4, O_2	CO_2	Pt	β"- Al_2O_3	180-300	$5 \cdot 10^4$	4	
CH_4, O_2	CO_2, C_2H_4, C_2H_6	Ag	ZrO_2-Y_2O_3	650-850	5	30	yes
CH_4, H_2O	CO, CO_2, H_2	Ni	ZrO_2-Y_2O_3	600-900	3	2	yes
CO, O_2	CO_2	Pd	ZrO_2-Y_2O_3	400-550	$1 \cdot 10^3$	1.5	
CO_2, H_2	CH_4, CO	Rh	ZrO_2-Y_2O_3	390-450	40	2	yes
C_2H_6, O_2	CO_2	Pt	ZrO_2-Y_2O_3	400-500	300	20	(*)
CO, O_2	CO_2	Ag	ZrO_2-Y_2O_3	350-450	20	5	
CO, O_2	CO_2	Pt	ZrO_2-Y_2O_3	300-550	$2 \cdot 10^3$	3	
CH_4, O_2	CO_2	Pt	ZrO_2-Y_2O_3	600-750	5	70	yes
CH_3OH, O_2	H_2CO, CO_2	Pt	ZrO_2-Y_2O_3	300-500	10^4	4	yes
Electrophilic effect ($\Delta r > 0$ with $I < 0$)							
CH_3OH	H_2CO, CO, CH_4	Ag	ZrO_2-Y_2O_3	550-750	-25	6	yes
CH_3OH	H_2CO, CO, CH_4	Pt	ZrO_2-Y_2O_3	300-500	-10	3	yes
C_3H_6, O_2	CO_2	Pt	ZrO_2-Y_2O_3	250-400	$-3 \cdot 10^3$	6	(*)
C_2H_6, O_2	CO_2	Pt	ZrO_2-Y_2O_3	400-500	-100	7	(*)
CO, O_2	CO_2	Ag	ZrO_2-Y_2O_3	350-450	-800	15	
CO, O_2	CO_2	Pt	ZrO_2-Y_2O_3	300-550	-500	6	
CH_4, O_2	CO_2	Pt	ZrO_2-Y_2O_3	600-750	-5	30	yes
CH_3OH, O_2	H_2CO, CO_2	Pt	ZrO_2-Y_2O_3	300-500	-10^4	15	

If small currents and reversed cell operation are employed, Na^+ depletion is avoided and it is not necessary to maintain the counter and reference electrodes in contact with molten Na [Vayenas, 1991a]. The enhancement factor Λ is not a very meaningful quantity when using β"-Al_2O_3, since Na is not a reactant nor a product; "infinitely" large Λ values can be obtained if the current were to vanish at steady-state after having caused a steady-state rate increase Δr [Yentekakis, 1994].

The catalytic oxidation of C_2H_4 over Pt/YSZ is one of the systems which exhibits the most striking electrophobic NEMCA effect (Table 2.1). The dramatic increases are obtained in fuel-lean gaseous compositions, where the rate is first order in C_2H_4 and zeroth order in O_2 (§2.3). According to the Eley-Rideal mechanism, the reaction between chemisorbed oxygen and gaseous ethylene is then rate limiting. The rate increases regularly with increasing current until a plateau is reached. When this happens the order of the reaction changes abruptly and becomes zero in C_2H_4 and first order in O_2. The oxygen adsorption step becomes rate limiting and the reaction rate does not increase any longer with current [Bebelis, 1989]. The different behavior between the fuel-rich and fuel-lean sides shows that O^{2-} pumping has practically no effect on the oxygen adsorption kinetic constant and has a pronounced effect on the kinetic constant for the reaction.

The electrophobic behaviour of the system is explained by the weakening, with increasing $e\Phi$, of the Pt = O chemisorptive bond, the cleavage of which is involved in the rate-limiting step [Bebelis, 1989]. However, a study on the homomolecular oygen isotopic exchange on Pt/YSZ [Sobyanin, 1993] contradicts the above explanation: neither anodic nor cathodic polarizations of the Pt electrode influenced the rate of oxygen exchange with respect to its open-circuit value. The authors conclude that the strength of the oxygen chemisorptive bond on Pt remains unchanged during polarization.

The CO oxidation over Pt occurs via a Langmuir-Hinshelwood mechanism, where both reactants are in the adsorbed state and volcano-type behaviour is observed. The location of the rate maximum is not significantly affected with increasing potential and $e\Phi$, indicating that both chemisorptive bonds are weakened. So, the reaction rate is enhanced until the coverages become very low and the rate starts to decrease [Vayenas, 1995]. The CO disproportionation and subsequent carbon combustion was proposed to explain the pronounced electrophilic effect [Yentekakis, 1988].

The CO oxidation is known to exhibit oscillatory behaviour under certain conditions. The oscillations can be started or stopped at will by the enforcement of an appropriate current, and the potential oscillates at the same frequency as the rate [Yentekakis, 1988]. Variations in CO and O coverages on a Pt(110) surface during oscillations were visualized using a recently developed photoemission electron microscope for which the contrast is determined by variations in the local work function associated with the dipole moments of the adsorbates [Ertl, 1990].

The ethane oxidation over Pt/YSZ was studied in an undivided cell and exhibits mixed NEMCA behaviour. The open-circuit kinetics indicate that the oxygen coverage is always predominant and the ethylene coverage low. The electrophobic effect is then attributed to enhanced ethane chemisorption and a weakening in the Pt=O bond [Vayenas, 1995]. To explain the rate enhancement with negative currents

($V_{WR} < V°_{WR}$) one must take into account that, since in this case no backspillover of ions can take place, the surface oxygen coverage must decrease to obey the equation $\Delta(e\Phi) = \Delta V_{WR}$. Consequently, the rate increase can again be attributed to the electrochemically induced decrease in oxygen coverage and enhancement in ethane chemisorption [Vayenas, 1995].

A seventyfold increase in methane oxidation rate was obtained in 10 kPa CH_4 and 0.25 kPa O_2 and is also due to the weakening of the Pt=O bond with increasing work function [Vayenas, 1995]. The electrophilic effect is probably due to the fact that decreasing $e\Phi$ strengthens the Pt=O bond and thus enhances the activation of the C-H bond in CH_4 to form CH_3· radicals which can then be rapidly oxidized in the gas phase [Vayenas, 1995]. Mar'ina et al. [Mar'ina, 1993] confirmed the enhancement of methane oxidation over Pt upon oxygen pumping to the catalyst and believe that "new" active sites are created due to the formation of platinum oxide. In the temperature range 650-720°C, they also observed a slight enhancement of the methane oxidation over Au, but the rate increase could be explained by direct electrochemical oxidation.

Harkness and Lambert [Harkness, 1995] reported the electrochemical promotion of the ethylene oxidation by NO over Pt films supported on β"-Al_2O_3, when Na^+ ions are supplied to the catalyst. A finite value of $\rho = 15$ was obtained under specific experimental conditions, but, in a range of temperature and gas composition, the open-circuit rate was immeasurably small, yielding infinite values of the rate enhancement factor.

2.4.4 Origin of NEMCA

The spillover phenomenon can be defined as the transport of an active species from a donor phase, where it is adsorbed or formed to an acceptor phase, where it could not be adsorbed or formed. As Delmon noted [Delmon, 1994], the spillover phenomenon has been faced with a steady scepticism. It has been shown to account for acceleration of solid-state reactions, increase of selectivity, acceleration of catalytic reactions, inhibition of catalyst deactivation and creation of catalytic sites, but, at each stage of the discoveries, the scientific community resisted accepting it [Delmon, 1994].

Some species on the surface of industrial catalysts play a crucial role in regulating activity and selectivity. Atoms are known to be highly mobile on surfaces. When these mobile species come from a phase distinct from the catalyst and have to travel a certain distance to accomplish their regulating role, this corresponds to a sort of "remote control" [Delmon, 1994].

Oxygen and hydrogen are the most studied spillover species [Delmon, 1993; Fujimoto, 1993; Inui, 1993; Haruta, 1993; Moro-oka, 1993; Barrett, 1993; Li, 1993a] and were found to play the role of coke scavenger, when hydrocarbons are involved as reactants, or co-catalysts in redox control, preserving and tuning the right valency state on cations. Spillover oxygen is assumed to be monoatomic O species electrically charged or not, such as O, O^- and O^{2-}. If Brönsted acid sites are generated by oxygen spillover and Lewis acid sites by hydrogen spillover, a supported metal or oxide catalyst might become bifunctional [Teichner, 1993]. Isocyanate, CO, methoxy and formate species or hydrocarbons have also been found to

spill from a donor to an acceptor site [Laboratoire des Matériaux et procédés catalytiques, 1993]. Water is not required for spillover but can assist in the exchange process [Conner Jr., 1993].

Nam and Silveston proposed a mathematical model for spillover [Nam, 1993], where the catalyst surface is deemed to consist of an active region where reaction and adsorption/desorption occur, and an inactive region where dissociatively adsorbed species are stored. Reaction is considered possible while the spillover species migrate to or from the inactive region. The authors believe that spillover can be positively identified in a system by imposing periodic operation.

An X-ray photoelectron spectroscopy (XPS) investigation of Pt films on YSZ under positive current application [Ladas, 1993] showed the simultaneous presence of normally chemisorbed atomic oxygen (O1s at 530.2 eV) and of an oxidic spillover oxygen (O1s at 528.8 eV). This observation provides an explanation for the origin of NEMCA over YSZ, schematically represented in figure 2.14: spillover oxide ions (O^{2-}, O^{-} or $O^{\delta-}$) generated at the TPB upon electrochemical O^{2-} pumping to the catalyst spread over the gas-exposed catalyst-electrode surface. They are accompanied by their compensating charge in the metal, thus forming spillover dipoles. Due to the strong lateral repulsive interactions between the parallel-oriented surface dipoles, their migration on the surface is fast. The surface dipoles establish an effective electrochemical double layer which increases the catalyst surface work function and affects the strength of chemisorptive bonds. The binding strength or adsorption heat of covalently bonded adsorbates is affected both via direct electrostatic interactions in the double layer (usually termed through-the-vacuum interactions) or through-the-metal interactions [Vayenas, 1994b].

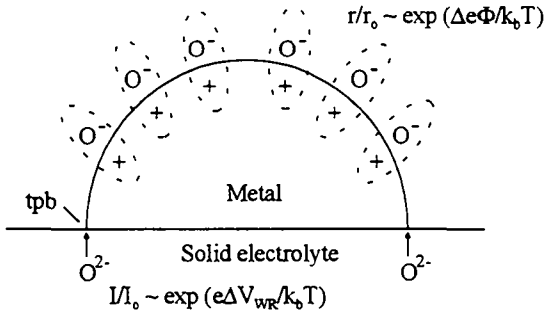

Fig. 2.14 Origin of NEMCA: upon polarization of the metal-solid electrolyte interface the catalyst potential changes by ΔV_{WR} and the catalyst work function by $\Delta e\Phi = e\Delta V_{WR}$ due to ion spillover [Vayenas, 1992b].

The oxidic state of spillover oxygen is *less* reactive than chemisorbed oxygen and the slow growth of its signal parallels the slow increase in the catalytic rate. This oxidic state is proposed to increase the reactivity of chemisorbed oxygen. Gas-phase supplied oxygen cannot produce the same surface species [Ladas, 1993].

The distances to be covered by spillover ions are surprisingly long (1-40μm), yet the spillover ion hypothesis is consistent with the observation that the catalytic rate relaxation time constant τ_N upon constant current application is of the order of 2FN/I, where N is the total metal catalyst area [Ladas, 1993]. The current dependence of the time constant τ_N is explained by the fact that the RDS for spillover is the formation of the spillover dipoles at the TPB and not their surface diffusion on the catalyst surface [Vayenas, 1993b].

In the case of β"-Al_2O_3, the solid electrolyte allows a controllable, measurable and reversible dosing of Na onto the catalyst surface. The existence of a threshold eΦ value, below which the catalytic rate is insensitive to work function variations, could be related to the formation of Na_2O, NaOH or Na_2CO_3 on the surface, in the presence of O_2, H_2O and CO_2 in the reactor. Such reactions can explain why a very small current (<1μA) is sustained at steady state [Vayenas, 1991a].

The fact that very small Na coverages suffice to induce a pronounced decrease in the rate of C_2H_4 oxidation rules out the possibility of a purely geometrical interpretation of the effect [Vayenas, 1991a]. Whether activation and poisoning by adsorbed species are short-range effects involving adjacent sites or long-range effects mediated through the electronic band structure, is a long-standing question. The NEMCA effect supports the idea that long-range influences are essential: if the effect were localized only to the catalyst atoms immediately adjacent to adsorbed Na, the expected rate decrease would be an order of magnitude smaller than the observed one [Vayenas, 1991a]. However, "short-range" explanations cannot be easily ruled out: if the spillover ions were producing a short-range effect but their mobility were so high that their average surface migration time from one catalytic site to another were shorter than the catalytic reaction time, then one would macroscopically observe a "long-range" effect [Vayenas, 1991a].

In conclusion, solid electrolytes can act as dopant donor phases to significantly enhance metal catalyst performance. The NEMCA effect does not appear to be limited to any specific type of catalytic reaction, metal catalyst or electrolyte. It is a general effect in heterogeneous catalysis with numerous potential theoretical and practical applications. At the very least, it will allow a systematic study and enhanced understanding of the promoters' role in heterogeneous catalysis [Vayenas, 1995].

CHAPTER 3

EXPERIMENTAL

The experimental apparatus has been primarily conceived for the study of the catalyst under an electrochemical polarization regime. The coupling of different electrochemical and heterogeneous catalysis techniques implies some practical problems. For these reasons, the apparatus and especially the reactor have not been optimized for the study of the catalytic oxidation kinetics.

The global experimental setup, presented in figure 3.1, is composed of the feed unit, the reactor, and the analysis unit, which will be subsequently presented in detail.

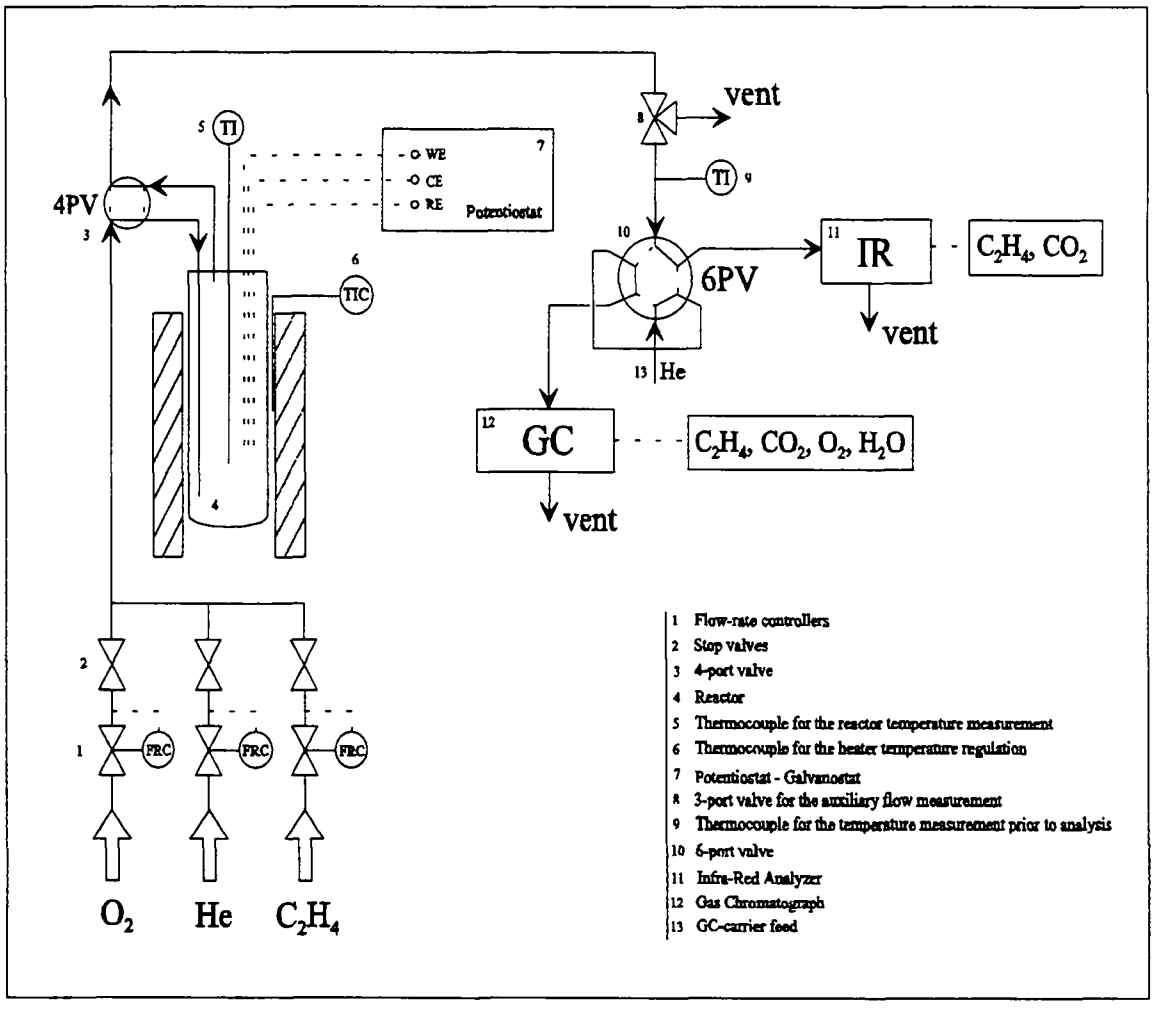

Fig. 3.1 Global experimental setup

3.1 THE FEED UNIT

The reactants are certified mixtures from Carbagas of 1% C_2H_4 and 20% O_2 or 1% O_2 in ultrapure He (99,999%), which can be further diluted with pure He (99,996%). The mass flow of each reactant can be regulated in the range 0-500 Nml/min by a mass flow controller (Bronkhorst Hi-Tec, F-201c) via a control panel (Bronkhorst Hi-Tec, E-5514-FA), which allows a very precise variation of the reactants' concentration while keeping the total flow rate constant. The mass flow controllers have been calibrated under an inlet pressure of 180 kPa, with a bubble-flowmeter.

The choice of the low ethylene mixture concentration (1% in helium) has been based on two considerations. First, for security reasons, because with a 1% initial mixture the explosion limits of the ternary system C_2H_4 - O_2 - He (inert) [Doepper, 1988] would never be approached. Second, because in some early experiments interesting cyclic voltammograms were obtained in very low oxygen concentrations and the most promising catalyst polarization effects found in highly oxidative conditions.

The reactants are mixed at ambient pressure and get into the reactor via a four-port valve (4PV), which gives the possibility to bypass the reactor for a direct analysis of the feed.

Except for the connections to the reactor, stainless steel pipes of 1/8" external diameter were used. The reactor input and output tubes have a 4mm inner diameter and are made of alumina (Firag, KER 610), in order to avoid the presence of steel in the reaction zone. The alumina tubings are connected to the 4PV via PVC tubings.

In the preliminary experiments, synthetic air of controlled quality from Carbagas and pure N_2 (99,995%) as the inert gas are utilized. The synthetic air however contains an important quantity of carbon dioxide (0,033%) compared to the one produced by ethylene oxidation. In addition, the separation of N_2 and O_2 in the chromatographic analysis would require a second column, and the time for an analysis would double.

3.2 THE REACTOR

The reactor (Fig. 3.2) is a 19 cm long quartz tube (2.9 cm i.d. and 3.3 cm o.d.) with a 110 cm^3 volume. The home-made cover consists of two teflon plates with a *caoutchouc* plate in between, pressed together and sealed with silicone (Dow Corning® 732). Two alumina tubes (Firag, KER 610) with two inner holes, for the three gold wires (electrical conductors) and the thermocouple to be kept apart, cross these plates. In this way, the gold wires and the stainless steel sheeth of the thermocouple are not in contact with the reactants, and the ensemble is more rigid and easy to handle. In order to prevent the gas leaks and electrical shortcircuits, a two-components paste (Fischer Elektronik) with excellent dielectric properties and resistant up to 150°C was used to stick the wires and the alumina together.

The reactor is lowered in an oven made of two heating elements (Sotelem, 350W-220V and 500W-220V), with the upper part remaining outside in order to protect the cover from excessive heating. The heating elements consist of two symmetric segments which are hinged on one side and can be closed on the

other by spring loaded clips. The temperature of each heating zone is regulated separately by a PID controller (RKC, REX-F7) and a thermocouple in contact with the reactor.

In order to characterize the extent of nonideal flow in the vessel, several pulses of CO_2 tracer were injected in the stream entering the reactor [Nicole, 1995]. The resulting residence time distribution could be fitted with a simple mathematical model consisting of two ideal flow reactors in series. It seems reasonable to assume a constant flow stirred tank reactor around the pellet, where the reaction takes place, followed by an ideal plug-flow reactor. The plug-flow section would consist of the reactor's upper cold part and the pipes to the analysis apparatus.

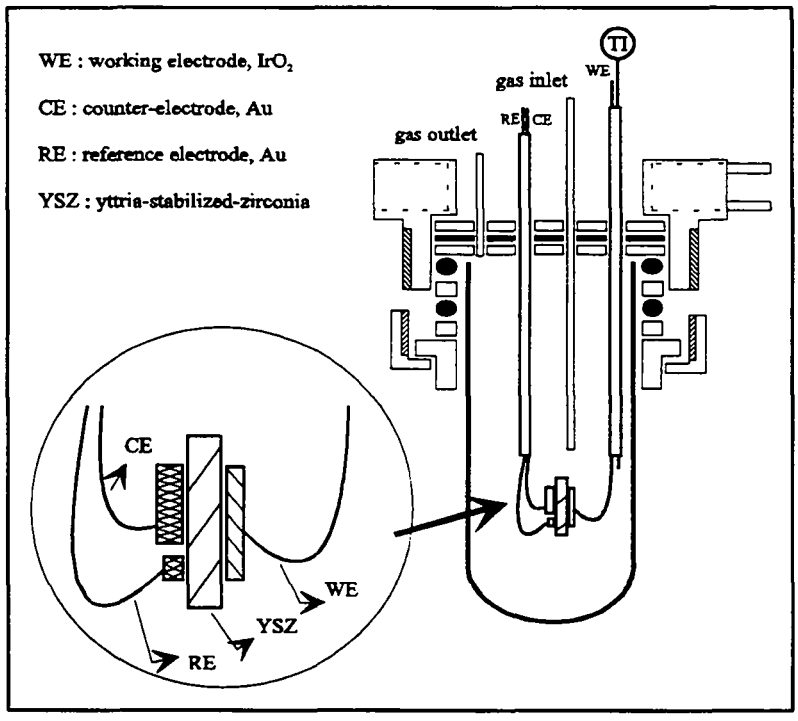

Fig. 3.2 Schematic representation of the reactor

3.2.1 The electrochemical cell

From the point of view of electrochemistry, the reactor functions as an electrochemical cell. The three-electrodes configuration is shown in figure 3.3 with a schematic representation of the electrical field, in the case where the catalyst (working electrode) is acting as the anode. The potential is applied between the working electrode (WE) and the counter electrode (CE) and it is measured between the WE and the reference electrode (RE), in order to avoid including the ohmic drop (R_e) in the electrolyte in the measurement. Although no current is supposed to pass through the RE, the current lines indicate that this is not exactly true. If the equipotential line, which cuts the RE, is drawn perpendicular to the current lines, some ohmic drop due to the uncompensated resistance (R_u) is still included in the measured potential V_{WR}.

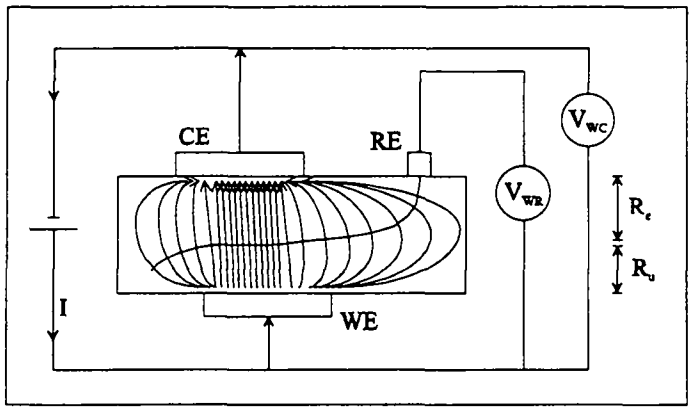

Fig. 3.3 The three-electrodes system with the working electrode acting as the anode

A simple equivalent electrical circuit for this configuration is presented in figure 3.4 where R_f is the faradaic resistance, C_d is the double layer capacitance, R_e is the ohmic contribution of the electrolyte which is eliminated by the use of the reference electrode, and R_u is the uncompensated resistance of the electrolyte. When no faradaic reaction takes place, for example when the applied overpotential is very small, the equivalent circuit can be even more simplified with only C_d in series with R_u between the RE and the WE.

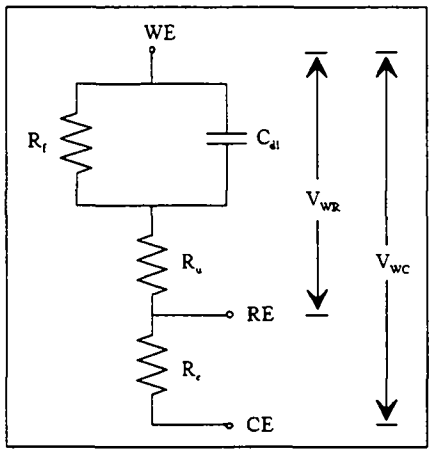

Fig. 3.4 A simple equivalent electrical circuit for the three-electrodes electrochemical system

Choice of the configuration

This configuration of the three-electrodes system, i.e. the relative position of the three electrodes, is not unique, although it is the most widely employed. Three different cell arrangements are presented in figure 3.5. In a divided cell, the RE should be preferably exposed to a gas of controlled composition (arrangement A or B). When the WE and RE are placed side by side (arrangement C) [VanManen, 1992; Velle, 1991; Robertson, 1990], the variation in the composition of the gas due to the reaction at the WE may affect the potential of the RE. The same problem can arise when the CE and RE lie on the same side (arrangement A), but to a much lesser extent.

Mizusaki et al. [Mizusaki, 1994] tested various configurations and chose the arrangement B in a divided cell on the basis of reduced polarization curves, I/σ_e vs overpotential, where σ_e is the electrode interface conductivity. The electrical field is very different and this case is difficult to compare with the two others. However, the proximity of the WE and CE is not suitable in our case, where a heterogeneous reaction takes place simultaneously with the electrochemical oxygen reaction. The carbon dioxide should be produced on the WE as far as possible from the CE in order to minimize its eventual adsorption.

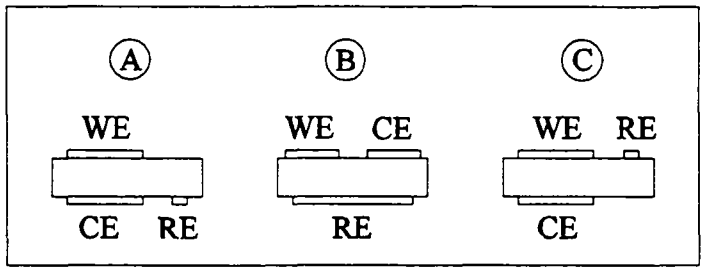

Fig. 3.5 Schematic illustration of three different cell configurations

Note that the simulated electrical field in figure 3.3 is not perfectly symmetrical, because the WE and CE are not exactly opposite, although they have the same surface for the current densities to be equal. The resulting equipotential line probably lies near the WE, minimizing the effect of the uncompensated resistance. However, the exact location of the equipotential line is not known, and it is not possible to predict it on the basis of the cell geometry.

Divided versus undivided electrochemical cell

The reactor type chosen is in fact an undivided cell: the working and the counter electrodes are both in contact with the reactive mixture. Undivided cells are most promising for industrial applications because of the simple and low-cost construction but divided cells are generally more appropriate for mechanistic studies.

In the divided cell, the yttria-stabilized-zirconia (YSZ) solid electrolyte plate would act as a separator between the working electrode (catalyst), in contact with the reactants, and the counter-electrode applied on the other side. The reference electrode, which lies on the same side as the counter-electrode, could then be maintained in a medium of invariable concentration such as air. In this case, a "zero" potential line can be defined with respect to air. This configuration presents a disadvantage when the oxygen partial pressure in the reaction mixture (WE-side) is much lower than in air (CE and RE-side): the YSZ being an oxygen ion conductor, there will be an oxygen flux towards the reaction zone under the influence of the concentration gradient.

In the undivided cell, the potential of the reference electrode changes with the composition of the medium. So, there is a "zero" potential for every composition. In this case, the reference electrode is just used in order to subtract from the potential measurement the ohmic loss in the electrolyte. Furthermore, the

counter and reference electrodes should not be able to catalyze the reaction under study, otherwise it would be difficult to draw any conclusions for the activity of the desired catalyst.

In the beginning, an undivided cell, which was easier to construct, was used. While experiments were performed a divided cell was developed and constructed. However it was not tested since a large amount of interesting results had already been obtained with the undivided cell; much time would have had to be spent to get a complete set of results with the new configuration.

Measurement of the uncompensated resistance

The overall polarization of the working electrode V_{WR} includes the electrode overpotential η and the ohmic drop due to the uncompensated resistance. The electrode overpotential η can be regarded as the potential difference which is needed to compensate the sum of the voltage drops through the electrochemical interface. When a reaction takes place at the interface between the electronically and ionically conducting medium, the rate may be limited by the charge-transfer (activation overpotential) or the mass-transfer (concentration overpotential). For the system of interest to be studied, the ohmic drop should therefore be subtracted from V_{WR}.

The uncompensated resistance R_u includes the resistance of the electrode, the solid electrolyte and that of the wire connections and can be measured by impedance spectroscopy [VanHerle, 1992] or by a current interruption technique [Newman, 1970; McIntyre, 1970; Lucesoli, 1970; Al-Zakri, 1991; Wang, 1979a; Yeager, 1970].

The current interruption technique is based on the fact that, upon a sudden interruption of the current, the ohmic drop disappears instantaneously (within around 10^{-5}s), whereas the other components decrease slowly, generally following exponential relationships. A schematic illustration of the voltage decay, which can be recorded on a storage oscilloscope, is depicted in figure 3.6, where the term IR_u appears as the vertical potential drop. The distinction between the vertical drop and the exponential tail may not be very precise.

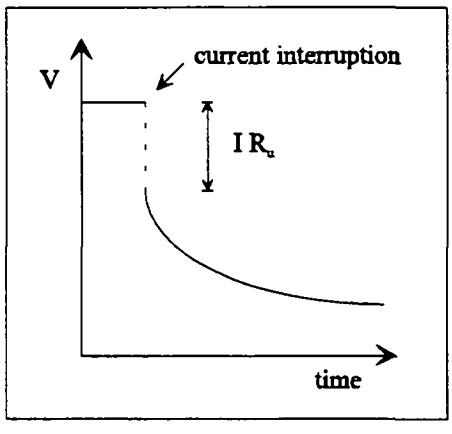

Fig. 3.6 Schematic illustration of the voltage decay upon interruption of the current

Although this method is currently used and IR-drop corrected V_{WR} values are generally presented in the literature, great care must be taken when it is applied on complex systems. The value measured corresponds to the primary current distribution [Newman, 1970]. If the current distribution is not uniform, the double-layer capacitance may prevent a portion of the ohmic loss from disappearing upon interruption of the current and an average value of the ohmic drop will be measured [Yeager, 1970].

Immediately after the current interruption and if the double layer was nonuniformly charged, the current density is not necessarily zero everywhere. In an attempt to uniformize the state of charge a characteristic time for the current to flow may be calculated by:

$$\tau = l_o C_d / \sigma$$

where l_o is a characteristic length of the electrode and σ is the electrolyte conductivity. For an ideally polarizable electrode, this process will precede the decay of charge by a faradaic reaction. The time constant for the double-layer capacity to be discharged by a faradaic reaction may be approximated by

$$\tau = R_f T C_d / F\, i_0$$

where i_0 is the exchange current density. A subsequent potential drop may occur by decay of the concentration overpotential. However, if the surface and concentration overpotentials are small compared to the ohmic drop, the current distribution will approximate the primary distribution and the current interruption method may give the desired ohmic drop [Newman, 1970].

The uncompensated resistance R_u is not necessarily a constant value over a wide range of overpotential and current. It may change due to electrolyte reduction, surface film formation or destruction and current distribution variation. The ohmic drop of the system was measured at several experimental conditions. The value obtained at a given set of temperature, gas phase composition and potential is reproducible with a precision of 10%. For an applied voltage of 0.5V, the ohmic drop never exceeded 5mV. However, when 1V is applied, the ohmic drop varies from 30mV in pure He to 100mV in 20% O_2. The ohmic drop should therefore be measured for each set of conditions. Since this is not always possible, especially in transient conditions (e.g. cyclic voltammetry and rapid potentiostatic pulses), all the results presented here are not IR-drop corrected.

3.2.2 The Yttria-Stabilized-Zirconia solid electrolyte and catalyst support

The solid electrolyte, which also acts as a catalyst support in this study, is cubic zirconia fully stabilized with 6mol% Y_2O_3 (Metoxit AG, 6YSZ). It is prepared by hot isostatic pressing of the precursor powder with an average grain size of 20-30μm and it is non-porous. Some characteristics of the zirconia, given by the supplier, are presented in the table 3.1.

The 26 × 13 × 1 mm YSZ plates are polished with sandpaper (Vitex, P320) to remove the "sinter dust" remaining from the preparation procedure. Then they are washed with deionized water in an ultrasonic bath for one hour.

Table 3.1 Properties of the 6YSZ samples, given by the supplier (Metoxit AG)

specific gravity	5800 kg/m^3
thermal expansion coefficient	10^{-7} K^{-1}
thermal conductivity	2 W/mK
specific heat	550 J/kg K
electrical resistivity at 20°C	10^{15} Ω cm
electrical resistivity at 1000°C	3 Ω cm

In-plane and cross-plane conductivity measurements on different YSZ (6-8% mol) samples showed that the electrolyte is isotropic and of good conductance only if it is highly or totally dense. Van Herle [VanHerle, 1992] measured the conductivity of the YSZ (6% mol) samples used in this work by four different techniques and found it isotropic (identical in-plane and cross-plane conductivities). The Arrhenius plot is shown in figure 3.7 and presents a break at around 600°C, probably due to ion blocking at the grain boundaries [VanHerle, 1992].

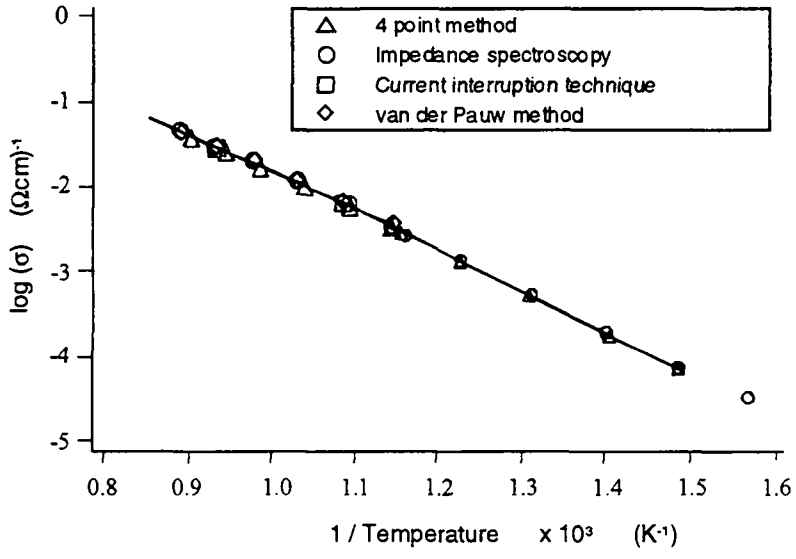

Fig. 3.7 The conductivity of YSZ (6% mol) samples as a function of temperature [VanHerle, 1992]

In the temperature range of interest for our study (250-450°C) the ionic conductivity is quite low, with an important grain boundary resistance and the electronic conductivity is negligible.

In order to make sure that only the cubic phase is present in the 6YSZ sample, an X-ray diffraction analysis (XRD) was performed at grazing angle incidence from $2\theta=25°$ to $2\theta=65°$. The X-ray diffractometer (Rigaku) has a $CuK_{\alpha 1}$ radiation source ($\lambda=1.5406$ Å) and the results can be treated with a pattern-processing software (JADE). No other phase was found indeed, and the pattern (Fig. 3.8) fits very well to the one reported in the JCPDS file No 30-1468 for 8% mol cubic zirconia. A "reduced" sample was also analyzed which had been exposed to high voltages and exhibited a color change from yellow to deep

brown in the region of the electrical field. This is the so called "blackening" of zirconia, the effect of which on the structure and properties of the zirconia is still unclear (see §4.1). The XRD analysis did not reveal any peaks due to the tetragonal phase, which means that the reduced sample is still stabilized in the cubic structure.

The relative intensity of the reflections on the cubic structure planes and the plane spacing is presented in the table 3.2 for the new 6YSZ sample, the "reduced" 6YSZ sample and the 8YSZ standard of the JCPDS data bank. Note that the (220) and (311) planes are less developed in the 6YSZ new sample (reduced relative intensity) and that the peaks shift to slightly higher angles, especially for the less developed planes.

The plane spacing d is calculated by the Bragg law:

$$\lambda = 2d \sin\theta$$

This law states the essential condition for diffraction to occur when a beam of perfectly monochromatic X-rays of wavelength λ is incident on a crystal at an angle θ, where θ is measured between the incident beam and the crystal plane.

Table 3.2 Comparison of the X-Ray reflections intensity and the plane spacing of our 6mol%YSZ sample with an 8mol%YSZ standard (JCPDS No 30-1468).

	6YSZ	Metoxit	new	6YSZ	Metoxit	reduced	8YSZ	JCPDS	30-1468
hkl	**2θ**	d [Å]	Intensity %	**2θ**	d [Å]	Intensity %	**2θ**	d [Å]	Intensity %
1 1 1	**30.155**	2.961	100	**30.147**	2.962	100	**30.084**	2.968	100
2 0 0	**35.001**	2.561	23.4	**34.949**	2.565	25.8	**34.868**	2.571	25
2 2 0	**50.249**	1.814	42.3	**50.246**	1.814	50.8	**50.136**	1.818	55
3 1 1	**59.752**	1.546	26.4	**59.747**	1.547	33.2	**59.597**	1.550	40
2 2 2	**62.744**	1.480	4.4	**62.653**	1.482	2.4	**62.538**	1.484	6

The plane spacing in a cubic structure of lattice parameter *a* is also given by the relation:

$$d = a / (h^2 + k^2 + l^2)^{1/2}$$

which shows that the lowest index planes are the more spaced [vanMeerssche, 1976]. The lattice parameter *a* of the cube, determined from the different plane spacings, is presented in the table 3.3 for a fresh 6YSZ sample, a reduced one and the 8YSZ standard. It increases with the yttria content, since the Y^{3+} radius is higher than the Zr^{4+} one. Note that the reduced sample also presents a slightly higher lattice parameter compared to the fresh sample. This may be due to the strain induced by the reduction of some Zr^{4+} ions to the Zr^{3+} state with a concomitant increase in the ionic radius.

Table 3.3 The cubic lattice parameter *a* for a new 6YSZ sample, a reduced one and the 8YSZ standard

	6YSZ Metoxit new	6YSZ Metoxit reduced	8YSZ JCPDS 30-1468
hkl	*a* [Å]	*a* [Å]	*a* [Å]
1 1 1	5.129	5.130	5.141
2 0 0	5.122	5.130	5.142
2 2 0	5.131	5.131	5.142
3 1 1	5.128	5.131	5.141
2 2 2	5.127	5.134	5.141

Consider a face of the zirconia cube with an area equal to a^2. There are 2 zirconium ions in this area. A simple calculation shows that 3.8 10^{14} Zr^{4+} ions correspond to a 0.5 cm^2 surface, equal to the geometric catalyst surface.

The cubic lattice parameter of stabilized zirconia can be estimated as a function of the stabilizer mole percentage by the Aleksandrov model [Ingel, 1986]. This model assumes spherical packing of ions and uses the calculated mean number of anion vacancies per unit cell. For the binary system Y_2O_3-ZrO_2, the equation can be expressed as follows:

$$a = A\left[R_{Zr} + R_O + \frac{P_Y(R_Y - R_{Zr})M}{100 + M}\right]$$

The constant A is based on the geometry of the unit cell, i.e. $A = 4 / \sqrt{3} = 2.3094$, the ionic radius of Zr^{4+} is R_{Zr} = 0.81 Å, the ionic radius of O^{2-} is R_O = 1.40 Å and the ionic radius of Y^{3+} is R_Y = 0.90 Å; the term P_Y is the number of stabilizer ions per unit cell and is equal to 2 for Y_2O_3; M is the mole percentage of the stabilizer. Substituting these values, the equation becomes:

$$a = 2.3094\left(0.221 + \frac{0.018\,M}{100 + M}\right)$$

Using this equation for the 6YSZ sample, with M=6, *a* = 5.127 Å is obtained, which is in excellent agreement with the experimental value *a* = 5.129 Å (Table 3.3).

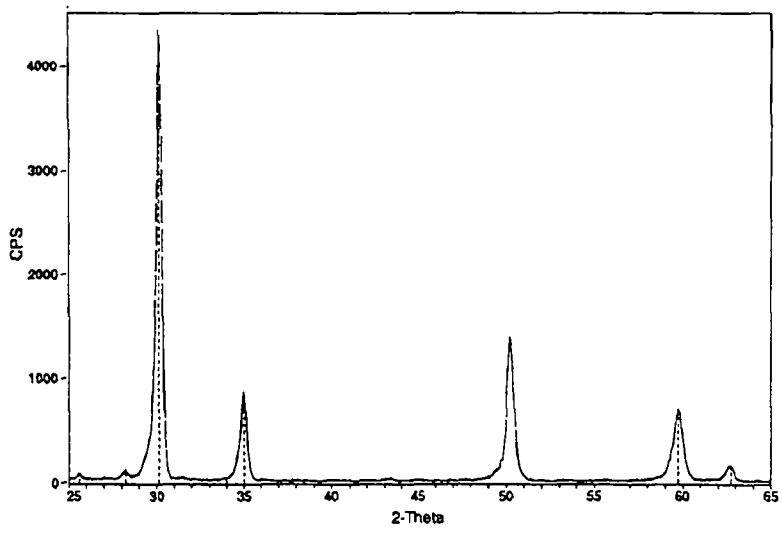

Fig. 3.8 The X-ray diffractogram of a new 6YSZ Metoxit sample obtained at a scan rate of 5°/min

3.2.3 The IrO_2 catalyst preparation and characterization

The IrO_2 catalyst is prepared by the thermal decomposition method [Comninellis, 1991a]. The precursor solution is prepared by dissolving a precise amount of hexachloroiridic acid $H_2IrCl_6.6H_2O$ (Fluka) in isopropanol. With a micropipet, 1 µl of the $H_2IrCl_6.6H_2O$ 0.093M solution is applied on a 0.5 cm^2 area on the YSZ support. The support is placed in the oven at 80°C for the solvent to evaporate and then gradually heated up to 550°C (heating-rate 3°C/min), where the temperature is kept constant for one hour. The sample is cooled down slowly in the oven, in order to avoid thermal shocks: the thermal expansion coefficients of the catalyst and the support differ enough for the deposit to get cracked. This operation is repeated three times. The application of 3 µl in one step is avoided because the deposition of successive layers provides a more homogeneous sample. The IrO_2 deposit exhibits a very good adherence.

The thermogravimetric curve of $H_2IrCl_6.6H_2O$ shows that the decomposition occurs according to the following reactions [Vercesi, 1991]:

$$H_2IrCl_6 \cdot 6H_2O \xrightarrow{150°C} IrCl_4 + 6H_2O + 2HCl$$

$$IrCl_4 + 2H_2O \xrightarrow{>500°C} IrO_2 + 4HCl$$

The counter and reference electrode preparation always precedes the catalyst deposition because, in this case, temperatures as high as 850°C are needed and such a thermal treatment might influence the catalyst structure.

The catalyst weight can not be measured because the YSZ plate is too heavy for a microbalance to be used. The weight can be estimated under the assumption that there is no loss in the applied solution and that the decomposition of the precursor to IrO_2 is complete (100% yield). Therefore, the catalyst mass is 63 µg and the catalyst geometric surface is 0.5 cm^2.

The electrical connections are prepared in the following manner. A gold wire (0.4 mm diameter)

with a flat end is finely soldered on the electrode with a hint of gold paste. In order to enhance the mechanic stability of the connection, the wire is stuck on the YSZ plate with a two-component alumina cement (Firag, Feuerfestkitt 1500). The plate is then heated at 550°C for one hour.

From the electrochemical point of view, the working electrode (catalyst) must be polarizable. An electrode is called ideally polarizable if no charge-transfer can take place through the electrode-elecrolyte interface for any applied potential. The interface then acts as a capacitor. In practice, the electrode is polarizable only within some precise voltage limits. Above or below these limits, a faradaic reaction can take place. This polarizability requirement is essential for the present study in order to observe important non-faradaic catalytic changes. On the contrary, electrodes developed for SOFC applications must be less polarizable, for high currents to flow under small applied voltages.

The IrO_2 catalyst is porous [Comninellis, 1991a] and, as a consequence, has a long catalyst-zirconia-gas TPB. However, it is polarizable, as can be seen by the horizontal line portion in current-potential curves (see §4).

X-Ray Diffraction analysis

The catalyst structure is characterized by XRD [Cullity, 1978; Feidenhans'l, 1989]. Since the effective depth of X-ray penetration is generally higher than 1μm and increases as θ increases, the analysis was performed on a 1.1 mg IrO_2 sample prepared with the same thermal decomposition technique. Although electron diffraction would be more suitable when information is required from very thin surface films, such as our IrO_2 catalyst, the penetration depth can be reduced to a certain limit by using radiation which is highly absorbed.

The diffractogram of the YSZ supported IrO_2 sample obtained at a scan rate of 5°/min is presented in figure 3.8; a good fitting is observed with the one reported in the JCPDS file No 15-870 for tetragonal IrO_2. The results of a detailed analysis in the ranges 2θ=38° to 48° and 2θ=52° to 58° at a scan rate of 0.5°/min for enhanced sensitivity are also presented in figure 3.8. The IrO_2 peaks show a severe X-ray line broadening as compared to the YSZ peaks, due to the very small size of the IrO_2 particles. The fact that the intensity of the YSZ peaks is much higher than that of the IrO_2 means that the deposit thickness is much lower than 1μm. The relative intensities of the IrO_2 reflections are presented in the table 3.4 and they have been calculated assuming a 100% intensity for the main IrO_2 peak at 2θ=28°. Generally, the peaks of the two substances are distinct. However, at 2θ=35°, there is an overlap of the YSZ (200) plane and the IrO_2 (101) plane. Since the relative intensity of the YSZ peak is already known (see table 3.2), this contribution was subtracted from the peak at 2θ=35°.

Although it has been reported in the literature (see §2.2) that iridium is also present in the IrO_2 deposit, especially when the precursor solution contains $IrCl_3$, no iridium phase could be detected in the present sample. In the table 3.4, these results are compared with the values reported in the JCPDS files No 15-870 for tetragonal IrO_2 and No 6-598 for cubic Ir. The absence of the two main peaks of Ir at $2\theta=40.662°$ and $47.313°$ is also clear on the detailed diffractogram in figure 3.9. Note also the peak at $2\theta=57.740°$ detected at the slow rate analysis only, which may correspond to the IrO_2 (220) plane at $2\theta=57.941°$.

Table 3.4 The peak intensities and interplanar distances of the IrO_2 phase. Comparison with the standards reported in the JCPDS data bank for tetragonal IrO_2 and cubic Ir

	IrO_2			IrO_2	JCPDS	15-870	Ir	JCPDS	6-598
hkl	**2θ**	d [Å]	Intensity %	**2θ**	d [Å]	Intensity %	**2θ**	d [Å]	Intensity %
1 1 0	**28.051**	3.178	100	**28.054**	3.178	100			
1 0 1	**34.945**	2.566	51	**34.714**	2.582	90			
2 0 0	**39.996**	2.252	28	**40.062**	2.249	25	**40.662**	2.217	100
							47.313	1.920	50
2 1 1	**53.952**	1.698	50	**54.024**	1.696	55			
2 2 0	**57.740**			**57.941**	1.590	12			
1 1 2	**66.347**	1.408	1.7	**66.052**	1.413	14			
3 0 1	**69.349**	1.354	2.2	**69.334**	1.354	14	**69.142**	1.358	40

The peak intensities of the YSZ sample with 1.1 mg IrO_2 are presented in the table 3.5. The measured values are closer to those of the JCPDS file than the values obtained on the new Metoxit sample.

Table 3.5 The peak intensities and interplanar distances of the 6YSZ phase in the sample with 1.1mg IrO_2. Comparison with the standard reported in the JCPDS data bank for the 8mol%YSZ

	6YSZ	with	IrO_2	6YSZ	Metoxit	new	8YSZ	JCPDS	30-1468
hkl	**2θ**	d [Å]	Intensity %	**2θ**	d [Å]	Intensity %	**2θ**	d [Å]	Intensity %
1 1 1	**30.105**	2.966	100	**30.155**	2.961	100	**30.084**	2.968	100
2 0 0	**34.945**	2.566	23.4	**35.001**	2.561	23.4	**34.868**	2.571	25
2 2 0	**50.205**	1.816	45	**50.249**	1.814	42.3	**50.136**	1.818	55
3 1 1	**59.748**	1.547	24	**59.752**	1.546	26.4	**59.597**	1.550	40
2 2 2	**62.651**	1.482	2.5	**62.744**	1.480	4.4	**62.538**	1.484	6
4 0 0	**73.893**	1.282	1				**73.660**	1.285	5

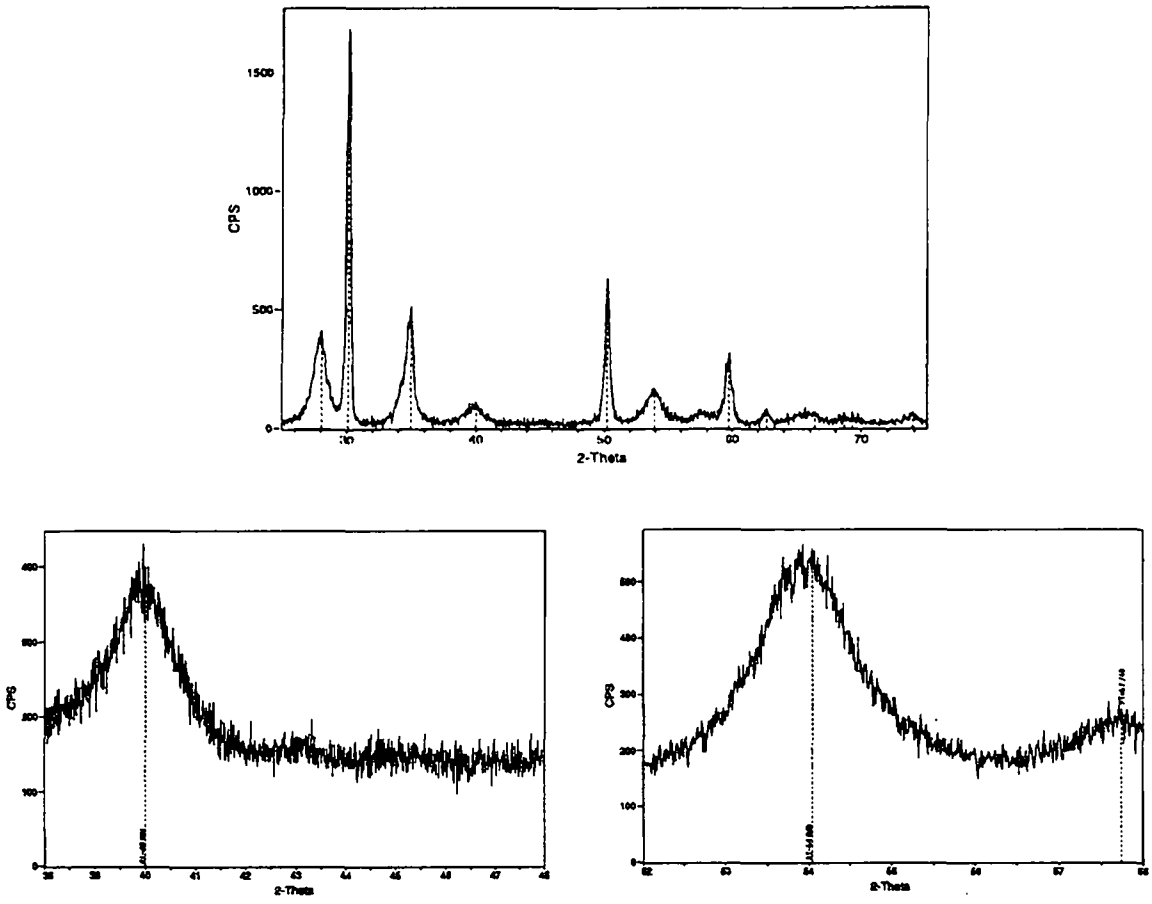

Fig. 3.9 X-ray diffractograms of the YSZ supported IrO_2 sample at a scan rate of 5°/min (top) and 0.5°/min (bottom)

3.2.4 The counter-electrode

The gold paste (Demetron, Leitgold M8000) counter electrode is applied by brush on a 0.56 cm^2 area and fired at 850°C in air during 1h. The gold wire electrical connection is taken directly into the deposit, which is a few μm thick. Although the heating rate is low (3-5°C/min) to avoid thermal stress between the ceramic support and the metallic coating, the adherence of the gold electrode is poor and the film can be partially removed by slight scratching. The gold wire must be cemented on the zirconia plate (see §3.2.3), otherwise the deposit is taken off easily when the electrical connections are manipulated. However, a time-dependent increase in gold-oxide substrate adhesion is frequently observed [Martin, 1986].

The XRD analysis of the YSZ supported gold electrode (Fig. 3.10) shows that the polycrystalline sample is of cubic structure, with a preferred (111) orientation. The location of the peaks and the calculated interplanar distances (Table 3.6) are in excellent agreement with those reported in the JCPDS file No 4-784 for high purity gold (99.997% Au). Four YSZ peaks are also present on the diffractogram, because the counter-electrode does not cover the entire solid electrolyte surface.

Table 3.6 The peak intensities and interplanar spacing of the gold counter-electrode. Comparison with the standard reported in the JCPDS data bank for high purity cubic Au.

	Au	counter	electrode	Au	JCPDS	4-784
hkl	**2θ**	d [Å]	Intensity %	**2θ**	d [Å]	Intensity %
1 1 1	**38.209**	2.354	100	**38.184**	2.355	100
2 0 0	**44.408**	2.038	42	**44.392**	2.039	52
2 2 0	**64.641**	1.441	11	**64.576**	1.442	32

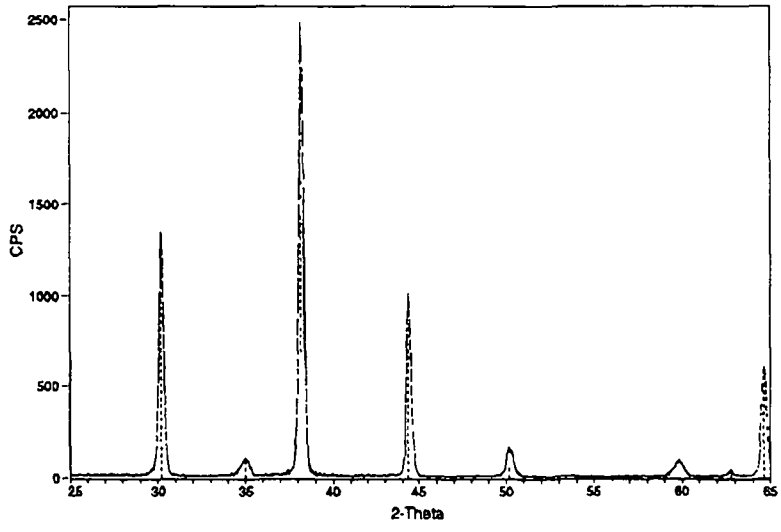

Fig. 3.10 The X-ray diffractogram of the gold counter-electrode obtained at a scan rate of 5°/min

3.2.5 The reference electrode

The reference electrode serves two purposes: first, it fixes the potential on some reference scale and second, it separates the overpotential of the working electrode from the overpotential of the counter-electrode and the ohmic drop in the electrolyte. It must be non-polarizable, which means that the potential is kept constant even if some current flows through the electrode, and must return rapidly to the equilibrium potential after polarization in either direction. In the case of an undivided cell, it should also be chemically and electrochemically inactive.

In aqueous electrochemistry, the internationally accepted primary reference is the normal hydrogen electrode (NHE), with all the components at unit activity:

$$2H^+ + 2e^- \Leftrightarrow H_2(g)$$

Its potential is arbitrarily taken as zero at all temperatures and the half-cell potential of every redox couple can be measured against the NHE. Since the NHE is difficult to construct and use, other reference electrodes have been developed using some stable redox systems (e.g. calomel electrode).

In solid state electrochemistry, there is no reference scale and most redox processes do not have a

reproducible potential. However, in undivided cells, the potentials are often reported against the reference electrode YSZ // Pt / air with respect to the half cell:

$$O_2(g) + 2e^- \Leftrightarrow 2O^{2-}$$

Although the fist aim of a reference electrode is not fulfilled in our case, the second one, which consists in isolating the working electrode overpotential from the other voltage contributions, can be satisfied (see §3.2.1).

The gold reference electrode is prepared in the same way as the counter electrode. Its area is small (0.07 cm^2) and it is applied at a 2 mm distance from the counter electrode. The total electrical resistance of the deposit and the current collectors connected to the potentiostat is only 0.2Ω. The same resistance has been measured in the case of the counter electrode.

The influence of the gold presence in the reactor as counter and reference electrode will be discussed in the results section (§4.1).

3.3 THE ANALYSIS UNIT

Upon leaving the reactor, the products pass through a water-cooled tubing with a thermocouple (Philips, TKA) at the end, in order to verify that the products have been sufficiently cooled prior to analysis. The flow rate can be measured with a bubble-flowmeter through a vent. The gases then enter in the Infra-Red analyzer (Siemens, Ultramat 5E), where the ethylene and carbon dioxide concentrations are continuously monitored, via a 6-port valve. The 6-port valve (Valco, Vici UW) has an electric actuator and a 5 cm^3 loop for the injection of a precise volume sample in the gas chromatography analyzer (Shimadzu GC-8A).

The gas chromatograph has a set of two columns and a thermal conductivity detector (TCD). It is connected to an integrator (Shimadzu, Chromatopac C-R6A) for the peaks area evaluation. All the products are analyzed on a Porapak Q packed column (100/120 mesh) under a 25 cm^3 /min He flow. In the present work an isothermal analysis at an oven temperature of 60°C and the TCD at 120°C and 120mA is generally performed. A typical chromatogram is presented in figure 3.11.

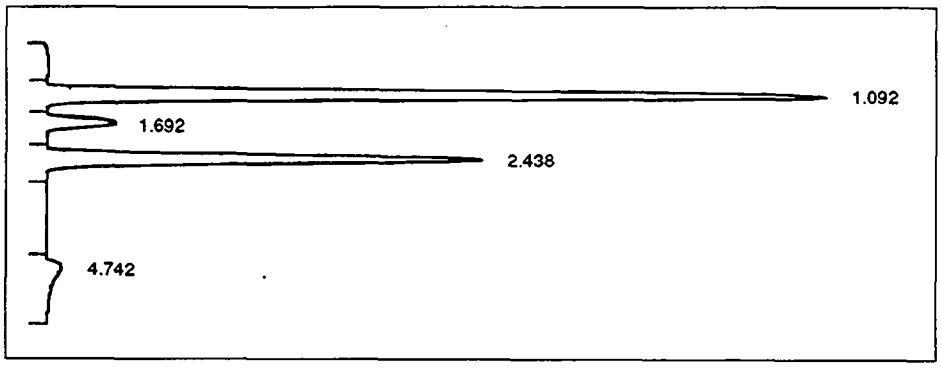

Fig. 3.11 A typical chromatogram at 60°C, with the peaks appearing in the order O_2, CO_2, C_2H_4, H_2O

The IR analyzer has two channels for the percentage volume measurement of C_2H_4 and CO_2 in the range 0.000-1.000%. Since the concentrations are very small, no additional filter or moisture trap prior to the analysis unit was added in order to minimize the eventual adsorption of the products and the dead volume. However, there is a fine filter mounted in the analyzer, before the cell entrance. The output channels of the analyzer are connected to a recorder (Bryans, BS-273). The on-line IR analysis of the carbon containing products allows the continuous verification of the carbon mass balance. The GC analysis, which takes 20 minutes approximately for three injections, is therefore omitted when the precise knowledge of the oxygen or water content in the effluent is not necessary. In some experiments, another IR analyzer (Horiba, PIR-2000) with only one channel was also used for the CO_2 concentration measurement in three different ranges (0-0.05, 0-0.15 and 0.025%). This analyzer has a sensitivity limit of 0.0005%.

The indications of the IR analyzer in %vol must be divided by 100 in order to obtain the molar fractions of the carbon dioxide y_c and ethylene y_e. The molar flow rate of the carbon dioxide $\dot{n}_c$ is given by the relation:

$$\dot{n}_c = y_c \frac{\dot{V}_{tot}}{\upsilon} \left[\text{mol } CO_2 / s\right]$$

where $\dot{V}_{tot}$ $[Nl/s]$ is the total volumetric flow rate and υ = 22.4 Nl/mol is the molar volume under normal conditions.

Considering the ethylene oxidation complete, the rate of reaction or rate of oxygen consumption is expressed as:

$$r = 3 \cdot \dot{n}_c \text{ [mol O /s]}$$

In order to verify that the reactor is differential, the conversion is always estimated for the minor reactant, which is usually ethylene. The ethylene conversion X_e is calculated from the equation:

$$X_e = \frac{\dot{n}_{e,in} - \dot{n}_{e,out}}{\dot{n}_{e,in}} \cdot 100 \quad [\%]$$

where $\dot{n}_{e,in}$ [mol / s] is the initial ethylene molar flow and $\dot{n}_{e,out}$ [mol / s] is the ethylene molar flow at the exit of the reactor.

The electrochemical measurements were made with a scanning potentiostat-galvanostat (EG&G Princeton Applied Research, Model 362). The cell cable of the potentiostat has an electrical resistance of 0.1 Ω and is connected to the gold wires of the three electrode system. The cyclic voltammograms are traced on an electronic recorder (Rikadenki Kogyo Co., RW-201T).

A complete data acquisition on a personal computer (Mitsui AT 80286) through analog/digital input/output boards (Analog Device, RTI-815, RTI-820 and STB-TC thermocouple panel) allows a rapid treatment of the results.

CHAPTER 4

RESULTS AND DISCUSSION

The experimental results are presented in four distinct sections. In the first section, the influence on the ethylene oxidation rate of parameters such as the thermal reactions and the gold presence in the system is accounted for. The optimum experimental conditions for the study of the polarized YSZ supported IrO_2 catalyst are established, based upon various preliminary experiments. The second section concerns the in-situ study of the catalyst by cyclic voltammetry, which is in fact a special case of electrochemical polarization. The "open-circuit" results, i.e. the kinetic measurements on the catalytic ethylene oxidation, are presented in the third section, and the "closed-circuit" results, or kinetic measurements under an electrochemical polarization regime, in the fourth.

The rate of ethylene oxidation is always expressed in terms of the atomic oxygen consumption [molO/s], in order to facilitate the comparison with the rate of oxygen ion transport through the electrolyte. The carbon mass balance is always in excellent agreement with the assumption that ethylene oxidation is complete on IrO_2 / YSZ. Except for some slight deviations within the experimental error, there was no indication for the presence of another reaction product but CO_2.

4.1 PRELIMINARY EXPERIMENTS

Before any measurements were performed on the catalytic rate, it was verified that no reaction takes place in the absence of the IrO_2 catalyst. Then, different experimental conditions were scanned, to identify the most promising for the polarization study. During these preliminary experiments, some intriguing features were observed, such as electrolyte color change and catalytic rate enhancement both by positive and negative potentials.

4.1.1 Reactor testing for eventual thermal reactions

Thermal reactions, i.e. heterogeneous reactions taking place on the hot surfaces of the reactor and homogeneous reactions occurring spontaneously in the gas phase, should be avoided because they mask the effect of the catalytic rate. The eventual presence of thermal reactions was tested by admitting the reactants in the system without the zirconia supported catalyst. The oxygen to ethylene partial pressure ratio was varied from 3 to 10 in the reactive mixture, because this range covers most of the experimental conditions used. Although homogeneous reactions are reported for temperatures higher than 340°C [Schmid, 1988], no oxidation products were detected in the temperature range 250°C to 370°C. On the Horiba IR-analyzer however, which has a higher sensitivity, some CO_2 traces appeared for temperatures higher than 370°C. At 400°C, this thermal contribution is responsible for less than 1% of the conversion attained in presence of the catalyst.

4.1.2 The influence of the gold counter-electrode

As far as gold catalytic activity is concerned, the apparatus was tested by admitting the reactants in the reactor containing a stabilized zirconia plate with only the gold counter and reference electrodes. Under the experimental conditions used in the test for thermal reactions, the presence of the gold deposits did not induce any significant difference. At 400°C, the carbon dioxide detected on the Horiba IR-analyzer is still less than 1% of the carbon dioxide produced in presence of the IrO_2 catalyst. Since this quantity is very close to the analysis sensitivity limits, a separate quantification of the thermal contribution and the "open-circuit" gold activity was not possible.

The overvoltages (V_{RC}) measured during oxygen pumping were large and indicate that the gold electrode is slow. This remark is in agreement with other studies on ceria or zirconia supported gold electrodes. Although gold is known to be active for the electrochemical reduction of CO_2 to CO in aqueous and aprotic media [Kedzierzawski, 1994], it seems that at low CO_2 concentrations in the gas phase and at high temperature it is not a good catalyst. This corroborates the present results since no CO was ever detected in the products.

In the light of these observations, it seems reasonable to neglect the catalytic and electrocatalytic contribution of the gold electrode. The rate enhancement induced by oxygen pumping to the IrO_2 catalyst (see §4.1.3) is too important to be explained by the gold activity.

Since potential measurements are always presented here with respect to the reference electrode (V_{WR}), the counter electrode overpotential (V_{RC}) does not seem important at a first glance. This overpotential contributes to the total power consumption "V_{WC}·I", which is always small because of the low current values. Generally, the consumption during potential application does not exceed 0.3 mW and in extreme cases (high temperature, high overvoltage) it may attain 1 mW.

However, if the counter electrode is not a "sufficiently good" electrode for the oxygen reaction, the O^{2-} flux through the electrolyte may be perturbed. The gold reactivity in the oxygen transfer reaction has been presented in §2.1. Although the studies reported in the literature have been done at high temperature (700-1000°C), the counter electrode may behave in a similar way in the temperature range of this work (300-500°C). The current is generally small upon polarization at these low temperatures but the cathodic overpotential is quite high. In some of the present experiments, the oxygen reduction at the counter-electrode may be limited by the diffusion of the adsorbed oxygen species along the gold-zirconia interface. This is particularly true for low oxygen partial pressures in the gas phase.

During some early experiments, the colour of the zirconia electrolyte changed from yellow to brown underneath the gold counter-electrode, used as a cathode, in the proximity of the electrical connection. The coloration was not visible on the opposite side of the zirconia plate. On other occasions, when the plate had been polarized during several hours at high overpotentials, this coloration was observed on both sides of the plate and through the electrolyte bulk. The coloration is well-delimited, restricted in the

region of the electrical field, and varies from brown to black as the zones of high current density are approached. This is probably the "zirconia blackening" or zirconia partial reduction, due to electron injection from the metal electrode into the electrolyte. This coloration does not need the passage of high currents and starts on the gold cathode side. It can disappear completely by heating the reduced sample in air at 800°C approximately for one hour. Since this reduction is not accompanied by a structural change (see §3.2.2), it is difficult to establish its influence on the measurements.

Although a gradual reduction of the zirconia support was observed, no relation with the electrochemical modification of the ethylene oxidation rate was found. The slight increase in electronic conductivity and concomitant decrease in ionic conductivity, which is undesirable in the SOFC applications, would simply mean that the enhancement factor Λ, calculated under the assumption that the current is purely ionic, is underestimated. On the other hand, the establishment of mixed conduction in the stabilized zirconia would make the oxygen reaction possible on the electrolyte surface alone. The eventual augmentation of electrochemical reaction sites should not be important, since the zirconia is known to be less active than the gold electrode [VanHerle, 1994]. The same remark stands for the catalytic activity which remains probably low in the case of the reduced zirconia too. The most important effect of the electrolyte reduction probably lies in the modification of the double-layer structure and properties.

4.1.3 Scanning of the experimental conditions for the NEMCA effect study

The exploratory investigation of the IrO_2 / YSZ interface was performed with the electrodes deposited on zirconia stabilized with 8% mol yttria (Didier Werke, Zircoa composition 1373). The solid electrolyte disk (8YSZ) had a diameter of 13 mm and was 1.7 mm thick. The 0.16 mg IrO_2 catalyst (WE) was applied over a 0.3 cm^2 area. The gold CE and RE were deposited on the opposite side of the disk (0.3 cm^2 and 0.1 cm^2 respectively).

The reactor was operated at a total pressure of approximately 100 kPa. The flow of the reactants was not automatically controlled. The manual adjustment of the flowmeters is relatively imprecise, so the results are semi-quantitative.

The IrO_2 catalyst is very active for the ethylene oxidation. At 390°C, P_{O_2} = 0.8 kPa and $P_{C_2H_4}$ = 0.16 kPa, the catalytic rate is of the order of $2 \cdot 10^{-7}$ molO/s. The polarization of the catalyst did not have any effect on the reaction rate at such low oxygen partial pressures. The currents measured are also very low due to the abundant presence of inert gas which reduces the zirconia conductivity.

At higher oxygen concentrations in the gas phase, the open-circuit rate is slightly lower, but the effect of catalyst polarization increases dramatically. The carbon dioxide production is enhanced by applying positive potentials to the IrO_2 catalyst (electrochemical pumping of oxide ions to the catalyst) and the enhancement is more pronounced at high potentials. In order to rapidly detect the most promising experimental conditions, potential steps of 3V were applied during this preliminary study. Such high potentials accelerate the "blackening" of zirconia and were only used with this IrO_2 / 8YSZ catalyst. The ohmic drop through the electrolyte was important, especially at low temperatures.

A typical potentiostatic experiment is presented in figure 4.1a where the rate of CO_2 production, the potential and the current are simultaneously traced. The parameters used to describe the system have been defined in §2.4. Initially, the system is at steady state and the reaction rate is $r_o = 1.1 \cdot 10^{-8}$ molO/s. The potential of the catalyst with respect to the reference electrode is approximately $V°_{WR}$ = -50 mV and the current is zero. At time t = 0, the potential is stepped to 3V and the ohmic-drop-free potential becomes V_{WR} = 1.8V. The response of the system to the polarization is very rapid and after a few minutes the reaction rate stabilizes at a value $r' = 6.9 \cdot 10^{-8}$ molO/s. This value is $\rho = 6$ times higher than the initial catalytic rate. The enhancement $\Delta r = 5.8 \cdot 10^{-8}$ molO/s corresponds to a current I = 150 μA, which means that each oxygen atom formed makes $\Lambda = 73$ oxygen atoms to react.

Upon interrupting the current, the reaction rate decreases slowly towards the initial value r_o. The process is indeed reversible but the decrease is always slower than the increase. This feature indicates that there is a difference between the "activation" and the "deactivation" mechanism. In the above examples, the system responds very quickly to polarization. This is not the case for a fresh catalyst, as will be discussed later.

The theoretical reaction rate r'(electrochemical), depicted in figure 4.1a by a dashed line, corresponds to the sum of the open-circuit rate and the electrochemical ethylene oxidation predicted by Faraday's law with a 100% current efficiency. The electrochemical reaction can be written as:

$$C_2H_4 + 6O^{2-} = 2CO_2 + 2H_2O + 12e^-$$

and the electrochemical rate for a current of 150 μA is $I / 12F = 1.3 \cdot 10^{-10}$ molO/s. The simple addition of the catalytic and electrocatalytic rates cannot explain the observed enhancement.

The current response to the potential step is different in figures 4.1a and 4.1b. In the case (a), the current raises quickly to approximately the steady-state value. This response is observed when the catalyst has been polarized positively during the preceding experiment. In the case (b), the current increases rapidly to a certain value, indicated by an arrow, where it remains stable for a laps of time before raising again towards the final value. This is observed when the catalyst is polarized negatively prior to the application of the positive potential step, even if the catalyst was left to return to the "open-circuit" rate for half an hour between the two experiments. The high cathodic polarization probably provokes the reduction of some species to a stable state, which needs many hours or high anodic potentials to be reoxidized.

A similar effect of the catalyst history on the response of the reaction rate during galvanostatic transients has been reported by Yentekakis and Vayenas [Yentekakis, 1988]. If negative currents were applied prior to the application of positive galvanostatic steps, the reaction rate raised rapidly to a maximum value and decreased towards the same steady-state value as in the case of previously applied positive currents.

The initial and temporary current limitation indicates that the reduced species represent an important resistance to the current passage and need to be reoxidized before the double layer becomes charged and the main faradaic reaction (oxygen evolution) take place freely. The magnitude of the initial current step depends principally on the temperature. A definite amount of charge is needed for the reduced

quantity to be oxidized and could be calculated by integrating the current-time curve from t=0 to the time where the current starts raising again, if all the current were only due to this reaction.

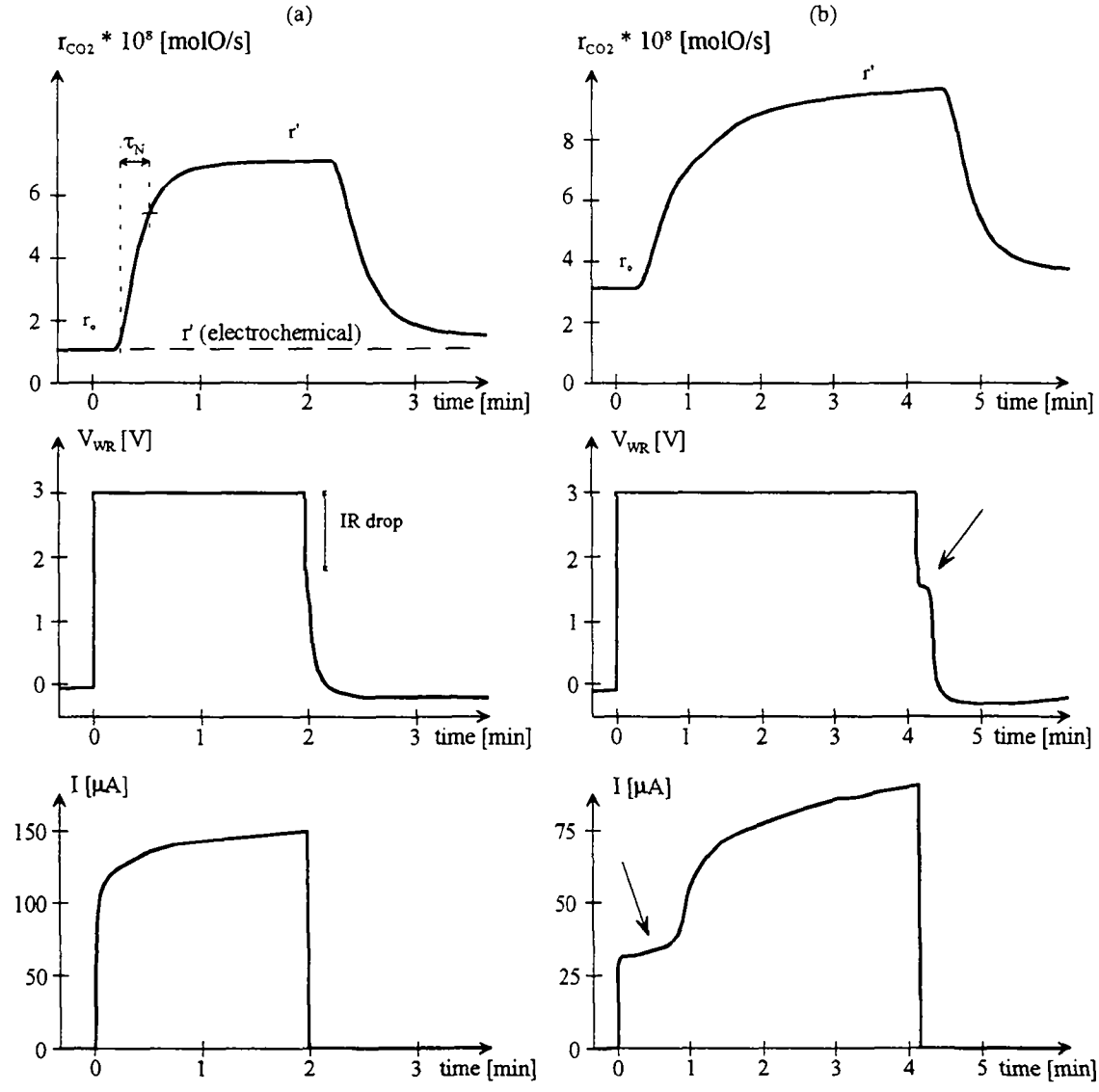

Fig. 4.1 Response of the CO_2 production rate to the application of a potential step at (a) 390°C, 20 kPa O_2 , 0.26 kPa C_2H_4 and (b) 370°C, 20 kPa O_2, 0.33 kPa C_2H_4; r_o is the regular catalytic rate and r' is the rate attained by catalyst polarization.

Supposing that the process is limited by the diffusion of some electroactive species, the current might obey to a relation of the type (see §2.1.3):

$$I \propto \sqrt{D}$$

Considering that only the activation energy for diffusion is temperature dependent, this equation can be rearranged in the form:

$$\ln\left(I^2 \cdot T\right) = -\frac{E_a}{R} \cdot \frac{1}{T} + \text{const.}$$

The experimental activation energy can then be determined from the slope of the $\ln(I^2T)$ vs 1/T plot (Fig. 4.2).

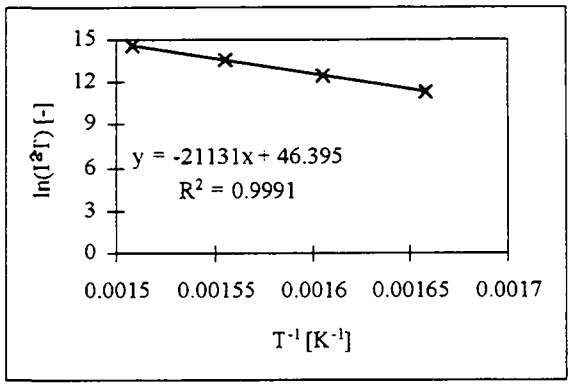

Fig. 4.2 Plot of $\ln(I^2T)$ vs 1/T for the determination of the activation energy for diffusion.

The value obtained is E_a = 176 kJ/mol and is relatively close to the value reported for the electron diffusion [VanHassel, 1992b]:

$$D_e = 213.8 \exp [-(192kJ/mol) / RT]$$

Part of the initial limiting current is certainly due to the oxygen reaction which occurs at any potential. The second parallel process should not be related to a redox couple, like the oxygen reaction, since a certain potential value is needed before it can occur. It may be due to the zirconia reduction during the cathodic step with injection of electrons and eventually formation of additional oxygen vacancies. The reoxidation of reduced zirconia would constitute an additional resistance to the flux of oxide ions.

Note that the reaction rate response to the potential step is not sensitive to the current behaviour and is similar for both cases in figure 4.1. This is in agreement with the statement that the NEMCA effect is related to the catalyst potential and not to the current through the circuit. As far as the open circuit rate r_o is concerned, it is higher at 370°C (Fig. 4.1b) than at 390°C (Fig. 4.1a), although the partial pressures of the reactants are similar. This "irregularity" will be discussed later, with the results on the catalytic ethylene oxidation.

Sometimes, the potential decay curve upon opening the circuit presents a shape like the one indicated by an arrow in figure 4.1b, after the ohmic drop. This delay in the potential decrease is not always in relation with the current plateau. It is observed at lower temperatures and longer polarization durations. It may be due to a diffusion limited electrode process like reduction of the previously oxidized IrO_2 surface. A similar feature has been observed in the potential decay following the cathodic polarization of a gold electrode [VanHerle, 1992]. It was explained by the slow reoxidation of the subsurface electrolyte, reduced by electron injection under strong cathodic polarization. In this study, no wave was observed in the potential decay after cathodic polarization of the IrO_2 catalyst.

The IrO_2 catalyst exhibits mainly electrophobic NEMCA behaviour, i.e. it is activated when oxide

ions are pumped to the catalyst. However, it can also exhibit electrophilic behaviour, i.e. it may be promoted by pumping oxide ions from the catalyst. At 330°C and 350°C, the application of positive potential steps enhances the reaction rate and the application of negative potential steps reduces the rate. At 370°C, the application of negative potentials does not affect the rate significantly and at 390°C, the rate is increased by both positive and negative potentials. The rate enhancement is always higher when the catalyst is subject to anodic than to cathodic polarizations. It is not clear yet why the system changes from purely electrophobic to mixed electrophobic and electrophilic behaviour at around 370°C.

The response of the system to a linear variation of the potential is particularly interesting under conditions where both positive and negative polarizations induce a rate enhancement. An example is shown in figure 4.3, where the variation with time of the CO_2 production rate, the potential and the current are simultaneously traced. The potential is varied from -2V to 3V (dashed curve) at three different scan rates, namely 100, 50 and 20 mV/s.

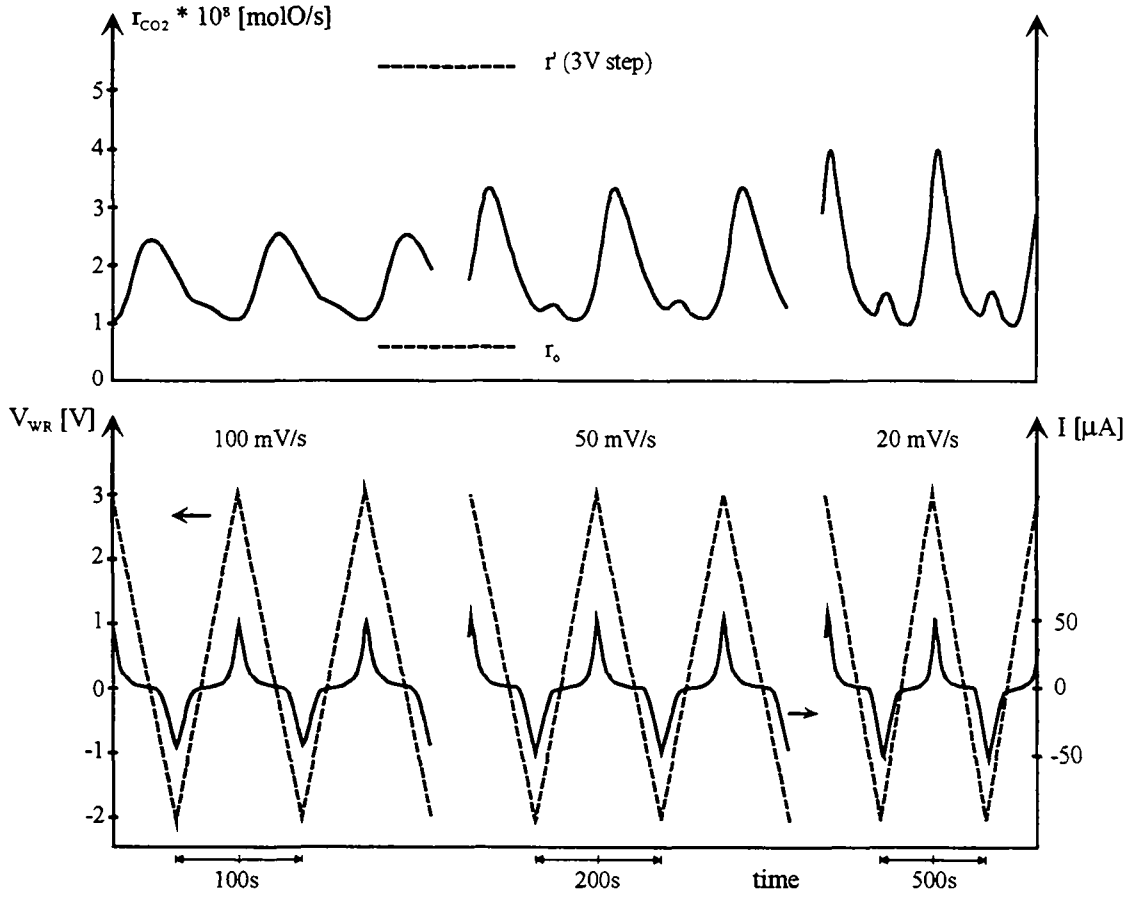

Fig. 4.3 Response of the CO_2 production rate to cyclic voltammetry in 20 kPa O_2 and 0.22 kPa C_2H_4, at 390°C.

The reaction rate changes in phase with the potential and passes through a maximum when the potential is at 3V and through a second "local" maximum when the potential is at -2V. The 30s shift between the rate and potential peaks is mainly due to the residence time in the reactor.

The open-circuit rate r_o and the rate r', obtained by polarizing the catalyst at 3V until the steady-state is reached, are indicated in the figure for comparison. During the cyclic voltammetry, the reaction rate is always higher than r_o and lower than r'. This is not surprising since, at 390°C, the IrO_2 catalyst is activated by both positive and negative potentials, but to a lesser extent for the latter. The reaction rate varies between a lower and an upper limit. The separation between the two limits decreases with increasing voltage scan rate. At 500 mV/s, the rate remains almost stable at an intermediate value (not shown in this figure). Although the voltage scan rate induces an important change in the upper and lower limits of the reaction rate, the mean value is not altered significantly and decreases from $1.9 \cdot 10^{-8}$ molO/s at 20mV/s to $1.8 \cdot 10^{-8}$ molO/s at 50mV/s and $1.7 \cdot 10^{-8}$ molO/s at 100mV/s.

The magnitude of the anodic and cathodic currents is the same for the voltage limits chosen. Integrating the current-time curve over a complete scan, the anodic and cathodic charges were found to be equal and the total charge to be zero. The enhancement factor Λ, calculated on the basis of the total charge would take an infinite value. This observation is particularly important since it proves that the species formed during polarization do not need to *react* for the NEMCA effect to occur. They are just stored at or near the interface and they are reduced during the reverse (cathodic) scan. The time constant of this process is very small and the migration of species other than electronic seems improbable.

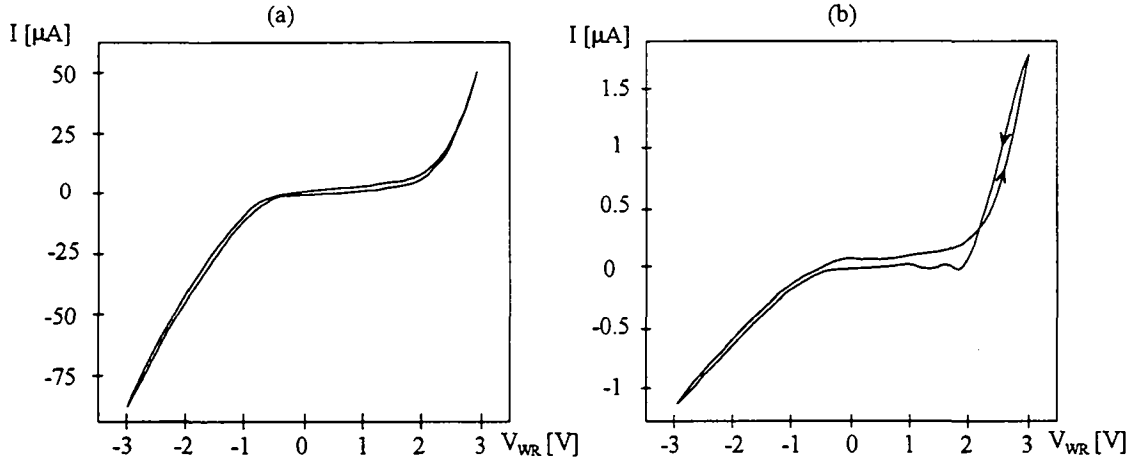

Fig. 4.4 Cyclic voltammograms of the IrO_2/YSZ catalyst at 200mV/s (a) in 20 kPa O_2, 390°C and (b) in 0.3 kPa O_2, 340°C.

Note that no limiting current is observed during the anodic scan, as was the case with the application of a potential step. This remark also stands for cyclic voltammetry from -3V to 3V. A similar process, eventually zirconia reduction, should take place from the thermodynamic point of view, but the system does not spend enough time at the cathodic limit for a measurable quantity of zirconia to be reduced. The "regularity" of the current response during cyclic voltammetry can be seen in figure 4.4a, where the

current-potential curve is traced for the same conditions as in figure 4.3, but for a cathodic limit of -3V and at 200 mV/s. There is no indication that zirconia reduction might take place.

The voltammogram in figure 4.4b was obtained in 0.3 kPa O_2 at 340°C. The significant decrease in zirconia conductivity at this low oxygen pressure and temperature is reflected in the small currents. Note the hysteresis loop at the anodic side. Above a threshold potential value of around 2.2V, an additional oxidative process seems to set in, which goes on upon reversal of the scan, yielding higher currents than during the anodic scan. The partial oxidation of IrO_2 to IrO_3 may explain the hysteresis. One or both of the cathodic peaks might be related to the reduction of the species formed above 2.2V.

On the other hand, the threshold potential value is similar to the zirconia decomposition voltage of 2.23V measured by Weppner [Weppner, 1977a] at 900°C with respect to air. Since the decomposition voltage value decreases with decreasing oxygen pressure value and increases with decreasing temperature, the hysteresis may be due to the partial zirconia reduction at the Au counter electrode. The knowledge of the corresponding potential V_{CR} at the counter-electrode with respect to the reference, could throw some more light on the process.

The main results obtained on this catalyst are presented in table 4.1. The total flow rate $\dot{V}_{tot}$ is indicated because it varied from one experiment to the other. The relaxation time constant τ_N was determined experimentally by measuring the time necessary for the reaction rate to attain 63% of its final value and subtracting the mean residence time in the reactor $V_R / \dot{V}_{tot}$. The reactive oxygen uptake of the catalyst N_t and the turnover frequency TOF are estimated from the following relations:

$N_t = \tau_N I / 2F$ [molO] and

$TOF = r' / N_t$ [s^{-1}]

The calculated values of the turnover frequency and catalytically active area are very similar to those measured and calculated for a Pt catalyst [Vayenas, 1992a], but there are no experimentally determined values for the IrO_2 / YSZ system. The 0.16 mg IrO_2 correspond to $7.1 \cdot 10^{-7}$ mol IrO_2 and, taking a mean value $N_t = 7.1 \cdot 10^{-9}$ molO, it seems that 1% of the total catalyst mass is active. The relaxation time constants are very small and indicate that the process involves surface rather than bulk diffusion or oxidation.

The rate enhancement is large in oxygen-rich gaseous compositions. A similar remark stands for ethylene oxidation over a Pt / YSZ catalyst, where it is believed that O^{2-} pumping to the catalyst does not affect the oxygen adsorption kinetic constant and has a pronounced effect on the kinetic constant of the reaction between gaseous ethylene and chemisorbed oxygen [Bebelis, 1989].

The partial pressure ratio of the reactants O_2:C_2H_4 is approximately 90:1 in the cases presented here. When oxygen is in such large excess, the catalytic rate of ethylene oxidation decreases with increasing temperature. This anomalous behaviour is studied in more detail in a following section. As a consequence of

this particularity, the reaction enhancement ratios ρ are higher at high temperatures, because the open-circuit reaction rates are lower. This observation shows that the effect is not due to a local Joule heating of the catalyst; if this were the case, the enhancement should be higher at low temperatures.

For a given system, the reaction enhancement factors Λ increase with decreasing reaction enhancement ratio ρ. The ρ and Λ values obtained in this preliminary study are comparable to the ones obtained with other systems (table 2.1). The effect is much more pronounced for the ethylene oxidation over Pt / YSZ than over IrO_2 / YSZ, but in both cases, no change in the selectivity was observed. The electrochemical oxygen pumping did not favour the partial oxidation to ethylene oxide but reinforced the total oxidation activity of the catalysts.

Table 4.1 Main results on the electrophobic NEMCA effect for the ethylene oxidation over IrO_2 / YSZ, obtained by the application of 3V steps. The oxygen partial pressure is 20 kPa excepted in the case marked *, where P_{O2} = 0.8 kPa.

T [°C]	$P_{C_2H_4}$ [kPa]	$\dot{V}_{tot}$ [cm^3/s]	r_o [10^{-8} molO/s]	ρ [-]	Λ [-]	τ_N [s]	N_t [10^{-9} molO]	TOF [s^{-1}]	f [-]	ΔT [°C]
390*	0.16*		20*						1.35-1.98	32
390	0.26	5	1.1	**6.3**	73	15	12	5.9	0.05-0.07	2
370	0.23	4.8	1.8	3.6	122	28	11	6.1	0.08-0.12	3
370	0.26	4.3	2	4.1	126	18	8.9	9.2	0.08-0.12	3
370	0.33	3.3	3.3	3.1	145	30	14	7.2	0.10-0.15	5
350	0.26	4.3	5.2	1.8	211	36	6.7	14	0.20-0.30	8
350	0.30	4.6	7.4	1.7	225	24	5.2	24	0.25-0.37	11
350	0.28	5	4.7	1.8	167	20	4.6	19	0.17-0.25	7
350	0.27	4.9	4.1	1.9	154	18	4.2	18	0.15-0.23	6
350	0.25	4.8	3.7	2.1	185	36	7.8	9.8	0.15-0.22	6
330	0.25	4.8	4.9	1.6	223	30	3.7	21	0.19-0.28	8
330	0.23	4.7	3.9	1.7	**251**	36	4.1	17	0.17-0.24	6
330	0.22	5	2.7	1.8	198	36	3.7	13	0.12-0.18	4
330	0.22	4	3.4	1.9	210	24	3.5	18	0.15-0.22	5

The reaction rate is not limited by external diffusion, since an increase of the total flow rate at a constant ratio of reactants causes the reaction rate to decrease. Porous catalysts must also be tested for strong pore resistance effects. Pore diffusion alone can never become controlling but may slow the reaction rate. Considering a first order reaction, the following criterion, developed by Weisz [Weisz, 1959] can

indicate if the mass transfer influences the rate [Levenspiel, 1972]:

$$f = \frac{\left(-r_{C_2H_4}\right)\cdot L^2}{D_e \cdot C_{C_2H_4\,(g)}} \qquad \begin{cases} f < 1 & \text{absence of pore resistance} \\ f > 1 & \text{strong pore resistance} \end{cases}$$

where D_e [cm^2/s] is the effective diffusivity of the fluid in the solid and

$$C_{C_2H_4} = \frac{P_{C_2H_4}}{RT}\left[mol/cm^3\right]$$

is the gas phase concentration of the reactant.

The reaction rate is based on the unit catalyst volume:

$$-r_{C_2H_4}\left[\frac{mol\,C_2H_4}{s\cdot cm^3}\right] = -\frac{1}{6}\cdot\frac{r_{CO_2}\,[molO/s]}{Vcat\left[cm^3\right]}$$

and the characteristic length L corresponds to the catalyst thickness:

$$L = \frac{\text{volume of catalyst}}{\text{exterior surface available for diffusion}} = \frac{V_{cat}}{A_{cat}} \quad [cm]$$

The thickness of the catalyst is not known but can be estimated from the specific gravity which is equal to 11.67 g/cm^3 for IrO_2. Considering the porosity to be between 10 and 40%, two catalyst volumes and corresponding L values were calculated. The thickness is L= 0.5 μm for $V_{cat} = 1.5\cdot10^{-5}$ cm^3 and L = 0.7 μm for $V_{cat} = 2\cdot10^{-5}$ cm^3. The respective values of the factor f, obtained for different experimental conditions using a typical value [Levenspiel, 1972] of the effective diffusivity $D_e = 1.4\cdot10^{-4}$ cm^2/s, are also given in table 4.1.

The range of the f-factors is smaller than 1 in all the cases except one. The first line in table 4.1 refers to an experiment at low oxygen pressure, where the open-circuit rate was very high, the conversion exceeded 20% and the polarization had no effect. It seems that internal diffusion strongly influences the rate. The criterion was applied to the open-circuit rate r_o. If r_o were replaced by the enhanced rate $r' = \rho\cdot r_o$ upon polarization, the factor values would remain below the unity value but would approach it. So, a slight influence of pore resistance on the reaction rate cannot be completely excluded. This observation indicates that a less pronounced NEMCA effect may be encountered in some cases due to internal diffusion limitations.

The ethylene oxidation is very exothermic (ΔH_r = -1322 kJ/mol); if the heat released is not removed rapidly enough, the catalyst will be hotter than the surrounding gas. The gas temperature is measured very close to the catalyst, but the thermocouple is not in contact with the catalyst to avoid an electrical short-circuit. A simple calculation can tell if nonisothermal effects are present. Equating the rate of heat generation and of heat removal, the temperature difference between the gas and the catalyst is obtained:

$$\Delta T = \left(T_c - T_g\right) = \frac{-r_{C_2H_4}\left[\text{mol}\,C_2H_4/s\right]\cdot \Delta H_r\left[\text{kJ/mol}\right]}{h\left[\text{kJ/s cm}^2\,\text{K}\right]\cdot A_{cat}\left[\text{cm}^2\right]}$$

where the area of the catalyst is 0.3 cm^2 and the global heat transfer coefficient is taken from correlations in the literature [Levenspiel, 1972] h = 4.65 10^{-6} kJ/s·cm^2 K. The same coefficient was used for all the experimental conditions, without any correction for the differences in the flow rate.

The calculated ΔT values for the open-circuit rates are shown in table 4.1 with the other results. The corresponding temperature gradient for the electrochemically promoted rate can be determined with a multiplication by the ρ factor. The catalyst is indeed hotter than the gas by 2 to 10°C under open-circuit conditions and by 10 to 20°C under potentiostatic steps. Interestingly, the smaller ΔT values are obtained in the case of the most pronounced effect (ρ = 6.3), while higher values correspond to smaller rate enhancement. The highest ΔT is obtained for the low oxygen pressure where the reaction rate is very high and is not influenced by polarization.

Note that only the gas-exposed catalyst surface was taken into account for the heat evacuation. However, the thermal conductivity of the 6YSZ sample (2 W/mK) is high enough for the electrolyte surface to be included in the surface of heat exchange. The corresponding ΔT values never exceed 5°C.

The additional heat generated by the current passage is not taken into account. In fact, under the conditions treated here, the electrical power "V_{WC}·I" varies from 0.1 to 0.7 mW. For comparison, the heat produced by the conversion of $1\cdot10^{-8}$ mol C_2H_4 /s is 13 mW. Since there is no correlation between the rate enhancement and the local catalyst heating, no explanation of the NEMCA effect can be based on a local temperature increase.

4.2 In-situ Study of the Catalyst by Cyclic Linear Sweep Voltammetry

Cyclic voltammetry is very useful for the study of non-steady state phenomena. Although it has been extensively used in aqueous electrochemistry, very few attempts have been recently made in the solid electrolyte field at high temperature [VanManen, 1992; Fabry, 1979; Seiersten, 1991; Jacobsen, 1991; Metcalfe, 1992; VanHassel, 1992b; Vayenas, 1991b; Jiang, 1993; Chao, 1991; Baker, 1993], where the interpretation of the voltammograms is more delicate.

In aqueous electrochemistry, the study of an electrochemical system is only possible in a certain potential range fixed by the water stability limits: the oxygen evolution at positive potentials and the hydrogen evolution at negative potentials. In electrochemistry with solid electrolytes, the potential range for the electrochemical investigation is also subject to a similar restriction, depending on the decomposition voltage of the electrolyte. In this case however, the detection of the potential limits is not straightforward. The zirconia decomposes via the reaction $ZrO_2 \rightarrow Zr + O_2$, at a potential varying with the temperature and the gas-phase composition.

On the other hand, in an atmosphere containing oxygen, the current in a voltammogram rises at high anodic and cathodic potentials due to the oxygen evolution $2O^{2-} \Leftrightarrow O_2 + 4e^-$ at the WE and CE respectively. So, it is quite difficult to make the distinction between the oxidation of the O^{2-} ions diffusing through the electrolyte and the ones belonging to the electrolyte lattice.

4.2.1 High temperature cyclic voltammetry on Pt/YSZ electrodes

The first voltammetric studies were performed on a cell of the type $O_2(g)$ / Pt // YSZ (8% mol) // Au / $O_2(g)$. Although platinum is widely used in electrochemistry with zirconia electrolytes, there are very few systematic investigations based on cyclic voltammetry [Chao, 1991; Vayenas, 1991b; Jiang, 1993]. Some voltammograms have also been reported as a part of a larger study [Isaacs, 1982; Schouler, 1987] using dc polarization or impedance measurements.

Figure 4.5 shows a typical cyclic voltammogram of a Pt film at 435°C and exposed to an O_2-N_2 mixture with an oxygen partial pressure of 0.5 kPa. The potential V_{WR} is scanned from -0.4V to 0.6V at a rate of 100 mV/s. The general appearance of the voltammetric curve is quite similar to the ones reported in the other studies [Chao, 1991; Vayenas, 1991b; Jiang, 1993], although the electrode configuration and preparation method were often different.

At high positive potentials, the current rises due to the oxidation of oxygen anions diffusing through the electrolyte to the TPB. The desorption being very rapid at high temperatures, the presence of an intermediate step implying adsorbed oxygen is difficult to establish:

$$2O_o^x \rightarrow O_2(g) + 2V_{\ddot{o}} + 4e^-$$

At high negative potentials, the current rises again due to the reverse reaction or the reduction of an adsorbed oxygen species, while the oxygen evolution occurs at the CE. The reduction of oxygen probably occurs via dissociative adsorption (see §2.1.3), although the direct reaction of oxygen from the gas phase cannot be excluded:

$$O_2\,(g) \rightarrow 2O_{ads}$$

$$2O_{ads} + 2V_o^{\cdot\cdot} + 4e^- \rightarrow 2O_o^x$$

or

$$O_2\,(g) + 2V_o^{\cdot\cdot} + 4e^- \rightarrow 2O_o^x$$

The most striking feature in the voltammogram is the cathodic peak called (a). This peak is present in a wide range of temperatures and oxygen partial pressures. Under some experimental conditions, the peak is asymmetrical and presents a "tail" in the region indicated by an arrow. This may be due to the existence of a second small peak, hidden by the main one. The same observation has already been reported [Jiang, 1993; Chao, 1991]. The anodic "hump" called (a'), might well be the anodic peak associated with (a), but it is ill-defined and not observed in all the voltammograms. A similar remark stands for the small cathodic peak (b), which seems perturbed by the high cathodic currents due to the reduction of the main oxygen species. At the portion of the anodic scan denoted (b'), no hump was ever clearly distinguished under various experimental conditions. Therefore, it is not excluded that the anodic peak at (a') corresponds to the cathodic (b), even if the separation is very large.

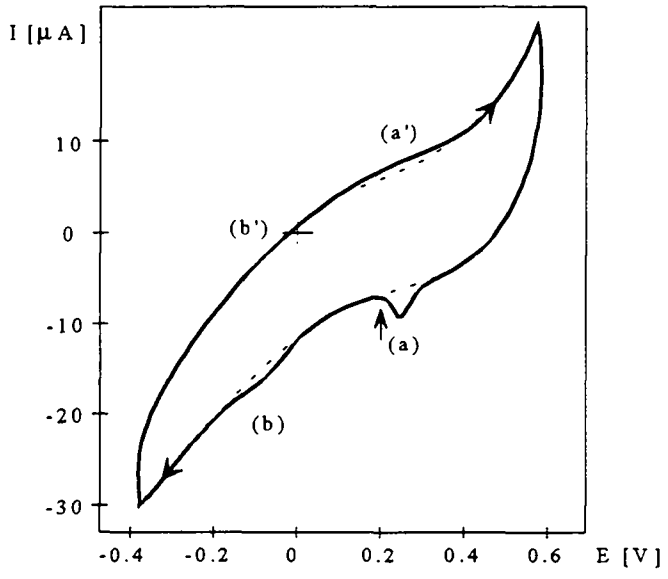

Fig. 4.5 Typical cyclic voltammogram of a Pt film at a 100 mV/s scan rate, exposed to an O_2-N_2 mixture (P_{O2} = 0.5 kPa), at 435°C

The behaviour of the cathodic peak at (a) was subsequently studied by varying the voltage scan rate, the reversal potential, the holding time at a fixed positive potential and the temperature. As far as information from the peaks at (a') and (b) is concerned, their low definition does not allow any precise measurement of the peak current and potential. The electrode potential is always given with respect to the Au reference electrode exposed to the same oxygen partial pressure as the working electrode. Consequently, the dependence of the peak potential shift on different variables should be interpreted with great care.

The potential cycling in all the voltammograms always started at the cathodic limit. No particular

anodic or cathodic treatment was applied prior to the cycling. Every voltammogram was recorded after 5 cycles, except for the voltammograms under low scan rates (2 and 5 mV/s) which were recorded after 2 cycles, because the stabilization is more rapid. The reproducibility is generally good under a certain set of experimental conditions. However, in these preliminary experiments the oxygen partial pressure was controlled by adjusting the flow with a bubble flowmeter. So, some slight differences observed in the voltammograms were attributed to the relative imprecision of the oxygen partial pressure control.

There are several methods for the evaluation of the peak current and the subject is still under discussion among scientists. In the absence of capacitive effects, the peak current of the cathodic wave should be measured from the decaying anodic current as a baseline [Bard, 1980]. This method is not applicable in the absence of a reverse peak. In aqueous electrochemistry, the influence of the double layer charging current is reduced by subtracting from the I-E curve for the test solution, the I-E curve for the electrolyte solution in the absence of the electroactive species [Greef, 1990]. Such a subtraction is not possible with the zirconia electrolyte, since the absence of oxygen modifies the ionic conductivity. In high temperature electrochemistry, the most frequently applied method is to measure the current from a baseline, such as the one depicted in figure 4.5, which reproduces artificially the voltammogram in the absence of the peak. Unfortunately, it is not always easy to trace such a baseline and the measurement is not precise. If the baseline is assumed to delimit the portion of the current due to the double layer charging, then the current at the baseline should depend linearly on the scan rate. However, this test is not systematically applied. In the absence of capacitive effects, it is also possible to measure the peak current from the line of zero current. Here, the peak currents are systematically calculated with respect to a baseline, although some measurements from the zero line are also reported. In order to avoid confusion, the current determined from the zero current line will be called I_z and the one estimated from the baseline I_b.

Effect of scan rate

The effect of varying the potential sweep rate v on the cyclic voltammogram is shown in figure 4.6. The potential is scanned from -0.2V to 0.6V at 435°C in figure 4.6a and from -0.5V to 0.7V at 330°C in figure 4.6b. Both series of voltammograms were obtained under an oxygen partial pressure of 0.3 kPa. Increasing v causes an increase in the peak current I_p and a negative shift to the cathodic peak potential E_p.

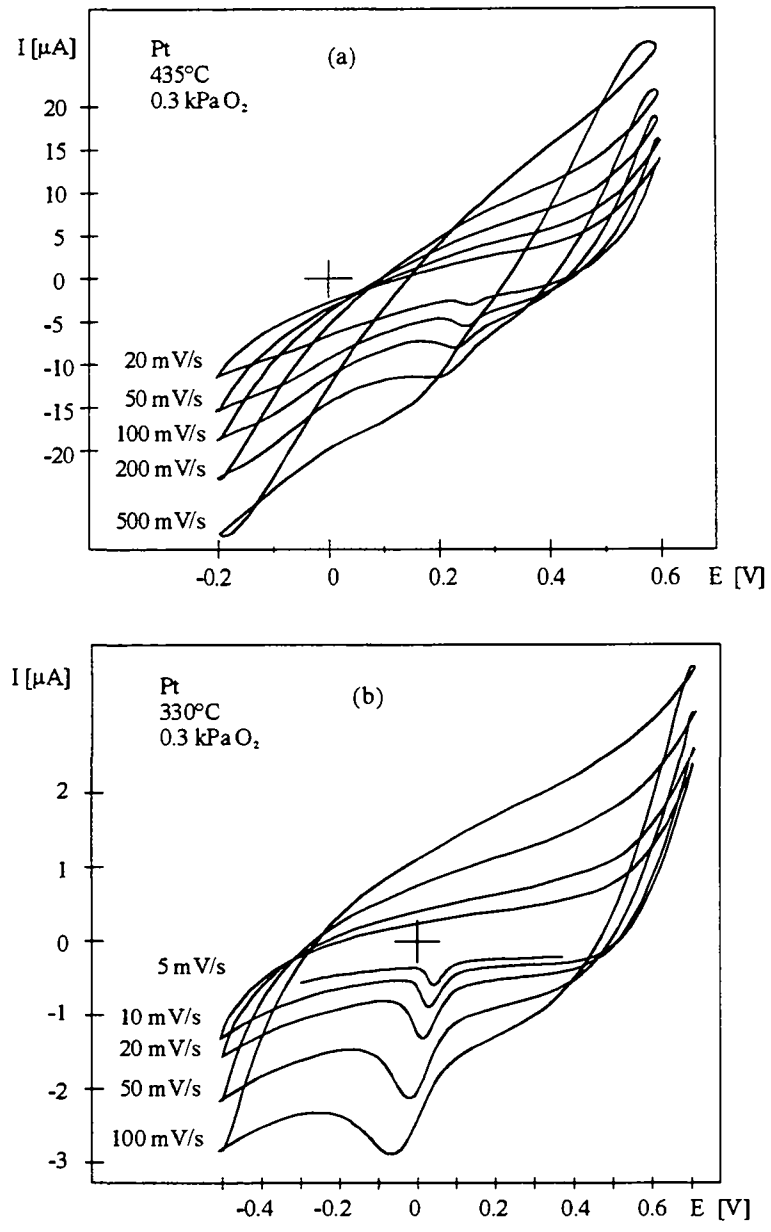

Fig. 4.6 Cyclic voltammograms of Pt films exposed to P_{O2} = 0.3 kPa for various scan rates (a) at 435°C from -0.2V to 0.6V and (b) at 330°C from -0.5V to 0.7V.

The peak current is proportional to the square root of the scan rate. The linear relation between I_p and $v^{1/2}$ is shown in figure 4.7a for several sets of experimental conditions. It is known from the literature on aqueous electrochemistry (see §2.1.3) that a linear dependence of I_p on $v^{1/2}$ is characteristic of an electrochemical process where the reactant is diffusing to the reaction site, while a linear dependence of I_p on v suggests a process implying a reactant in the adsorbed state. Jiang et al. [Jiang, 1993] reported the same I_p dependence on $v^{1/2}$ while Chao et al. [Chao, 1991] conclude that I_p is not proportional to v nor to $v^{1/2}$, although the latter seems to be the case in their plots at low temperatures. Vayenas et al. [Vayenas, 1991b] found a linear dependence of I_p on v and attributed the peak to the reduction of oxygen adsorbed at the TPB.

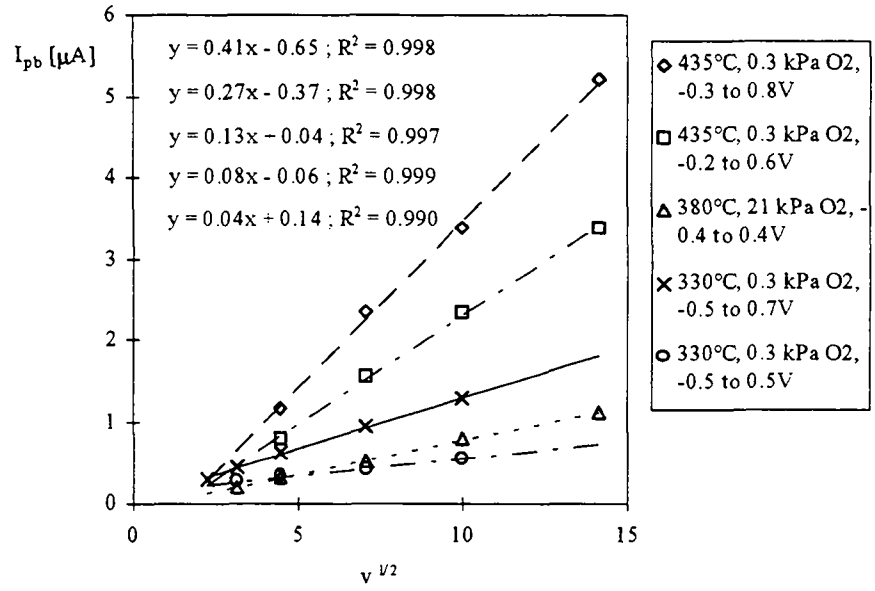

(a)

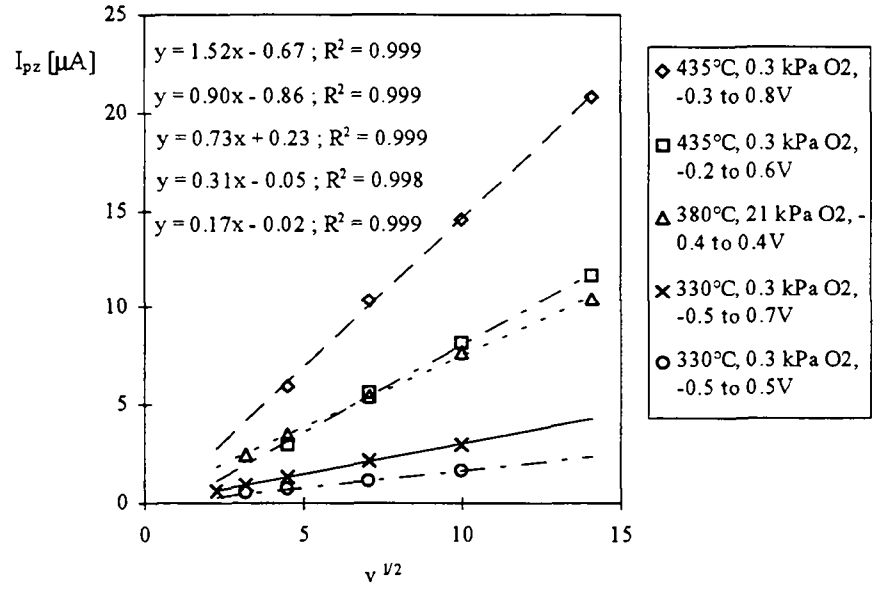

(b)

Fig. 4.7 The dependence of the peak current on $v^{1/2}$ under various experimental conditions; the scan rate is expressed in mV/s.

In the present study, the redox reaction is diffusion controlled and any perturbation from a chemical reaction preceding or following the charge-transfer step can be excluded, at least in the range of scan rates studied. The peak may be assigned to the decomposition of a platinum surface oxide:

$$PtO_x + 2xe^- + xV_{\ddot{o}} \rightarrow Pt + xO_o^x$$

The formation of the oxide by the reverse reaction during the anodic scan is probably slow due to the competition between the incorporation of the oxygen in the platinum oxide and the discharge of the oxygen anions.

The process is not reversible since there is no anodic peak and the peak potential is not independent of the scan rate. The absence of a reverse peak can be partially due to the formation of platinum oxide by a chemical reaction, which is known to be slow [Chao, 1991]. The variation of the peak potential with ln(v) is shown in figure 4.8. The relation is linear only in air at 380°C, indicating an irreversible reaction, but not at lower oxygen pressures. Chao et al. [Chao, 1991] did not observe any linearity in air while Jiang et al. [Jiang, 1993] observed a linear relationship under various conditions with only slight deviations at low oxygen pressures.

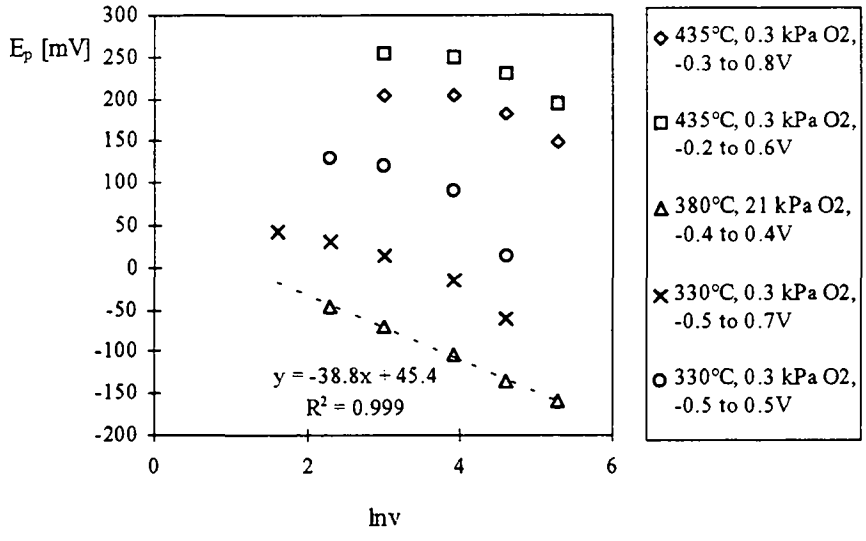

Fig. 4.8 The dependence of the peak potential on the logarithm of the scan rate; same conditions as in figure 4.7

Interestingly, the linear relation between the peak current and $v^{1/2}$ (Fig. 4.7a) is also respected when the current is measured from the zero current line (Fig. 4.7b). Since I_{pb} and I_{pz} obey the square root law, the difference I_{pz}-I_{pb} will also obey it. If the baseline were due to the double-layer charging, then I_{pz}-I_{pb} would be proportional to the scan rate. This observation suggests that the contribution of the capacitive component to the global current is negligible. The current is due to the superposition of two distinct faradaic processes. Although a linear dependence of both I_{pb} and I_{pz} on $v^{1/2}$ has already been reported [Fabry, 1979; VanHassel, 1992b], the authors did not draw any conclusion concerning the origin of the baseline current.

In order to learn more about the faradaic process, which is not related to the peak, the current I_z was measured at various cathodic and anodic potentials around the peak potential. The plots of I_z versus $v^{1/2}$ in 0.3 kPa O_2, at 330°C are given in figure 4.9 for the cyclic voltammograms depicted in figure 4.6b. The peak current I_{pb} is reported with the cathodic currents I_{cz} in figure 4.9a, while the anodic currents I_{az} are shown in figure 4.9b.

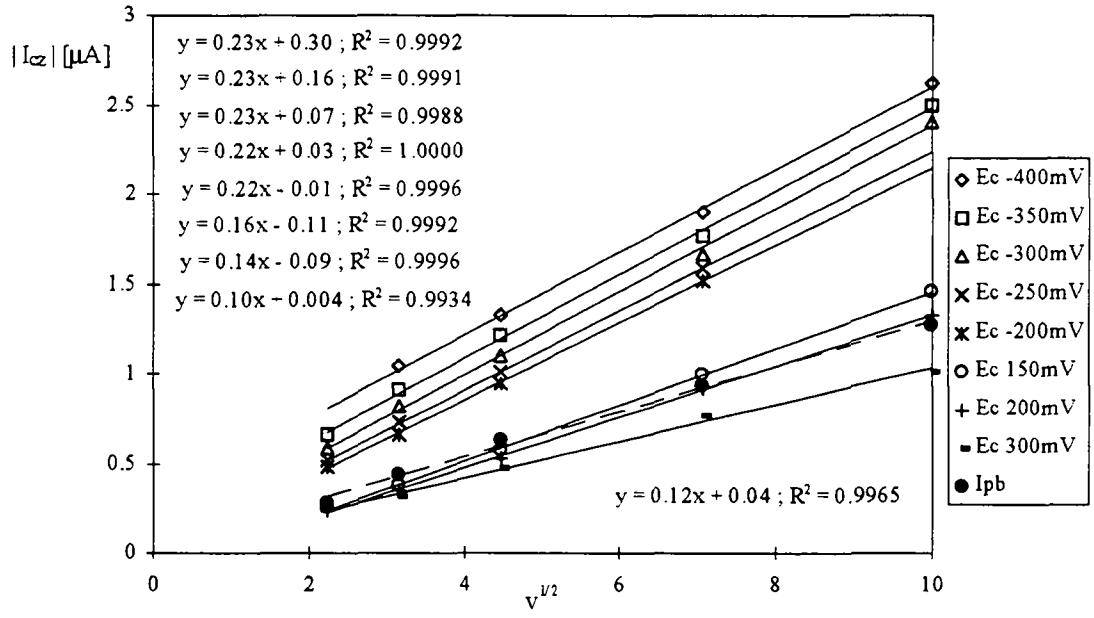

(a)

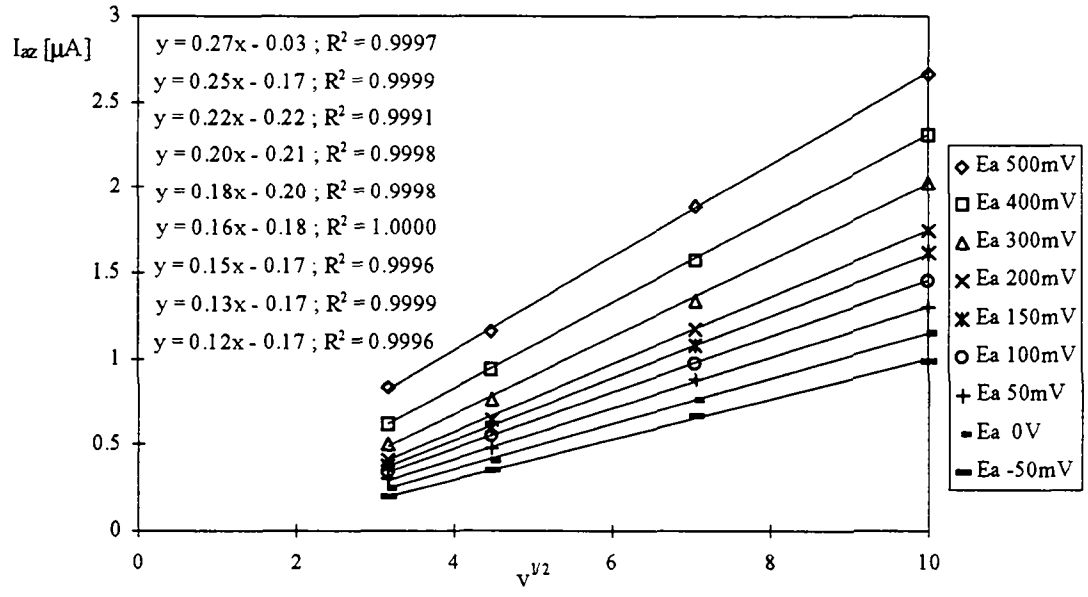

(b)

Fig. 4.9 Dependence of the cathodic (a) and anodic (b) current I_z (measured from the zero current line) on $v^{1/2}$ at several potentials. The voltage was scanned from -0.5V to 0.7V in 0.3 kPa O_2, at 330°C. The peak current I_{pb} (measured from the estimated baseline) is reported in (a). The corresponding cyclic voltammograms are shown in figure 4.6b.

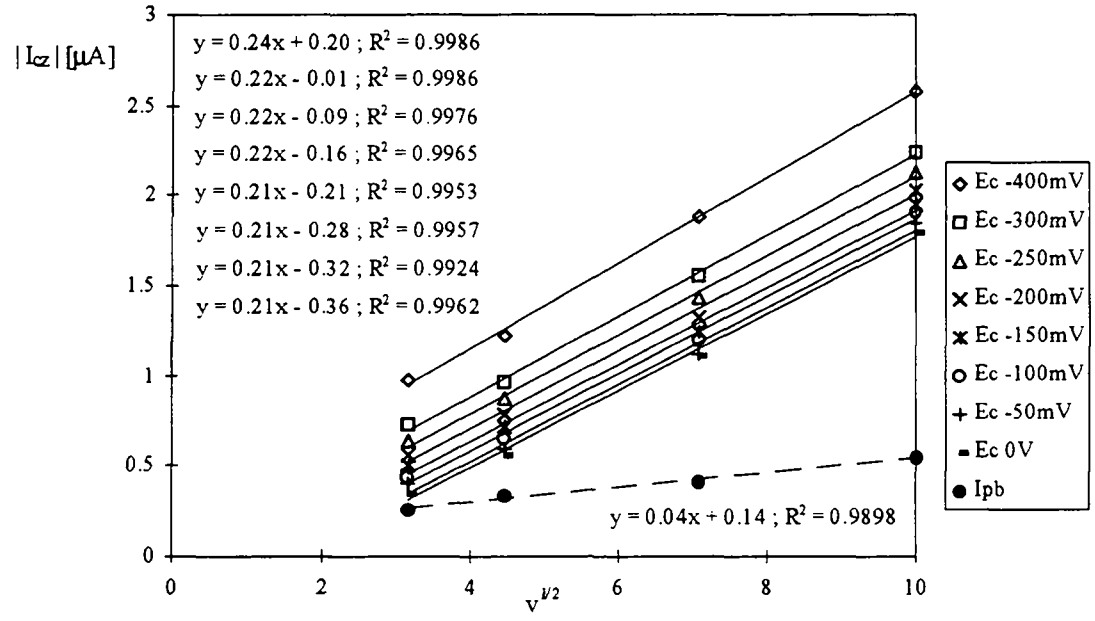

(a)

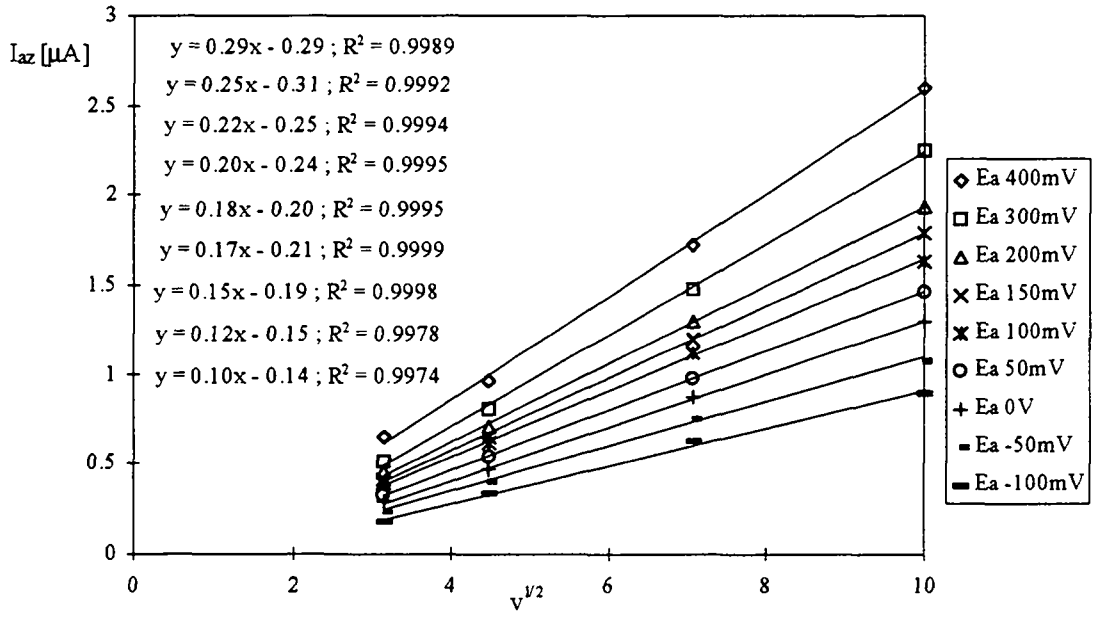

(b)

Fig. 4.10 Dependence of the cathodic (a) and anodic (b) current I_z (measured from the zero current line) on $v^{1/2}$ at several potentials. The voltage was scanned from -0.5V to 0.5V in 0.3 kPa O_2, at 330°C. The peak current I_{pb} (measured from the estimated baseline) is reported in (a).

The dependence of the cathodic currents on $v^{1/2}$ is linear and presents two distinct regions. At potentials more negative than the peak potential, the linear plots of I_{cz} vs $v^{1/2}$ have approximately the same slope, which differs markedly from the slope at the peak potential. It seems that the faradaic process occurring in this region is not perturbed by other reactions. The absence of a distinguishable peak due to this process may be due to the fact that the reaction takes place in the whole potential range. The reaction is probably reversible since there is no potential shift.

The cathodic current at positive potentials and the anodic current at all potentials also depend linearly on $v^{1/2}$, but the slope of the lines changes constantly with the potential. The variation of the slope can be explained by the interference of the two faradaic processes. Note that the peak currents I_{pb} and I_{pz} are not measured at a fixed potential but at the peak potential which shifts towards negative values with increasing scan rate. The linear dependence of the "baseline" current on $v^{1/2}$ occurs at a fixed potential, but the current does not change much with slight variations of the potential.

The I_z versus $v^{1/2}$ plots in figure 4.10 are similar to those in figure 4.9 and were obtained from voltammograms with an anodic reversal potential of 0.5 V instead of 0.7 V. In figure 4.10a, all the cathodic currents I_{cz} were measured at potentials lower than the peak potential E_{pc} and all the plots have the same slope.

The faradaic process responsible for the basic cathodic current may be due to the oxygen reaction which occurs slowly in the whole potential range and is accelerated at high negative potentials. The reverse reaction would take place during the whole anodic scan and would be particularly enhanced at high positive potentials.

Effect of reversal potential

The voltammograms obtained by varying the anodic reversal potential E_{ra} on the cathodic peak is shown in figure 4.11. Increasing E_{ra} causes an increase in the peak current and a shift of the peak potential to the negative direction. The cathodic peak disappears when the E_{ra} is smaller than approximately 0.3V. The exact E_{ra} value for which the peak is no longer visible is difficult to establish, and many curves are omitted in the figure for clarity. Note the hysteresis loops at the anodic side. Upon reversing the potential, the oxidation reaction goes on fast enough for the current to be higher during the reverse scan, until a "crossing" potential is reached. The hysteresis loops are more pronounced at high scan rates and temperatures but their relation to the cathodic peak is still unclear.

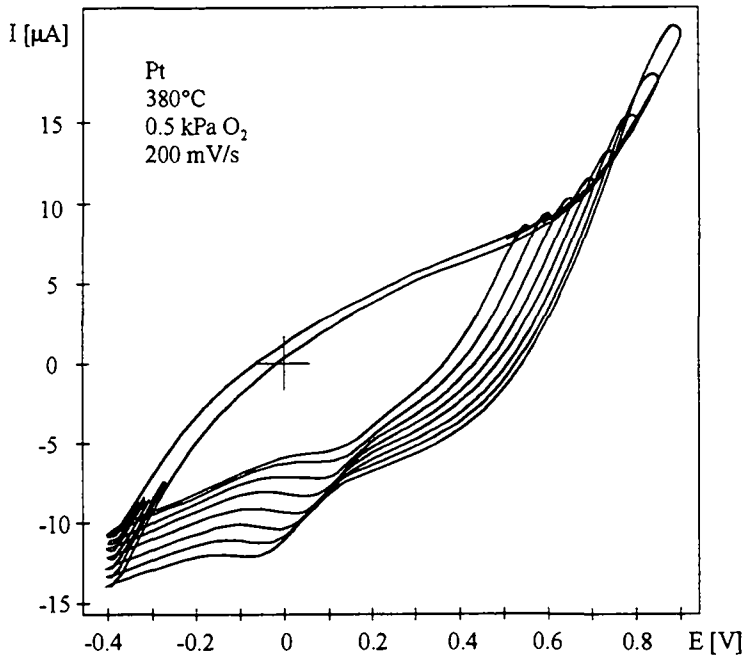

Fig. 4.11 Platinum voltammograms in 0.5 kPa O_2, with a cathodic reversal potential of -0.4V and the anodic reversal potential E_{ra} varied from 0.90V to 0.55V by steps of 0.05V. The temperature is 380°C and the voltage scan rate 200 mV/s.

The current increase and potential decrease with increasing E_{ra} is depicted on figures 4.12 and 4.13 respectively. The dependence of the current I_{pz} (Fig. 4.12b) on E_{ra} is linear, while the peak current I_{pb} (Fig. 4.12a) tends to a saturation state with increasing E_{ra}. The saturation state is reached earlier for low scan rates. A similar tendency was observed with the charge accumulated on the surface. The charge related to the peak is calculated by dividing the geometric area of the peak by the voltage scan rate. The charge first increases with increasing E_{ra} and then reaches a limiting value. Since the charge decreases with increasing scan rate, the saturation will be attained for a higher E_{ra} value. Under the same conditions, the second faradaic process, responsible for the current baseline, does not approach a saturation state.

The dependence of the peak potential on E_{ra} is linear and the negative shift may be due to the accumulation of oxygen in the surface oxide. A slight cathodic shift in the onset potential is also observed in figure 4.13. This can be explained by considering the presence of two peaks corresponding to two electrochemically active states of platinum oxide [Chao, 1991]. The second peak should form at higher anodic potentials or at a lower rate. Alternatively, the initially formed platinum oxide might rearrange to a more stable state, as in aqueous systems, requiring a higher cathodic potential for reduction [Chao, 1991].

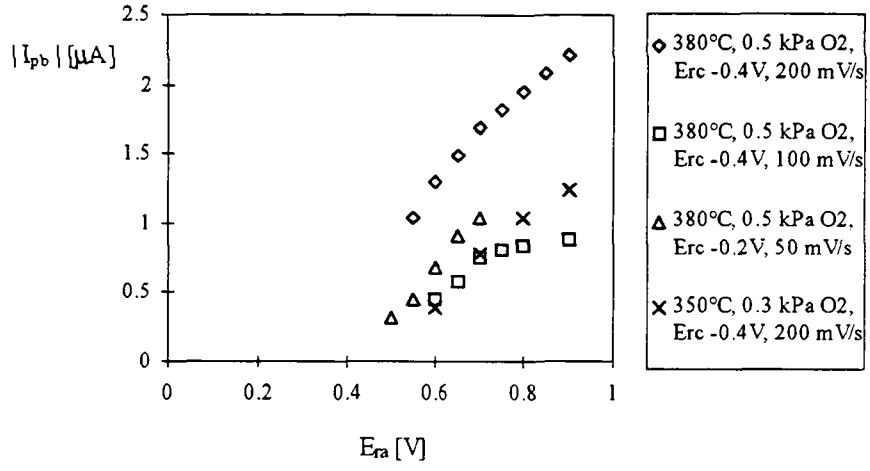

(a)

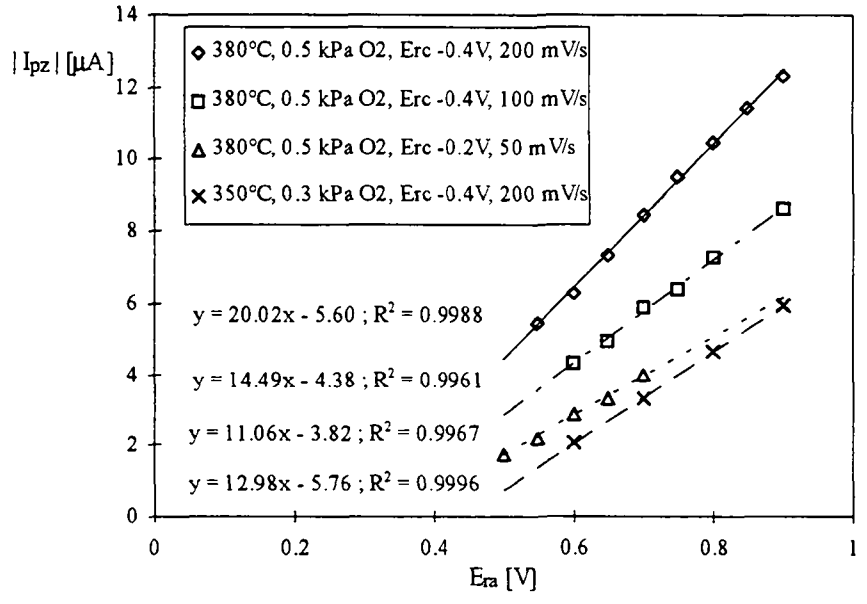

(b)

Fig. 4.12 Effect of the anodic reversal potential E_{ra} on the cathodic peak current I_{pb} (a) and I_{pz} (b).

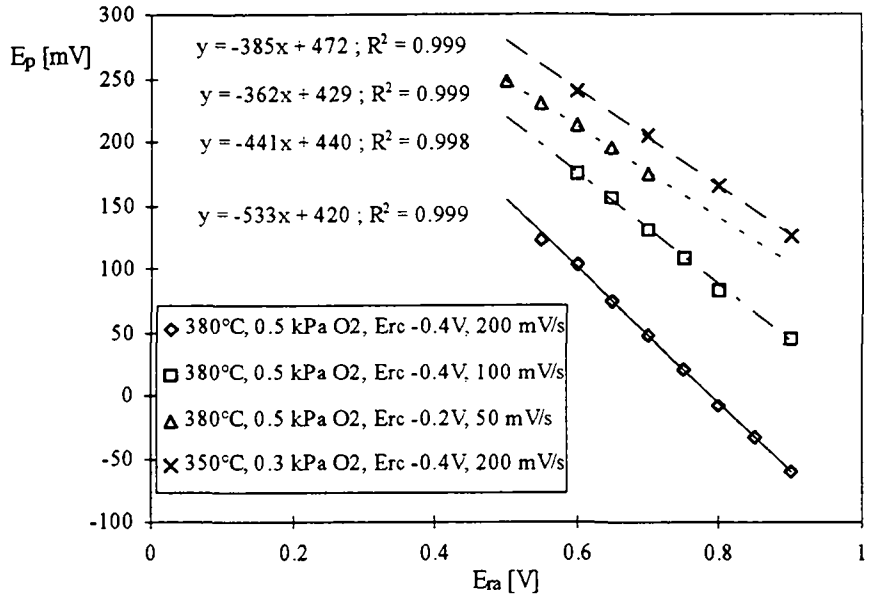

Fig. 4.13 Effect of the anodic reversal potential E_{ra} on the cathodic peak potential E_p.

Effect of holding time at fixed anodic potential

The voltammograms obtained by holding the anodic potential at a fixed value for different lapses of time is depicted in figure 4.14. The voltammogram is plotted once without interruption. The potential is then kept at the anodic limit for a holding time t_h, and the cathodic scan is recorded. After each cathodic scan, the system is allowed to return to the initial state by sweeping the voltage continuously for approximately ten cycles. The peak broadens with increasing t_h and might well encompass two peaks. The effect of keeping the potential at the anodic limit for a period of time is similar to the one of increasing the E_{ra}, as long as no additional reaction sets in because of the higher E_{ra} value. Since both the cathodic peak and the cathodic baseline are related to processes occurring in the anodic region, it is not easy to study them apart.

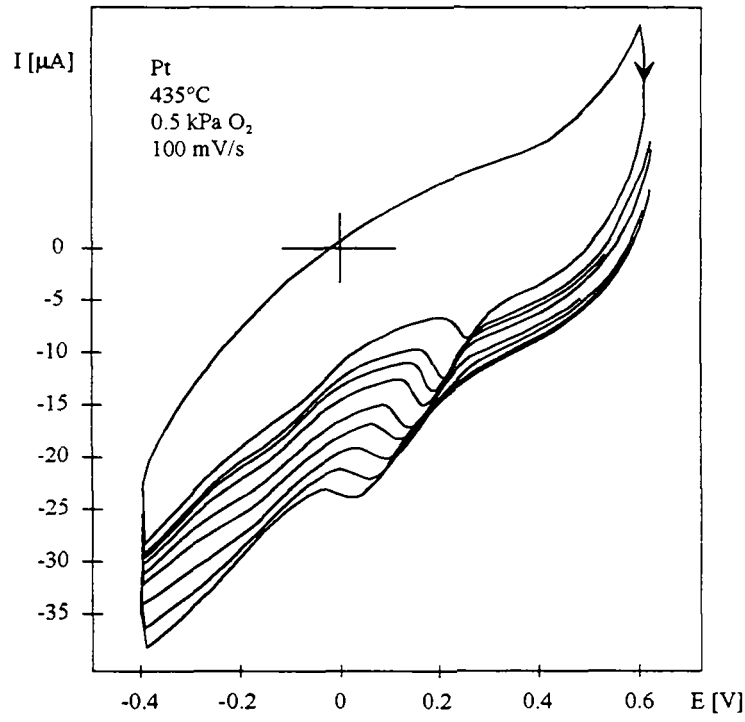

Fig. 4.14 Platinum voltammograms in 0.5 kPa O_2 for several holding times at 0.6V: continuous, 3s, 6s, 12s, 24s, 48s, 2min, 5min and 10min. The temperature is 435°C and the scan rate 100 mV/s.

The effect of holding time on the cathodic current and the peak potential is shown in Fig. 4.15. The peak current I_{pb} and the peak charge attain their highest value within approximately 6s and then remain stable. The cathodic current I_{pz} initially increases rapidly with holding time and approaches a plateau. The absence of saturation in the voltammograms with increasing E_{ra} is compatible with the present result if the timescale of the two experiments is compared. Increasing the E_{ra} from 0.6 to 0.9V for voltammograms at a 100mV/s scan rate can be juxtaposed to holding the anodic potential at 0.6V for 6s.

The cathodic current I_{pz} related to the oxygen reaction

$$O_{ads} + V_{\ddot{o}} + 2e^{-} \rightarrow O_o^{x}$$

increases linearly with $\ln(t_h)$, as shown in figure 4.16. Jiang et al. [Jiang, 1993] observed a similar linear increase for the peak current I_{pb} and explained it with the Elovich equation for the adsorption rate. This explanation is consistent with their attribution of the peak to the reduction of oxygen adsorbed at the TPB. In addition, the authors remark that the Elovich equation being derived on the assumption of linear decrease in chemisorptive bond strength with coverage, it is related to the interpretation of NEMCA [Jiang, 1993]. In the present study, the oxygen reaction is assumed to be limited by the diffusion of the oxygen vacancies to the reaction sites, because of the linear current dependence on the scan rate square root. However, upon holding the potential at an anodic value for some time, it cannot be excluded that a change occurs in the limiting step. The oxygen adsorption step may then control the reaction rate.

The peak potential shifts cathodically with t_h and tends to an equilibrium value. It decreases

linearly with $\ln(t_h)$ and the slope is independent of the anodic potential at which the system is polarized, at least within restricted limits (Fig. 4.16).

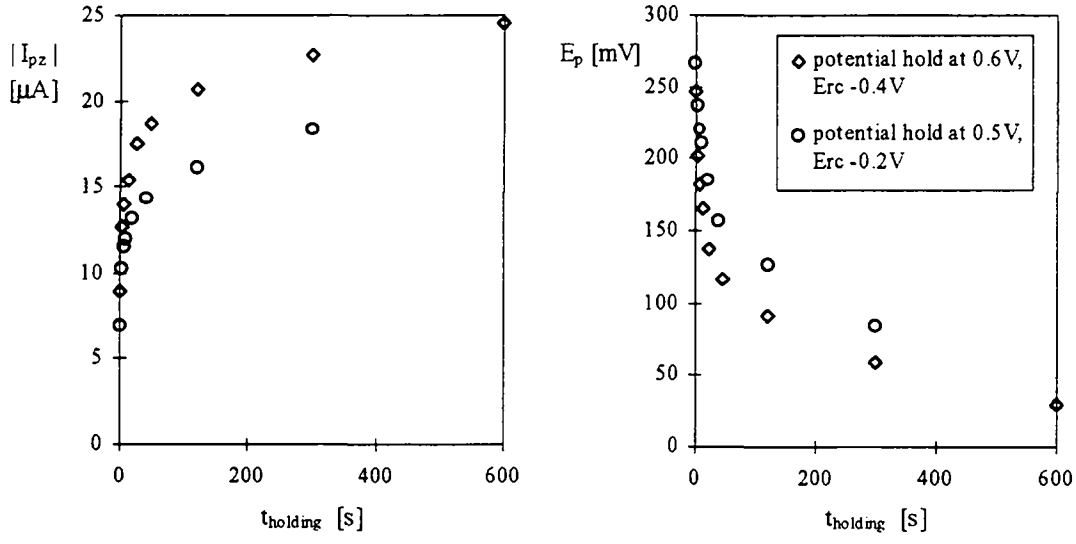

Fig. 4.15 Effect of holding time at 0.6V and 0.5V on the cathodic peak current and potential, in 0.5 kPa O_2 and at 435°C. The scans are recorded at 100 mV/s and the cathodic reversal potentials are -0.4V and -0.2V respectively.

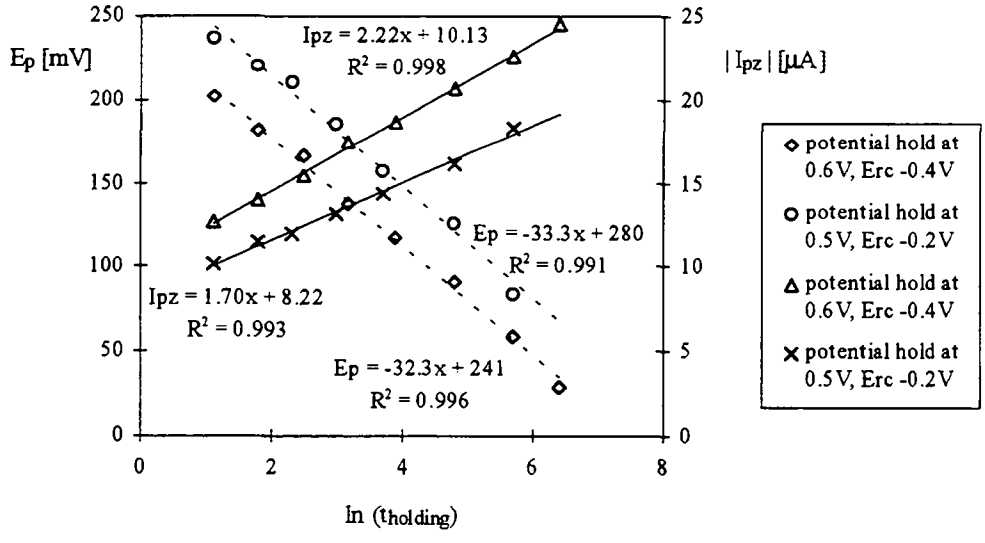

Fig. 4.16 Dependence of the peak potential and cathodic peak current I_{pz} on the logarithm of the holding time, at 435°C, 100 mV/s and 0.5 kPa O_2.

Effect of temperature

The influence of the temperature on the cathodic peak is shown in figure 4.17: The peak current increases with temperature in the range from 300°C to 450°C, while the peak potential slightly shifts positively (Fig. 4.18a). In a voltammogram obtained at 585°C in air, the peak had almost vanished. Vayenas et al. [Vayenas, 1991b] observed a similar behaviour with the peak size increasing with temperature to a maximum near 450°C then decreasing and finally disappearing near 570°C.

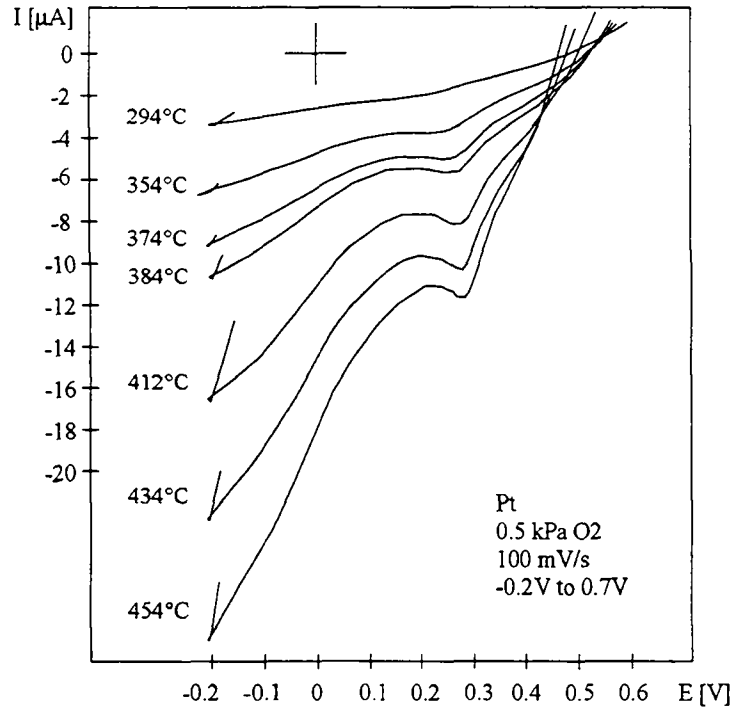

Fig. 4.17 Platinum voltammograms at several temperatures in 0.5 kPa O_2, with the potential scanned from -0.2 to 0.7V at 100mV/s.

The apparent activation energy of the diffusion process is estimated by rearranging the equation of the peak current dependence on the scan rate. The latter can be written in the form:

$$I_p^2 T = \text{const.} \cdot \exp(-E_a / RT)$$

assuming that the preexponential factor of the diffusivity does not depend on temperature. The activation energy is then calculated from the slope of the plot of $\ln(I_p^2 T)$ vs 1/T. Two such plots are presented in figure 4.18b, related to the platinum oxide reduction (I_{pb}) and the oxygen reduction process (I_{cz}). The apparent activation energies are 91 kJ/mol (0.9 eV) and 114 kJ/mol (1.2 eV) respectively. The cathodic current I_{cz} is measured at -100mV, where there is no contribution from the peak current.

The calculated values of the activation energy are very close to those reported by West [West, 1995] for the defect motion in YSZ (0.9 eV) and by van Hassel and Burggraaf [VanHassel, 1992b] for the diffusion of electron holes (111 kJ/mol). The activation energy for the diffusion of electrons (192 kJ/mol) is too high to be compared with the present results. Taking into account these values, the reduction of

platinum oxide is controlled by the diffusion of the oxygen vacancies, while the oxygen reduction is controlled by the diffusion of electron holes. The corresponding reaction can then be rewritten in the form:

$$O_{ads} + V_{\ddot{o}} \rightarrow O_o^x + 2h^{\cdot}$$

For this reaction to occur, some electronic conductivity in the solid electrolyte is necessary. The platinum electrode can act as the electron donor in the electrochemical reaction at the TPB, but not as an electron hole acceptor.

Yet another possibility for the oxygen reduction reaction is the control by the diffusion of dissociated oxygen along the platinum surface to the TPB. A value of 111 kJ/mol (1.15 eV) is reported for the activation energy of oxygen diffusion on the platinum surface [Moghadam, 1986]. In this case, the diffusing species would be the adsorbed oxygen and no hole injection in the electrolyte is needed.

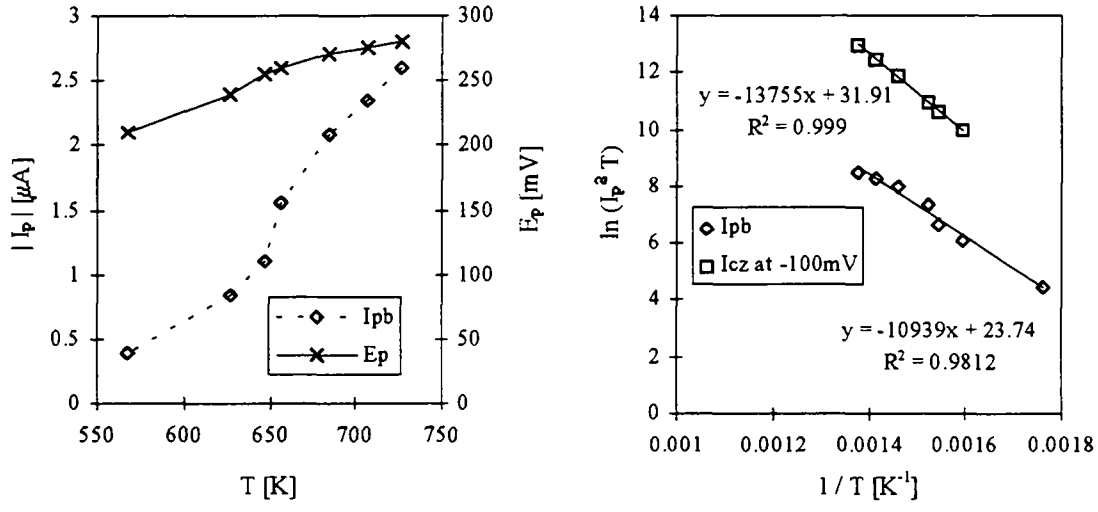

Fig. 4.18 Effect of temperature on the peak current and potential (a) for platinum electrodes in 0.5 kPa O_2. Determination of the apparent activation energy from the plots of $\ln(I_p^2T)$ vs 1/T for the two faradaic processes (b).

Effect of oxygen partial pressure

The influence of the oxygen partial pressure on the platinum voltammograms is complex. In this work, it has not been systematically studied, but some qualitative trends have been observed. The current increases and the open-circuit potential shifts negatively with increasing oxygen partial pressure. The voltammograms in figure 4.19 were obtained at 450°C after stopping the air flux to the reactor and continuously admitting nitrogen gas at a 20 cm^3 /s rate. The peak current decreases and the peak potential shifts positively with decreasing oxygen partial pressure. The size of the hysteresis loop at high anodic potentials also decreases with the peak size. The behaviour of the hump at more negative potentials, which has not been attributed to any particular faradaic process, is difficult to explain.

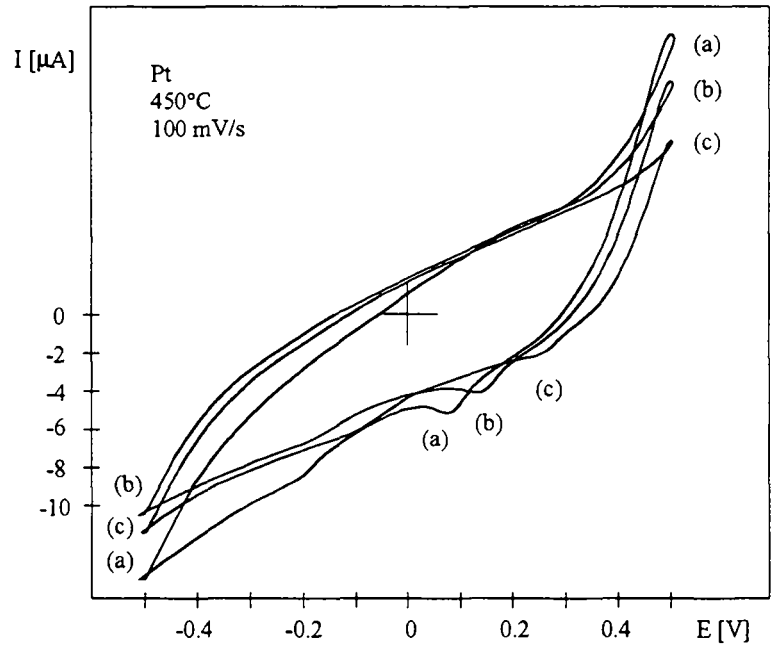

Fig. 4.19 Qualitative effect of oxygen partial pressure on the platinum voltammograms at 450°C. The curves a, b, c are plotted in the order of oxygen partial pressure decrease.

The presence of the peak even at very low oxygen pressures confirms the participation of lattice oxygen in the formation of platinum oxide by the reaction:

$$Pt + xO_o^x \rightarrow PtO_x + 2xe^- + xV_{\ddot{o}}$$

The contribution of oxygen gas in the oxide formation can be accounted for by assuming that the above reaction is indirectly enhanced at high oxygen partial pressures. The zirconia conductivity and lattice oxygen availability increase because of the second reaction:

$$O_2\,(g) \rightarrow 2O_{ads}$$

$$2O_{ads} + 2V_{\ddot{o}} + 4e^- \rightarrow 2O_o^x$$

In the above mentioned scheme, the oxygen vacancies in the zirconia lattice are the diffusing species for both cathodic reactions.

In conclusion, the preliminary investigation of the Pt / 8YSZ interface by cyclic voltammetry allowed a qualitative description of the system. Purely capacitive effects, due to the double-layer charging, seem absent and so do adsorption controlled processes. Evidence is advanced for the occurrence of a faradaic reaction in the whole potential range studied. The main cathodic peak on the voltammograms is attributed to the destruction of a platinum oxide and the current baseline to the oxygen reaction, occurring in the whole potential range.

4.2.2 High temperature cyclic voltammetry on IrO_2/YSZ electrodes

The voltammetric study was performed on two different cells of the type $O_2(g)$ / IrO_2 // YSZ // Au / $O_2(g)$. The first cell was identical to the one used for the preliminary results. The 160 μg IrO_2 (0.3 cm^2) catalyst was applied on a disk (13mm diameter, 1.7mm thickness) of zirconia stabilized with 8% mol yttria (8YSZ). The second cell is the one with which the main investigations (§4.2.3 and 4.2.4) were performed. The 63 μg IrO_2 (0.5 cm^2) catalyst was applied on a plate (26mm × 13mm and 1mm thick) of zirconia stabilized with 6% mol yttria (6YSZ).

The situation is much more complicated than for platinum and it is difficult to choose a "typical" voltammogram. In air, most voltammograms are featureless, with the current rising at high and low potentials due to the gaseous oxygen evolution. Several peaks become distinct as the oxygen partial pressure decreases. The two cells gave rise to apparently different voltammograms. An example is shown in figure 4.20. The main difference between the two cells lies in the thickness of the solid electrolyte. The currents are smaller by an order of magnitude in the case of the thicker electrolyte (Fig. 4.20a). The inclination of the whole voltammogram is also more pronounced than in figure 4.20b, because of the higher ohmic drop. The electrolyte doping does not play a significant role, nor does the lower partial pressure of oxygen in figure 4.20a.

The main anodic peak A1 at 170 mV (Fig. 4.20a) has no visible cathodic counterpart here, while the anodic hump A2 may be related to the cathodic C2. The anodic hump A1' (Fig. 4.20b) with the corresponding cathodic C1' are probably due to the same process as the peak A1. The cathodic peak C2' at around 500 mV is better defined than the equivalent C2. The wide peak A1 is double, but the two peaks can only be distinguished at higher scan rates. The letters A_n and C_n refer to the YSZ (8% mol) and the letters A'_n and C'_n refer to the YSZ (6% mol).

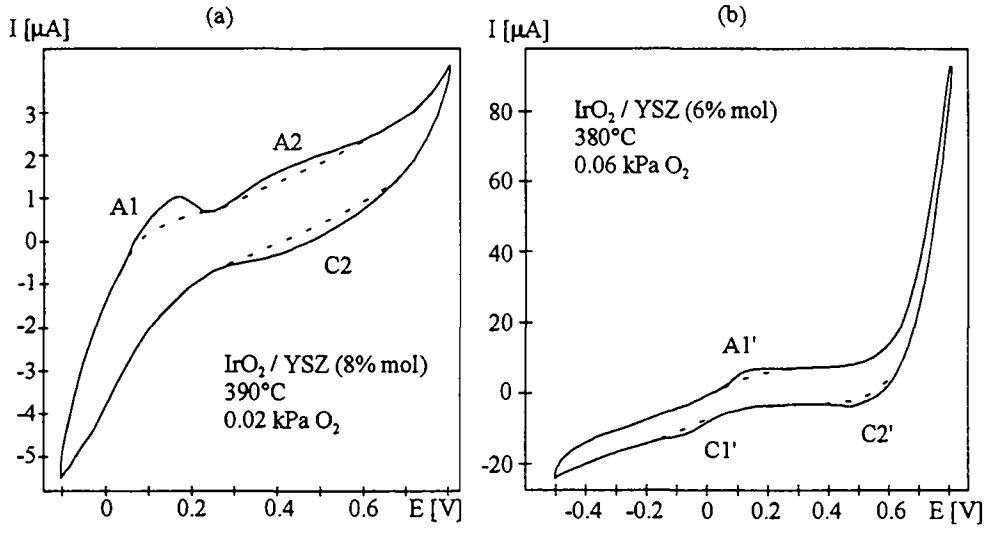

Fig. 4.20 Cyclic voltammograms of an IrO_2 catalyst supported on 8YSZ (a) and 6YSZ (b). Both current-potential curves were recorded at a 10 mV/s scan rate.

The effect of the oxygen partial pressure on the two redox processes is difficult to establish. The peaks are better defined in low oxygen pressures, where the peaks of the main faradaic reaction, i.e. the oxygen reaction, are sufficiently spaced. The voltammograms become almost featureless at a partial pressure of 1 kPa O_2 for low scan rates. The cathodic peak C2', however, is obvious even in air for voltage scan rates above 100 mV/s.

The investigation proceeded as in the case of platinum (§4.2.1.). In order to identify the different processes taking place during the potential scanning, the voltammograms were traced at several scan rates, reversal potentials and temperatures. The evaluation of the peak current is more problematic with IrO_2 than with Pt, because the peaks appear in regions where the current baseline has an important curvature. Here, all the currents are measured from the line of zero current.

Effect of scan rate

The effect of varying the potential sweep rate v on the cyclic voltammograms is shown in figures 4.21 and 4.22. In figure 4.21, the potential is scanned from -0.5V to 0.8V at 380°C, in the IrO_2 / 6YSZ cell. The anodic hump at around 50 mV and the cathodic one at -50 mV are not very well defined. There is no experimental indication that the anodic hump might hide two peaks. On the other hand, the cathodic peak called C2' is clearly traced and shifts negatively with increasing scan rate. The most striking feature in this series of voltammograms is the existence of two "invariant" points, where all the curves meet. For any voltage scan rate, the current is 6 μA at 610 mV on the anodic side and -12 μA at -340 mV on the cathodic side. No explanation was found for this observation, reproduced on several occasions.

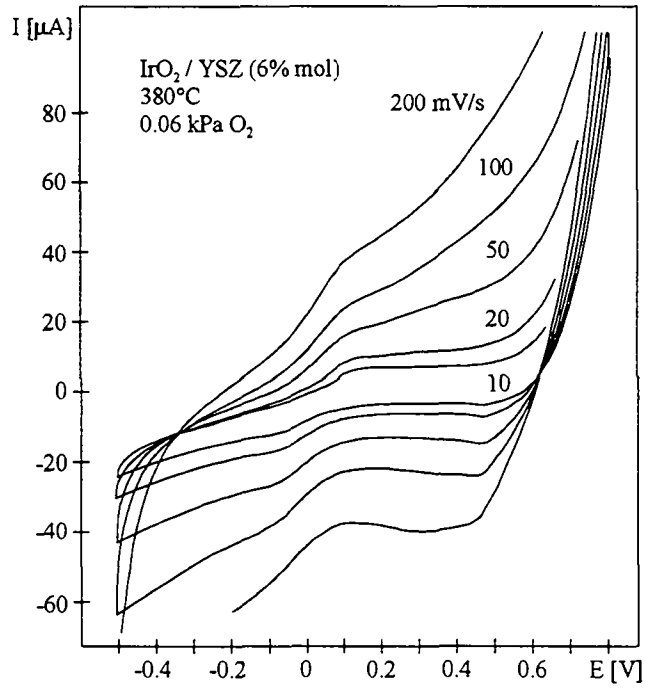

Fig. 4.21 Cyclic voltammograms of the IrO_2 / 6YSZ catalyst exposed to 0.06 kPa O_2 , from -0.5V to 0.8V.

In figure 4.22, the potential is scanned from -0.1V to 0.8V at 390°C, in the IrO_2 / 8YSZ cell. The wide anodic peak at low scan rates is separated in two peaks as the scan rate is increased above 50 mV/s. The global current increases with increasing v, but the effect on the peak currents is not clear. When the scan rate is increased from 2 mV/s to 5 and 10 mV/s, the wide peak potential shifts negatively. This may be due to an enhanced contribution of the peak at lower potential to the global peak. At higher scan rates, there is a positive shift of both anodic peak potentials E_{p1} and E_{p2}. At 2 mV/s, a cathodic hump is visible at around 50 mV. It is probably related to the anodic peak, since, at low potential sweep rates, the ratio of the electron transfer rate to the mass transfer rate is higher and the process approaches the reversibility.

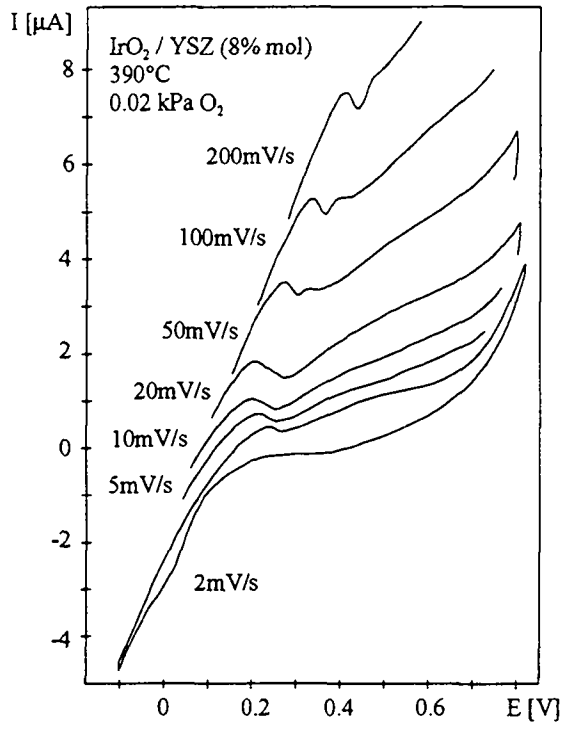

Fig. 4.22 Cyclic voltammograms of the IrO_2 / 8YSZ catalyst exposed to 0.02 kPa O_2 , from -0.1V to 0.8V.

The anodic peak current, measured from the zero current line, was found to vary linearly with the square root of the scan rate, like in the case of Pt electrodes. So, the corresponding faradaic process is diffusion limited. The linear relation between I_p and $v^{1/2}$, in the IrO_2 / 8YSZ cell, is shown in figure 4.23 for several sets of experimental conditions.

This anodic process is not reversible on the timescale of the experiment, since the peak potential increases linearly with ln(v). This means that the electron transfer rates at all potentials are significantly slower than the rate of mass transport. Therefore, no Nernstian equilibrium is maintained at the electrode surface. Two examples of the peak potential variation with ln(v) are shown in figure 4.24 for the IrO_2 / 8YSZ cell. The potential was scanned from 0 to 0.7V at 340°C and 390°C. At the lower temperature, only one peak could be distinguished at the low scan rates used. At higher temperature, the two peaks were more or less clearly defined and the linear dependence is obeyed for both E_{p1} and E_{p2}. The slope of the line is very

similar for both peaks, suggesting that they are related to the same faradaic process, i.e. the double anodic peak in figure 4.22.

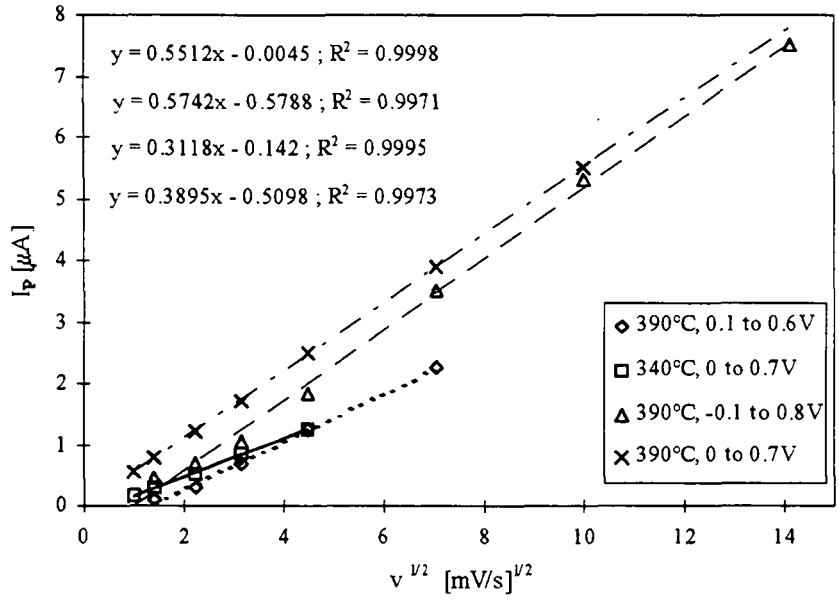

Fig. 4.23 The dependence of the peak current on $v^{1/2}$, for the IrO_2 / 8YSZ catalyst in 0.02 kPa O_2.

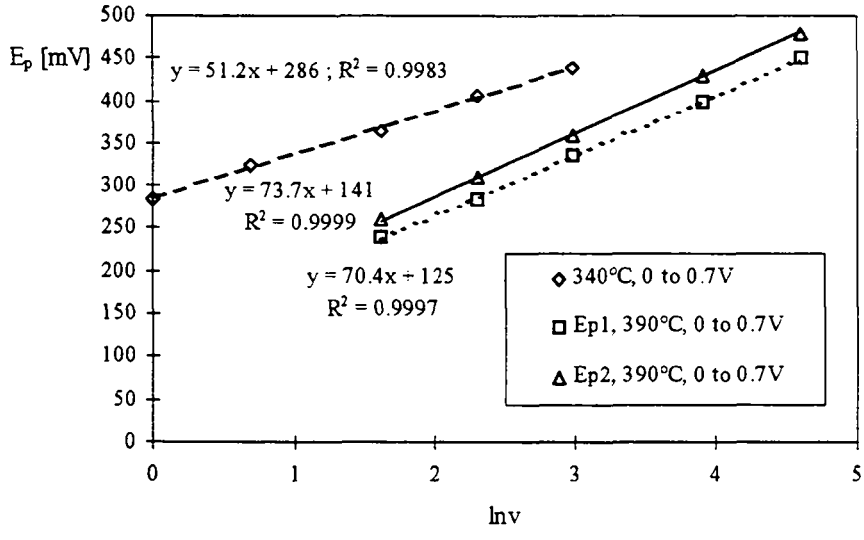

Fig. 4.24 The dependence of the anodic peak potential on the logarithm of the scan rate, for the IrO_2 / 8YSZ catalyst in 0.02 kPa O_2.

The baseline current also depends linearly on $v^{1/2}$ as is shown in figure 4.25, where the current is measured at several anodic (Fig. 4.25a) and cathodic (Fig. 4.25b) potentials. The linearity is not observed for potentials in the region of the peak. It seems that the contribution of the peak to the global current is prevailing in that region and explains why a linear relation is observed between I_p and $v^{1/2}$, where I_p is measured at the *peak* potential and not at *fixed* potential. The linear correlation in figure 4.25a is not very

satisfactory for the anodic currents at 0 mV and 50 mV, probably because the current still includes some contribution from the peak process at low scan rates.

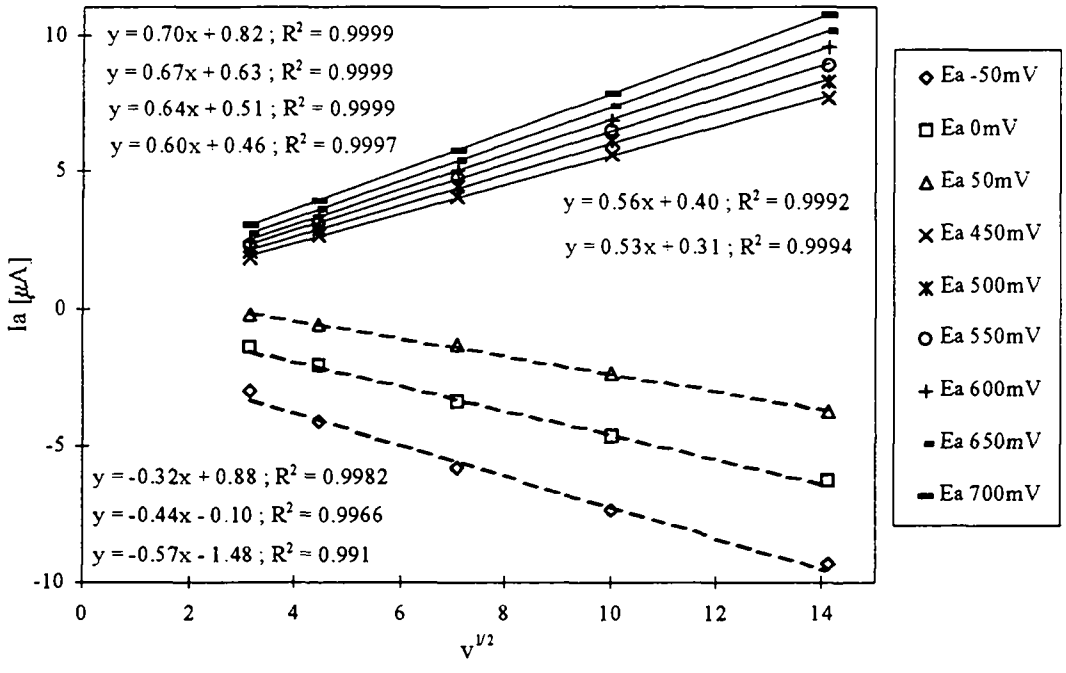

(a)

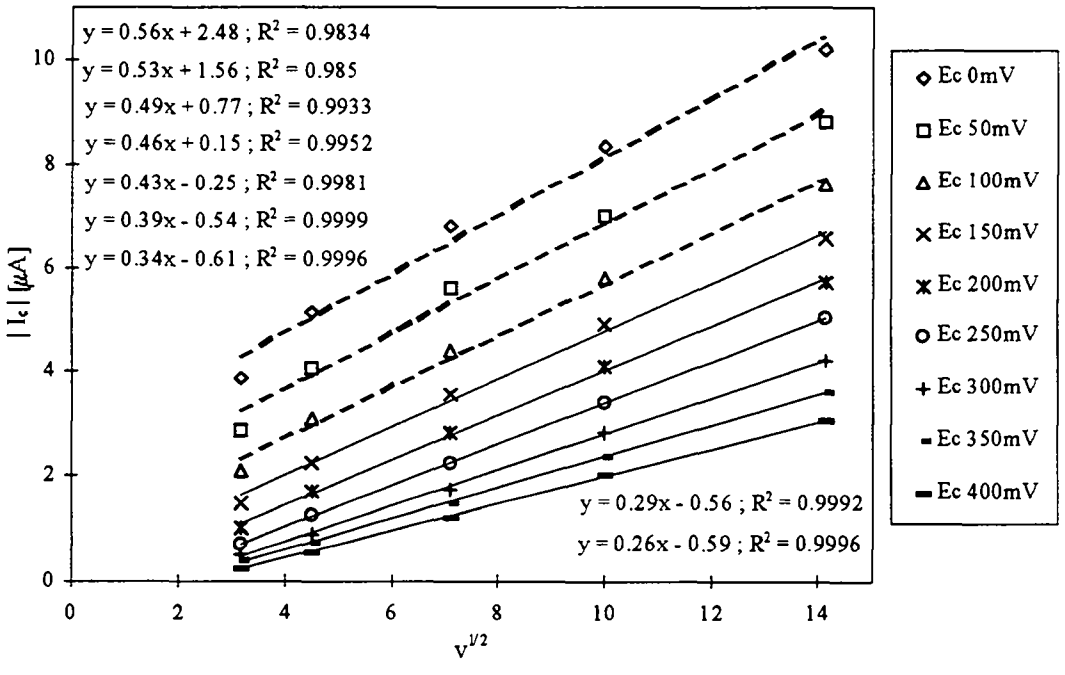

(b)

Fig. 4.25 Dependence of the anodic (a) and cathodic (b) current on $v^{1/2}$ at several potentials, for the voltammograms depicted in figure 4.22. The voltage was scanned from -0.1V to 0.8V in 0.02 kPa O_2, at 390°C.

The same remark stands for the cathodic currents measured in the potential range from 0 mV to 150 mV (Fig. 4.25b). This observation indicates that a second faradaic process is interfering in that range, probably related to the anodic one, even if there is no distinguishable peak. The linear correlation in the range from 200 to 400 mV is perfect, so the quality of the correlation can be used to determine if more than one processes coexist in a given potential range.

The fact that the current is strictly dependent on $v^{1/2}$ in the whole potential range is very astonishing. It implies that purely capacitive effects are absent. The charge accumulation at the double layer is still possible, but only due to the slow supply or removal of electroactive species at the interface. The double layer charging is thus associated to an electrochemical reaction. In aqueous electrochemistry, the term "pseudocapacitance" is generally used to describe the charge accumulation at the interface through a redox reaction. The term "capacitance" is used when the charged species accumulate at the interface without any faradaic reaction taking place. Purely capacitive effects are frequent in wet electrochemistry, especially at high scan rates.

In order to verify if the absence of capacitive effects is limited to a given set of experimental conditions, the effect of the scan rate was studied in a series of experiments at reduced timescale. The potential was scanned in a restricted range around the open-circuit, from 50 mV to 150 mV. The oxygen reaction is very slow and the time required for a complete scan is short. An example is given in figure 4.26a, where the scan rate is varied from 5 to 100 mV/s. The current measured from the zero line is proportional to the scan rate and a slight deviation from linearity is observed at scan rates above 100 mV/s. Supposing that no faradaic reaction takes place at this potential, in such a short time interval, the linear relation between the current and the scan rate is attributed to the charging of the double layer interface.

The capacitance C_d of the electrode-electrolyte interface can be calculated from the width δI of the voltammogram, according to the relation [Bard, 1980]:

$$\delta I = 2 \cdot v \cdot C_d$$

A series of voltammograms was recorded in air, but the reproducibility of the capacitance values was not always satisfying. The width of the voltammograms was found to depend on the humidity level in the reactor. The voltammetric curves in figure 4.26b were obtained in air, saturated with water vapour at 24°C. The synthetic air feed was forced through a closed water reservoir, and the vapor content in the feed was analyzed by gas chromatography. The calibration of the GC-analyzer for the water measurement is very difficult, so the quantity of water is reported as the area of the peak on the chromatogram. It is a relative measure, but the capacitance values are reproducible at a given humidity level in the reactor. Indicative values of the vapour content are peak areas of "w260000" for air saturated with water vapour (Fig.4.26b) and "w500" for dry air.

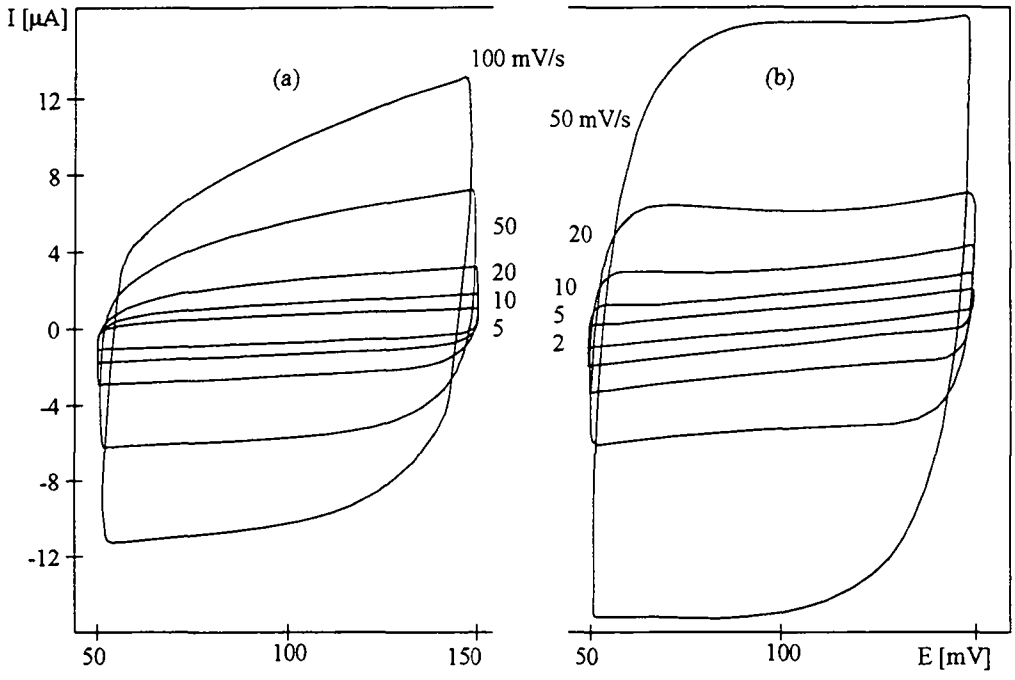

Fig. 4.26 Cyclic voltammograms of the IrO_2 / 6YSZ electrode, recorded from 50 to 150 mV, in 20 kPa O_2 , at 400°C (a) the scan rate v is 5, 10, 20, 50 and 100 mV/s ; (b) the scan rate v is 2, 5, 10, 20 and 50 mV/s and the oxygen feed is saturated with water at 24°C.

After a period of inactivity, during which no feed is supplied to the reactor, the water vapour content in the reactor is high ("w4000"). The diffusion of ambient vapour, as well as carbon dioxide, is detected in the beginning of each set of experiments. The gas mixtures of the feed contain a negligible level of humidity, so the humidity is greatly reduced in a few hours ("1000"). The water production by the ethylene oxidation is undetectable; the water peak area does not change when ethylene is added to the oxygen feed.

The influence of the vapour content on the cyclic voltammograms and the interface capacitance is studied in the following experiment. The feed (20 kPa O_2 in He) is first supplied to the reactor via a closed vessel containing water at 24°C. Then, the saturator is removed from the feed and the water content in the reactor starts to decrease. Several voltammograms are recorded and corresponding GC analyses performed during this decrease. The voltage is scanned from 50 to 150 mV, at 400°C. The capacitive current I_{cap}, defined as half the width of the cyclic voltammogram, is measured at 100 mV and depends linearly on the scan rate v, as is shown in figure 4.27a. The capacitance of the interface is given by the slope of the linear correlations between I_{cap} and v. Interestingly, the capacitance increases linearly with the water content, at least in the range studied. The evolution of the capacitance C_d with the water vapour content in the reactor is given in figure 4.27b.

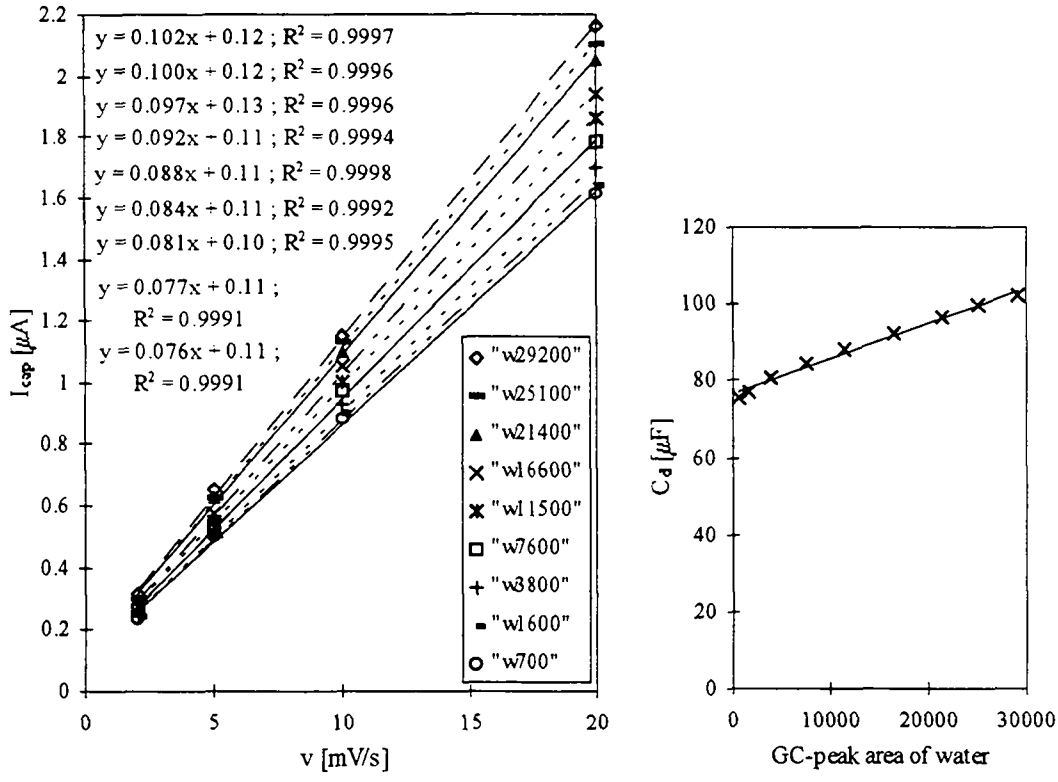

Fig. 4.27 The water influence on the cyclic voltammograms of the IrO_2 / 6YSZ electrode at 400°C, recorded in 20 kPa O_2 , from 50 to 150 mV; (a) effect of the scan rate v on the capacitive current for several water vapour contents in the reactor; (b) effect of the vapour content on the capacitance of the electrode-electrolyte interface.

The capacitance values are further increased in presence of ethylene. The current is also proportional to v when the potential is scanned in a restricted range around the open-circuit voltage. Water and ethylene do not dissolve in the solid electrolyte but can only adsorb on the surface of the catalyst and/or electrolyte. So, the enhancement of the capacitance at the electrode-electrolyte interface, by the presence of water vapour or ethylene in the gaseous phase, shows unambiguously that the processes occurring at the electrochemical interface and those occurring at the solid-gas interface are related. This observation is not surprising since the theory of the NEMCA effect precisely establishes this relation. However, it proves that the processes at the electrode-electrolyte and electrode-gas interfaces are linked, even in the absence of a catalytic gas phase reaction. On the other hand, the assumption that no faradaic reaction takes place is not necessarily valid. The linear dependence of the current on the scan rate can also be explained by an adsorption controlled redox process. In the latter case, the double-layer charging would not be of purely capacitive origin. Therefore, the question remains whether capacitive currents exist in high temperature electrochemistry with solid electrolytes or not. The present results indicate that only pseudocapacitive and faradaic currents are possible.

Effect of reversal potential

The voltammograms obtained by varying the cathodic reversal potential E_{rc} on the anodic peak of the IrO_2 / 8YSZ catalyst is shown in figure 4.28a. Decreasing E_{rc} causes an increase in the peak current and a shift of the peak potential to the negative direction. The anodic peak becomes ill-defined when the E_{rc} is higher than approximately 0.3V. The peak current tends towards saturation readily and the E_{rc} decrease below -0.3V does no longer provoke a current enhancement. As far as the peak potential is concerned, the shift is very small and rather irregular. The relative importance of the two hidden peaks might play some role. The main conclusion from this experiment is that the anodic peak is indeed related to some cathodic process, but the quantity of electroactive species involved is very small.

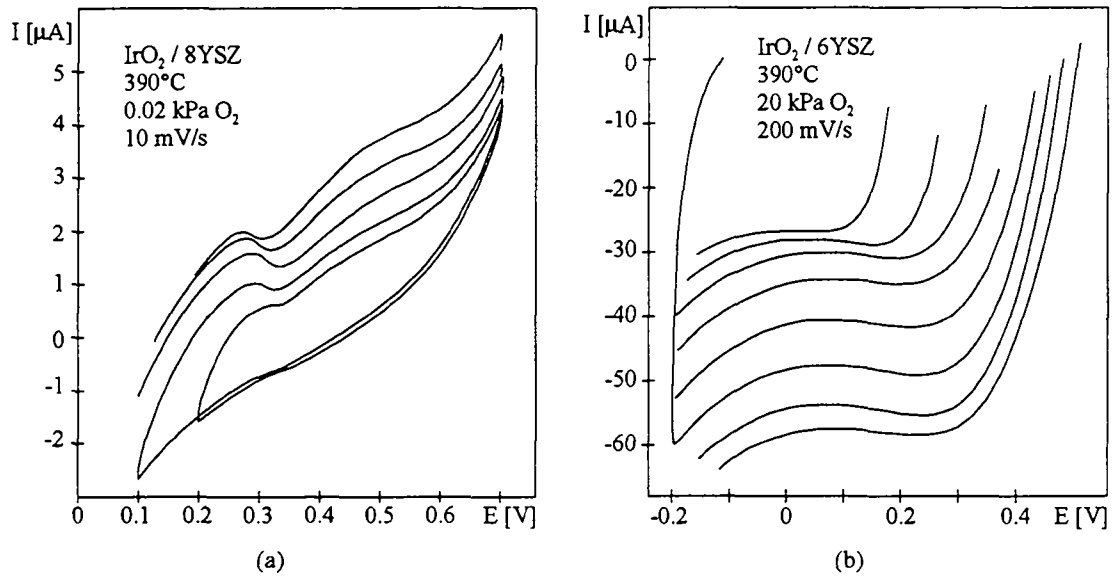

Fig. 4.28 Effect of varying the reversal potential on the cyclic voltammograms of the IrO_2 / YSZ catalysts; (a) the cathodic reversal potential is varied from -0.2V to 0.2V by steps of 0.1V, for an anodic reversal potential of 0.7V; (b) the anodic reversal potential is varied from 0.2V to 0.9V by steps of 0.1V, for a cathodic reversal potential of -0.2V.

The influence of an anodic reversal potential variation on the cathodic peak at the IrO_2 / 6YSZ electrode is shown in figure 4.28b. In air, this peak is not easily distinguishable at scan rates lower than 100 mV/s. Upon increasing the anodic termination potential, an increasing quantity of charge is accumulated and subsequently restored during the reverse scan. The saturation state is not attained as rapidly as in the case of the anodic peak at the IrO_2 / 8YSZ electrode.

Effect of holding time at fixed anodic potential

The voltammograms of the IrO_2 / 6YSZ catalyst obtained by holding the anodic potential at a fixed value for different lapses of time is depicted in figure 4.29. The voltammogram is plotted once without interruption. The potential is then kept at the anodic limit for a holding time t_h, before recording again the cathodic scan. After each cathodic scan, the system is allowed to return to the initial state by sweeping the voltage continuously for approximately ten cycles.

The current and the charge of the cathodic peak at 420 mV increase with increasing holding time, until a saturation state is attained. The most remarkable increase occurs for t_h < 1min, because almost all of the anodic charge accumulated seems to be restored to the cathodic peak. For longer holding times, an important part of the accumulated charge is responsible for the global current increase in the potential range from 0 to -0.5 V. The current peak no longer increases for t_h > 10 min.

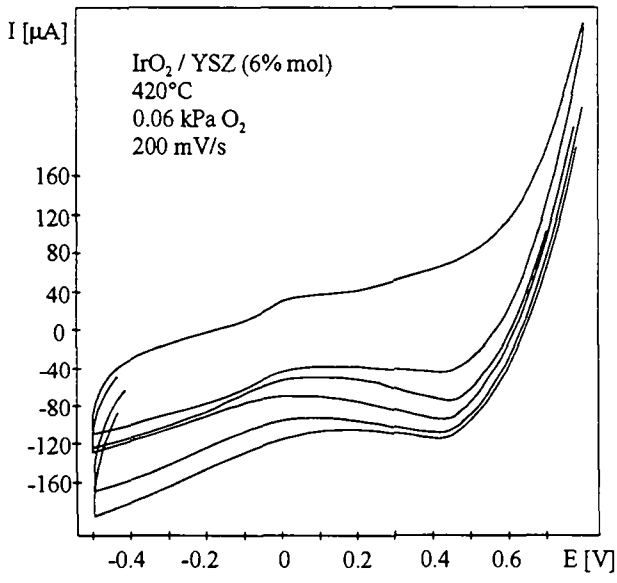

Fig. 4.29 Effect of holding time at 0.8V on the cyclic voltammogram of the IrO_2 / 6YSZ catalyst: continuous, 10s, 30s, 2min and 6min.

Effect of temperature

The influence of the temperature on the cyclic voltammograms of the IrO_2 / 6YSZ catalyst is shown in figure 4.30. The voltammogram is almost featureless at 300°C. The main cathodic peak called C2' is clearly defined for temperatures above 340°C and shifts to lower potentials with increasing temperature. The processes related to the anodic A1' and cathodic C1' humps are also greatly promoted with increasing temperature. At 420°C and especially at 440°C, a second anodic hump can also be distinguished.

The rate enhancement of all these processes with increasing temperature supports the already established conclusion of diffusion control. In the case of adsorption controlled processes, an increase in temperature should result in a rate decrease.

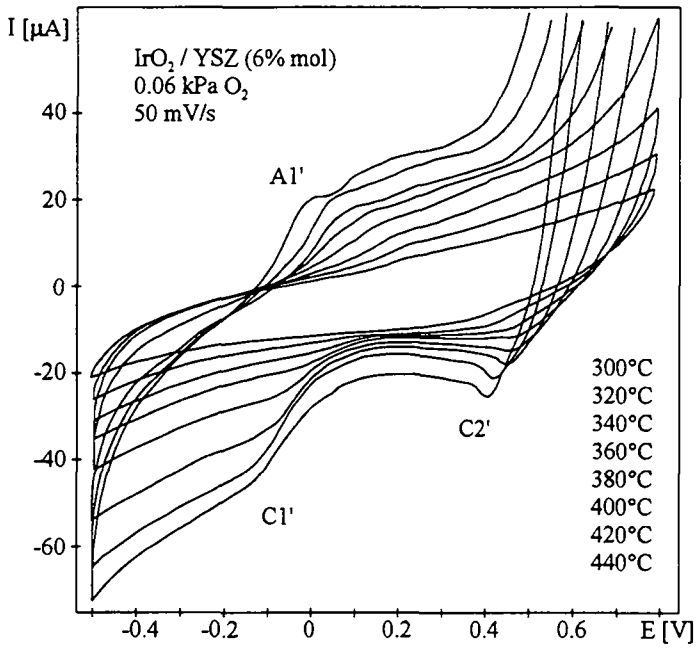

Fig. 4.30 Cyclic voltammograms of the IrO_2 / 6YSZ catalyst at several temperatures in 0.06 kPa O_2, with the potential scanned from -0.5 to 0.8V.

The apparent activation energy of the diffusion process, calculated from the slope of the plot of $\ln(I_p^2 T)$ vs (1/T) is 77 kJ/mol. This value is lower than the activation energy reported for the diffusion of oxide ions in stabilized zirconia (91 kJ/mol). It may be attributed to the diffusion of oxygen anions from a thin layer of $IrO_{2+\delta}$ oxide to the electrode-electrolyte interface. The transitions from Ir(IV) to Ir(V) and Ir(VI) probably occur at high anodic potentials and the $IrO_{2+\delta}$ oxide thus formed is reduced during the reverse scan. Such transitions have been reported in aqueous electrochemistry just prior to the oxygen evolution with the Ir(IV/V/VI) waves overlapping in the cathodic scan [Pickup, 1988b].

The redox process A1/C1 in figure 4.20a could be due to the transition Ir(III/IV). Very negative potentials are indeed necessary for the reduction of IrO_2 which is very stable. This redox couple, however, cannot explain the presence of a double peak. The characteristics of the double anodic peak A1 are reminiscent of the hydrogen peaks on platinum, in aqueous electrochemistry [Frelink, 1995]. Taking into account the fact that protons H^+ do not exist in the gas phase nor in the zirconia electrolyte, the electrochemical reduction of water can be schematically presented as follows:

$$2\ IrO_2 + H_2O + 2e^- \leftrightarrow 2\ IrO_2\text{---}(H_{ads}) + O^{2-}$$

In analogy with platinum, a weakly and a strongly adsorbed hydrogen species may exist, giving rise to the double peak observed. Even if the water reaction is not of the type presented above, the contribution of water to the redox process cannot be excluded. In fact, comparing the figures 4.26a and 4.26b, the differences in the voltammograms are only due to the quantity of water vapour present. A small anodic peak appears near the cathodic potential limit (50 mV) upon reversing the scan in figure 4.26b, where the air is saturated with water vapour. This peak is probably due to the redox process A1'/C1'.

This voltammetric study of the IrO_2 / YSZ cell, far from being exhaustive, revealed many interesting features of the electrochemical interface. More investigations are needed to definitely attribute the voltammetric peaks to a given redox process. The water presence seems to strongly influence the surface processes but is not well understood yet. The cyclic voltammetry in restricted potential ranges can give valuable information on the solid electrolyte-catalyst interface.

4.3 CATALYTIC ETHYLENE OXIDATION OVER AN YSZ SUPPORTED IrO_2 CATALYST

In the literature, no reference was found on the kinetics of the complete catalytic ethylene oxidation over an IrO_2 catalyst, in the temperature range from 250° to 450°C. Here are reported some basic kinetic measurements at steady-state. The influence of temperature and of the reactants' partial pressure on the reaction rate is discussed semi-quantitatively. No partial oxidation products were detected, nor were any saturated hydrocarbons found. The carbon mass balance calculations indicate a selectivity of 1 for carbon dioxide formation. The only reaction taking place is the following:

$$C_2H_4 + 3\ O_2 \rightarrow 2\ CO_2 + 2\ H_2O \qquad \Delta H_{r,\,600K} = -\ 1322\ kJ/mol$$

The mechanism of the ethylene oxidation over Pt or Ag, which has been studied for more than 40 years, is still controversial. A great number of kinetical models have been proposed for these catalysts. The purpose of this work is rather to provide a qualitative description of the system than to propose a model for the ethylene oxidation over a supported IrO_2 catalyst.

The experimental apparatus and especially the continuous flow reactor is not well suited for kinetical measurements, because it has not been designed for this purpose. However, based on the time distribution and the geometry of the reactor [Nicole, 1995], the reaction can be reasonably assumed to occur in a continuous stirred tank reactor (space around the catalyst) followed by a tubular section where the gases flow without reacting (upper part of the reactor and tubing to the analysis unit). The composition of the effluent stream is considered identical to the composition of the gas phase within the reaction vessel.

4.3.1 Steady-state kinetic measurements

The measurements were not performed on a fresh catalyst, but on the IrO_2 / 6YSZ catalyst which had already served for more than 2000 hours under various experimental conditions: oxidizing or reducing ambient gas, thermal cycling or electric potential cycling. The reaction rate is expressed in terms of atomic oxygen consumption [molO/s], calculated from the CO_2 molar flow rate.

The activity of the catalyst is very stable and, upon changing the gas concentrations at fixed temperature, the new steady-state is attained in approximately 10 minutes. The reproducibility of the measurements is very good when the partial pressure of one reactant is varied at constant temperature and total flow rate. The measurements at increasing and decreasing partial pressures give the same rate of CO_2 formation. When the concentration of the reactants is kept constant and the temperature is changed, the steady-state is attained very slowly and the measurements at increasing temperature often differ from the ones at decreasing temperature.

The dependence of the steady-state reaction rate on the partial pressure of ethylene is shown in figure 4.31. The reaction is studied at four distinct temperatures, namely 260, 300, 340 and 380°C, at a constant oxygen partial pressure of 2.2 kPa. The partial pressure of C_2H_4 is varied from 0.2 to 0.9 kPa, and the rate is plotted against the ratio of reactants $P_{C_2H_4} / P_{O_2}$. The volumetric flow rate $\dot{V}$ is 7.4 cm^3/s, reported at normal conditions. The corresponding space-time is $V_R / \dot{V} = 15s$. The fluid, however, does not

spend 15s in the reacting zone, since the temperature in the reactor is high and the reacting zone is a small part of the reactor. The conversion of the minor reactant lies in the range $2\% < X < 10\%$.

At low C_2H_4 partial pressures, the reaction rate increases linearly with increasing C_2H_4 partial pressure. A rate maximum is attained at a critical ethylene concentration and the reaction rate decreases with further increasing the ethylene concentration. The shape of the curve excludes an Eley-Rideal mechanism. The presence of the maximum indicates a catalytic reaction occurring between the reactants at the adsorbed state. Oxygen and ethylene seem to compete for the same adsorption sites. Based on the electronic and structural properties of IrO_2 (§2.2), oxygen probably adsorbs dissociatively.

Generally, a rate maximum is observed when the reactants are present at the stoechiometric ratio. For the ethylene reaction, the gas phase stoechiometric ratio lies at $P_{C_2H_4} / P_{O_2} = 0.33$. The rate maximum observed in figure 4.31 lies below the gas phase stoechiometric ratio at low temperatures and shifts towards higher values of $P_{C_2H_4}$ with increasing temperature. At 380°C, the maximum lies slightly above the gas phase stoechiometric ratio.

Since both reactants are in the adsorbed state, the rate maximum probably corresponds to the *surface* optimum ratio. The optimum ratio of the reactants' surface concentration is not necessarily equal to the stoechiometric ratio for the complete ethylene oxidation. The catalytic reaction may proceed through an intermediate, the formation of which necessitates less than 3 O_2 molecules.

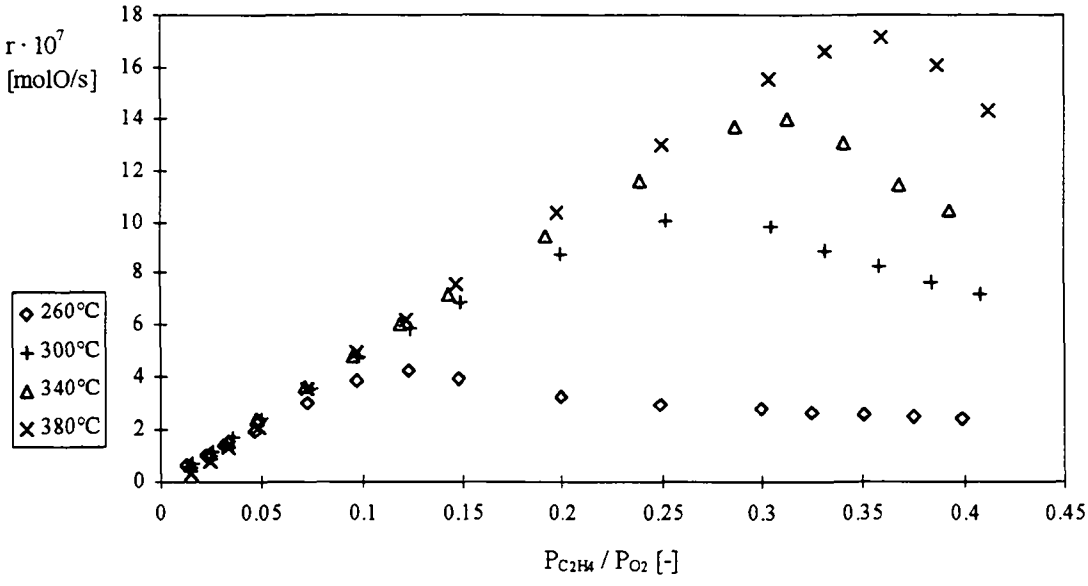

Fig. 4.31 Steady-state rate dependence on $P_{C_2H_4}$ at a constant oxygen partial pressure of 2.2 kPa and at a total volumetric flow rate of 7.4 cm^3 /s (normal conditions).

In order to obtain more information about the rate dependence on $P_{C_2H_4}$ in an ethylene excess, the steady-state rate is also measured for a constant P_{O_2} = 1.1 kPa at 340°C. The results are presented in

figure 4.32, with the corresponding values of the open-circuit potential. The rate measured for a constant P_{O_2} = 2.2 kPa at 340°C is also shown for comparison. The rate maximum is observed at the same $P_{C_2H_4} / P_{O_2}$ ratio for both oxygen pressures, indicating that the maximum location is only temperature-dependent.

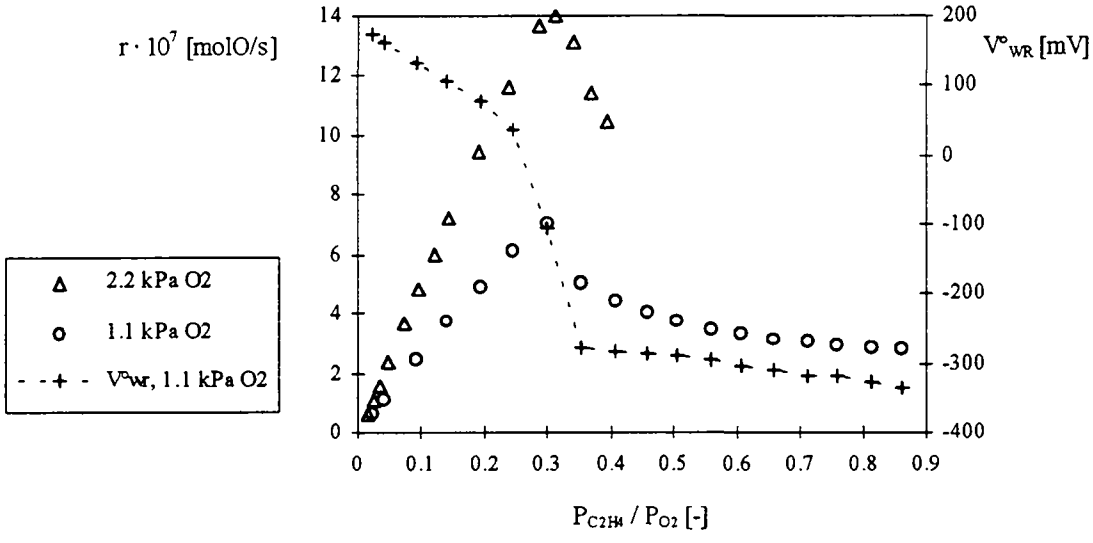

Fig. 4.32 Steady-state rate dependence on $P_{C_2H_4}$ at constant oxygen partial pressures 1.1 kPa and 2.2 kPa, at 340°C ($\dot{V}$ = 7.4 cm^3 / s). The open-circuit potential $V°_{WR}$ corresponding to 1.1 kPa O_2 is also reported.

The open-circuit potential $V°_{WR}$ strongly depends on the activity of the adsorbed species. The adsorption of ethylene is known to decrease the catalyst work function [Margolis, 1963] and the work function is directly related to the catalyst potential V_{WR} (see § 2.4.2). In figure 4.32, at low $P_{C_2H_4}$, $V°_{WR}$ decreases linearly with increasing $P_{C_2H_4}$ until the pressure value corresponding to the rate maximum is reached. A remarkable drop in the $V°_{WR}$ value occurs close to the rate maximum. Upon further increasing the $P_{C_2H_4}$, $V°_{WR}$ decreases slightly and almost linearly. The behavior of the $V°_{WR}$ supports the idea that the rate maximum corresponds to the passage from a predominantly oxygen covered, to an ethylene covered catalyst surface.

The reaction rate dependence upon the partial pressure of oxygen is presented in figures 4.33 and 4.34 for a constant ethylene partial pressure of 0.7 kPa and 0.3 kPa respectively. The P_{O_2} is varied from 0.4 to 14 kPa at distinct temperatures. In figure 4.33, the normal volumetric flow rate is $\dot{V}$ = 9 cm^3 /s and the space-time $V_R / \dot{V}$ = 12s, while in figure 4.34, $\dot{V}$ = 8.2 cm^3 /s and $V_R / \dot{V}$ = 13s. The conversion is generally kept below 7% and does not exceed 10%.

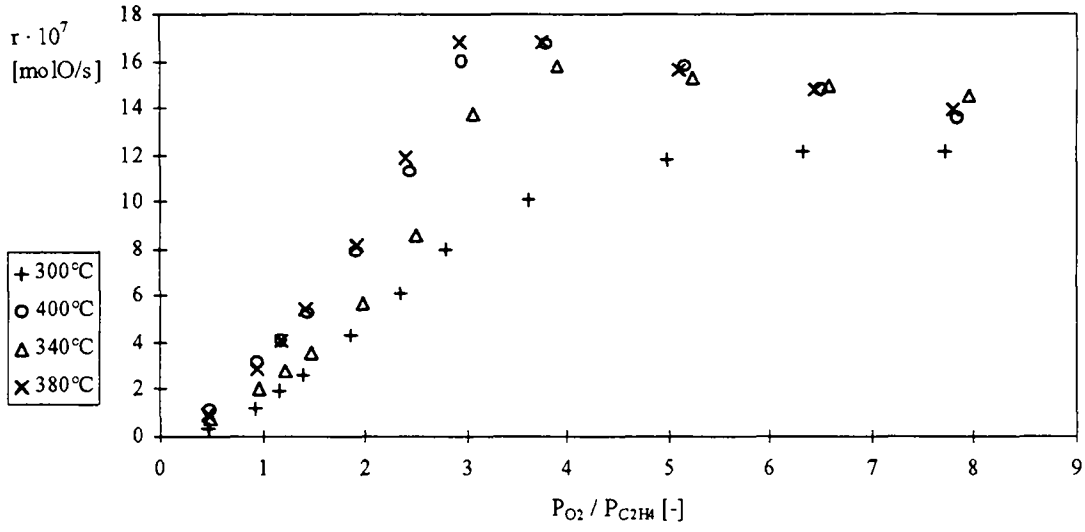

Fig. 4.33 Steady-state rate dependence on P_{O_2} at a constant ethylene partial pressure of 0.7 kPa and at a total volumetric flow rate of 9 cm^3 /s (normal conditions).

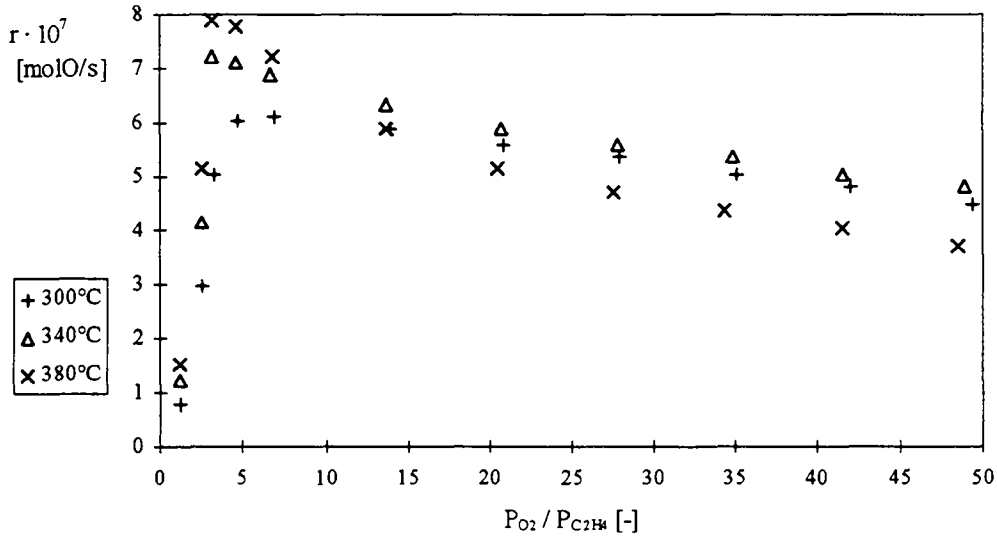

Fig. 4.34 Steady-state rate dependence on P_{O_2} at a constant ethylene partial pressure of 0.3 kPa and at a total volumetric flow rate of 8.2 cm^3 /s (normal conditions).

At low oxygen partial pressures, the reaction rate increases with increasing oxygen partial pressure, but the increase is not linear and can be approximated by a power law:

$$r_o = \text{const.}\, P_{O_2}{}^{3/2}$$

An example is given in figure 4.35, where the abscissa of figure 4.33 is extended for better visualisation.

The reaction rate is plotted against the P_{O_2} for $P_{C_2H_4}$ = 0.7 kPa. The reaction rate passes through a maximum at a P_{O_2} corresponding approximately to the gas phase stoechiometric ratio and starts decreasing with increasing oxygen partial pressure. The assumption of a competitive adsorption between oxygen and ethylene molecules is therefore confirmed. If adsorbed oxygen reacted with gaseous ethylene, an increase in P_{O_2} at constant $P_{C_2H_4}$ would not provoke a decrease in the rate. The reaction rate would reach a plateau once a unity coverage were attained.

The dependence of the rate on $P_{O_2}^{3/2}$ may be explained by assuming that the RDS in excess ethylene is the formation of a very reactive intermediate, which decomposes readily to CO_2 and cannot be detected at the exit. The oxidation of ethylene to glyoxal HCOCHO and water needs 3 oxygen atoms and can account for the order 3/2 in gaseous oxygen. As the surface becomes predominantly covered with oxygen, the formation of the glyoxal would no longer be the RDS, or the reaction would proceed via another pathway.

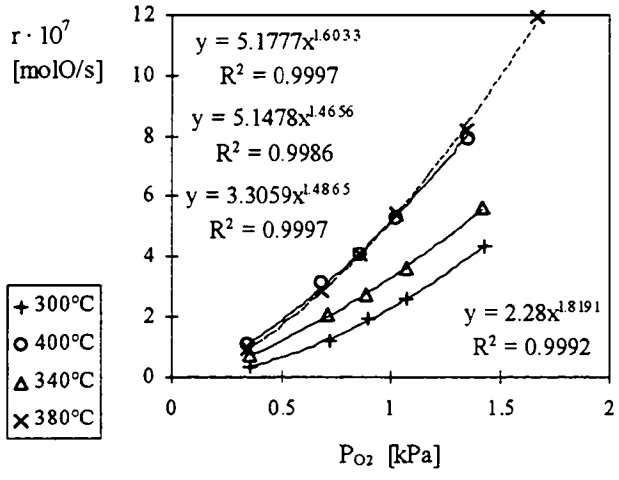

Fig. 4.35 Steady-state rate dependence on P_{O_2} at a constant ethylene partial pressure of 0.7 kPa and at a total volumetric flow rate of 9 cm^3 /s (normal conditions).

4.3.2 The temperature influence on the catalytic rate

The effect of the temperature on the steady-state rate measurements is complex. Upon increasing the temperature, a point will usually be reached beyond which the rate of the homogeneous reaction will exceed the rate of the catalyzed reaction. This is certainly not the case here.

In figure 4.31, the linear dependence of the rate on the partial pressure of C_2H_4 is very well respected, almost up to the sharp rate maximum. In this domain of slight oxygen excess, there is almost no influence of the temperature on the reaction rate. The rate is described by a relation of the form:

$$r_o = \text{const.} \cdot P_{C_2H_4}$$

An apparent activation energy of E_{app} = 7 kJ/mol is calculated from the slope of the ln(const.) vs 1/T plots. This value is too low to correspond to the kinetic constant of a reaction or adsorption.

The reaction rate decreases linearly with increasing $P_{C_2H_4}$ in a restricted range above the maximum rate, where an apparent activation energy of 83 kJ/mol was calculated.

The results in figure 4.31 show that the optimum ratio of reactants is achieved in oxygen-rich gas phase compositions at low temperatures and in oxygen-lean compositions at high temperatures. Ethylene adsorption seems to be favoured with respect to oxygen adsorption at low temperatures, while oxygen adsorption becomes more and more competitive with increasing temperature. No conclusion can be drawn from this observation on the characteristics of the oxygen and ethylene adsorption on IrO_2, since the surface coverage is not constant.

When the P_{O_2} is varied at constant $P_{C_2H_4}$, a rate enhancement with temperature is again observed in ethylene-rich mixtures, up to 380°C (Fig. 4.35). In this range, where the rate depends on $P_{O_2}^{3/2}$, an apparent activation energy of E_{app} = 32 kJ/mol is calculated from the slope of the ln(const.) vs 1/T plot. In figure 4.33 and especially in 4.34, the effect of the temperature on the reaction rate is particularly interesting at high oxygen partial pressures. There is almost no effect on the rate when the temperature is raised from 300 to 340°C, while a further increase in temperature provokes a rate decrease (Fig. 4.34). This observation indicates that an adsorption step is rate limiting, because the rate of adsorption decreases with increasing temperature.

In fuel-lean conditions, the reaction rate is probably limited by the ethylene adsorption. Near the rate maximum (Fig. 4.31), the overall rate seems to depend on the surface reaction between adsorbed ethylene and oxygen. An apparent activation energy of the order of 80 kJ/mol is obtained in this region. In fuel-rich conditions, the reaction may proceed via a reactive intermediate, the formation of which yields an E_{app} of the order of 30 kJ/mol. It is not possible to describe the steady-state kinetics of the ethylene oxidation over IrO_2 using the approach of a unique RDS. The attempts to correlate the data with a Langmuir-Hinshelwood type expression failed. Simulations were performed considering both molecular and dissociative oxygen adsorption, ethylene and CO_2 adsorption, with the reaction as the limiting step. The influence of water was ignored, because its concentration is unknown. However, the water level was kept approximately constant throughout the experiments ("w1300 ± 200").

In the range of the present operating conditions, several processes affect the reaction rate. The reaction order with respect to ethylene and oxygen significantly depend on the reaction conditions. In order to understand the overall behaviour of the catalyst, the interaction of each reactant and product with the catalyst surface should be considered. In particular, the adsorption-desorption characteristics of ethylene and oxygen must be studied at constant coverage to determine the k_{ads}, E_{ads} and ΔH_{ads} values. The dependence of the adsorption characteristics on surface coverage is also important.

4.4 Catalytic Ethylene Oxidation over an Electrochemically Modified IrO_2 / YSZ Catalyst

All the results presented in this section were obtained on the IrO_2 / 6YSZ catalyst. They are qualitatively similar to the preliminary results over the IrO_2 / 8YSZ catalyst. The reaction rate is of the same order of magnitude for both catalysts under a given set of conditions and passes through a maximum when the ratio of the reactants' partial pressure is close to the stoechiometric ratio for ethylene oxidation. Both catalysts exhibit mainly electrophobic NEMCA behaviour and some electrophilic behaviour at temperatures above 380°C. However, large discrepancies exist between the two catalysts in the quantitative response to polarization. The currents are much higher in the IrO_2 / 6YSZ system, where the solid electrolyte is thinner. The influence of the electrolyte thickness on the NEMCA effect could not be quantitatively established by comparing the two systems, since the mass and thickness of the catalyst also differed.

The fact that only one catalyst was systematically studied, limits the reliability of the conclusions drawn from the experimental results. Therefore, in the case of the IrO_2 / 6YSZ catalyst, it was attempted to trace the history of the catalyst and avoid the application of high currents at the early stage of its life. Initially, the system was heated up to 300°C in an atmosphere containing 1 kPa O_2 in helium. It was maintained at these conditions for two days and was subject to cyclic voltammetric measurements in a reduced potential range (-0.5V to 0.5V).

When the reactive mixture containing 10 kPa O_2 and 0.48 kPa C_2H_4 in helium was first admitted in the reactor at 300°C, the oxygen consumption rate attained the value of $2.3 \cdot 10^{-8}$ molO/s within one hour and remained stable at this value for ten hours. The catalyst potential was then raised to V_{WR} = 0.5V (45μA). The reaction rate started to increase within 30 seconds, and half an hour later, the rate was $1.9 \cdot 10^{-7}$ molO/s and was still increasing. The current was then switched off and the system was allowed to return to its initial state. Eleven hours later, the rate was already stabilized at $1.24 \cdot 10^{-7}$ molO/s for one hour, a much higher value than the initial one. This behaviour had not been observed on the IrO_2 / 8YSZ catalyst, which had suffered severe polarizations during some voltammetric experiments, prior to the study of the ethylene oxidation. The catalyst used responds readily to polarization and attains a steady-state value within a few minutes.

In order to attain the conditions for a "reversible" study of the NEMCA effect, the catalyst was polarized at several intervals at 1V (120mA), under the same experimental conditions. The evolution of the rate is shown in figure 4.36, where the open-circuit rate r_o is designated by (-) and the rate r' upon polarization by (+). After 70 hours of service life, the r_o value was $4.7 \cdot 10^{-7}$ molO/s. The concentration of the reactants was then changed and several polarization treatments were applied, but are not shown here. After 132 hours of service life, the r_o value in 10 kPa O_2 and 0.48 kPa C_2H_4 was $6.1 \cdot 10^{-7}$ molO/s (fig. 4.36), but the catalyst already responded more rapidly to polarization; a steady-state value was attained within 1 hour, upon polarization. This initial experiment was then stopped, for the main study to start. The response time continued to decrease and the "reversibility" of the polarization, i.e. the return to the initial rate r_o after a potentiostatic pulse, was improved as the service life increased. After approximately 1500 hours and 3000

hours of experiment, the catalyst activity seems to be stabilized, with r_o values of $8.8 \pm 0.5 \cdot 10^{-7}$ molO/s at 300°C, in 10 kPa O_2 and 0.48 kPa C_2H_4.

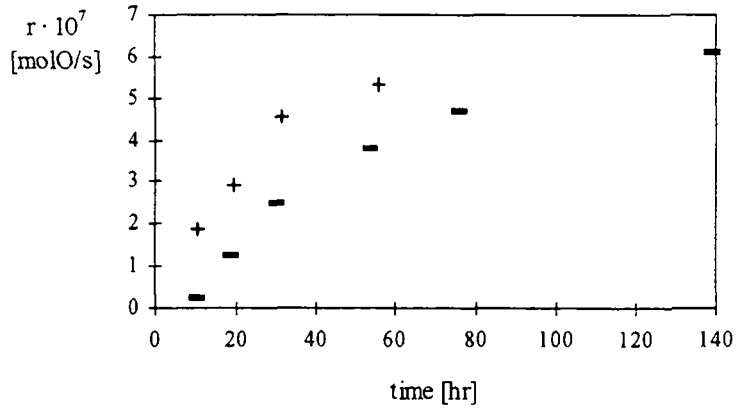

Fig. 4.36 The rate of ethylene oxidation at the beginning of the catalyst life and its evolution by the application of successive potential steps in 10 kPa O_2, 0.48 kPa C_2H_4, at 300°C; (-) refer to the open-circuit rate and (+) refer to the rate upon polarization.

4.4.1 Steady-state polarization and determination of the exchange current density

The response of the system to the electrochemical polarization is a key parameter of the NEMCA effect and the right use of the term polarization is of primary importance in the interpretation of the results.

The catalyst potential with respect to the reference electrode is:

$$V_{WR} = V^{\circ}_{WR} + IR_u + \eta_W + \eta_R$$

where

V°_{WR} is the open-circuit potential

Ir_u is the ohmic-drop due to the uncompensated resistance

η_W is the catalyst overpotential and

η_R is the overpotential at the reference electrode, considered negligible.

Generally, in electrochemistry, the term polarization refers to the overpotential η_W: when a potential V_{WR} is applied to an electrochemical system, the working electrode is said to be polarized by an amount

$$\Delta V_{WR} = V_{WR} - V^{\circ}_{WR} - IR_u = \eta_W .$$

In most NEMCA studies, the term polarization is indeed used in this sense and the reported values of V_{WR} are corrected for the ohmic drop. In this study, the potential values are not ohmic-drop-free. The general term polarization is abusively used when a potentiostatic pulse of V_{WR} is applied to the catalyst. This is due to the difficulty encountered in the precise measurement of the ohmic drop. The IR_u term varies from 30mV to 100 mV for V_{WR} = 1V and increases to approximately 1V for V_{WR} = 3V. Since the current magnitude does not only depend on the temperature but also on the composition of the gas phase, it should

be measured for each potentiostatic pulse. This systematic measurement would take too much time and is almost impossible in cyclic voltammetric measurements. The influence of the IR_u term is more important at high applied potentials, which are generally avoided here.

The open-circuit potential $V°_{WR}$ is also strongly dependent on the gas phase composition and, to a lesser extent, on the temperature. Its evaluation is not easy, nor sufficiently reproducible. For a given set of conditions, the measured $V°_{WR}$ values present a 50% error. When the feed composition and temperature are changed, or at the interruption of a potentiostatic pulse, the $V°_{WR}$ does not reach a steady-state before several hours. It seems that it is much more sensitive to the experimental conditions than the rate of CO_2 formation, which attains a steady-state after a few minutes, for a used catalyst. When the system is allowed to rest overnight in the reactive mixture, the $V°_{WR}$ value is stable enough, i.e. does not change for half an hour, and is used to determine the polarization term

$$\Delta V_{WR} = V_{WR} - V°_{WR}$$

In a divided cell, the measured $V°_{WR}$ value can be used to determine the thermodynamic activity of oxygen on the catalyst (Eqn. 2.7), which differs substantially from the gas-phase oxygen activity if oxygen adsorption is not in equilibrium [Bebelis, 1989]. The reference electrode must be made of the same material as the working electrode (catalyst) and maintained at constant gas-phase composition. The oxygen activity was thus determined on a platinum catalyst, during ethylene oxidation [Bebelis, 1989]. In this work, no correlation was found between the $V°_{WR}$ values and the oxygen partial pressure.

The polarization curve I vs ΔV_{WR} , of the IrO_2 / 6YSZ interface in 0.13 kPa C_2H_4 and 17.5 kPa O_2 at 400°C, is shown in figure 4.37. The current is zero at $V°_{WR}$ = 214 mV. The catalyst is highly polarizable and the overpotential is particularly important on the cathodic side. The asymmetrical curve indicates that the oxidation of O^{2-} anions to atomic oxygen is better catalyzed than the reduction of oxygen to O^{2-} anions. The current is very low for cathodic overpotentials smaller than ΔV_{WR} = -0.5V, indicating that concentration overpotential is predominant in the polarization term. For higher cathodic overpotentials, the current seems to increase exponentially with the potential, indicating that activation overpotential is prevailing.

The activation overpotential is described by the Butler-Volmer equation (Eqn. 2.10), which predicts a linear dependence of the current on ΔV_{WR} at low overpotentials (Eqn. 2.12) and an exponential dependence at high overpotentials (Eqn. 2.11). The plot of ln | I | vs ΔV_{WR} , where I is measured in Amperes, is shown in figure 4.38. The exchange current I_o and the charge transfer coefficients, for the oxygen reaction, can be determined from the linear part of the plot, called Tafel region, where the high field approximation (ΔV_{WR} > 100 mV) holds (Eqn. 2.11). The Butler-Volmer equation reduces to

$$\ln (I) = \ln (I_o) + (\alpha_a F / RT)\, \Delta V_{WR}$$

for anodic overpotentials, where α_a is the anodic charge-transfer coefficient and

$$\ln (|I|) = \ln (I_o) - (\alpha_c F / RT)\, \Delta V_{WR}$$

for cathodic overpotentials, where α_c is the cathodic charge-transfer coefficient.

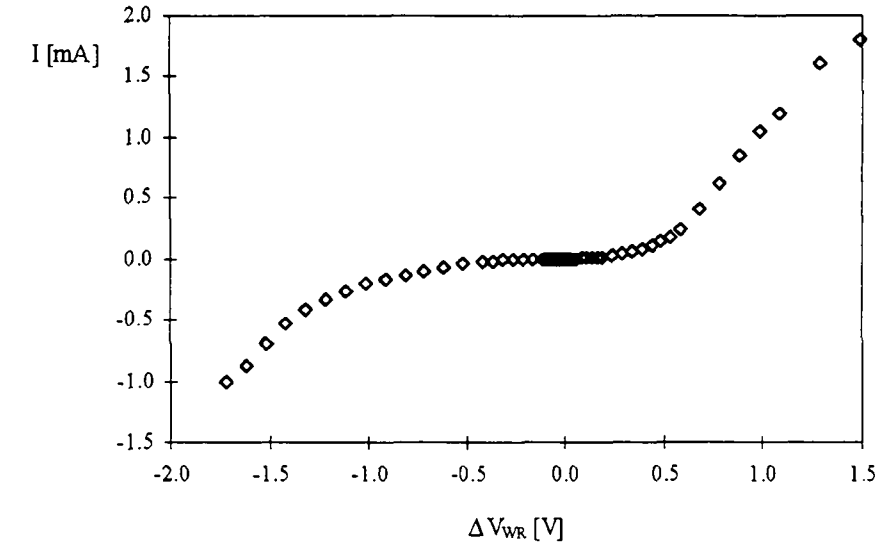

Fig. 4.37 Polarization curve of the IrO_2 / 6YSZ interface in 0.13 kPa C_2H_4 and 17.5 kPa O_2 at 400°C

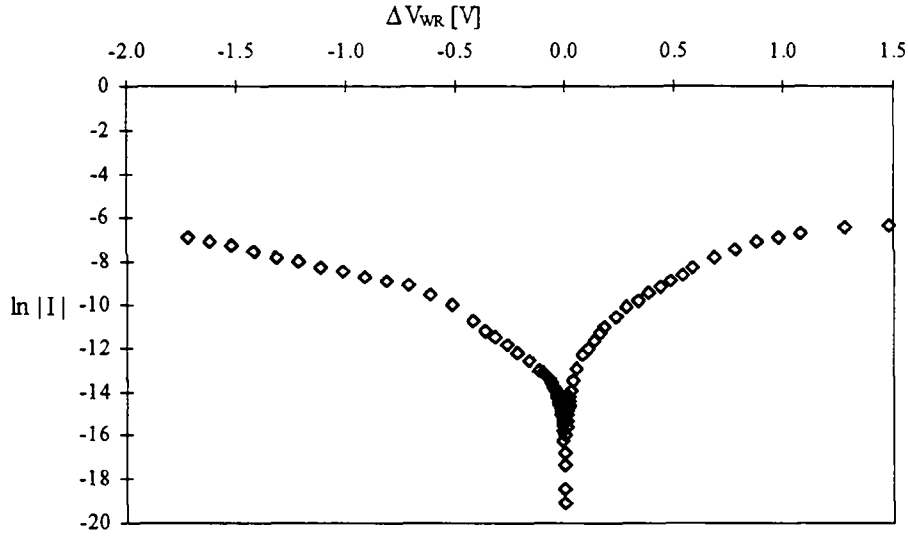

Fig. 4.38 Plot of ln | I | vs ΔV_{WR} in 0.13 kPa C_2H_4 and 17.5 kPa O_2 at 400°C

On the cathodic side of the ln | I | vs ΔV_{WR} plot (Fig. 4.38), there is a well-defined Tafel region at $\Delta V_{WR} < -0.6V$. The values of $I_o = 20$ μA and $\alpha_c = 0.14$ were extracted from this cathodic Tafel region. On the anodic side, the ln | I | vs ΔV_{WR} plot is regularly curved and it is difficult to define a Tafel region. The values of $I_o = 9$ μA and $\alpha_a = 0.3$ were extracted from the linear plot in the interval $0.3 < \Delta V_{WR} < 0.8V$. The accuracy of these values can be checked using the low-field approximation (Eqn. 2.12) to extract the value of $(\alpha_a + \alpha_c)\cdot I_o$ from the slope of the curve in figure 4.37. This attempt was not satisfying, although a strict linearity is observed at $| \Delta V_{WR} | < 30$ mV. The extracted values of I_o, α_a and α_c, should thus be considered with care. Since I_o is known to depend on the oxygen coverage of the catalyst surface [Bebelis, 1989], the measurements may be perturbed by the eventual withdrawal of adsorbed oxygen by ethylene.

The order of magnitude of the enhancement factor Λ can be approximately estimated by the relation [Vayenas, 1994b]:

$$\Lambda \approx 2 F r_o / I_o$$

In this case, $r_o = 1.75 \cdot 10^{-8}$ molO/s and the Λ values, corresponding to an exchange current of 20 μA and 9μA, are 1700 and 3800 respectively. These values are largely underestimated, since enhancement factors of up to 20000 were measured in 0.13 kPa C_2H_4 and 17.5 kPa O_2 at 400°C, as will be shown later in the chapter.

4.4.2 Effect of the gas phase composition on the polarization behaviour

In the preliminary results, it was established that the effect of catalyst polarization is particularly dramatic in reactive mixtures with a large oxygen excess. The effect of the gas phase composition on the NEMCA behaviour is presented in a more systematic way in figure 4.39. The steady-state rate under open-circuit conditions (symbol ◊) and under an applied potential V_{WR} = 0.5V (symbol +) are reported as a function of the reactants' partial pressure. When the oxygen partial pressure is varied at constant $P_{C_2H_4}$ = 0.7 kPa, the application of a positive potential in the fuel-rich region has almost no effect on the reaction rate and seems even to provoke a slight rate decrease (Fig. 4.39a). The effect is more pronounced when the oxygen partial pressure is higher than the gas-phase stoechiometric ratio for the ethylene oxidation. In figure 4.39b, the reaction rate is given as a function of the ethylene partial pressure at constant P_{O_2} = 2.2 kPa. The application of a positive potential seems to have no effect in the range of $P_{C_2H_4}$ studied. This is intriguing, since the low $P_{C_2H_4}$ values correspond to approximately a five-fold excess of gaseous oxygen. The polarization effect should then be considerable. This anomalous behaviour is explained by taking into account the variation of $V°_{WR}$ with the gaseous composition. Since the $V°_{WR}$ values increase with decreasing $P_{C_2H_4}$, the application of a potential V_{WR} = 0.5V will correspond to a lower overpotential V_{WR} - $V°_{WR}$ at low $P_{C_2H_4}$ than at high $P_{C_2H_4}$. The comparison of the figures 4.39c and 4.39d, where the oxygen partial pressure is varied at constant $P_{C_2H_4}$ = 0.3 kPa, shows that the NEMCA effect increases with increasing oxygen excess and with increasing temperature. In fact, the rate enhancement by electrochemical polarization is maximum at low $P_{C_2H_4}$, high P_{O_2} and high temperature.

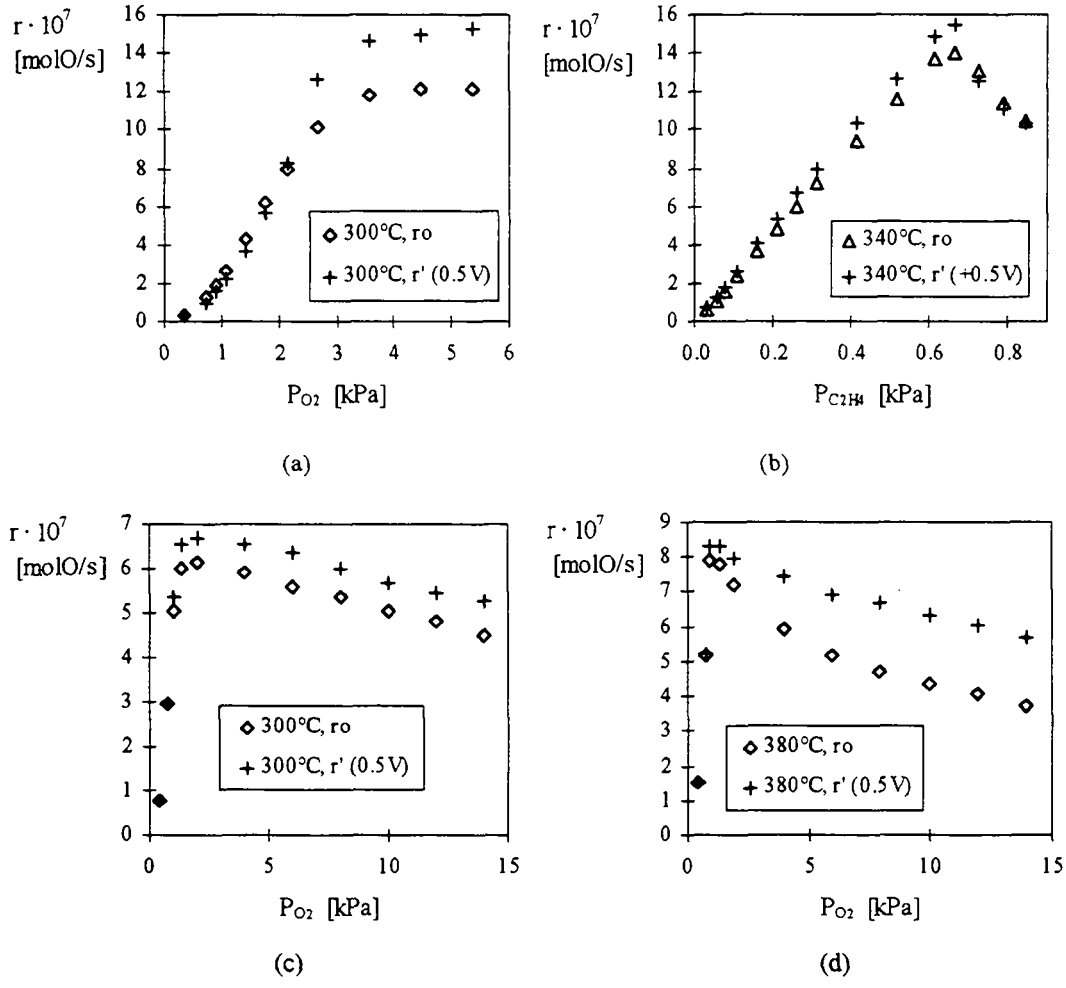

Fig. 4.39 Effect of the gas-phase composition on the NEMCA behavior; (a) in 0.7 kPa C_2H_4; (b) in 2.2 kPa O_2; (c) in 0.3 kPa C_2H_4 at 300°C; (d) in 0.3 kPa C_2H_4 at 380°C. The open-circuit rate r_o corresponds to open symbols, and the rate under an applied V_{WR} = 0.5V corresponds to (+)

The dramatic effect of the polarization in oxygen-rich gas-mixtures, where the catalyst surface is predominantly covered with oxygen and the rate is likely to depend on ethylene adsorption, can be explained by the weakening of the bond between IrO_2 and adsorbed oxygen with increasing potential. The application of positive potentials is believed to favour the oxygen desorption and consequently to facilitate the ethylene adsorption on the liberated surface sites.

4.4.3 Effect of the overpotential on the ethylene oxidation rate

The ethylene oxidation rate under polarization in 0.13 kPa C_2H_4 and 17.5 kPa O_2 is shown in figure 4.40 as a function of the applied potential V_{WR}, at 380°C and 400°C. The two curves are very similar with the curve at 400°C lying below the one at 380°C, in the whole potential range. At zero current, $V°_{WR}$ = 255 mV and $r_o = 5.25 \cdot 10^{-8}$ molO/s at 380°C, and $V°_{WR}$ = 214 mV and $r_o = 1.75 \cdot 10^{-8}$ molO/s at 400°C. The rate decrease with increasing temperature was already discussed in the previous chapter. Here, the two

curves are reported to show that the temperature does not influence the mechanism of catalyst activation. The measurements are made at decreasing applied potential, but the measurements at increasing potential give a similar curve, while the rates are higher by approximately 3% in the whole range. The rate "step", observed in the region of low overpotentials, is due to the great number of measurements done in that region. It shows that the open-circuit potential $V°_{WR}$ is not stable throughout the experiment. During the application of high positive potentials, the system is maintained at a state corresponding to a higher $V°_{WR}$ value than the "equilibrium" one. The "step" is not observed when the system is allowed to rest for an hour after each potential application.

The shape of the curve under anodic polarization is very similar to the ones reported for the ethylene oxidation over Pt/YSZ [Bebelis, 1989]: initially, the rate increases very rapidly with increasing overpotential and attains a plateau at high overpotentials. Oxygen is an electron acceptor, and provokes an increase in the catalyst work function upon adsorption [Margolis, 1963]. The application of positive potentials results in a weakening of the catalyst-adsorbed oxygen bond. The ethylene molecule is an electron donor and the strength of the catalyst-adsorbed ethylene bond should increase with increasing potential. The oxygen partial pressure is more than 100 times higher than the ethylene partial pressure. Since ethylene adsorption is probably limiting the rate, the dramatic rate increase observed is explained by an enhancement of the oxygen desorption and ethylene adsorption.

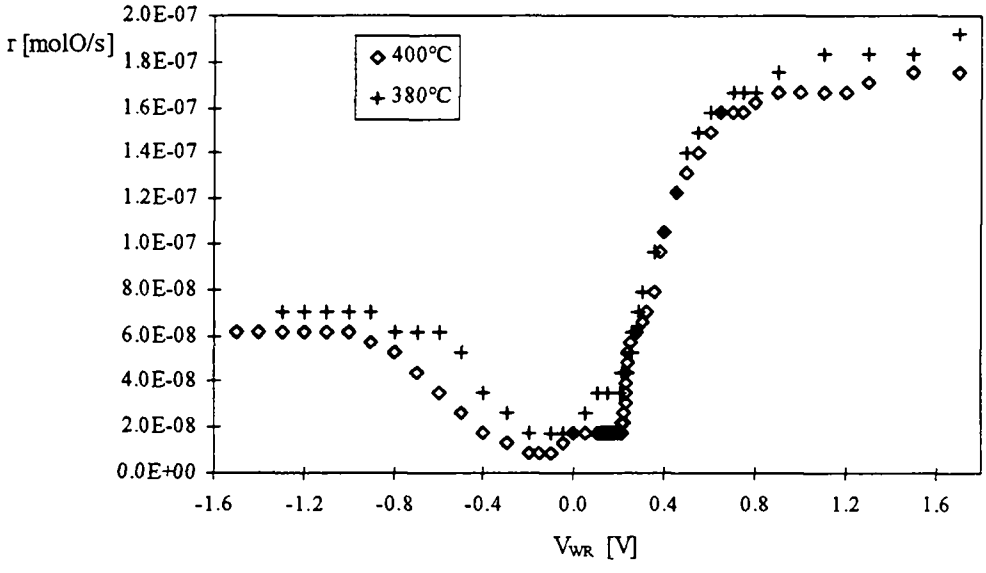

Fig. 4.40 Effect of the potential V_{WR} on the ethylene oxidation rate in 0.13 kPa C_2H_4 and 17.5 kPa O_2. The total volumetric flow rate at normal conditions is 6.5 cm^3 / s

The rate enhancement $\Delta r = r' - r_o$ is shown in figure 4.41 as a function of the rate of O^{2-} ions' supply I / 2F. A very low O^{2-} supply provokes a dramatic increase in the reaction rate. Note that there is no use increasing the rate of O^{2-} supply above $1 \cdot 10^{-9}$ molO/s, since it does not provoke any further rate enhancement. The NEMCA effect is more pronounced at the higher temperature (400°C), since the open-

circuit rate r_o is lower at 400°C than in 380°C. In fact, in most NEMCA studies [Vayenas, 1992a], the most remarkable rate enhancements were observed at low temperatures. This difference is only due to the temperature dependence of the open-circuit kinetics of a given reaction.

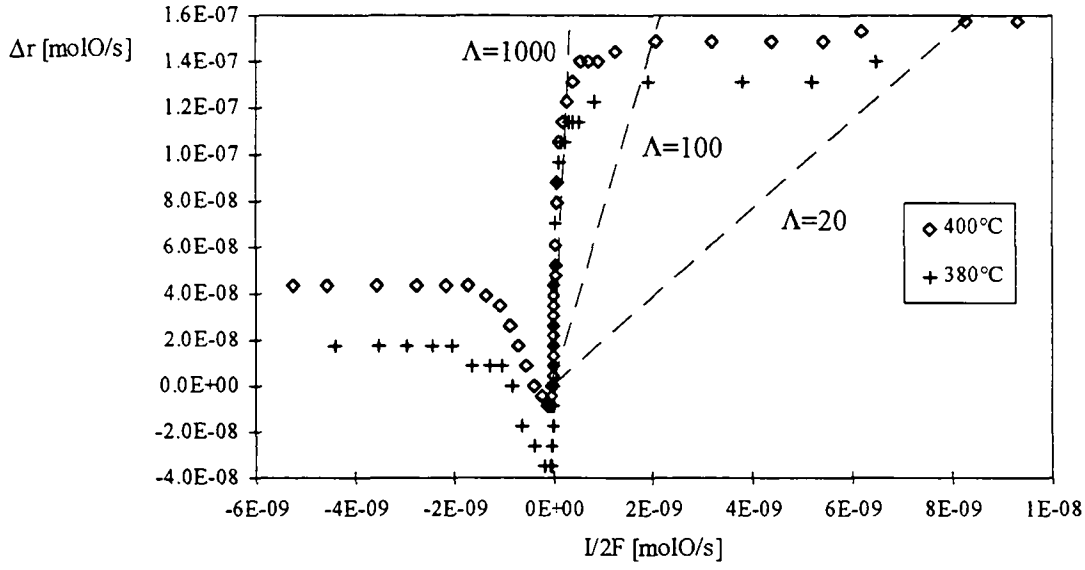

Fig. 4.41 The rate enhancement in 0.13 kPa C_2H_4 and 17.5 kPa O_2, as a function of the rate of O^{2-} supply

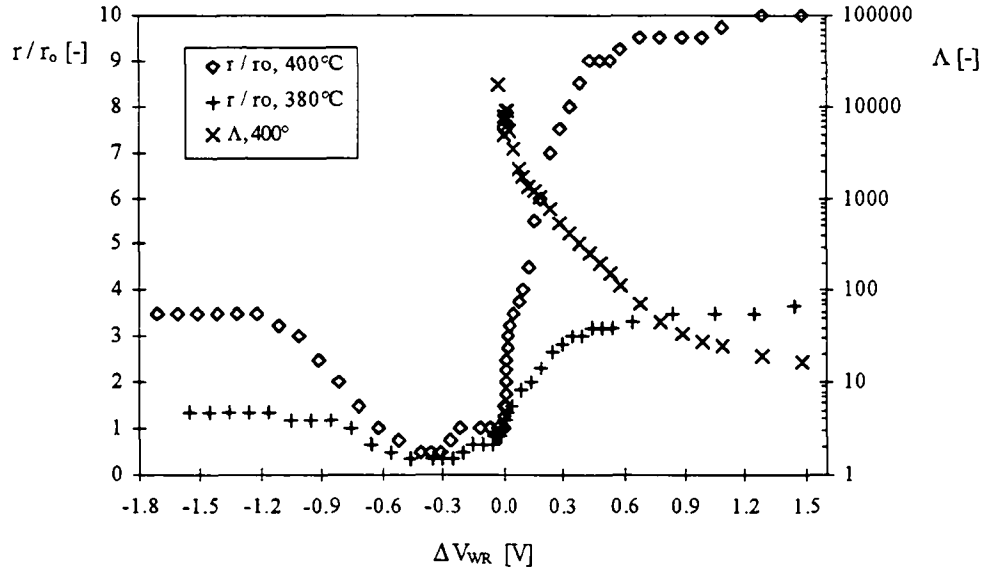

Fig. 4.42 The rate enhancement ratio r'/ r_o and the enhancement factor Λ as a function of the applied overpotential in 0.13 kPa C_2H_4 and 17.5 kPa O_2

The ratio Δr / (I/2F) defines the enhancement factor Λ (§2.4), which is reported in figure 4.42 with the enhancement ratio r = r' / r_o, as a function of the overpotential. The rate enhancement ratio ρ = r' / r_o

increases exponentially with the overpotential in a very limited range of ΔV_{WR} values ($0 < \Delta V_{WR} < 80$ mV), but there is no threshold value below which the rate is unaffected as in the case of ethylene oxidation over Pt / YSZ [Bebelis, 1989]. When the ρ values increase, the Λ values decrease. The highest ρ value shown here is 10, which means that the ethylene oxidation rate over the IrO_2 catalyst, polarized by $\Delta V_{WR} = 1.3$V, is 10 times higher than under open-circuit conditions. The corresponding Λ value is only 20, which means that, each O^{2-} ion discharged at the catalyst makes 20 oxygen atoms to react. The most impressive Λ value, namely 20000, is observed when the reaction rate is only enhanced by a factor 1.2.

Upon switching off the current at the end of a potentiostatic or galvanostatic pulse, the deactivation rate of the catalyst, i.e. the relaxation towards the initial open-circuit rate, is slower than the activation rate. This fact was already pointed out in the preliminary results and indicates that the application of successive potentiostatic pulses could be used to maintain the reaction rate at an enhanced level with a lower power consumption. A spectacular demonstration of the NEMCA effect by applying successive, positive, galvanostatic pulses to the IrO_2 / 6YSZ catalyst is shown in figure 4.43. After each applied pulse of a certain duration, the system is at rest for the same duration. The following pulses were applied successively: 3 pulses of 120s at 100 μA, 8 pulses of 60s at 100 μA, 8 pulses of 30s at 100 μA, 11 pulses of 30s at 200 μA.

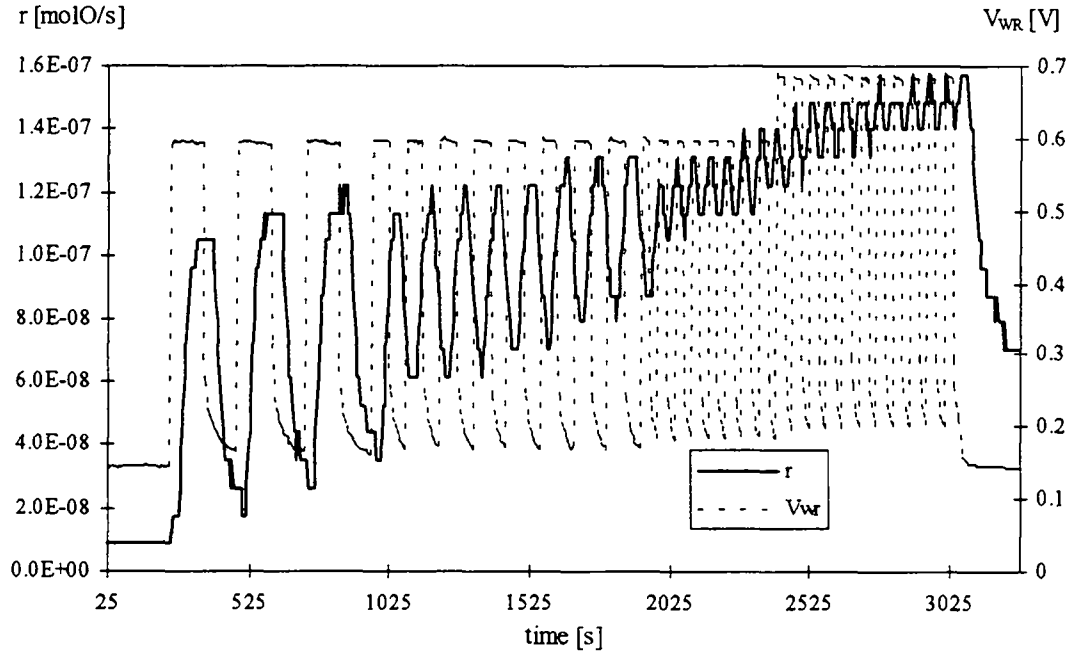

Fig. 4.43 Pulsed galvanostatic operation on the IrO_2 / 6YSZ catalyst in 0.13 kPa C_2H_4 and 18 kPa O_2 at 400°C. The total volumetric flow rate at normal conditions is 6.7 cm^3 /s

The open-circuit initial rate is $r_o = 0.9 \cdot 10^{-8}$ molO/s (Fig. 4.43). The application of a 100 μA galvanostatic pulse during 120s enhances the rate to $10.5 \cdot 10^{-8}$ molO/s. The rate enhancement ratio is 11. When the current is switched off, the rate starts to decrease towards the initial value. The next galvanostatic step provokes a further increase in the rate. After each step, the rate is globally enhanced, until a "steady-

state" is reached, where the rate "oscillates" between two fixed values. The polarization step is better exploited in this kind of periodic operation. As far as the rate of O^{2-} supply is concerned, the application of 100 μA for 30s every 60s can be compared to the continuous application of 50 μA. The pulsed operation at 100 μA results in a rate increase by a factor $\rho = 14$, whereas the steady-state rate attained by the continuous application of 50 μA is only $\rho = 8$ times higher than the open-circuit rate.

Consider an average enhancement factor $\overline{\Lambda}$, defined from the equation:

$$\overline{\Lambda} = \frac{\int_0^{t'} \Delta r \, dt}{\int_0^{t'} (I/2F) dt}$$

This $\overline{\Lambda}$ factor can be compared to the L value at the top of the rate peaks. Average $\overline{\Lambda}$ values of 243, 326 and 302 are obtained for t' = 960s, 2400s and 3070s respectively. The corresponding Λ values, namely 219, 252 and 138, are lower. The pulsed operation seems more effective as the frequency is increased.

The experiment in figure 4.43 is performed on a used catalyst. The system responds very rapidly to polarization, namely in a few seconds. Note that, at the end of the experiment, the rate has rapidly decreased to $7 \cdot 10^{-8}$ molO/s. One hour later (not shown in the figure), the rate is $6 \cdot 10^{-8}$ molO/s, and approximately 20 hours later, $1 \cdot 10^{-8}$ molO/s. There are clearly two stages in the deactivation, the first being rapid and the second very slow. The latter may be attributed to a diffusion process in the bulk solid.

In figure 4.40, the reaction rate does not increase any more with increasing overpotential, for overpotential values higher than 0.7V. When the rate is maximum, the ethylene conversion is only 8% and the ethylene adsorption should still limit the reaction rate. The reaction rate should continue to increase, unless the effect of the potential on the adsorptive bonds is limited above a certain potential value. Limitations by internal diffusion in the catalyst pores can be excluded under the present conditions, because the Weisz factor f [Weisz, 1959] equals 0.0002 and is much smaller than 1 (see §4.1).

Since the activation process upon polarization proceeds through the electrical charging of the catalyst-electrolyte interface, the rate enhancement limitation can be attributed to the existence of a maximum storage capacity at the interface. Upon electrochemical pumping of O^{2-} to the catalyst, the oxygen species are stored at the surface of the catalyst which is thus oxidized to a higher oxide, according to the reaction:

$$IrO_2 + \delta O^{2-} \Leftrightarrow IrO_{2+\delta} + 2\delta e^-$$

The positive electrical charge in the catalyst film (on the iridium ions) is compensated by an equal and negative charge in the solid electrolyte. The excess oxygen species can diffuse over the catalyst surface, provoking the oxidation of the gas-exposed catalyst surface. The activity of the partially oxidized surface for the ethylene oxidation should be greater than the activity of the stoechiometric IrO_2 catalyst. The number of O^{2-} ions, discharged at the IrO_2 catalyst, which can be stored in the form of $IrO_{2+\delta}$ at the surface, is probably limited. When the maximum storage capacity is reached, the excess O^{2-} ions, pumped to the catalyst, will be released in the gas-phase as molecular oxygen and will not participate to the activation process.

The activation process is related to the electrochemical interface, so, it should also occur in the absence of ethylene. In order to check whether the activated state of the catalyst, eventually an $IrO_{2+\delta}$ state, is more stable if it is formed in absence of a fuel which reacts with oxygen, the following experiment is carried out. The reactor is maintained in an atmosphere containing 17.5 kPa O_2 in helium and a galvanostatic step of 300 μA is applied for 15 minutes. Upon switching off the current, ethylene is allowed to flow in the reactor, at a partial pressure of 0.13 kPa. The result is depicted in figure 4.44. The second galvanostatic step of 300 μA is applied in the presence of ethylene.

The catalyst is indeed activated in absence of ethylene and it is clear that the fuel only acts as a tracer. The maximum in the rate observed upon injection of ethylene is slightly lower than the maximum rate attained by the second polarization. This difference is due to the experimental manipulations, and the coordination of the current interruption and the ethylene injection. Astonishingly, the deactivation rate is almost identical in presence and in absence of ethylene. The activated state is not more stable if it is formed in absence of fuel, at least as far as the first stage of deactivation is concerned. This experiment was reproduced several times, but no information can be drawn for the second stage of deactivation, i.e. the time needed to return to the open-circuit rate, since r_o is unknown.

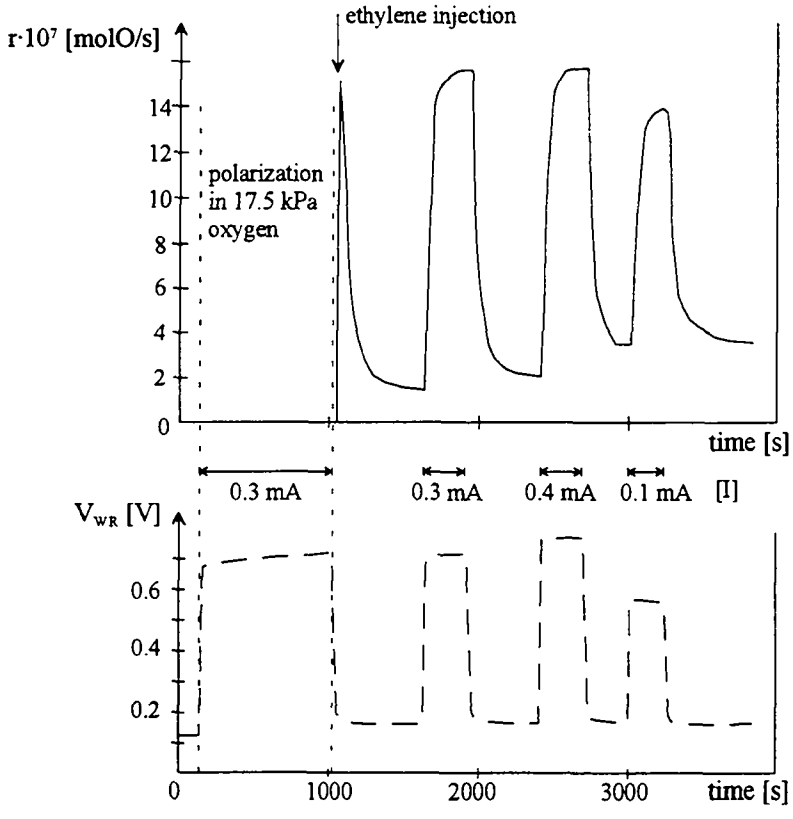

Fig. 4.44 Polarization of the catalyst in 17.5 kPa O_2, injection of C_2H_4 upon interruption of the current and subsequent polarizations in 17.5 kPa O_2 and 0.13 kPa C_2H_4, at 400°C.

In order to learn more about the "destruction" mechanism of the activated state, the following experiment is performed. The catalyst is polarized until the steady-state rate is reached. As soon as the

current is switched off, several cyclic voltammograms are recorded, at different time intervals, during the rate decay. The potential is swept from 0.05 to 0.15V at a scan rate of 50 mV/s. These potential limits are chosen close to the $V°_{WR}$ value, so as to disturb the rate decay as little as possible. The total electric charge, measured from the surface of the voltammogram, is then compared to the corresponding ethylene oxidation rate. Two examples are shown in figure 4.45, where the reaction rate is reported against the total voltammetric charge Q. In one case, the catalyst was subject to a galvanostatic step of 200 μA for 11 minutes and, prior to the interruption, the rate was $1.5 \cdot 10^{-6}$ molO/s. In the other case, the voltammograms were recorded after a galvanostatic step of 100 μA for 9 minutes, and the steady-state rate during polarization was $1.4 \cdot 10^{-6}$ molO/s. The 6.5 cm^3 /s gas feed contains 0.13 kPa C_2H_4 and 17.5 kPa O_2, at 400°C. Another example has already been published by Varkaraki et al. [Varkaraki, 1995].

The linear relation, observed between the catalytic oxidation rate and the voltammetric charge at the catalyst-electrolyte interface, is one of the most important findings in this work. The rate decrease is accompanied by a concomitant decrease in the charge stored at the electrochemical interface. During the positive polarization of the catalyst, the O^{2-} ions are discharged and incorporated at the catalyst surface which is partially oxidized to $IrO_{2+\delta}$. The rate of O^{2-} supply increases with increasing potential, and so does the charge stored at the interface, until the maximum pseudocapacitance of the interface is reached. If the rate of O^{2-} supply is further increased, the discharged ions will be released in the gas phase as molecular oxygen. This description accounts for the continuous current increasing with increasing potential and the rate enhancement limitation to a certain potential value (Fig. 4.40).

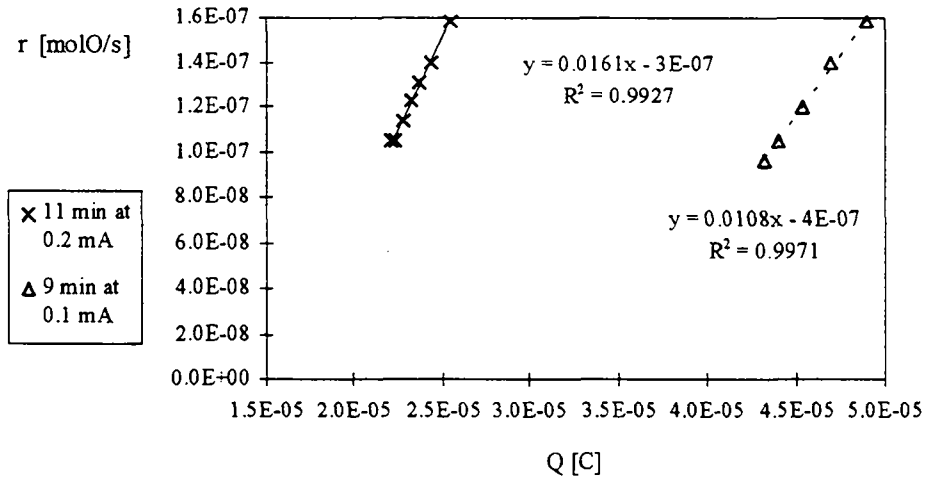

Fig. 4.45 The relation between the ethylene oxidation rate in 0.13 kPa C_2H_4 and 17.5 kPa O_2 at 400°C and the total voltammetric charge Q

The magnitude of the voltammetric charge depends on the time elapsed between the current interruption and the cyclic voltammetric measurement. The first voltammogram upon interruption of the 200 μA galvanostatic step was recorded 10s later than the first voltammogram upon interruption of the 100

μA step. The difference in the Q values can only be partly explained by such a small lapse of time. It seems that it is mainly due to the difference in the water vapour content in the reactor. In fact, the GC area for the water peak is "w1100" in the case of the 200 μA step, and "w2700" in the case of the 100 μA step.

The extrapolation of the linear correlation of the experimental points crosses the line of zero rate at a non-zero value of charge. The charge predicted at a zero rate is 19 μC for the 200 μA step and 37 μC for the 100 μA step. Considering the activation procedure, this observation can be explained by supposing that the oxygen initially stored in the form of $IrO_{2+\delta}$ is not active, because it is firmly bonded to the catalyst. As the higher oxide grows, the mobility of the oxygen stored over the first monolayer or, most probably, part of a monolayer, may be higher, and the surface diffusion towards the gas-exposed catalyst surface is facilitated. The gradual formation of a surface oxide $IrO_{2+\delta}$ over the gas-exposed catalyst surface, should result in an increase of the work function. The distinction between surface oxidation and oxygen adsorption is mainly based on the strength difference of the bonds involved in each case. However, since oxygen adsorption provokes an increase of the work function, the surface oxidation probably also provokes it. Therefore, the attribution of the enhanced catalyst activity to a surface $IrO_{2+\delta}$ oxide is consistent with the observed work function increase on the gas-exposed catalyst-electrode surface under NEMCA conditions [Vayenas, 1992b].

4.4.4 The catalyst stability

The alternation between "open-circuit" and "closed-circuit" experiments at variable intervals make it difficult to establish a coherent history of the catalyst. However, some general remarks can be pointed out.

The selectivity did not change throughout the experiments. The carbon mass balance is always respected, assuming that all the ethylene converted is transformed to CO_2 . The precision of the mass balance depends on the quantity of CO_2 formed. At high rates of formation, the carbon mass balance is respected at ± 1%, while at very low rates, it is only respected at ± 10%, because the CO_2 partial pressure is close to the sensitivity limit of the IR-analyzer.

No evidence of poisoning or coking of the catalyst was noted over the course of the study, even in reducing atmospheres. The system was regularly tested by letting oxygen flow through the reactor at the end of a series of experiments, at a slightly higher temperature. The continuous monitoring of the CO_2 concentration at the exit did not reveal any subsequent CO_2 formation. This result is in agreement with the literature (§2.2), where Ir catalysts are known to promote coke destruction. No catalyst sintering seems likely to have taken place, because the temperatures used ($T < 500°C$) were always lower than the preparation temperature of the catalyst ($T = 550°C$).

The response of the fresh catalyst to electrochemical activation by galvanostatic or potentiostatic pulses differs significantly from the response of the used catalyst. The catalyst was often submitted to electrochemical "activation" treatments (O^{2-} pumping to the catalyst by applying positive potentials) alternated with periods at rest. The catalyst did not spend more than 100 hours under "deactivating" conditions (O^{2-} withdrawal by applying negative potentials) is comparatively lower.

The IrO_2 catalyst used for approximately 3000 hours of experiment does not present any signs of deactivation. On the contrary, an activity increase is observed between the beginning and the end of the investigations. Under a given set of temperature, flow rate and gas phase composition, the measured rate increased from $2.3 \pm 0.1 \cdot 10^{-8}$ molO/s to $8.8 \pm 0.5 \cdot 10^{-7}$ molO/s. The activity increase principally occurred during the first half of the catalyst life. During the same period, the electrochemical modification of the catalytic activity was not completely reversible. In the second half of the catalyst life, where the response of the catalyst to the electrochemical polarization is very rapid and reversible, the reaction rates seem stable. Initially, the catalyst may have been subject to a permanent modification, the nature of which has not been elucidated.

CHAPTER 5

GENERAL DISCUSSION AND PERSPECTIVES

The use of cyclic voltammetry for the in-situ study of catalyst surfaces in undivided cells is a technique which provides valuable information on the processes involved, although further investigation is needed to be fully understood. In a divided cell, where the reference electrode can be maintained in a stable environment like air, the interpretation of voltammograms should be simplified. Since the IrO_2 / YSZ cell is usually operated in a large oxygen excess, oxygen leakage through the solid electrolyte membrane should not be a problem with a divided cell.

In the cyclic voltammetric study of the IrO_2 catalyst, the well-defined cathodic peak with no visible anodic counterpart is attributed to the coupled transitions Ir (IV/V/VI). When the potential is held for some lapse of time at the anodic reversal potential, the surface of the peak during the cathodic scan is greatly enhanced. This peak must be related to the activation process of the catalyst and, more precisely, to the higher $IrO_{2+\delta}$ oxide. In this non-stoechiometric oxide, part of the Ir^{4+} cations in the catalyst lattice are oxidized to the Ir^{5+} and Ir^{6+} states. In this work, the behaviour of the peak has not been studied under the experimental conditions used for the investigation of the NEMCA effect. Further investigation in presence of ethylene in the gas phase should provide more insight into the mechanisms of electrochemical promotion.

The cyclic voltammetric work also showed that the properties of the electrochemical interface depend on the water vapour content of the gas phase. The water vapour is probably at the origin of the anodic peak observed in platinum voltammograms. It also causes an increase of the capacity at the catalyst-electrolyte interface. Some recent studies have shown that water is not required for spillover to occur, but can assist in the exchange process [Conner Jr., 1993]. Since the presence of moisture influences the catalytic and electrocatalytic behaviour of oxide catalysts, via the regulation of the surface coverage by OH groups, the moisture content should be maintained at known level during all the experiments. The role of water should certainly be further investigated in relation with the NEMCA effect.

The ethylene oxidation kinetics are complex. The quantitative evaluation of the adsorption and desorption kinetics of the reactants is necessary for the elucidation of the reaction mechanism and the development of a suitable kinetic model.

It would be interesting to study the ethylene oxidation in an undivided cell with both working and counter electrodes in IrO_2 . This configuration may throw more light on the rate enhancement by both anodic and cathodic catalyst polarization under a given set of conditions.

The catalytic reactor and electrochemical cell should be improved prior to further investigations. The simplicity of construction and maintenance of the present configuration are valuable for the prompt collection of semi-quantitative results. However, a reliable model for the reaction kinetics can only be obtained in a well-characterized reactor from the hydrodynamic point of view. The dead zones can be minimized by filling the upper part of the reactor with a temperature resistant ceramic rod, containing

several holes for the gas feed and for the passage of electrical leads and thermocouples. The dead volume from the reactor exit to the analysis unit can also be minimized by an appropriate arrangement of the apparatus. If the reactor volume is reduced to a few cm^3 , the conversion can be kept at a low level without the need of very high volumetric flow rates and without problems due to the analysis limits.

The thickness of the YSZ support should be reduced to, at least, half of its actual value (1mm). The plate would still be mechanically resistant, and the electrolyte conductivity would be enhanced. In this way, the ethylene oxidation and the NEMCA effect can be studied at temperatures as low as 200°C. The results would probably be even more spectacular at very low temperatures, where the regular catalytic rate is also low.

In this respect, an improvement of the electrical contacting procedure would be welcome: instead of "soldering" a one point contact on the catalyst, the gold current lead could terminate in a fine gold net, which can be "taken into" the catalyst during the last application of the precursor solution. Usually, such multiple contact points are used in SOFCs to reduce the contact resistance [VanHerle, 1992]. In the studies of the NEMCA effect, the multiple contact procedure would allow a better current distribution in the catalyst. Even if the IrO_2 is a good metallic conductor, the in-plane resistance of very thin porous films is not necessarily negligible. In fact, the observation of localized zirconia blackening during some preliminary experiments indicates that the catalyst surface in contact with the electrolyte is not always an equipotential.

It has been pointed out in the literature (§2.1) that the electrode performance can be ameliorated when the surface layer of the solid electrolyte is made active with respect to oxygen adsorption, surface diffusion and electron transfer processes. This can be realized by current blackening or by applying an oxidic layer showing mixed conductivity. Ong et al. observed that anodic currents can be increased up to two orders of magnitude by using the electrolyte in a highly reduced state. However, the results in this work are very similar prior to and after zirconia reduction. The absence of a significant effect positive or negative on the catalyst performance, may be due to the fact that the visual effect of current blackening is much more important than the electrocatalytic one. On the other hand, a systematic study of the electrochemical promotion on a solid electrolyte with a mixed conduction layer adjacent to the electrode might help to elucidate the mechanism of the activation. Electronic conduction is supposed to be harmful, since it provokes some ionic current loss, but the eventual enhancement of the electrolyte activity in the process might be beneficial.

Iridium oxide is very expensive, so it could be mixed with or replaced by other conducting or semi-conducting oxides. Some insufficiently documented results, not presented here, showed that mixed oxides of iridium and tin also exhibit the NEMCA effect. A mixed oxide of IrO_2 and Ta_2O_5 may also give interesting results. The high temperature α phase of Ta_2O_5 was reported to exhibit oxygen ion conductivities comparable with stabilized zirconia at temperatures in the vicinity of 800°C [Weber, 1993]. Insensitivity to doping showed that Ta_2O_5 is indeed an intrinsic oxygen ion conductor with an activation energy of about 1eV.

IrO_2 can be advantageously replaced by RuO_2 which possesses similar properties and especially metallic conductivity. RuO_2 was not chosen at the first place because it is not very stable at high temperatures. Thermal stability should not be a problem if the temperature is maintained below 400°C. An additional benefit for the NEMCA effect study on RuO_2 catalysts comes from the fact that the open-circuit kinetics for several reactions are well documented over such catalysts.

In order to study the effect of polarization for reduction reactions over oxide catalysts, the mixed oxides of RuO_2 and TiO_2 would be of special interest. These mixed oxides are well characterized with respect to their catalytic and electrocatalytic properties. In addition, TiO_2 could play the role of support, since it was recently successfully used as a solid electrolyte in a NEMCA application [Kaloyannis, 1995]. Electronic oxides, in addition to temperature sensitivity, are often sensitive to the oxygen partial pressure. In the case of TiO_2 oxygen sensors, the ionic conductivity, although representing only a small fraction of the total conductivity, is essential to the operation and response time of the device [Weber, 1993].

The CO oxidation by NO over IrO_2 / YSZ would be a particularly interesting reaction with respect to the NEMCA effect. Iridium catalysts are reported to be selective towards CO_2 formation in oxygen rich atmospheres (§2.2). If the IrO_2 selectivity is enhanced by polarization and the reduction of CO and NO_x emissions is coupled to a high activity for the complete oxidation of hydrocarbons in oxygen-rich conditions, then the IrO_2 / YSZ cell might be suitable as a car-exhaust catalyst.

In this work, the IrO_2 catalyst supported on YSZ is shown to be very active for the complete ethylene oxidation. The kinetics show a Langmuir-Hinshelwood type behaviour and a complex temperature dependence. The two reactants are in competition for the adsorption sites and the reaction may take place via a reactive intermediate. The NEMCA effect is observed for the first time over an oxide catalyst. The electrochemical promotion probably proceeds via a higher $IrO_{2+\delta}$ oxide.

The area of investigations related to the electrochemical promotion is huge and awareness of this new field is growing. It can be expected that the researchers' community of electrochemistry and electrocatalysis will direct an increasing interest toward this topic in the future.

REFERENCES

Al-Zakri, A. S., Gultekin, S., Al-Saleh, M. A., Celiker, H. S. (1991). "A method of IR drop measurements using a current interruption technique: an application to half cell studies with porous gas diffusion electrodes." J. Appl. Electrochem. **21**: 368.

Andersen, A. G., Hayakawa, T., Suzuki, K., Shimizu, M., Takehira, K. (1994). "Electrochemical methane conversion over $SrFeO_{3-x}$ perovskite on an yttrium stabilized zirconia membrane." Catal. Lett. **27**: 221.

Aramata, A., Toyoshima, I., Enyo, M. (1992). "Study of methanol electrooxidation on Rh-Sn oxide, Pt-Sn oxide and Ir-Sn oxide in comparison with that on the Pt metals." Electrochim. Acta **37**(8): 1317.

Ardizzone, S., Carugati, A., Trasatti, S. (1981). "Properties of thermally prepared iridium dioxide electrodes." J. Electroanal. Chem. **126**: 287.

Ardizzone, S., Fregonara, G., Trasatti, S. (1990). ""Inner" and "outer" active surface of RuO_2 electrodes." Electrochim. Acta **35**(1): 263.

Atkinson, A. (1989). "Defects and diffusion in metal oxides" in *Selected topics in high temperature chemistry*, (O. Johannesen, A.G. Andersen, Ed.), Elsevier, vol. 9, p.29.

Augustynski, J., Koudelka, M., Sanchez, J., Conway, B. E. (1984). "ESCA study of the state of iridium and oxygen in electrochemically and thermally formed iridium oxide films." J. Electroanal. Chem. **160**: 233.

Azzoni, C. B., Paleari, A. (1991). "Paramagnetic-defect kinetics in yttria-stabilized zirconia." Solid State Ionics **44**: 267.

Badwal, S. P. S., Nardella, N. (1990). "Polarization studies on solid electrolyte cells with a fully automated galvanostatic current interruption technique." Solid State Ionics **40/41**: 878.

Bae, J.-M., Park, S.-J. (1992). "Surface conduction characteristic of 8 mol% Y_2O_3 - ZrO_2." Solid State Ionics **53-56**: 798.

Baker, R. T., Metcalfe, I. S., Middleton, P. H., Petrolekas, P., Steele, B. C. H. (1993). "Catalytic behavior of $LiFeO_2$ anode for solid oxide fuel cells" in *New frontiers in catalysis*, (L. Guczi, Ed.), Elsevier Science Publishers, p. 2127.

Baker, D. R., Verbrugge, M. W. (1994). "Mathematical analysis of potentiometric oxygen sensors for combustion gas streams." AIChE J. **40**(9): 1498.

Balko, E. N., Nguyen, P. H. (1991). "Iridium-tin mixed oxide anode coatings." J. Appl. Electrochem. **21**: 678.

Bard, A. J., Faulkner, L. R. (1980). Electrochemical methods: fundamentals and applications, John Wiley & Sons.

Barlow Jr., C. A. (1970). "The electrical double layer" in *Physical Chemistry: an advanced treatise*, Academic Press, vol. 9A, p. 167.

Barrett, E. P. S., Blackburn, A. J.; Yates, M. A.; Wang, Y.; Sermon, P. A. (1993). "Catalysis and spillover" in *New aspects of spillover effect in catalysis*, Elsevier, vol. 77, p. 207.

Bebelis, S., Vayenas, C. G. (1989). "Non-faradaic Electrochemical Modification of Catalytic Activity 1. The case of ethylene oxidation on Pt." J. Catal. **118**: 125.

Belyaev, V. D., Sobyanin, V. A., Mar'ina, O. A. (1993). "Oxidative conversion of methane on Cu and Ag-Ni electrodes at artificial unsteady-state mode of the SOFC reactor operation." in *New aspects of spillover effect in catalysis*, Elsevier, vol. 77, p. 213.

Belzner, A., Gür, T. M., Huggins, R. A. (1990). "Measurement of the chemical diffusion coefficient of oxygen in mixed conductors by a solid state electrochemical method." Solid State Ionics **40/41**: 535.

Ben-Michael, R., Tannhauser, D. S. (1991). "Visual observation of chemical diffusion in stabilized zirconia." Appl. Phys. A **53**: 185.

Benedetti, A., Polizzi, S., Riello, P., DeBattisti, A., Maldotti, A. (1991). "X-ray diffraction characterization of iridium dioxide electrocatalysts." J. Mater. Chem. **1**(4): 511.

Berlowitz, P. J., Peden, C. H. F., Goodman, D. W. (1988). "Kinetics of CO oxidation on single-crystal Pd, Pt, and Ir." J. Phys. Chem. **92**: 5213.

Biswas, J., Bickle, G. M., Gray, P. G., Do, D. D., Barbier, J. (1988). "The role of deposited poisons and crystallite surface structure in the activity and selectivity of reforming catalysts." Catal. Rev.-Sci. Eng. **30**(2): 161.

Bockris, J. O., Reddy, A. K. N. (1970). Modern electrochemistry. Plenum Press, New York.

Bockris, J. O., Minevski, Z. S. (1994). "Electrocatalysis: past, present and future." Electrochim. Acta **39**(11-12): 1471.

Böld, W., Breiter, M. (1961). "Untersuchung des anodischen aufbaus und der kathodischen reduktion der sauerstoff-belegung am Rhodium und Iridium." Electrochim. Acta **5**: 169.

Borman, P. C., Westerterp, K. R. (1995). "An experimental study of the kinetics of the selective oxidation of ethene over a silver on a-alumina catalyst." Ind. Eng. Chem. Res. **34**: 49.

Boukamp, B. A., VanHassel, B. A., Vinke, I. C., DeVries, K. J., Burggraaf, A. J. (1993). "The oxygen transfer process on solid oxide / noble metal electrodes, studied with impedance spectroscopy, dc polarization and isotope exchange." Electrochim. Acta **38**(14): 1817.

Brainina, K., Neyman, E. (1993). "Electroanalytical stripping methods" in *Chemical Analysis*, John Wiley & Sons, p. 5.

Brook, R. J., Pelzmann, W. L., Kröger, F. A. (1971). "Platinum electrodes and calcia-stabilized zirconia." J. Electrochem. Soc. **118**(2): 185.

Bruce, P. G. (1995). Solid state electrochemistry. Cambridge University Press.

Buckley, D. N., Burke, L. D. (1975). "The oxygen electrode Part 5. Enhancement of charge capacity of an iridium surface in the anodic region." J. Chem. Soc. Faraday Trans. **1**: 1447.

Burke, L. D., Murphy, O. J., O'Neill, J. F., Venkatesan, S. (1977). "The oxygen electrode. Part 8: Oxygen evolution at ruthenium dioxide anodes." J.C.S. Faraday I **73**: 1659.

Burke, L. D. (1980). "Oxide growth and oxygen evolution on noble metals" in *Electrodes of conductive metallic oxides*. Elsevier, p. 141.

Burke, L. D., Whelan, D. P. (1984). "A voltammetric investigation of the charge storage reactions of hydrous iridium oxide layers." J. Electroanal. Chem. **162**: 121.

Burkhard, D. J. M., Hanson, B., Ulmer, G. C. (1991). "ZrO_2 oxygen sensors: an evaluation of behavior at temperatures as low as 300°C." Solid State Ionics **47**: 169.

Butler, J. A. V., Drever, G. (1936). "The mechanism of electrolytic processes. Part I: The anodic oxidation of some metals of the Pt group." Trans. Far. Soc. **32**: 427.

Canning, N. D. S., Outka, D., Madix, R. J. (1984). "The adsorption of oxygen on gold." Surf. Sci. **141**: 240.

Cant, N. W., Hall, W. K. (1970). "Catalytic oxidation II. Silica supported noble metals for the oxidation of ethylene and propylene." J. Catal. **16**: 220.

Cant, N. W., Hall, W. K. (1972). Ethylene oxidation in the presence of iridium metal. US Patent No 3641139, Gulf Research & Development Co.

Cant, N. W., Hicks, P. C., Lennon, B. S. (1978). "Steady-state oxidation of carbon monoxide over supported noble metals with particular reference to platinum." J. Catal. **54**: 372.

Chao, T., Walsh, K. J., Fedkiw, P. S. (1991). "Cyclic voltammetric study of the electrochemical formation of platinum oxide in a Pt / YSZ cell." Solid State Ionics **47**: 277.

Che, M., Tench, A. J. (1983). "Characterization and reactivity of molecular oxygen species on oxide surfaces" in *Advances in Catalysis*, Academic Press, vol. 32, p. 3.

Chesters, M. A., Somorjai, G. A. (1975). "The chemisorption of oxygen, water and selected hydrocarbons on the (111) and stepped gold surfaces." Surf. Sci. **52**: 21.

Chiang, P. H., Eng, D., Alqahtany, H., Stoukides, M. (1992). "Nonoxidative methane coupling with the aid of solid electrolytes." Solid State Ionics **53-56**: 135.

Choudhary, C. B., Maiti, H. S.; Subbarao, E. C. (1980). "Defect structure and transport properties" in *Solid electrolytes and their applications*, (E. C. Subbarao, Ed.), Plenum Press, New York, p. 1.

Comninellis, C., Vercesi, G. P. (1991a). "Characterization of DSA-type oxygen evolving electrodes: choice of a coating." J. Appl. Electrochem. **21**: 335.

Comninellis, C., Vercesi, G. P. (1991b). "Problems in DSA coating deposition by thermal decomposition." J. Appl. Electrochem. **21**: 136.

Comninellis, C. (1994). "Electrocatalysis in the electrochemical conversion/combustion of organic pollutants for waste water treatment." Electrochim. Acta **39**(11-12): 1857.

Conner Jr., W. C. (1993). "Spectroscopic insight into spillover" in *New aspects of spillover effect in catalysis*, Elsevier Sci. Publ., vol. 77, p. 61.

Conway, B. E., Mozota, J. (1983). "Surface and bulk processes at oxidized iridium electrodes II. Conductivity-switched behaviour of thick oxide films." Electrochim. Acta **28**(1): 9.

Copcutt, R. C., Maskell, W. C. (1992). "CO/CO_2 electrochemistry on zirconia electrolyte with Pt electrodes in relation to amperometric oxygen sensors." Solid State Ionics **53-56**: 119.

Cullity, B. D. (1978). Elements of X-Ray diffraction. Addison-Wesley.

DaSilva, P. N., Guenin, M., Leclercq, C., Frety, R. (1989). "Metallic area of supported iridium catalysts." Appl. Cat. **54**: 203.

Davydov, A. A. (1990). Infrared spectroscopy of adsorbed species on the surface of transition metal oxides. John Wiley & Sons.

De Battisti, A., Barbieri, A., Giatti, A., Battaglin, G., Daolio, S., Boscoletto, A. B. (1991). "Depth profiles and electrochemical properties of IrO_2 electrocatalysts stabilized with TiO_2." J. Mater. Chem. **1**(2): 191.

Delmon, B. (1993). "The control of selectivity and stability of catalysts by spillover processes" in *New aspects of spillover effect in catalysis*, Elsevier Sci. Publ., vol. 77, p. 1.

Delmon, B. (1994). "The control of reaction selectivity and stability of catalysts by spillover processes." Het. Chem. Rev. **1**: 219.

Deportes, C., Duclot, M.; Fabry, P.; Fouletier, J.; Hammou, A.; Kleitz, M.; Siebert, E.; Souquet, J.-L. (1994). Electrochimie des solides. Presses Universitaires de Grenoble.

Dieterich, W. (1990). "Recent developments in the theory of solid electrolytes." Solid State Ionics **40/41**: 509.

Doepper, R. (1988). Etude cinétique de l'acétoxydation d'éthylène en régime transitoire. Thesis No 750, EPFL, Lausanne.

Dufour, L.-C., Morin, F. (1988). "Surface and morphology of oxide materials for advanced water electrolysis." Mat. Sci. Forum **29**: 275.

Elzanowska, H., Birss, V. I. (1993). "Reversible ageing of iridium oxide electrodes in acidic solutions." J. Appl. Electrochem. **23**: 646.

Eng, D., Stoukides, M. (1991a). "The catalytic and electrocatalytic coupling of methane over YSZ." Catal. Lett. **9**: 47.

Eng, D., Stoukides, M. (1991b). "Catalytic and electrocatalytic methane oxidation with solid oxide membranes." Catal. Rev.-Sci. Eng. **33**(3/4): 375.

Ertl, G. (1990). "Elementary steps in heterogeneous catalysis." Angew. Chem. Int. Ed. Engl. **29**: 1219.

Etsell, T. H., Flengas, S. N. (1971). "Overpotential behavior of stabilized zirconia solid electrolyte fuel cells." J. Electrochem. Soc. **118**(12): 1890.

Fabry, P., Kleitz, M. (1979). "Electrochemical characterization of the point defects associated with copper dissolved in stabilized zirconia." J. Electrochem. Soc. **126**(12): 2183.

Feidenhans'l, R. (1989). "Surface structure determination by x-ray diffraction." Surf. Sci. Rep. **10**: 105.

Ferloni, P., Magistris, A. (1994). "New materials for solid state electrochemistry." J. Phys. IV **4**: C1.

Ferrer, J. E., Victori, L. (1994). "Study of the oxygen evolution reaction on the Ir electrode in acid medium by EIS." Electrochim. Acta **39**(5): 667.

Foger, K., Jaeger, H. (1981). "Interpretation of temperature-programmed reduction (TPR). Experiments of platinum-iridium catalysts." J. Catal. **67**: 252.

Forbes, C. A., Pierre, J. F. (1993). "The solid fuel-cell future." IEEE Spectrum **october**: 40.

Frelink, T., Visscher, W., van Veen, J. A. R. (1995). "The third anodic hydrogen peak on platinum; subsurface H2 adsorption." Electrochim. Acta **40**(5): 545.

Fujimoto, K. (1993). "Catalyst design based on spillover theory" in *New aspects of spillover effect in catalysis*, Elsevier Sci. Publ., vol. 77, p. 9.

Fung, S. C. (1994). "Regenerating a reforming catalyst." Chemtech **24**(1): 40.

Gellings, P. J., Koopmans, H. J. A., Burggraaf, A. J. (1988). "Electrocatalytic phenomena in gas phase reactions in solid electrolyte electrochemical cells." Appl. Cat. **39**: 1.

Goffe, R. A., Mason, D. M. (1981). "Electrocatalytic oxidation of hydrocarbons on a stabilized-zirconia electrolyte employing gold or platinum electrodes." J. Appl. Electrochem. **11**: 447.

Goodenough, J. B. (1995). "Crystalline solid electrolytes II: material design" in *Solid state electrochemistry*, (P. G. Bruce, Ed.), Cambridge University Press, p. 43.

Goto, T., Vargas, R., Hirai, T. (1993). "Preparation of Ir and Pt films by MOCVD and their properties." J. Phys. IV **3**: 297.

Gottesfeld, S., Srinivasan, S. (1978). "Electrochemical and optical studies of thick oxide layers on Ir and their electrocatalytic activities for the oxygen evolution reaction." J. Electroanal. Chem. **86**: 89.

Gozzi, D., Carnevale, G., Cignini, P. L., Petrucci, L., Tomellini, M. (1988). "Zirconia based electrochemical cells to study the reaction kinetics between materials and oxygen at high temperature" in *Zirconia'88. Advances in Zirconia Science and Technology*, (S. Meriani, C. Palmonari, Ed.), Elsevier, p. 99.

Grant, R. B., Lambert, R. M. (1985). "A single crystal study of the silver-catalysed selective oxidation and total oxidation of ethylene." J. Catal. **92**: 364.

Greef, R., Peat, R., Peter, L. M., Pletcher, D., Robinson, J. (1990). Instrumental methods in electrochemistry. Ellis Horwood.

Gulliver, D. J., W. Levason, W. (1982). "The chemistry of Ru, Os, Rh, Ir, Pd and Pt in the higher oxidation states." Coord. Chem. Rev. **46**: 1.

Gundry, P. M., Tompkins, F. C. (1968). "Surface potentials" in *Experimental methods in catalytic research*, (R. B. Anderson, Ed.), Academic Press, vol. 1, p. 100.

Gür, T., Raistrick, I., Huggins, R. (1980). "Steady state dc polarization characteristics of the O_2, Pt / YSZ interface." J. Electrochem. Soc. **127**: 2620.

Harkness, I. R., Lambert, R. M. (1995). "Electrochemical promotion of the NO + ethylene reaction over platinum." J. Catal. **152**: 211.

Hartley, T. N., Price, D. (1970). "Anodic oxidation of hydrocarbons." J. Electrochem. Soc. **117**(4): 448.

Haruta, M., Tsubota, S., Ueda, A., Sakurai, H. (1993). "Synergism in the catalysis of supported gold" in *New aspects of spillover effect in catalysis*, Elsevier Sci. Publ., vol. 77, p. 45.

Hayakawa, T., Sato, K., Tsunoda, T., Suzuki, K., Shimizu, M., Takehira, K. (1994). "Partial oxidation of ethane into acetaldehyde by active oxygen generated electrochemically on gold through yttria-stabilized zirconia." J. Chem. Soc. Chem. Commun. : 1743.

Heras, J. M., Viscido, L. (1988). "The behavior of water on metal surfaces." Catal. Rev.-Sci. Eng. **30**(2): 281.

Hildenbrand, H.-H., Lintz, H.-G. (1989). "Solid Electrolyte Potentiometry at an oxide electrode." Appl. Cat. **49**: L1.

Hildenbrand, H.-H., Lintz, H.-G. (1990). "Phase-composition and selectivity: Solid Electrolyte Potentiometry aided study of the oxidation of propene on copper oxides." Appl. Cat. **65**: 241.

Hino, M., Arata, K. (1995). "Synthesis of highly active superacids of SO_4/ ZrO_2 with Ir, Pt, Rh, Ru, Os, and Pd substances for reaction of butane." Catal. Lett. **30**: 25.

Hoare, J. P. (1964). "On the mixed potentials observed in the Iridium-Oxygen-Acid system." J. Electrochem. Soc. **111**(8): 988.

Hoare, J. P. (1967). "The oxygen electrode on noble metals" in *Advances in electrochemistry and electrochemical engineering*, (P. Delahay, C. W. Tobias, Ed.), John Wiley & Sons, vol. 6, p. 202.

Honig, J. M. (1980). "Electronic band structure of oxides with metallic or semiconducting characteristics" in *Electrodes of conductive metallic oxides Part A*, (S. Trasatti, Ed.), Elsevier, p. 1.

Huang, Y.-J., Fung, S. C., Gates, W. E., Mc Vicker, G. B. (1989). "Pt-Ir/Al_2O_3 catalysts - The effect of Pt-Ir interaction on Ir agglomeration and catalytic performance." J. Catal. **118**: 192.

Hüppauff, M., Lengeler, B. (1993). "Valency and structure of iridium in anodic iridium oxide films." J. Electrochem. Soc. **140**(3): 598.

Hutchings, R., Müller, K., Kötz, R., Stucki, S. (1984). "A structural investigation of stabilized oxygen evolution catalysts." J. Mat. Sci. **19**: 3987.

Ingel, R. P., Lewis, D. (1986). "Lattice parameters and density for Y_2O_3-stabilized ZrO_2." J. Am. Cer. Soc. **69**(4): 325.

Inoue, M., Kurusu, A., Terada, K., Inui, T. (1991). "Alcohol synthesis from syngas on alumina-supported iridium-based catalysts. Effects of transition-metal compound additives." Appl. Cat. **67**: 203.

Inoue, T., Hoashi, K., Eguchi, K., Arai, H. (1993). "An effect of microstructure on the interface resistance between a perovskite-type oxide electrode and YSZ." J. Mat. Sci. **28**: 1532.

Inui, T. (1993). "Spillover effect as the key concept for realizing rapid catalytic reactions" in *New aspects of spillover effect in catalysis*, Elsevier Sci. Publ., vol. 77, p. 17.

Isaacs, H. S., Olmer, L. J. (1982). "Comparison of materials as oxygen catalytic electrodes on zirconia electrolyte." J. Electrochem. Soc. **129**(2): 436.

Jacob, K.-H., Knözinger, E., Benfer, S. (1993). "Adsorption sites on polymorphic zirconia." J. Mater. Chem. **3**(6): 651.

Jacobsen, T., Zachau-Christiansen, B., West, K., Skaarup, S. (1991). "Linear sweep voltammetry on $La_{0.85}Sr_{0.15}MnO_3$" in *2nd International Symposium on SOFC*, Athens (GR), p. 795.

Jiang, Y., Kaloyannis, A., Vayenas, C. G. (1993). "High temperature cyclic voltammetry of Pt catalyst-electrodes in solid electrolyte cells." Electrochim. Acta **38**(17): 2533.

Johannesen, O. (1989). "Enhanced ionic conductivity in inorganic solids" in *Selected topics in high temperature chemistry*, (O. Johannesen, A.G. Andersen, Ed.), Elsevier, vol. 9, p. 143.

Jung, D.-Y., Demazeau, G. (1995). "High oxygen pressure and the preparation of new iridium (VI) oxides with perovskite structure: Sr_2MIrO_6 (M=Ca, Mg)." J. Solid State Chem. **115**: 447.

Kaloyannis, A. C., Pliangos, C. A., Tsiplakides, D. T., Yentekakis, I. V., Neophytides, S. G., Bebelis, S., Vayenas, C. G. (1995). "Electrochemical promotion of catalyst surfaces deposited on ionic and mixed conductors", in *4th Panhellenic symposium on catalysis*, Papingo (GR), p. 129.

Kameyama, K., Tsukada, K., Yahikozawa, K., Takasu, Y. (1994). "Surface characterization of RuO_2-IrO_2-TiO_2 coated titanium electrodes." J. Electrochem. Soc. **141**(3): 643.

Kanski, J., Rhodin, T. N. (1977). "Chemisorptive bonding and reaction of nitric oxide on Ir(100) and Ir(111) surfaces." Surf. Sci. **65**: 63.

Kedzierzawski, P., Augustynski, J. (1994). "Poisoning and activation of the gold cathode during electroreduction of CO_2." J. Electrochem. Soc. **141**(5): L58.

Kenjo, T., Horiuchi, Y., Osawa, S. (1990). "Determination of the rate constants of oxygen reduction in high-temperature air electrodes on solid oxide electrolytes." J. Electrochem. Soc. **137**(8): 2423.

Khandkar, A. C., Joshi, A. V. (1993). "Solid electrolytes: emerging applications and technologies." Electrochem. Soc. Interface **summer**: 26.

Kip, B. J., van Grondelle, J., Martens, J. H. A., Prins, R. (1986). "Preparation and characterization of very highly dispersed iridium on Al_2O_3 and SiO_2." Appl. Cat. **26**: 353.

Kirschner, E. M. (1995). "Production of top 50 chemicals increased substantially in 1994." C&EN **April 10**: 16.

Kleitz, M., Besson, J., Deportes, C. (1967). "Cinétique des réactions d'électrode dans les oxydes électrolytes solides" in *Compte rendu des 2ièmes Journées Internationales d'étude de piles à combustibles*, Bruxelles, p. 354.

Kleitz, M., Siebert, E., Fouletier, J. (1983). "Recent developments in oxygen sensing with a solid electrolyte cell" in *Chemical Sensors*, Elsevier, Amsterdam, p. 262.

Kötz, R., Neff, H., Stucki, S. (1984). "Anodic iridium oxide films." J. Electrochem. Soc. **131**(1): 72.

Krishnamurthy, S., Landolt, G. R., Schoennagel, H. J. (1982). "The stoichiometry of hydrogen and CO chemisorption on Ir / γ-Al_2O_3." J. Catal. **78**: 319.

Küppers, J., Plagge, A. (1976). "Interaction of CO and O_2 with Ir(111) surfaces." J. Vac. Sci. Technol. **13**(1): 259.

Kurumchin, E. K., Perfiliev, M. V. (1990). "An isotope exchange study of the behaviour of electrochemical systems." Solid State Ionics **42**: 129.

Kuzin, B. L., Komarov, M. A. (1990). "Adsorption of O_2 at Pt and kinetics of the oxygen reaction at a porous Pt electrode in contact with a solid oxide electrolyte." Solid State Ionics **39**: 163.

Laboratoire des Matériaux et procédés catalytiques, U. C. B. L. (1993). "Attempt at the characterization of spillover adsorbed species during catalysis" in *New aspects of spillover effect in catalysis*, Elsevier Sci. Publ., vol. 77, p. 85.

Ladas, S., S. Bebelis, S., Vayenas, C. G. (1991). "Work function measurements on catalyst films subject to in situ electrochemical promotion." Surf. Sci. **251/252**: 1062.

Ladas, S., Kennou, S., Bebelis, S., Vayenas, C. G. (1993). "Origin of non-faradaic electrochemical modification of catalytic activity." J. Phys. Chem. **97**(35): 8845.

Légaré, P., Hilaire, L., Sotto, M., Maire, G. (1980). "Interaction of oxygen with Au surfaces: a LEED, AES and ELS study." Surf. Sci. **91**: 175.

Levenspiel, O. (1972). Chemical Reaction Engineering. 2nd Ed., John Wiley & Sons.

Lezna, R. O., Kunimatsu, K., Ohtsuka, T., Sato, N. (1987). "In situ IR spectroscopy of iridium oxide." J. Electrochem. Soc. **134**(12): 3090.

Li, C., Chen, Y., Li, W., Xin, Q. (1993a). "Spillover of atomic oxygen and reverse spillover of dioxygen species on Pt/CeO_2 catalyst" in *New aspects of spillover effect in catalysis*, Elsevier Sci. Publ., vol. 77, p. 217.

Li, C., Xin, Q., Guo, X., Onishi, T. (1993b). "Surface oxygen species and their reactivities in the oxidation of CH_4, C_2H_6 and C_2H_4 over cerium oxide at mild temperatures" in *New frontiers in catalysis*, (L. Guczi, Ed.), Elsevier Sci. Publ. p. 1955.

Liaw, B. Y., Weppner, W. (1990). "Low temperature limiting-current oxygen sensors using tetragonal zirconia as solid electrolytes." Solid State Ionics **40/41**: 428.

Lin, S.-M., Wen, T.-C. (1993). "Oxygen evolution on Ir-Ru-Sn ternary oxide-coated electrodes in H_2SO_4 solution." J. Electrochem. Soc. **140**(8): 2265.

Lin, Y.-S., Wang, W., Han, J. (1994). "Oxygen permeation through thin mixed-conducting solid oxide membranes." AIChE J. **40**(5): 786.

Lincoln, W. W., Olinger, J. L. (1975). "Enhancement of gaseous adsorption on metal surfaces trough the use of an applied ac voltage." AIChE Symp. Ser. **71**(152): 77.

Lodi, G., De Battisti, A., Benedetti, A., Fagherazzi, G., Kristof, J. (1988). "Formation of iridium metal in thermally prepared iridium dioxide coatings." J. Electroanal. Chem. **256**: 441.

Lodi, G., De Battisti, A., Bordin, G., Asmundis, C. D., Benedetti, A. (1990). "Microstructure and electrical properties of IrO_2 prepared by thermal decomposition of $IrCl_3.xH_2O$." J. Electroanal. Chem. **277**: 139.

Lohrengel, M. M. (1993). "Pulse measurements for the investigation of fast electronic and ionic processes at the electrode/electrolyte interface." Ber. Bunsenges. Phys. Chem. **97**(3): 440.

Lucesoli, D., Degobert, P., Kochaniak, E. (1970). "Determination of the ohmic contribution to the polarization of fuel cell electrodes." J. Electrochem. Soc. **117**(7): 975.

Mahmood, M. N., Bonanos, N. (1992). "Application of the mixed potential model to the oxidation of methane on silver and nickel-zirconia catalysts." Solid State Ionics **53-56**: 142.

Mann, R. S., Khulbe, K. C. (1970). "The hydrogenation of ethylacetylene III. Reaction of ethylacetylene with hydrogen catalyzed by platinum and iridium." J. Catal. **17**: 46.

Mar'ina, O. A., Sobyanin, V. A., Belyaev, V. D. (1992). "The methane oxidation on a gold electrode in a solid electrolyte fuel cell." Mat. Sci. Eng. **B13**: 153.

Mar'ina, O. A., Sobyanin, V. A., Belyaev, V. D., Parmon, V. N. (1993). "The effect of electrochemical pumping of oxygen on catalytic behaviour of metal electrodes in methane oxidation" in *New aspects of spillover effect in catalysis*, Elsevier Sci. Publ., vol. 77, p. 337.

Marecot, P., Peyrovi, S., Bahloul, D., Barbier, J. (1990a). "Regeneration by hydrogen treatment of bifunctional catalysts deactivated by coke deposition I. Regeneration of precoked catalysts." Appl. Cat. **66**: 181.

Marecot, P., Peyrovi, S., Bahloul, D., Barbier, J. (1990b). "Regeneration by hydrogen treatment of bifunctional catalysts deactivated by coke deposition II. Regeneration of catalysts impregnated by coronene." Appl. Cat. **66**: 191.

Margolis, L. Y. (1963). "Catalytic oxidation of hydrocarbons" in *Advances in Catalysis*, Academic Press, vol. 14, p. 429.

Martin, P. J. (1986). "Ion-enhanced adhesion of thin gold films." Gold Bull. **19**(4): 102.

Mayer, J. W. (1984). "Gold contacts to semiconductor devices." Gold Bull. **17**(3): 18.

Mc Daniel, C. L., Schneider, S. J. (1967). "Phase relations in the systems TiO_2-IrO_2 and SnO_2-IrO_2 in air." J. Res. Nat. Bur. Stand. **71A**: 119.

Mc Intyre, J. D. E., Peck, J. W. F. (1970). "An interrupter technique for measuring the uncompensated resistance of electrode reactions under potentiostatic control." J. Electrochem. Soc. **117**(6): 747.

Mc Vicker, G. B., Garten, R. L., Baker, R. T. K. (1978). "Surface area stabilization of Ir/Al_2O_3 catalysts by CaO, SrO, and BaO under oxygen atmospheres: implications on the mechanism of catalyst sintering and redispersion." J. Catal. **54**: 129.

Metcalfe, I. S., Middleton, P. H., Petrolekas, P., Steele, B. C. H. (1992). "Hydrocarbon activation in solid state electrochemical cells." Solid State Ionics **57**: 259.

Michaels, J. N., Vayenas, C. G., Hegedus, L. L. (1986). "A novel cross-flow design for solid-state electrochemical reactors." J. Electrochem. Soc. **133**(3): 522.

Minh, N. Q. (1993). "Ceramic fuel cells." J. Am. Cer. Soc. **76**(3): 563.

Miura, N., Yan, Y., Sato, M., Yao, S., Shimizu, Y., Yamazoe, N. (1994). "Stabilized zirconia based CO_2 sensors combined with carbonate auxiliary phase." Chem. Lett. : 393.

Miyahara, Y. (1992). "Characterization of sputtered yttria-stabilized zirconia thin film and its application to a metal-insulator-semiconductor structure." J. Appl. Phys. **71**(5): 2309.

Mizusaki, J., Amano, K., Yamauchi, S., Fueki, K. (1983). "Response and electrode reaction of zirconia oxygen gas sensor" in *Chemical Sensors*, Elsevier, Amsterdam, p. 279.

Mizusaki, J., Amano, K., Yamauchi, S., Fueki, K. (1987). "Electrode reaction at Pt, O_2(g) / stabilized zirconia interfaces. Part I: Theoretical consideration of reaction model. Part II: Electrochemical measurements and analysis." Solid State Ionics **22**: 313.

Mizusaki, J., Tagawa, H., Miyaki, Y., Yamauchi, S., Jueki, K., Koshiro, I., Hirano, K. (1992). "Kinetics of the electrode reaction at the CO-CO_2, porous Pt / stabilized zirconia interface." Solid State Ionics **53-56**: 126.

Mizusaki, J., Tagawa, H., Isobe, K., Tajika, M., Koshiro, I., Maruyama, H., Hirano, K. (1994). "Kinetics of the electrode reaction at the H_2-H_2O porous Pt / stabilized zirconia interface." J. Electrochem. Soc. **141**(6): 1674.

Moghadam, F. K., Stevenson, D. A. (1986). "Oxygen diffusion and solubility in Ag and Pt using AC impedance spectroscopy." J. Electrochem. Soc. **133**(7): 1329.

Monk, P. M. S., Mortimer, R. J., Rosseinsky, D. R. (1995). "Through a glass darkly." Chemistry in Britain **31**(5): 380.

Moro-oka, Y. (1993). "Oxygen spillover for the design of industrial oxidation catalysts" in *New aspects of spillover effect in catalysis*, Elsevier Sci. Publ., vol. 77, p. 95.

Moulijn, J. A., Ponec, V. (1993). "Heterogeneous catalysis" in *Catalysis. An integrated approach to homogeneous, heterogeneous and industrial catalysis*, (J. A. Moulijn, P.W.N.M. van Leeuwen, R.S. van Santen, Ed.), Elsevier, p. 159.

Mozota, J., Conway, B. E. (1983). "Surface and bulk processes at oxidized iridium electrodes I. Monolayer stage and transition to reversible multilayer oxide film behaviour." Electrochim. Acta **28**(1): 1.

Murakami, Y., Tsuchiya, S., Yahikozawa, K., Takasu, Y. (1994). "Preparation of ultrafine IrO_2-Ta_2O_5 binary oxide particles by a sol-gel process." Electrochim. Acta **39**(5): 651.

Murphy, M. M., van Herle, J., Mc Evoy, A. J., Thampi, K. R. (1994). "Electroless deposition of electrodes in solid-oxide fuel cells." J. Electrochem. Soc. **141**(8): L94.

Nakagawa, N., Kuroda, C., Ishida, M. (1992). "Electrode reaction at fixed Pt film - fixation of Pt film on stabilized zirconia electrolyte and its effect on the electrode performance of the solid-electrolyte cell." J. Chem. Eng. Jap. **25**(1): 55.

Nam, Y. W., Silveston, P. L. (1993). "A mathematical model for spillover" in *New aspects of spillover effect in catalysis*, Elsevier Sci. Publ., vol. 77, p. 235.

Neophytides, S. G., Tsiplakides, D., Stonehart, P., Jaksic, M. M., Vayenas, C. G. (1994). "Electrochemical enhancement of a catalytic reaction in aqueous solution." Nature **370**: 45.

Neuimin, A. D., Kotlyar, A. G., Pal'guev, S. F., Strekalovskii, V. N., Batrakov, N. A. (1972). "The structure and conductivity of the ZrO_2-Y_2O_3 systems containing iron, manganese, cobalt, and nickel oxides" in *Electrochemistry of molten and solid electrolytes*, (S. F. Pal'guev, Ed.), Consultants Bureau, vol. 9, p. 73.

Newman, J. (1970). "Ohmic potential measured by interrupter techniques." J. Electrochem. Soc. **117**(4): 507.

Nguyen, B. C., Lin, T. A., Mason, D. M. (1986a). "Electrocatalytic reactivity of hydrocarbons on a zirconia electrolyte surface." J. Electrochem. Soc. **133**(9): 1807.

Nguyen, B. C., Rincon-Rubio, L. M., Mason, D. M. (1986b). "Mechanism of the electrocatalytic reduction of oxygen in a tubular solid oxide electrolyte flow reactor." J. Electrochem. Soc. **133**(9): 1860.

Nicholas, M. G. (1988). Interactions at oxide-metal interfaces. External and internal surfaces in metal oxides. Trans Tech. 127.

Nicholson, R. S., Shain, I. (1964). "Theory of stationary electrode polarography." Anal. Chem. **36**(4): 706.

Nicole, J. (1995). Modification de l'activité catalytique de l'oxyde d'iridium par application de potentiel. Diploma work (internal report), EPFL, Lausanne.

Nieuwenhuys, B. E., Ponec, V., van Koten, G., van Leeuwen, P. W. N. M., Santen, R. A. (1993). "Bonding and elementary steps in catalysis" in *Catalysis. An integrated approach to homogeneous, heterogeneous and industrial catalysis*, (J. A. Moulijn, P.W.N.M. van Leeuwen, R.S. van Santen, Ed.), Elsevier, p. 89.

Norby, T., Middleton, H., Hansen, E. W., Dahl, I., Andersen, A. G. (1993). Oxidation of methane on a $SrFeO_3$/Au//YSZ electrode characterised by mass spectrometry and $^{18}O_2$ pulses. Internal report.

Norby, T., Middleton, P. H., Hansen, E. W., Dahl, I., Andersen, A. G. (1995). "Oxidation of methane on a Au+$SrFeO_{3-\delta}$//YSZ electrode characterised by mass spectroscopy and $^{18}O_2$ pulses." Chem. Eng. Technol. **18**: 139.

Okamoto, H., Kawamura, G., Kudo, T. (1983). "Study of oxygen adsorption on platinum through observation of exchange current in a solid electrolyte concentration cell." Electrochim. Acta **28**(3): 379.

Orera, V. M., Merino, R. I., Chen, Y., Cases, R., Alonso, P. J. (1990). "Intrinsic electron and hole defects in stabilized zirconia single crystals." Phys. Rev. B **42**(16): 9782.

Orera, V. M., Merino, R. I., Chen, Y., Cases, R., Alonso, P. J. (1991). "Electron and hole trapped defects produced by thermoreduction or irradiation in stabilized zirconia." Rad. Eff. Def. Sol. **119-121**: 907.

Orera, V. M., Merino, R. I., Pena, F. (1994). "Ce^{3+} / Ce^{4+} conversion in ceria-doped zirconia single crystals induced by oxido-reduction treatments." Solid State Ionics **72**: 224.

Orliukas, A., Sasaki, K., Bohac, P., Gauckler, L. J. (1991). "Ionic conductivity of ZrO_2-Y_2O_3 prepared from ultrafine coprecipitated powders" in *2nd International Symposium on SOFC*, Athens (GR), p. 377

Ownby, P. D., Burt, D. D., Stewart, D. V. (1991). "Experimental study of the thermal expansion of yttria stabilized zirconia ceramics." Thermochim. Acta **190**: 39.

Parravano, G. (1970). "Equilibrium hydrogen transfer between benzene and C_6 hydrocarbons over supported metal catalysts." J. Catal. **16**: 1.

Paspek, S. C. (1980). Experimental and theoretical investigation of ethylene oxidation in a fixed-bed reactor. Thesis. Notre Dame University, Indiana.

Pickup, P. G., Birss, V. I. (1987). "A model for anodic hydrous oxide growth at iridium." J. Electroanal. Chem. **220**: 83.

Pickup, P. G., Birss, V. I. (1988a). "Chemical analysis of the ionic content of hydrous iridium oxide films." J. Electroanal. Chem. **240**: 171.

Pickup, P. G., Birss, V. I. (1988b). "The kinetics of charging and discharging of iridium oxide films in aqueous and non-aqueous media." J. Electroanal. Chem. **240**: 185.

Pilla, A. A. (1967). "Use of electrode impedance studies for the elucidation of electrochemical hydrocarbon oxidation kinetics" in *Compte rendu des 2ièmes Journées Internationales d'étude de piles à combustibles*, Bruxelles, p. 186.

Pizzini, S., Bianchi, M., Colombo, P., Torchio, S. (1973). "On the influence of the annealing temperature and heavy current treatments on the porous structure of platinum electrodes and on the kinetics of the oxygen reaction at high temperatures." J. Electrochem. Soc. **120**(3): 153.

Podlovchenko, B., Shterev, G., Semkova, R., Kolyadko, E. (1990). "Peculiarities of the electrocatalytic properties of surface skeleton iridium electrodes." Electrochim. Acta **35**(1): 191.

Pritchard, J. (1990). "Electrochemical promotion." Nature **343**: 592.

Psaro, R., Dossi, C., DellaPergola, R., Garlaschelli, L., Calmotti, S., Marengo, S., Bellatreccia, M., Zanoni, R. (1995). "Methanol from synthesis gas over cluster-derived FeIr/MgO catalysts." Appl. Cat. **121**: L19.

Ramanarayanan, T. A., Ling, S., Anderson, M. P. (1991). "Electrochemical analysis of mixed conduction in ceramic oxide membranes" in *2nd International Symposium on SOFC*, Athens (GR), p. 777.

Rasser, J. C. (1977). Platinum-iridium reforming catalysts. Thesis. Technische Hogeschool Delft, Netherlands.

Rickert, H. (1982). Electrochemistry of solids. Springer-Verlag, Berlin.

Robertson, N. L., Michaels, J. N. (1990). "Oxygen exchange on platinum electrodes in zirconia cells: location of electrochemical reaction sites." J. Electrochem. Soc. **137**(1): 129.

Robertson, N. L., Michaels, J. N. (1991). "Double layer capacitance of porous platinum electrodes in zirconia electrochemical cells." J. Electrochem. Soc. 138(5): 1494.

Rolewicz, J. (1987). Développement d'une électrode stable du type: métal support/dépôt conducteur. Thesis No 662, EPFL, Lausanne.

Rolewicz, J., Comninellis, C., Plattner, E., Hinden, J. (1988). "Récent Développement d'électrodes du type métal support-dépôt catalytique." Chimia **42**(2): 75.

Roof, R. B. (1976). Los Alamos Sci. Laboratory. Chem. Abstr. 86, 19, 8367 (1977).

Sachtler, W. M. H., Backx, C., van Santen, R. A. (1981). "On the mechanism of ethylene epoxidation." Catal. Rev.-Sci. Eng. **23**(1&2): 127.

Sadaoka, Y., Sakai, Y., Manabe, T. (1992). "CO2 sensing characteristics of a solid-state electrochemical sensor based on a sodium ionic conductor." J. Mat. Chem. **2**(9): 945.

Sakuma, T., Hata, H. (1988). "The domain structure of tetragonal zirconia in ZrO_2-Y_2O_3 alloys" in *Zirconia'88. Advances in Zirconia Science and Technology*, (S. Meriani, C. Palmonari, Ed.), Elsevier, p. 283.

Sammes, N. M., Steele, B. C. H. (1994). "The catalytic oxidation of ammonia in a ceramic electrochemical reactor, using metal oxide electrodes." J. Catal. **145**: 187.

Sanjinés, R., A. Aruchamy, A., Lévy, F. (1989). "Thermal stability of sputtered iridium oxide films." J. Electrochem. Soc. **136**(6): 1740.

Saracco, G., Specchia, V. (1994). "Catalytic inorganic-membrane reactors: present experience and future opportunities." Catal. Rev.-Sci. Eng. **36**(2): 305.

Sato, T., Endo, T., Shimada, M. (1988). "Post-sintering hot isostatic pressing of ceria-doped tetragonal zirconia/alumina composites" in *Zirconia'88. Advances in Zirconia Science and Technology*, (S. Meriani, C. Palmonari, Ed.), Elsevier, p. 293.

Satterfield, C. N. (1980). Heterogeneous catalysis in practice. McGraw-Hill.

Sawata, A., Tsuneyoshi, K., Mizusaki, J., Tagawa, H. (1990). "Oxygen chemical potential profile in a solid oxide fuel cell and simulation of electrochemical performance." Solid State Ionics **40/41**: 415.

Schmid, M. (1988). Etude de l'oxydation catalytique de l'éthylène en régimes stationnaire et transitoire. Thesis No 732, EPFL, Lausanne.

Scholl, K. L., Fletcher, E. A. (1993). "Y_2O_3-doped ZrO_2 membranes for solar electrothermal and solarthermal separations II: electron hole conductivity of yttria-stabilized zirconia." Energy **18**(1): 69.

Schouler, E. J. L., Kleitz, M. (1987). "Electrocatalysis and inductive effects at the gas, Pt / stabilized zirconia interface." J. Electrochem. Soc. **134**(5): 1045.

Schrader, M. E. (1977). "Auger electron spectroscopic study of chemisorption of oxygen to (111)-oriented gold surfaces." J. Coll. Interf. Sci. **59**(3): 456.

Schwank, J. (1983). "Catalytic gold." Gold Bull. **16**(4): 103.

Seiersten, M. E., Middleton, P. H. (1991). "Redox behavior of plasma sprayed nickel anodes" in *2nd International Symposium on SOFC*, Athens (GR), p. 569.

Setoguchi, T., Sawano, M., Eguchi, K., Arai, H. (1990). "Application of the stabilized zirconia thin film prepared by spray pyrolysis method to SOFC." Solid State Ionics **40/41**: 502.

Shelef, M., Graham, G. W. (1994). "Why Rhodium in automotive three-way catalysts?" Catal. Rev.-Sci. Eng. **36**(3): 433.

Silveston, P., Hudgins, R. R., Renken, A. (1995). "Periodic operation of catalytic reactors-introduction and overview." Catalysis Today **25**: 91.

Sinfelt, J. H., Via, G. H. (1979). "Dispersion and structure of Platinum-Iridium catalysts." J. Catal. **56**: 1.

Slin'ko, M. M., Jaeger, N. I. (1994). Oscillating heterogeneous catalytic systems. Elsevier.

Smith, O. I., Solomon, W. C. (1982). "Kinetics of hydrazine decomposition on Ir surfaces." Ind. Eng. Chem. Fundam. **21**: 374.

Snel, R. (1987). "Olefins from syngas." Catal. Rev.-Sci. Eng. **29**(4): 361.

Sobyanin, V. A., Sobolev, V. I., Belyaev, V. D., Mar'ina, O. A., Demin, A. K., Lipilin, A. S. (1993). "On the origin of the non-faradaic electrochemical modification of catalytic activity (NEMCA) phenomena. Oxygen isotope exchange on Pt electrode in cell with solid oxide electrolyte." Catal. Lett. **18**: 153.

Srinivasan, S., Wroblowa, H., Bockris, J. O. (1967). "Electrocatalysis" in *Advances in Catalysis*, Acad. Press, vol. 17, p. 352.

Stoukides, M., Eng, D. (1991). "Catalytic and electrocatalytic methane oxidation with solid oxide membranes." Catal. Rev.-Sci. Eng. **33**(3-4): 375.

Stoukides, M., Eng, D., Chiang, P.-H., Alqahtany, H. (1993). "Electrochemical modification of the activity and selectivity of metal catalysts" in *New frontiers in catalysis*, (L. Guczi, Ed.), Elsevier Sci. Publ. p. 2131.

Strekalovskii, V. N., Zubankov, V. N., Pal'guev, S. F. (1972). "High-temperature X-ray measurements of oxides. I. Study of the monoclinic-tetragonal transition of zirconium dioxide" in *Electrochemistry of molten and solid electrolytes*, (S. F. Pal'guev, Ed.), Consultants Bureau, vol. 9, p. 95.

Subramanian, S., Schwarz, J. A. (1991). "Stoichiometric composition of Platinum, iridium and platinum-iridium catalytic precursors." Appl. Cat. **68**: 131.

Suzuki, M., Sasaki, H., Otoshi, S. (1991). "Development of Ru / ZrO_2 SOFC anode" in *2nd International Symposium on SOFC*, Athens (GR), p. 585.

Takahashi, T., Suzuki, Y. (1967). "Time dependence of electrical conductivity of stabilized zirconias" in *Compte rendu des 2ièmes Journées Internationales d'étude de piles à combustibles*, Bruxelles, p. 354.

Takasu, Y., Tsukada, K., Nishimura, K., Hiromine, T., Yahikozawa, K. (1992). "An application of the thermal desorption method to the surface characterization of RuO_2-IrO_2 and RuO_2-TiO_2 coated titanium electrodes." Electrochim. Acta **37**(6): 1029.

Takeuchi, K., Perry, S. S., Salmeron, M., Somorjai, G. A. 1995). "The bonding properties of hydrogenated and fluorinated molecules to zirconium oxide thin films: influence of surface defects and water coadsorption." Surf. Sci. **323**: 30.

Tauster, S. J., Murrell, L. L. (1976). "The NO-CO reaction in the presence of excess oxygen as catalyzed by Iridium." J. Catal. **41**: 192.

Taylor, K. C. (1989). "Automobile catalytic converters" in *Catalysis - Science and Technology*, Akademic Verlag Berlin, p. 141.

Taylor, K. C., Schlatter, J. C. (1980). "Selective reduction of nitric oxide over noble metals." J. Catal. **63**: 53.

Teichner, S. J. (1993). "The history and perspectives of spillover" in *New aspects of spillover effect in catalysis*, Elsevier Sci. Publ., vol. 77, p. 27.

Thomas, J. M. (1994). "Turning points in catalysis." Angew. Chem. Int. Ed. Engl. **33**(9): 913.

Thomas, J. M., Thomas, W. J. (1967). Introduction to the principles of heterogeneous catalysis. Academic Press, London.

Thomson, S. J. (1987). "Promotion in heterogeneous catalysis: retrospect and prospect." J. Chem. Soc. Faraday Trans. **I83**: 1893.

Tournayan, L., Marcilio, N. R., Frety, R. (1991). "Promotion of hydrogen uptake in cerium dioxide. The role of iridium." Appl. Cat. **78**: 31.

Trasatti, S., Lodi, G. (1980). "Properties of conductive transition metal oxides with rutile-type structure" in *Electrodes of conductive metallic oxides*, Elsevier, p. 301.

Trasatti, S. (1991). "Physical electrochemistry of ceramic oxides." Electrochim. Acta **36**(2): 225.

Turner, J. E., Sales, B. C., Maple, M. B. (1981). "Oscillatory oxidation of CO over Pd and Ir catalysts." Surf. Sci. **109**: 591.

Vallet, C. E., Choudhury, A., Sobol, P. E., White, C. W. (1993). "XPS characterization of anodic layers grown on Ir- and Rh-implanted titanium." Electrochim. Acta **38**(10): 1313.

Van Hassel, B. A., Boukamp, B. A., Burggraaf, A. J. (1991). "Electrode polarization at the Au, O_2(g) /YSZ interface. Part I: Theoretical considerations of reaction model. Part II: Electrochemical measurements and analysis." Solid State Ionics **48**: 139.

Van Hassel, B. A., Boukamp, B. A., Burggraaf, A. J. (1992a). "Oxygen transfer properties of ion-implanted YSZ." Solid State Ionics **53-56**: 890.

Van Hassel, B. A., Burggraaf, A. J. (1992b). "Characterization of Fe implanted YSZ by cyclic voltammetry." Solid State Ionics **51**: 175.

Van Herle, J. (1993a). Oxygen reduction reaction mechanisms at solid oxide fuel cell cathodes. Thesis No 1187, EPFL, Lausanne.

Van Herle, J., Mc Evoy, A. J. (1993b). "Impedance characteristics of Pt electrodes on YSZ." Ber. Bunsenges. Phys. Chem. **97**(3): 470.

Van Herle, J., Mc Evoy, A. J., Thampi, K. R. (1994). "Oxygen reduction at porous and dense cathodes for solid oxide fuel cells." Electrochim. Acta **39**(11/12): 1675.

Van Manen, P. A., Weewer, R., De Wit, J. H. W. (1992). "High temperature cyclic voltammetry on metal/metal oxide systems." J. Electrochem. Soc. **139**(4): 1130.

Van Meerssche, M., Feneau-Dupont, J. (1976). Introduction à la cristallographie et à la chimie structurale. Leuven, Oyez.

Van Santen, R. A., Kuipers, H.P.C.E. (1987). "The mechanism of ethylene epoxidation." Adv. Catal. **35**: 265.

Varkaraki, E., Nicole, J., Plattner, E., Comninellis, C., Vayenas, C. G. (1995). "Electrochemical promotion of IrO_2 catalyst for the gas phase combustion of ethylene." J. Appl. Electrochem. **25**: 978.

Vayenas, C. G., Lee, B., Michaels, J. (1980). "Kinetics, limit cycles, and mechanism of the ethylene oxidation on platinum." J. Catal. **66**: 36.

Vayenas, C. G., Georgakis, C., Michaels, J., Tormo, J. (1981). "The role of PtO_x in the isothermal rate oscillations of ethylene oxidation on platinum." J. Catal. **67**: 348.

Vayenas, C. G., Bebelis, S., Despotopoulou, M. (1991a). "Non-faradaic Electrochemical Modification of Catalytic Activity 4. The use of beta-alumina as the solid electrolyte." J. Catal. **128**: 415.

Vayenas, C. G., Ioannides, A., Bebelis, S. (1991b). "Solid electrolyte cyclic voltammetry for in situ investigation of catalyst surfaces." J. Catal. **129**: 67.

Vayenas, C. G., Bebelis, S., Yentekakis, I. V., Lintz, H. G. (1992a). "Non-faradaic Electrochemical modification of catalytic activity: a status report." Catalysis Today **11**(3): 303.

Vayenas, C. G., Bebelis, S., Yentekakis, I. V., Neophytides, S. (1992b). "Non-faradaic electrochemical modification of catalytic activity: the work function of metal electrodes in solid electrolyte cells." Solid State Ionics **53-56**: 97.

Vayenas, C. G., Bebelis, S., Yentekakis, I. V., Neophytides, S., Yi, J. (1993a). "Ion spillover as the origin of the NEMCA effect" in *New aspects of spillover effect in catalysis*, Elsevier Sci. Publ., vol. 77, p. 111.

Vayenas, C. G., Bebelis, S., Yentekakis, I. V., Tsiakaras, P., Karasali, H., Karavasilis, C. (1993b). "Solid electrolytes for in situ promotion of catalyst surfaces: the NEMCA effect" in *New frontiers in catalysis*, (L. Guczi, Ed.), Elsevier Sci. Publ. p. 2139.

Vayenas, C. G., Bebelis, S., Yentekakis, I. V., Karavasilis, C., Yi, J. (1994a). "Non-faradaic electrochemical modification of catalytic activity: solid electrolytes as active catalyst supports." Solid State Ionics **72**: 321.

Vayenas, C. G., Ladas, S., Bebelis, S., Yentekakis, I. V., Neophytides, S., Yi, J., Karavasilis, C., Pliangos, C. (1994b). "Electrochemical promotion in catalysis: non-faradaic electrochemical modification of catalytic activity." Electrochim. Acta **39**(11/12): 1849.

Vayenas, C. G., Jaksic, M. M., Bebelis, S. I., Neophytides, S. G. (1995). The electrochemical activation of catalytic reactions; to be published.

Velle, O. J., Norby, T., Kofstad, P. (1991). "The electrode system O_2 / Pt // ZrO_2:8Y_2O_3 investigated by impedance spectroscopy." Solid State Ionics **47**: 161.

Vercesi, G. P., Salamin, J.-Y., Comninellis, C. (1991a). "Morphological and microstructural study of the Ti/IrO_2-Ta_2O_5 electrode: effect of the preparation temperature." Electrochim. Acta **36**(5/6): 991.

Vercesi, G. P., Rolewicz, J., Comninellis, C., Hinden, J. (1991). "Characterization of DSA-type oxygen evolving electrodes. Choice of base metal." Thermochim. Acta **176**: 31.

Verhoef, R. W., Kelly, D., Weinberg, W. H. (1994). "Dynamics of trapping-mediated dissociative chemisorption of molecular oxygen on reconstructed Ir(110)." Surf. Sci. Lett. **306**: L513.

Vol, A. E., Kagan, I. K. (1986). Handbook of binary metallic systems, Oxonian Press.

Voskresenskaya, E. N., Roguleva, V. G., Anshits, A. G. (1995). "Oxidant activation over structural defects of oxide catalysts in oxidative methane coupling." Catal. Rev.-Sci. Eng. **37**(1): 101.

Vukovic, M. (1987). "Oxygen evolution reaction on thermally treated iridium oxide films." J. Appl. Electrochem. **17**: 737.

Wachs, I. E. (1983). "Research on gold in catalysis." Gold Bull. **16**(4): 98.

Wagner, C. (1970). "Adsorbed atomic species as intermediates in heterogeneous catalysis" in *Advances in Catalysis*, Academic Press, vol. 21, p. 323.

Wang, D. Y., Nowick, A. S. (1979a). "Cathodic and anodic polarization phenomenon at Pt electrodes with doped CeO_2 as electrolyte: I. Steady-state overpotential." J. Electrochem. Soc. **126**: 1155.

Wang, D. Y., Nowick, A. S. (1979b). "Cathodic and anodic polarization phenomenon at Pt electrodes with doped CeO2 as electrolyte: II. Transient overpotential and AC Impedance." J. Electrochem. Soc. **126**: 1166.

Wang, D. Y., Nowick, A. S. (1980). "Polarization phenomena associated with reduction of a doped ceria electrolyte." J. Electrochem. Soc. **127**(1): 113.

Wang, D. Y., Nowick, A. S. (1981). "Diffusion-controlled polarization of Pt, Ag and Au electrodes with doped ceria electrolyte." J. Electrochem. Soc. **128**(1): 55.

Wang, D. Y. (1990). "Electrode reactions at the surface of oxide ionic conductors." Solid State Ionics **40/41**: 849.

Watanabe, M., Uchida, H., Shibata, M., Mochizuki, N., Amikura, K. (1994). "High performance catalyzed-reaction layer for medium temperature operating SOFC." J. Electrochem. Soc. **141**(2): 342.

Weber, W. J., Tuller, H. L., Mason, T. O., Cormack, A. N. (1993). "Research needs and opportunities in highly conducting electroceramics." Mat. Sci. Eng. **B18**: 52.

Weisz, P. B. (1959). "Intraparticle diffusion in catalytic systems." Chem. Eng. Prog. Symp. Series **55**(25): 29.

Wendt, H., Rausch, S., Borucinski, T. (1994). "Advances in applied electrocatalysis" in *Advances in Catalysis*, Academic Press, vol. 40, p. 87.

Weppner, W. (1977a). "Electronic transport properties and electrically induced p-n junction in ZrO_2 + 10m/o Y_2O_3." J. Solid State Chem. **20**: 305.

West, A. R. (1995). Crystalline solid electrolytes I: general considerations and the major materials" in *Solid state electrochemistry*, (P. G. Bruce, Ed.), Cambridge University Press, p. 7.

Wiemhoefer, H.-D., Vohrer, U. (1992). "Spectroscopy and thermodynamics of electrons in YSZ." Ber. Bunsenges. Phys. Chem. **96**(11): 1646.

Wiemhofer, H.-D. (1993). "Processes at interfaces between solid electronic, ionic and mixed conductors. Characterization by voltage and frequency dependent electrical measurements." Ber. Bunsenges. Phys. Chem. **97**(3): 461.

Williams, J. M., Lee, I. S., Buchanan, R. A. (1992). "Charge injection properties of iridium oxide films produced on Ti-6Al-4V alloy substrates by ion beam mixing techniques." Surf. Coat. Tech. **51**: 385.

Winnubst, A. J. A., Scharenborg, A. H. A., Burggraaf, A. J. (1984). "The electrode resistance of ZrO_2-Y_2O_3 (Bi_2O_3) solid electrolytes with Pt electrodes." Solid State Ionics **14**: 319.

Woods, R. (1976). "Chemisorption at electrodes: hydrogen and oxygen on noble metals and their alloys" in *Electroanalytical Chemistry*, (A. J. Bard, Ed.), Marcel Dekker, vol. 9, p. 1.

Wright, J. D. (1995). "Chemical sensors: past, present and future." Chemistry in Britain **31**(5): 374.

Yamaguchi, T. (1994). "Application of ZrO_2 as a catalyst and a catalyst support." Catalysis Today **20**: 199.

Yamamoto, O. (1995). "Applications" in *Solid state electrochemistry*, (P. G. Bruce, Ed.), Cambridge University Press, p. 292.

Yanagida, H., Brook, R. J., Kröger, F. A. (1970). "Direct current-voltage characteristics of calcia stabilized zirconia with porous platinum electrodes." J. Electrochem. Soc. **117**(5): 593.

Yang, O. B., Woo, S. I., Kim, Y. G. (1994). "Comparison of Pt-Ir bimetallic catalysts supported on γ-alumina and HY-zeolite in n-hexane reforming reaction." Appl. Cat. **115A**: 229.

Yeager, E., Kuta, J. (1970). "Study of electrode processes" in *Physical Chemistry: an advanced treatise*, Academic Press, vol. 9A, p. 369.

Yentekakis, I. V., Vayenas, C. G. (1988). "The effect of electrochemical oxygen pumping on the steady-state and oscillatory behavior of CO oxidation on polycristalline Pt." J. Catal. **111**: 170.

Yentekakis, I. V., Moggridge, G., Vayenas, C. G., Lambert, R. M. (1994). "In situ controlled promotion of catalyst surfaces via NEMCA: the effect of Na on the Pt-catalyzed CO oxidation." J. Catal. **146**: 292.

Youngblood, G. E., Rice, R. W., Ingel, R. P. (1988). "Thermal diffusivity of partially and fully stabilized (yttria) zirconia single crystals." J. Am. Cer. Soc. **71**(4): 255.

Zschech, E., Auerswald, G., Klinkenberg, E. D., Novgorodov, B. N. (1991). "Short-range order in yttria-stabilized zirconia: an EXAFS study." Nucl. Instr. Meth. Phys. Res. **A308**: 255.

LIST OF SYMBOLS

A	area	[cm^2]
a	lattice parameter	[Å]
a_o	oxygen activity	[-]
C	capacitance	[F]
C_d	double layer capacitance	[F]
C_{Ox}	concentration of species Ox	[mol cm^{-3}]
$C_{Ox,b}$	bulk concentration of active species	[mol cm^{-3}]
C_{Red}	concentration of species Red	[mol cm^{-3}]
c_i	concentration of component i	[mol cm^{-3}]
D	diffusion coefficient	[cm^2 s^{-1}]
D_o	diffusion coefficient	[cm^2 s^{-1}]
D_{Ox}	diffusion coefficient of Ox	[cm^2 s^{-1}]
D_{Red}	diffusion coefficient of Red	[cm^2 s^{-1}]
d	interplate spacing	[Å]
E	electric field	[V·cm^{-1}]
E_a	activation energy	[kJ·mol^{-1}]
E_F	Fermi energy level for electrons	[eV]
E_i	initial potential	[V]
E_p	peak potential	[V]
$E_{p/2}$	half-peak potential	[V]
E_{pa}	anodic peak potential	[V]
E_{pc}	cathodic peak potential	[V]
E_{ra}	anodic reversal potential	[V]
E_{rc}	cathodic reversal potential	[V]
$e\Phi$	work function	[eV]
f	Weisz factor	[-]
I	current	[A]
I_o	exchange current	[A]
I_d	capacitive current component	[A]
I_f	faradaic current component	[A]
I_L	limiting current	[A]
I_p	peak current	[A]
I_{pa}	anodic peak current	[A]
I_{pb}	peak current measured from the baseline	[A]
I_{pc}	cathodic peak current	[A]
I_{pz}	peak current measured from the line of zero current	[A]
i	current density	[A cm^{-2}]
i_o	exchange current density	[A cm^{-2}]
k	reaction rate constant	*
k_{ads}	adsorption rate constant	*

k_{des}	desorption rate constant	*
K_i	adsorption equilibrium constant for component i	*
L	characteristic length	[cm]
L_D	Debye length	[cm]
l_o	characteristic electrode length	[cm]
M	mole percentage of stabilizer	[-]
N	number of surface sites	[mol]
N_t	number of catalyst surface sites	[mol]
n	charge number	[-]
n_a	number of electrons in the rate determining step	[-]
$\dot{n}_i$	molar flow rate of component i	[mol s^{-1}]
P_i	partial pressure of component i	[kPa]
q	charge	[A s]
Q_c	charge for adsorbed layer reduction	[A s]
R_e	electrolyte resistance	[Ω]
R_f	faradaic resistance	[Ω]
R_u	uncompensated resistance	[Ω]
R_O	ionic radius of O^{2-}	[Å]
R_Y	ionic radius of Y^{3+}	[Å]
R_{Zr}	ionic radius of Zr^{4+}	[Å]
r	reaction rate	[molO s^{-1}] or *
$\dot{r}$	reaction rate under polarization	[molO s^{-1}]
r_o	open circuit reaction rate	[molO s^{-1}]
T	temperature	[K] or [°C]
t	time	[s]
u	charge carrier mobility	[V cm^2 s^{-1}]
u_i	charge carrier mobility	[V cm^2 s^{-1}]
V	applied voltage	[V]
V_{cat}	catalyst volume	[cm^3]
$\dot{V}$	volumetric flow rate	[cm^3 s^{-1}]
$\dot{V}_{tot}$	total volumetric flow rate	[cm^3 s^{-1}]
V_R	reactor volume	[cm^3]
V_{WC}	potential	[V]
V^o_{WC}	potential	[V]
V_{WR}	potential	[V]
V^o_{WR}	potential	[V]
$V_{\ddot{o}}$	oxygen vacancies in a lattice (Kröger-Vink notation)	
v	voltage scan rate	[V s^{-1}]
v	mean velocity of mobile ions	[cm s^{-1}]
X_i	conversion of component i	[-]
y_i	molar fraction of component i	[-]
z_i	number of charges of species i	[-]

*dep. on the rate expr.

ΔG_m	motional free energy
ΔH_{ads}	enthalpy of adsorption
ΔH_m	enthalpy of motion
ΔH_r	enthalpy of reaction
Δr	steady-state reaction rate change
ΔS_m	entropy of motion
α	charge transfer coefficient
α_a	anodic charge transfer coefficient
α_c	cathodic charge transfer coefficient
η	electrode overpotential
θ	incident angle
θ_i	fraction of catalytically active sites occupied by component i
Λ	reaction enhancement factor
λ	wavelength
μ	chemical potential
$\mu^\circ_{O2.(g)}$	standard chemical potential of gaseous oxygen
$\mu^\circ_{O2.R}$	standard oxygen chemical potential at the reference electrode
$\mu^\circ_{O2.W}$	standard oxygen chemical potential at the catalyst electrode
$\bar{\mu}$	electrochemical potential
ν	molar volume
ρ	reaction enhancement ratio
ρ	resistivity
σ, σ_i	conductivity
σ_e	electrode interface conductivity/exchange current range density
τ	characteristic time constant
τ_N	NEMCA characteristic time constant electrode overpotential
Φ	electron extraction potential
ϕ	Galvani or inner potential
χ	surface potential
Ψ	Volta or outer potential

List of Constants

e	electron charge	$1.60\ 10^{-19}$	[A s]
F	Faraday constant	96480	[A s mol^{-1}]
k	Boltzmann constant	$1.38\ 10^{-23}$	[J K^{-1}]
R	gas constant	8.3143	[J K^{-1} mol^{-1}]
ε_o	permittivity of free space, dielectric constant	$8.854\ 10^{-12}$	[F m^{-1}] or [A s V^{-1} m^{-1}]
ν	molar volume under normal conditions	22.4	[N l mol^{-1}]

LIST OF ABBREVIATIONS

A.C.	Alternating Current
CE	Counter Electrode
CSZ	Calcia Stabilized Zirconia
D.C.	Direct Current
DSA	Dimensionally Stable Anodes
emf	electromotive force
EPR	Electron Paramagnetic Resonance
GC	Gas Chromatography
IR	Infra-Red analyzer
MOCVD	Metallorganic Chemical Vapour Deposition
NEMCA	Non-faradaic Electrochemical Modification of Catalytic Activity
NHE	Normal Hydrogen Electrode
OER	Oxygen Evolution Reaction
PID	Proportional Integral Derivative regulator
PVC	Poly Vinyl Chloride
RDS	Rate Determining Step
RE	Reference Electrode
SEP	Solid Electrolyte Potentiometry
SOFC	Solid Oxide Fuel Cell
TCD	Thermal Conductivity Detector
TOF	Turnover Frequency
TPB	Three Phase Boundary
WE	Working Electrode
XRD	X-Ray Diffraction analysis
XPS	X-ray Photoelectron Spectroscopy
YSZ	Yttria Stabilized Zirconia
4PV	Four Port Valve

CURRICULUM VITAE

Name:	**Varkaraki**
First name:	**Elli**
Date of birth:	March 30, 1967
Place of birth:	Athens
Nationality:	Greek
Civil status:	single

Professional Activities

1981-1984	High school in Athens (Moraitis School)
June 1984	Apolitirion "medical type" with distinction of excellence
1984-1985	Cours de Mathématiques Spéciales (CMS), EPFL
1985-1991	Studies of chemical engineering at the EPFL
January 1991	*Graduation in Chemical Engineering at the* **Ecole Polytechnique Fédérale de Lausanne EPFL** **Swiss Federal Institute of Technology, Lausanne, Switzerland**
since 1991	*Research work in the field of supercritical fluids, electrochemistry and heterogeneous catalysis, for the obtention of a Ph.D. at the* **Institute of Chemical Engineering** **Ecole Polytechnique Fédérale de Lausanne EPFL** **CH-1015 Lausanne, Switzerland**
	Assistant for undergraduate students' practical training courses
	Member of the Commission of Ethics at the EPFL
1991-1994	President of the Commission of Ethics at the EPFL

Languages spoken	Greek, French, English, Spanish, basic knowledge of German
	"Proficiency certificate" for the English Language "Diplôme d'Etudes Supérieures" at the "Institut Français d'Athènes"